



University of HUDDERSFIELD

University of Huddersfield Repository

Marangwanda, Gilbert Kudzai

COMPUTATIONAL FLUID DYNAMICS BASED DIAGNOSTICS AND PREDICTION TOOL FOR OPTIMAL DESIGN OF MULTISTAGE TRIM CONTROL VALVES

Original Citation

Marangwanda, Gilbert Kudzai (2020) COMPUTATIONAL FLUID DYNAMICS BASED DIAGNOSTICS AND PREDICTION TOOL FOR OPTIMAL DESIGN OF MULTISTAGE TRIM CONTROL VALVES. Doctoral thesis, University of Huddersfield.

This version is available at <http://eprints.hud.ac.uk/id/eprint/35710/>

The University Repository is a digital collection of the research output of the University, available on Open Access. Copyright and Moral Rights for the items on this site are retained by the individual author and/or other copyright owners. Users may access full items free of charge; copies of full text items generally can be reproduced, displayed or performed and given to third parties in any format or medium for personal research or study, educational or not-for-profit purposes without prior permission or charge, provided:

- The authors, title and full bibliographic details is credited in any copy;
- A hyperlink and/or URL is included for the original metadata page; and
- The content is not changed in any way.

For more information, including our policy and submission procedure, please contact the Repository Team at: E.mailbox@hud.ac.uk.

<http://eprints.hud.ac.uk/>

University of
HUDDERSFIELD
Inspiring global professionals

COMPUTATIONAL FLUID DYNAMICS BASED DIAGNOSTICS AND PREDICTION TOOL FOR OPTIMAL DESIGN OF MULTISTAGE TRIM CONTROL VALVES

A THESIS SUBMITTED IN PARTIAL FULLFILMENT OF THE REQUIREMENTS FOR
DEGREE OF DOCTOR OF PHILOSOPHY AT THE UNIVERSITY OF HUDDERSFIELD

by

Gilbert Kudzai Marangwanda

B.Eng. University of Huddersfield, UK, 2013

Director of Research: Prof Rakesh Mishra

Leader of Energy, Emissions, and the Environment Research Group

School of Computing and Engineering

University of Huddersfield

UK

December 2020

ABSTRACT

Control valves form an integral part of many industrial applications such as in the manufacturing, energy generation, aerospace, medical, civil, and environmental sectors. It is overly important and critical that accurate and explicit information on the local pressure and flow structure within a multi-stage trim control valve is known. Currently there is no known universal and scalable characterization methodology of local geometry of varying multiple aperture shape and size arrangements along a valve or flow handling device flow path, with local and Global flow and pressure parameters. Furthermore, at present the local pressure and flow structure within the vicinity of singularities, or flow passages within control valves is experimentally inscrutable with current experimental apparatus, mainly due to flow field intrusion, and impracticability of measuring probe or instrument insertion presented by complex local geometry. Extensive research is being carried out to improve the hydrodynamic performance efficiency and safe operation of control valves, as well as to develop viable and accurate scalable hydrodynamic performance prediction models within multiple flow passage trim control valves. Hence, the in-depth knowledge and understanding of the complex local pressure and flow phenomenon within multi-stage or multi-flow passage control valve trims is still an active subject of research. This is because most of the studies carried out on multi-stage control valve trims have severely limited information on the local geometric and flow field hydrodynamic interactive performance characteristics, or are based on globally derived empirical parameters for specific control valve types, and from which locally unquantified approximations of the local flow and pressure structure have been reported. The current hydrodynamic characterization methodologies presents a high risk of misrepresentation of the local and global flow and pressure structure. In addition, the current excessive empiricism presents ambiguity in selection of suitable and applicable methods and equations for a given flow restriction geometric shape, flow passages arrangement configuration, and flow physics. This leads to incorrect trim hydrodynamic design, and specification for an application. Consequently, this results in performance failures through cavitation and flashing damage, and inefficiency through choked flow and excessive pumping energy requirements. Hence this is the reason why this work is important.

The advent of advanced numerical flow analysis techniques has made it possible to simulate the complex local flow characteristics within multi-stage or multi-flow passage control valves and gain more detailed and in-depth information on the underlying local complex flow phenomenon. The work in this study is focused on the implementation of advanced numerical modelling tools to simulate flow inside multi-stage trim control valves with the objective of quantifying currently unmeasurable local geometric, flow and pressure characteristics within multi-stage trim control valves. The terminology control valves allude to devices that are used to critically regulate flow and pressure for designated downstream process requirements. Novel characterization methods of geometric, flow and pressure parameters have been developed and used to carry out investigations under various geometric and flow conditions

within multi-stage or multi-flow passage trim control valves. Comprehensive diagnostics have been performed qualitatively and quantitatively on the flow and pressure structure within multi-stage trims in control valves. A new and novel geometric based pressure loss coefficient (K_L) has been developed which is characteristic of geometry alone and independent of the current pressure loss coefficient prerequisites of pre-known pressure drop and flow rate across a flow passage or singularity. The pressure loss coefficient has been incorporated in the development of new and novel prediction tools that account for the observed combined effects of multiple apertures on the flow field, and as a function of the sequence of arrangement of their effective flow areas.

The prediction tools developed in this work have been incorporated to accurately predict local flow exit pressure, flow coefficient (CV), velocity, Pressure drop, and cavitation index and pumping energy requirements at each flow passage in a multi-stage trim, and as well as the global flow rate, pressure drop, and flow coefficient (CV), and pumping energy requirements. The flow coefficient is at present defined as a global parameter that characterises the flow and pressure drop across a flow restriction, and defines the efficiency at which flow is permitted through a flow restriction. It is practically expressed as the flow of water in US gallons/min at 60° Fahrenheit with a 1 PSI Global pressure drop across a valve.

From the developed hydrodynamic prediction tools, an optimization methodology based on the reduced gradient principle has been developed. The optimization model presented in this work is scalable, robust, and easily applicable. From the optimization model, the following determinations can be made:

- Optimal flow passages effective flow areas and their configuration of sequence of arrangement along the flow path can be simultaneously determined for optimal local flow Coefficient (CV) at any flow passage along a multi-stage trim flow path.
- Optimal flow passages effective flow areas and their configuration of sequence of arrangement along the flow path can be simultaneously determined for desired or prescribed local pressure drop at any flow passage along the flow path.
- Optimal flow passages effective flow areas and their configuration of sequence of arrangement along the flow path can be simultaneously determined for desired or prescribed cavitation characteristics at any flow passage along the flow path.
- Optimal flow passages effective flow areas and their configuration of sequence of arrangement along the flow path can be simultaneously determined for prescribed, desired and optimal local pumping energy requirements at any flow passage along the flow path.

DECLARATION

The author of this thesis owns any copyright in it and has given the University of Huddersfield the right to use such Copyright for any administrative, promotional, educational/and or teaching purposes. Copies of this thesis of any form, may be made in accordance with the regulations of the University Library. Details of these regulations may be obtained from the librarian. This page must form part of any such copies made.

The ownership of any patents, designs, trademarks, and all other intellectual property rights except for the Copyright (the intellectual property rights and any reproductions of copyright works, for example graphs and tables (Reproductions) which may be described in this thesis, may not be owned by the author, and may be owned by third parties. Such intellectual property rights and reproductions cannot and must not be available for use without the prior written permission of the owners(s) of the relevant intellectual property rights and/ or Reproductions.

ACKNOWLEDGEMENTS

It is with my greatest pleasure to honour and acknowledge the immense support from all who contributed towards the completion of this work. I would especially like to acknowledge and thank my late mother Nelia Sikala, Mubaiwa, Marangwanda whose dreams, hopes, and support was so immense it was inspirational. I thank God for giving me this opportunity and path to fulfil this work.

My acknowledgement for my supervisor Prof Rakesh Mishra is beyond putting into context as it is so immense and beyond words, he nurtured me in every aspect of Fluid Dynamics for which his command and intellect in the field is unfathomable, he became more than a supervisor with life changing advice and support in personal and work-related challenges throughout. I was blessed to have been under the supervision of Prof Rakesh Mishra. I would also want to acknowledge the support of the staff at the School of Computing and Engineering, particularly Chris Sentance for the overwhelming support and guidance throughout the course of the programme.

Finally, I would like to thank my Wife Stella Mpofu and my Children for their understanding, patience, and support through the journey of the PhD programme in eventful and non-eventful times.

CONTENTS

ABSTRACT	3
DECLARATION	5
ACKNOWLEDGEMENTS	6
CONTENTS	7
LIST OF FIGURES	10
LIST OF TABLES	15
NOMENCLATURE	16
SUBSCRIPTS	18
CHAPTER 1 INTRODUCTION	19
1.1. History of Control Valves	20
1.2. Typical Control Valve Components	22
1.3. Design Considerations for Control Valves	29
1.5. Control Valve Hydrodynamic Performance Prediction Governing Principles	34
1.6. ISA-75.01.01 Standard's Hydrodynamic Performance Predictions of a Control Valve:	36
1.6.1. Piping Geometry Factor	36
1.6.2. Valve Style Modifier	37
1.6.3. Reynolds Number Factor	38
1.6.4. Non-Choked Turbulent Flow:	39
1.6.5. Choked Turbulent Flow:	40
1.7. EN-60534-2-5 Standard's Hydrodynamic Performance Predictions for Fluid Flow Through Multistage Trim Control Valves with Interstage Recovery	41
1.7.1. Multistage Multi-path Control Valves	41
1.7.2. Multistage Single-Path Control Valves	42
1.7. Motivation.	52
1.8. Research Aims	53
1.9. Thesis Structure:	54
CHAPTER 2 LITERATURE REVIEW	56
2.1. Control Valves, Multi-Stage/Flow Passage Trims and Singularities.	56
2.2. Summary of Literature Regarding Multi-Flow Passages and Singularities Within Flow Control Valves.	74
2.3. Scope of Research.	74
2.4. Research Objectives:	76
COMPUTATIONAL FLUID DYNAMICS BASED DIAGNOSTICS AND PREDICTION TOOL FOR OPTIMAL DESIGN OF MULTI-STAGE TRIM CONTROL VALVES. BY GILBERT MARANGWANDA, SCHOOL OF COMPUTING AND ENGINEERING, UNIVERSITY OF HUDDERSFIELD	

Chapter 3 EMPIRICALLY BASED HYDRODYNAMIC PERFORMANCE PREDICTIONS OF A MULTI-STAGE TRIM CONTROL VALVE	77
3.1. Hydrodynamic Performance of a Control Valve.....	77
3.1.1. Valve Type Classification and Reference Criteria:	79
3.2. Empirically Based Hydrodynamic Performance Calculations:	82
CHAPTER 4 CFD BASED HYDRODYNAMIC PERFORMANCE EVALUATIONS OF A MULTI-STAGE CONTROL VALVE.....	85
4.1. Pre – Processing Set Up of CFD Model:.....	86
4.1.1. Configuration of Control Valve Geometry:.....	86
4.1.2. Meshing the Flow Domain:	87
4.1.3. Solver Execution:	88
4.2. Results of Single-Phase Flow in a Control Valve:	93
4.2.1. Pressure Loss and Pressure Recovery Downstream of the Valve Plug:	96
4.3. Choked Flow Analysis in a Control Valve with Multiphase Flow Model.	97
4.3.1. Physical Model Selection:	98
4.3.2. Choked Flow Characteristics Within a Control Valve	99
4.4. Summary of the Hydrodynamic Performance Analysis of The Baseline Valve:	102
Chapter 5 PARAMETRIC INVESTIGATIONS.....	104
5.1. Analysis of Single-Phase Flow in a Control Valve:	105
5.2.1. Mesh Independence Tests.....	107
5.2.2. Benchmark Tests	108
5.2.3. Valve Trim Geometric Effects on Local and Global CV	111
5.3. Analysis of Local and Global Geometric and Flow Parameter Correlations	116
5.3.1. Effects of Flow Passage Areas on Local Pressure Structure	116
5.3.2. Effects of Effective Flow Passage Areas on Local Flow Passage Differential Pressure:.....	118
5.3.3. Effects of The Global Pressure on the Extent of Cavitation within The Vicinity of the Multiple Flow Passages Along the Flow Path.....	120
5.4. Summary of Global Pressure Drop Effects and Outlet Pressure on Extent of Cavitation Within the Vicinity of the Multiple Flow Passages.....	124
5.4.1. Inlet Average Flow Velocity Effects on the Pressure Drop Ratio at the Valve Seat Flow Passage....	126
5.4.2. Effects of Flow Passage Effective Area Sizes and Sequence of Arrangement.....	127
5.5. Prediction Models.....	133
5.6. Summary of the Control Valve Analysis.....	138
Chapter 6 OPTIMIZATION OF A MULTI-STAGE TRIM CONTROL VALVE	139
6.1. Introduction	139
COMPUTATIONAL FLUID DYNAMICS BASED DIAGNOSTICS AND PREDICTION TOOL FOR OPTIMAL DESIGN OF MULTI-STAGE TRIM CONTROL VALVES. BY GILBERT MARANGWANDA, SCHOOL OF COMPUTING AND ENGINEERING, UNIVERSITY OF HUDDERSFIELD	

6.2. Optimization of a Multiple Flow Passage Control Valve.....	140
6.3. Pressure and Flow Output Objective Functions	140
6.4. Operation of The Optimization Model	142
6.4.1. Optimal Available Flow Coefficient (CV)	143
6.5. Optimization Model Limitations	145
6.6. Design Example 1, Multiple Flow Passage Control Valve	145
6.6.1. Summary a Control Valve Optimization.....	151
6.7. Design Example 2 for Water Flow in a 4 Stage-Passage Trim Control Valve.....	151
6.7.1. Specific Hydrodynamic Performance Optimization of a 4 Stage-Flow Passage Control Valve Trim.	157
6.8. Design Example of a Five Stage Continuous Resistance Trim with Liquid Helium Flow Media.	162
6.8.1. Optimal Trim Local and Overall Pressure Drop, CV and Pumping Energy Requirement.	170
6.8.2. Effects of Trim Geometric Configuration on the Trim Overall Maximum Allowable Flow Rate and Pressure Drop.	178
Chapter 7 CONCLUSIONS.....	185
7.1. Research Problem.....	185
7.2. Research Aims and Major Achievements	186
7.3. Thesis Conclusions.....	189
7.4. Thesis Contributions.....	194
REFERENCES	197
APPENDICES	206
A-1: Computational Fluid Dynamics	206
Introduction	206
Operation of CFD Codes.....	206
A-1.2: Empirical Flow and Pressure Relations and Derivations.....	211
A-1.2.1. Incompressible Flow CV and Resistance Coefficient.....	211
A-1.2.2. Derivations of Empirical Flow Equations	214
A-1.3. Empirical Derivations of Multi-Stage-Flow Passages Flow and Pressure Characteristics as a Function of Effective Flow Diameter and Area.	218
A-1.4. Derivations of Flow Coefficient (CV) From Crane TP-410 Parameter Characterization.....	221
A-2: ISA-75.01.01- Standard Hydrodynamic Performance Characteristics:	222
A-3: Examples of Sizing Calculations.....	230
A-4: Specific Hydrodynamic Performance in a Multi-Stage Trim Control Valve.....	232
A-5: Expressions for Flow and Pressure Structure in Multi-Stage Control Valves and Trims	237

LIST OF FIGURES

Figure 1-1 Roman Era Bronze Cock Stop Valve (Valvias, 2007-213) [85].....	20
Figure 1-2: Leonardo Da Vinci Sketch of Sophisticated Valves (Valvias, 2007-213) [85].....	21
Figure 1-3: Typical Components of a Guided Plug Globe Valve (Paktechpoint Valve Training Article – 2021) [86]	22
Figure 1-4: Fast Opening Characteristic Plug Configuration (Sivaranjith, Automation Forum.Co, 04/03/2018) [102]	30
Figure 1-5: (a) linear flow regulation characteristic relationship of flow rate and valve lift and (b) Plug shape for linear flow regulation characteristic. (Sivaranjith, Automation Forum.Co, 04/03/2018) [102]	31
Figure 1-6: (a) equal percentage flow regulating characteristic relationship of flow rate and valve lift, and (b) plug shape for equal percentage flow regulation characteristic. (Sivaranjith, Automation Forum.Co, 04/03/2018) [102].....	31
Figure 1-7: Extent of Cavitation Damage Within the Vicinity of a Valve Plug Flotech, 904-358-1849, 10/03/2018, [104]	32
Figure 1-8: Cavitation and Flashing pressure profile within a control valve (Instrumentation Tools, 2020, [103])	34
Figure 1-9: Example of a Multistage Multi Path Control Valve Trim (ISA 750101- EN 60534-2-5-2003-Page 6) [1].....	41
Figure 1-10: Example of a Multistage Single Path Control Valve (ISA 750101- EN 60534-2-5-2003Page 7) [1].	42
Figure 2-1 (a) Trim Geometry (b) Pressure Loss Variations Across Rows Across the Flow Path	58
Figure 2-2: Experimental and numerical Variations of the cavitation index w.r.t variations of the ball valve opening angle.....	59
Figure 2-3: Experimental and Numerical Variations of (a), the Head Loss Coefficient, and (b), the flow coefficient (CV) w.r.t Variations of the Ball Valve Opening Angle.	59
Figure 2-4: Throttle Valve Multi Flow Passages Arrangement.....	60
Figure 2-5: Depiction of Fluid Flow Across (a) Thin Orifice, and (b) Thick Orifice	61
Figure 2-6: Working Principle of Diaphragm Pump With 3 Inlets and 4 Outlets	65
Figure 2-7: Variations of Pressure Drop for (a) Double Orifice- 1D Spacing and (b) Double Orifice 2D Spacing.	67

Figure 2-8: Variations of the Flow Passages Equivalent Discharge Coefficient as a function of the Reynolds Number for (a) Single Plate-Stage, (b) Six Plate-Stages Inline Conditions, (c) 14 Plate Offset Conditions at Various Flow Area Ratios.	69
Figure 3-1 Control Valve Hydrodynamic Sizing Flow Chart	84
Figure 4-1 Valve Geometric Flow Domain	86
Figure 4-2 Valve Trim Flow Passages Along the Flow Path	87
Figure 4-3 Variations of Static Pressure (N/m^2) Within the Valve.	94
Figure 4-4 Variations of Static Pressure (N/m^2) Within the Valve Along the Mid Section of the Cage Holes Flow Passages. The Flow Section Holes are Defined as (FP1) In This Study.	95
Figure 4-5. Variations of Velocity (m/sec) with-in the Valve.....	95
Figure 4-6 Variations Of Velocity (m/sec) Within The Valve Along The Mid Section of the Cage Holes Flow Passages (FP1).....	96
Figure 4-7. Pressure Variations Downstream of the Valve Opening at Varying Outlet Pressure.	97
Figure 4-8. Variations of Volumetric Flow Rate as a function of Global Differential Pressure Across the Valve	99
Figure 4-9: Variations of Vapour Volume Fraction downstream of the Valve Plug Entrance.....	100
Figure 5-1. Variations of Water Flow Pressure in the Baseline Control Valve.....	106
Figure 5-2. Positions of stages-flow passages along the valve flow path Flow passage positions and flow parameter measuring points.....	107
Figure 5-3. Variations of Static Pressure Upstream and Downstream of The Valve Seat	107
Figure 5-4: Actual Test Rig Arrangement and Schematic Representative Diagram of Test Loop.	109
Figure 5-5: Validation of CFD Results and Experimental Results for Pressure Drop Across the Control Valve at Various Volumetric Flow Rates.....	112
Figure 5-6-Depiction of Flow Passage's Effective Flow Areas and Flow Area Ratio Variations.	113
Figure 5-7. Variations of Global Pressure Drop Across the valve for Various Sequential Flow Passage Area Ratios.....	114
Figure 5-8 Variations of Trim Flow Capacity for Various Sequential Flow Area Ratios (C_{FAR}).....	115
Figure 5-9 Flow Area Ratio (F_{AR}) Variations Along the Valve Flow Path	117
Figure 5-10. Differential Pressure Ratio Variations Along the Flow Path w.r.t Flow Passage Area Ratio Variations.	120
Figure 5-11. Variations of Local flow Passages Cavitation Number at Variations of Global differential pressure Ratio.	122

Figure 5-12. Variations of Vapour Volume Fraction at the Valve Seat Flow Passage at (a) 20 PSI Outlet Pressure, and at (b) 40 PSI Outlet Pressure.	124
Figure 5-13. Variations of Differential Pressure Ratio at Varying Combined Flow Area Ratios (CFAR)..	127
Figure 5-14. Variations of (a) Velocity and (b) Pressure, for Flow Passages Diameter FP1 = 38.1mm, FP2 = 30.5mm, FP3 = 25.4mm at flow rate of 148 Usgpm.	128
Figure 5-15. Variations of (a) Velocity and (b) Exit Pressure, for Flow passage 1 (FP1) 12 Holes of 11mm Diameter with Total Effective Diameter of 38.1mm at a Global Flow Rate of 148 Usgpm.	129
Figure 5-16: Variations of Differential Pressure across each Flow Passage and respective Local CV at for Flow Passages Diameter FP1 = 38.1mm, FP2 = 30.5mm, FP3 = 25.4mm at flow rate of 148 Usgpm.	130
Figure 5-17: Variations of Differential Pressure across each Flow Passage and Respective CV for Flow Passages Diameter FP1 = 26.4mm, FP2 = 20.3 mm, FP3 = 20.3 mm at flow rate of 148 Usgpm.	131
Figure 5-18: Variation of Vapour Volume Fraction Within the Vicinity of The Flow Passages, at Flow Passages Diameter FP1 = 26.4mm, FP2 = 20.3 mm, FP3 = 20.3 mm at flow rate of 148 Usgpm.	132
Figure 5-19: Variations of Prediction Model and CFD Results of The Flow Passages Downstream Exit Static Pressure.	137
Figure 6-1: Flow Chart of the Targeted Optimization Methodology	144
Figure 6-2: Variations of pressure drop and cavitation index at each flow passage along the flow path for the Baseline Geometric Configuration at the Given flow and Pressure Conditions Presented in Table 6.1.	147
Figure 6-3: Variations of Pressure Drop and Cavitation Index at Each Flow Passage Along the Flow Path for Iteration 1 of the Optimization Process.	149
Figure 6-4: Variations of Pressure Drop and Cavitation Index at Each Flow Passage Along the Flow Path for the Optimal Local Geometric Configuration.	150
Figure 6-5: Geometric Configuration for a Multi Hole Double Cage Trim Within a Control Valve (a) and velocity contours within cage trim flow passages.	152
Figure 6-6: Prediction Model and CFD Results of Pressure Drop Variations Across the Trim Flow Passages Along the Control Valve Flow Path for the Baseline Valve Trim.	154
Figure 6-7: Variations of Local Pressure Drop at Each of the Flow Passages and Corresponding Cavitation Index as a Function of the Ratio of Effective Inlet Flow Diameter and Respective Effective Flow Passage Diameter Along the Flow Path for the baseline Valve Trim Geometric Configuration.	155
Figure 6-8: Variations of Local Pressure Drop and CV Across the Trim Flow Passages Along the Flow Path, w.r.t the Ratio of Effective Inlet Flow Diameter and Respective Effective Flow Passage Diameter Along the Control Valve Flow Path.	156

Figure 6-9: Variations of Pressure Drop and Cavitation Index at the Flow Passages Along the Flow Path Within the Control Valve w.r.t the Optimal Flow Passages Effective Flow Area Magnitudes and Sequence of Arrangement Along the Control Valve Flow Path.	159
Figure 6-10: Variations of Pumping Energy Requirements w.r.t the Ratio of the Inlet Diameter to The Effective Flow Diameter at a Respective Flow Passage Along the Flow Path for the Baseline and Optimal Geometric Configuration.	160
Figure 6-11: Variations of Flow Coefficient (CV) and Pressure Drop w.r.t the Ratio of the Inlet Diameter to the Respective Flow Passage Effective Flow Diameter along the Control Valve flow path for the Optimal Geometric Configuration.	161
Figure 6-12: (a) Multi-Stage Trim Geometric Configuration and (b) Distribution of Flow Velocity Within the Trim.	163
Figure 6-13: Prediction Model and CFD Results of Variations of Local Static Pressure Drop Across The 5 Flow Passages Along the Trim Flow Path for the Baseline Valve Trim.	166
Figure 6-14: Variations of Normalised Pressure Difference and Stage/ Flow Passage Exit Static Pressure w.r.t the Ratio of The Inlet Diameter to The Effective Flow Diameter of a Respective Stage/Flow Passage Along the Trim Flow Path.	167
Figure 6-15: Variations of Pressure Drop and Flow Coefficient (CV) at Each of the Stages-Flow Passages Along the Trim Flow Path w.r.t the Ratio of the Inlet Diameter to the Respective Stage-Flow Passage Effective Flow Diameter Along the Trim Flow Path.	168
Figure 6-16: Variations of Pumping Power Requirements Across the Stages/Flow Passages Along the Trim Flow Path w.r.t the Flow Coefficient (CV) Across a Respective Stage-Flow Passage Along the Trim Flow Path.	170
Figure 6-17: Variations of Exit Pressure at Each Stage-Flow Passage Along the Trim Flow Path and Normalised Pressure Difference w.r.t the Optimal Ratio of the Inlet Diameter to the Effective Flow Diameter of a Respective Stage Flow Passage Along the Trim Flow Path.	172
Figure 6-18: Variations of Optimal CV and Pressure Drop Across the Trim Stages-Flow Passages Along the Flow Path w.r.t the Optimal Ratio of the Inlet Diameter to the Effective Flow Diameter of a Respective Stage-Flow Passage Along the Trim Flow Path.	173
Figure 6-19: Variations of Pressure Drop Across the Flow Passages for the Optimal and Baseline Trim as a Function of the Ratio of the Inlet Diameter to the Effective Flow Diameter of a Flow Passage Along the Trim Flow Path.	174
Figure 6-20: Variations of Normalised Pressure Difference for The Optimal and Baseline Trim Geometric Configuration.	175

Figure 6-21: Variations of Exit Static Pressure of the Trim Stages-Flow Passages Along the Trim Flow Path for the Optimal and Baseline Trim Geometric Configuration.....	176
Figure 6-22: Variations of Pumping Energy Requirements for the Optimal and Baseline Trim w.r.t the Ratio of the Inlet Diameter to the Effective Flow Diameter of a Flow Passage Along the Trim Flow Path.	177
Figure 6-23: Variations of Cavitation Index for The Optimal and Baseline Trim Geometric Configurations	179
Figure 6-24: Variations of Normalised Pressure Difference for the Optimal and Baseline Trim w.r.t the Ratio of the Control Valve Inlet Diameter to the Effective Flow Diameter of a Respective Stage-Flow Passage Along the Trim Flow Path.....	180
Figure 6-25: Variations of Pressure Drop Across the Trim Stages Flow Paths for the Optimal and Baseline Geometric Configurations.	181
Figure 6-26: Variations of Flow Coefficients (CV) Across the Stages-Flow Passages of the Optimal and Baseline Trim Geometric Configurations.....	182
Figure 6-27: Variations of Pumping Energy Requirements Across the Trim Stages-Flow Passages Effective Flow Diameters Along the Trim Flow Path for the Optimal and Baseline Trim Geometric Configurations.	183
Figure 6-28: Variations of Pumping Energy Requirements and Normalised Pressure Difference at the Stages-Flow Passages of the Optimal Trim Geometric Configuration.	184

LIST OF TABLES

Table 1-1: Control Valve Types	24
Table 2-1: Values of the Stage Interaction Factor k and Reheat Factor r	57
Table 3-1: Valve Operating Process Conditions.	78
Table 4-1: Mesh Independence Test Results	88
Table 4-2. Solver Boundary conditions.....	91
Table 4-3: Valve Hydrodynamic Performance Comparison	101
Table 5-1. Experimental and CFD Results Comparison	110
Table 5-2. Variations of Flow Passages Effective Flow Areas, Flow Area Ratios, and Combined Flow Area Ratios Along the Flow Path.....	112
Table 5-3. Variations of Flow Passages Diameters	117
Table 5-4: Variations of Flow Passages Diameters.....	118
Table 6-1. Variations of flow parameters w.r.t flow passage effective flow diameters for the.....	146
Table 6-2: Variations of Flow Parameters for Varied Effective Flow Passage Diameters For Optimization iteration 1.....	148
Table 6-3: Variations of Flow and Pressure Parameters for Varied Effective Flow Passage Diameters for Optimization Iteration 2.	149
Table 6-4: Control Valve Trim Geometric Parameter Configuration and Variations of Prediction Tool and CFD Results of Local and Global Flow Parameters.....	153
Table 6-5. Variations of The Control Valve Global and Local Trim Pressure and Flow Parameters for the Optimal Trim Flow Passages Effective Flow Area Sizes and Sequence of Arrangement Along the Flow Path.	158
Table 6-6: Stage Trim Geometric Parameter Configuration and Results of Local and Global Pressure and Flow Parameters for the Prediction Model and CFD Model.....	164
Table 6-7: Variations of the Specific Optimal Hydrodynamic Performance Characteristic of the Optimal Trim Geometric Configuration.....	171

NOMENCLATURE

CV	Flow Coefficient
\dot{m}	Mass Flow Rate
F_L	Fluid Pressure Recovery Factor
F_{LP}	Liquid Pressure Recovery Factor for Valves with Attached Fittings
F_F	Fluid Critical Pressure Ratio Factor
F_d	Valve Style Modifier
F_R	Reynolds Number Factor
P_1	Inlet Pressure (psi)
P_2	Outlet Pressure (psi)
P_V	Vapor Pressure (psi)
P_{VC}	Pressure at Vena-Contracta (psi)
Q	Volumetric Flow Rate (Usgpm)
Q_{MAX}	Maximum Volumetric Flow Rate (Usgpm)
ΔP	Pressure Drop
ΔP_{ch}	Pressure Drop Choked (psi)
S_G	Specific Gravity
D	Effective Flow Diameter
l	Travel (mm)
D_s	Flow passage/Stage outside diameter (mm)
Y	Expansion Coefficient
ρ	Density Fluid
μ	Dynamic Viscosity
ν	Kinematic Viscosity
N	Numerical Constant
β	Effective Flow Area Ratio
ζ_1	Upstream Velocity Head Loss Coefficient
ζ_2	Downstream Velocity Head Loss Coefficient
ζ_{B1}	Inlet Bernoulli Coefficient
ζ_{B2}	Outlet Bernoulli Coefficient

C_d	Discharge Coefficient
σ	Cavitation Index
K	Pressure Loss Coefficient
K_L	Geometry Pressure Loss Coefficient
FP	Flow Passage
G	Global

SUBSCRIPTS

FP	Flow Passage
eq	Equivalent Area
c	Contraction Coefficient
vc	Vena Contracta
J	Jet Pressure
W	Wetted Perimeter
dpr	Differential Pressure Ratio
AR	Area Ratio

CHAPTER 1

INTRODUCTION

Flow and pressure regulating valves form a fundamental part of many industrial applications where critical regulation of flow rates and pressure is required. The hydrodynamic performance of a control valve is critical in terms of designated design control requirements and safe operation. To comprehensively analyse the local complex flow characteristics eventuating within the control valve, it is paramount that the flow structure within a control valve is extensively understood. The local pressure losses and flow coefficients (CV) within a multi flow passage trim, and their effects on the global performance can be extended to assimilate the effects of the trim multiple flow passage effective flow areas and their pattern of arrangement along the flow path.

1.1. History of Control Valves

There is little known about the control of fluids prior to Roman times, water in irrigation channels was regulated by some form of isolation sluice gate valves, and the water clocks made by the Egyptians indicated that they possessed some form of knowledge on the principles of flow. The advent of numerous mechanical and hydraulic machines, and the initial use of complicated valve designs such as the plug cock valve was seen to have occurred in the Greek and Roman periods. The plug cock valve design remained virtually unchanged until the 19th century. The present swing and lift check valves are the modified and improved versions of the flap and coin valves respectively, and they were used in the water force pumps. Bronze and brass plug cocks were commonly used during the Roman era as stop valves on water mains and supply pipes to public and domestic buildings. The parts of the valve were a body, a holed pug, a bottom, and a long levy for turning the plug. A large bronze cock valve was found on Capri among the ruins of the Palace of Tiberius, built around AD25. Figure 1.1 shows the cock valve used in the Roman period.



Figure 1-1 Roman Era Bronze Cock Stop Valve (Valvias, 2020) [85]

The Romans also used a primitive diaphragm valve made of crude leather which was manually closed over a weir, to control flow and temperature of household bath water. Small valves and butterfly valves used as taps including butterfly valves used as taps were found at several Mediterranean towns of Rabat, Djemila, Istanbul, Avanches, Augusta, and in Naples where the plugs were cylindrical. There was no significant and important progress made in valve design during the Middle Ages. The advent of the construction of canals, irrigation systems, and other hydraulic equipment during the renaissance saw the introduction of more sophisticated valves.

Figure 1-2 shows a sketch of sophisticated valve samples by Leonardo Da Vinci

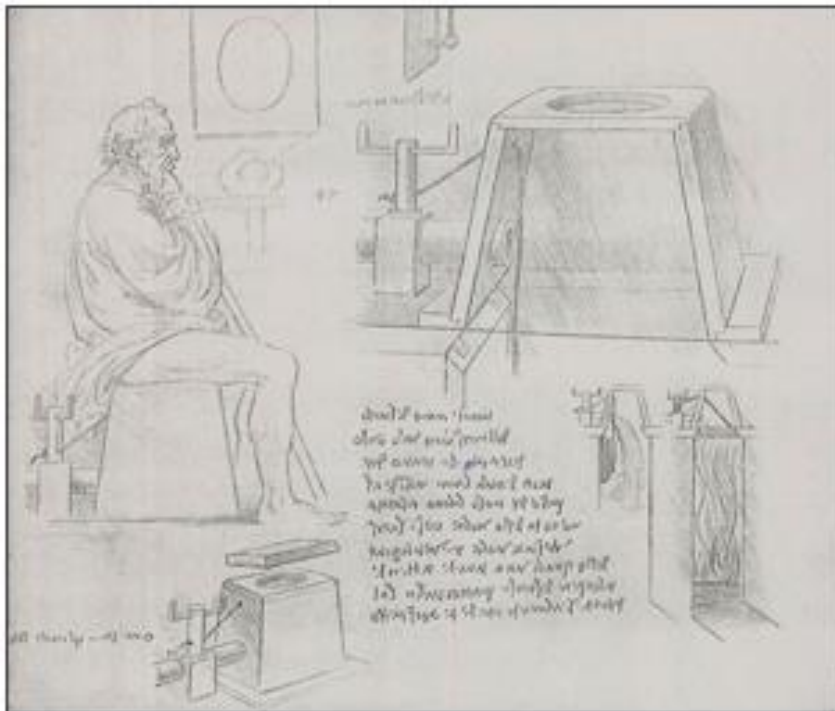


Figure 1-2: Leonardo Da Vinci Sketch of Sophisticated Valves (Valvias, 2020) [85]

The arrival of the steam engine invented by Thomas Newcomen in 1705, as a practical and commercial proposition at the commencement of the industrial revolution in the early 18th century meant that the steam engine required valves to regulate high pressure steam, and as more inventions came to realization, they facilitated the development of more variations of valve types. In the past 60 years, numerous other types of valves have been designed to make provision for new and hazardous processes. During the last 30 years, focus has been directed on ball valves by many manufacturers, resulting in the introduction of new and improved designs.

1.2. Typical Control Valve Components

In this present day, there are numerous types of valves and trim configurations available for Different applications and process conditions. Figure 1-3 shows the typical components of a guided globe control valve where the plug is guided by a cage.

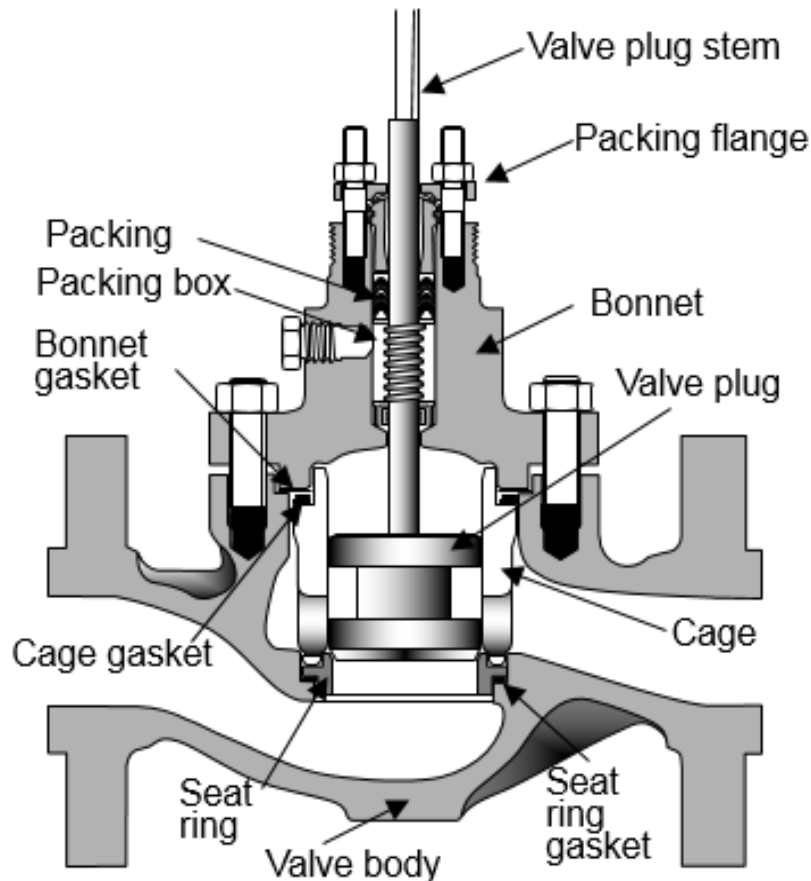


Figure 1-3: Typical Components of a Guided Plug Globe Valve (Paktechpoint Valve Training Article – 2020) [86]

➤ **The Body:**

The valve body forms the main flow path of the fluid and it houses the trim which mainly constitutes of the internal components of the valve through which other secondary flow passages exist to form the overall effective flow path across the entire valve.

➤ **Stem:**

The stem is coupled to the plug through various means to enable control of the fluid through actuation of the plug either in a linear or rotational manner.

The stem shown in figure 1-3, moves the plug in a linear manner by means of a thread. Actuation of the stem can also be achieved through hydraulic or pneumatic means.

➤ **Packing Flange:**

The packing flange facilitates for the compression of the stem sealing packings to achieve a seal and containment of the fluid within the valve.

➤ **Packing:**

The packing provides a seal around the stem, and there are different materials that can be used as packing seals with the most common being die formed graphite.

➤ **Packing box:**

The packing box provides the housing in which the packing seals are encapsulated.

➤ **Bonnet:**

The bonnet is the valve top cover which houses the stem packing configuration and can be used to provide a guide for the plug guide cage. The bonnet allows for the assembly of the trim parts through the top of the valve by design convenience.

➤ **Bonnet gasket:**

The bonnet gasket provides the joint seal between the body and the gasket.

➤ **Valve plug:**

The valve plug provides the fluid regulating element of the valve and depending on the fluid regulation requirements as a function of flow control characteristics, the plug can be of different shapes and configurations.

➤ **Cage:**


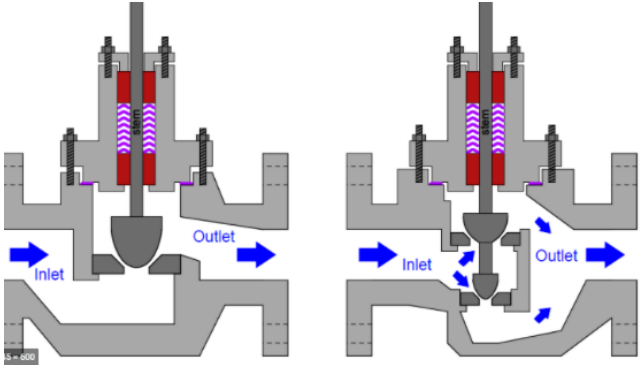
The cage primarily provides a guide for the plug but also forms an additional flow passage along the flow path.

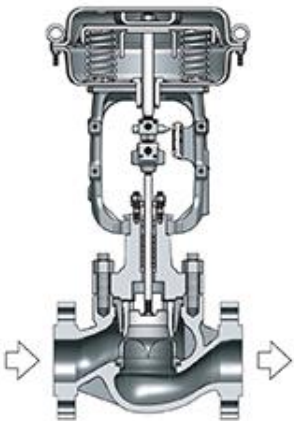
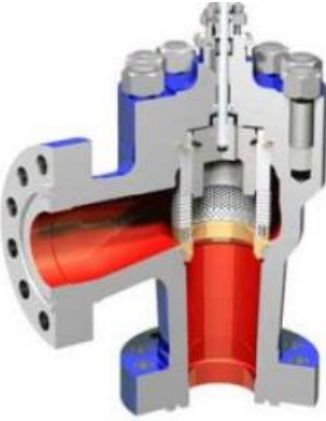
1.2.1. Control Valves Types

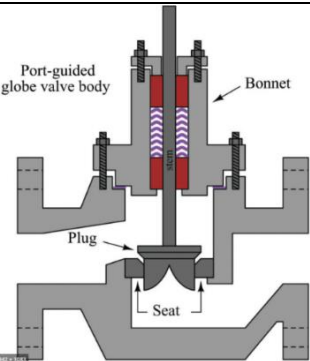
Control valve classification generally falls into two main categories with respect to the method of opening and closure, and these are linear motion or rotational. Within the

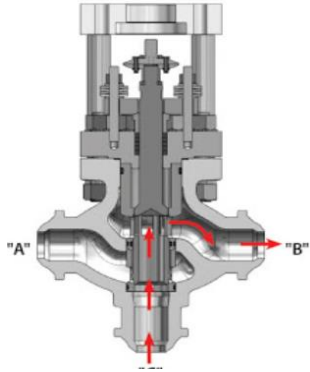
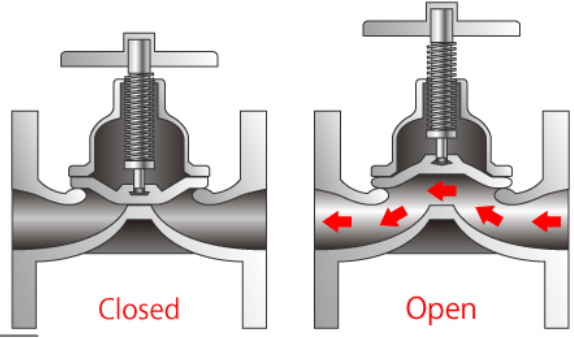
categories, valves are further classified with respect to specific trim (valve internal parts) geometric profiles. A list of common specific valve types falling under the linear motion and rotational motion categories is shown in table 1-1.

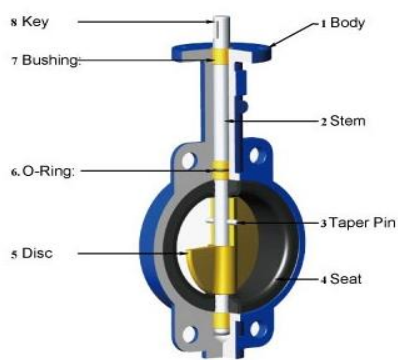
Table 1-1: Control Valve Types


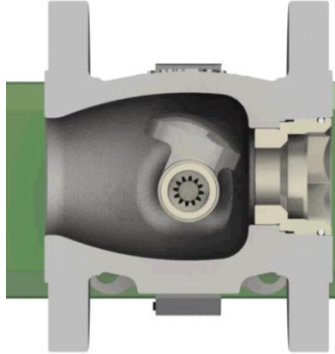
		General Valve Type Geometric Overview
Angle Valves	Cage Style Valves	 <p>Angle Seat Valve (Tameson B.V. 2020) [87]</p>
	Disk-Stack Style Valves	
	Angle Seat Piston Valves	
Globe Valve	Single and Double Port	 <p>Single and Double Ported Globe Valve (Control Automation- Sliding Stem Valves Chapter 30- 2020) [88]</p>

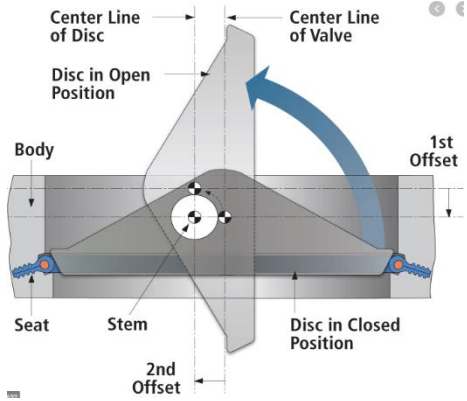
<p>Globe Valve</p>	<p>Balanced Plug-Cage Style</p>	 <p>Pressure Balanced Cage Type Control Valve (THINKTANK Optimal Fluid Solutions - 2020) [89]</p>
<p>Globe Valve</p>	<p>High-Capacity Cage Guided Valves</p>	 <p>Cage Guided Globe Valve- (Blakeborough BV992- Trillium Flow Technologies- 2020) [90]</p>

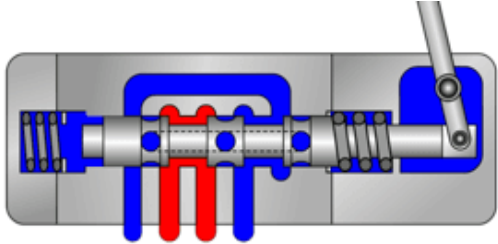
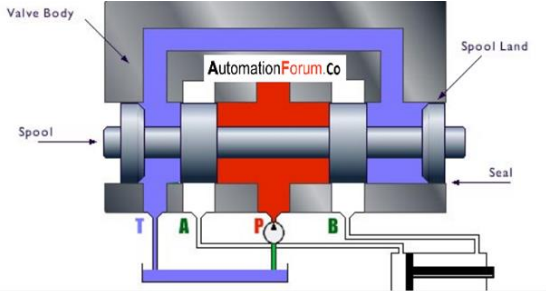
<p>Globe Valves</p>	<p>Port Guided Single-Port Valves</p>	 <p>Port Guided Single - Port Globe Valve (Control Automation- Sliding Stem Valves Chapter 30- 2020) [88]</p>
---------------------	---------------------------------------	---


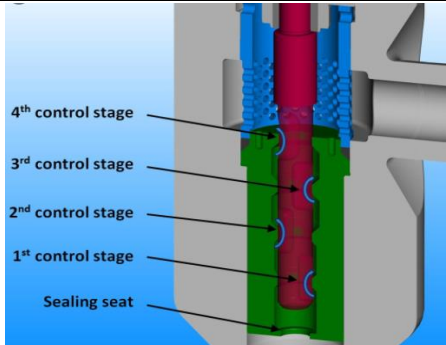
	<p>Three-Way Valves</p>	 <p>Three Way Globe and Plug Valve (Pnecon Automation - 2020) [91]</p>
<p>Diaphragm Valve</p>		 <p>Diaphragm Valve (GlobalSpec.com - Image Credit TLV- 2020) [92]</p>

<p>Rotary Valves</p>	<p>Butterfly Valve</p>	 <p>Butterfly Valve (Projectmaterials- Tecnos SA- 2020) [93]</p>
----------------------	------------------------	--

<p>Rotary Valves</p>	<p>V-notch Ball Valve</p>	 <p>V-Port Ball Valve (Pekos Valves-2020) [94]</p>
	<p>Eccentric-Pug Valves</p>	 <p>Eccentric Plug Rotary Valve (TRIMTECK OPTIMUX - 2020) [95]</p>

<p>Rotary Valves</p>	<p>Eccentric-Disk Valves</p>	 <p>Eccentric Disk Valve (Projectmaterials- 2020) [96]</p>
----------------------	------------------------------	--

Sliding Cylinder Valves	Directional Control Valves	 <p>Directional Control Valve (Lunchbox Sessions Training - 2020) [97]</p>
	Spool Valves	 <p>Directional Spool Valve (AutomationForum.Co - 2020) [98]</p>

Multi- Stage Trims	Anti-Cavitation Trim	 <p>Multi-Stage Anti Cavitation Trim (TRIMTECK OPTIMUX-2020) [99]</p>
	General Multiple Stage Trim	 <p>Multi-Stage Angle Type Valve (Valve and Automation - Total Valve & Control Solutions -2020) [100]</p>

1.3. Design Considerations for Control Valves

The design consideration within a control valve cover a wide aspect of parameters which fall under two main categories for which specific parameters are accounted for under each category. In this study the hydrodynamic parameters that have been considered are as follows.

➤ Hydrodynamic Parameters

- Geometric
- Flow control characteristics: (Equal percentage, linear, and quick opening)
- Cavitation
- Flow coefficient (CV)
- Flow rate
- velocity
- Pressure drop
- Flashing
- Noise

The behaviour of a fluid with regards to flow and pressure characteristics as it interacts with geometry within a control valve is overly complex. The design of a control valve constitutes of numerous considerations which may include, temperature, fluid toxicity, corrosion, pressure, type of fluid, structural integrity, and many more other specific considerations. Hydrodynamic performance considerations form a pivotal attribution to the functionality of a control valve to safely regulate fluid to the required process specifications safely and efficiently. The hydrodynamic performance of a control valve is benchmarked by the following parameters:

➤ Geometric Parameters

The hydrodynamic characteristics within a control valve are explicitly and exclusively dependent on the geometric profile of the flow path where the flow field is primarily sensitive to the effective flow area magnitudes of flow restrictions or flow passages along the flow path. In the case of a flow control valve consisting of multiple flow passages or stages, the pattern of arrangement of the flow passages along the flow path with regards to the effective flow area sizes along the flow path is substantially influential on the flow field characteristics. In addition, the change of direction of the flow passages where sudden or gradual angular changes exist along the flow path inclusively have substantial effect on the flow field characteristics. Furthermore, the flow control characteristic of a control valve which is defined by percentage change for a given percentage plug lift or opening is solely dependent on the geometric shape of the plug. The afore mentioned geometric parameters and the velocity, flow coefficient (CV) and pressure drop are interdependent, and hence, in order to design a control valve for optimal

hydrodynamic performance, all these parameters have to be simultaneously accounted for within the geometric constraints. An optimization model has been developed in this study for which the optimal flow passages effective flow areas and sequence of arrangement along the flow path can be determined for a desired global or local flow coefficient (CV), pressure drop, flow rate, and local cavitation index.

Flow Regulation Characteristics:

The primary purpose of a control valve is to control the rate of flow of a fluid, and the way the fluid is regulated is overly important for processes. The relationship between the valve opening and flow rate under constant pressure conditions defines the inherent flow characteristics of a control valve. The valve opening is defined as the position of the valve plug relative to its closed position. There are three main modes of flow regulating characteristics, and these have originated from specific requirements of a process. The three main types of flow characteristics are

➤ **Fast opening Characteristic.**

The fast-opening phenomenon is typified by a large variation of the flow rate for a small valve opening lift from the closed position. This characteristic does not necessarily provide any explicit regulation; hence it is described as an on and off characteristic. Figure 1-4 shows the fast-opening characteristic plug configuration.

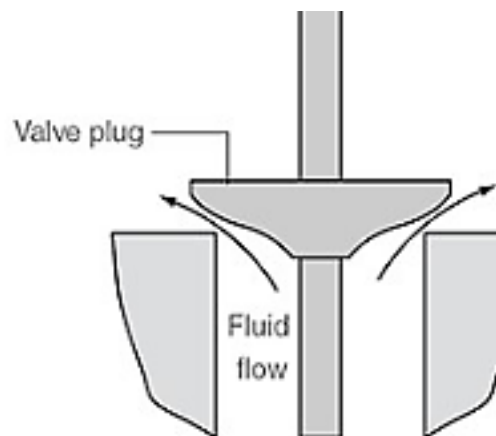


Figure 1-4: Fast Opening Characteristic Plug Configuration (Sivaranjith, Automation Forum.Co, 2020) [101]

➤ **Linear Characteristic:**

The linear flow regulating characteristic is where at a constant differential pressure there is direct proportionality between the flow rate and the valve lift, such that for example, a 40% valve lift, allows 40% of the full flow to pass through the valve plug. The relationship between the valve lift position and volumetric flow rate is linear. Figure 1-5 shows the linear relationship of the volumetric flow rate and valve lift for the linear flow regulation flow characteristic, and the plug shape for which this type of relationship is realized.

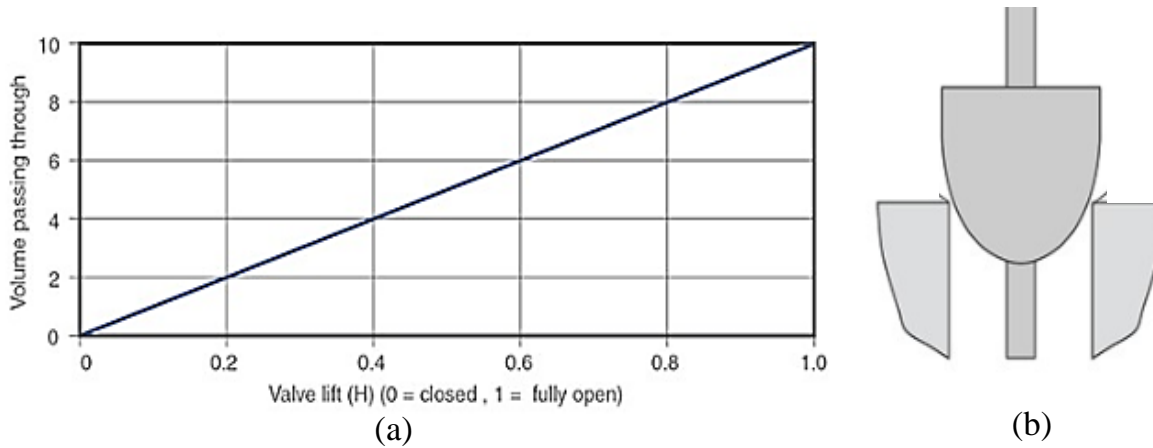


Figure 1-5: (a) linear flow regulation characteristic relationship of flow rate and valve lift and (b) Plug shape for linear flow regulation characteristic. (Sivaraniith, Automation Forum.Co, 2020) [101]

➤ Equal Percentage:

The equal percentage characteristic also termed as the logarithmic characteristic, is where the flow rate increases by a percentage of the prior flow rate for a given increment in the valve travel. For example, the flow rate can increase by 50% for every 10% increase of the valve travel, such that, given the flow rate is $100 \text{ m}^3/\text{min}$ at 20% valve travel, then at 30% valve travel the flow rate is $150 \text{ m}^3/\text{min}$, and at 40% travel it would be $225 \text{ m}^3/\text{min}$ and continues as such. Hence, this means that the flow rate increases by 50% for every 10% incremental increase in the valve travel. The equal percentage flow regulation characteristic relationship of the flow rate and valve lift is logarithmic and not linear. Figure 1-6 shows the equal percentage characteristic logarithmic relationship of the flow rate and valve lift.

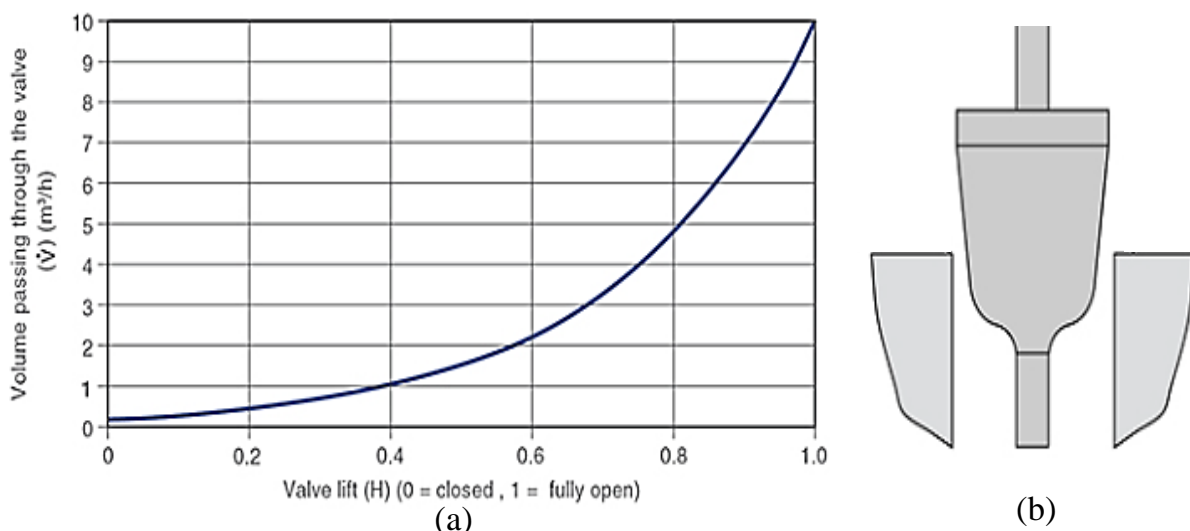


Figure 1-6: (a) equal percentage flow regulating characteristic relationship of flow rate and valve lift, and (b) plug shape for equal percentage flow regulation characteristic. (Sivaranjith, Automation Forum.Co, 04/03/2020) [101]

➤ Cavitation:

Cavitation flow condition is one major factor that can be accounted to have a significant contribution amongst other factors in control valves failure through erosion damage. The cavitation phenomenon is a frequent occurrence in pressure and flow regulating devices where tortuous flow paths are a standard design feature. Cavitation occurs in liquids when the pressure within a given region in the liquid falls below the vapour pressure of the liquid at the operating temperature. Cavitation generally follows a 3 step process for liquids, where the pressure at a given region within the liquid drops below the liquid saturation pressure at the relative temperature causing vapour bubbles to form within that region, and as the pressure rises to above the liquid saturation pressure, the bubbles implode as they collapse.

The implosion of the bubbles result in the development of shock waves which eventually cause extensive erosion damage to the valve trim within the vicinity of implosion occurrence. Furthermore, cavitation also results in noise and vibrations. Cavitation is an undesirable phenomenon in control valve design and is a major hydrodynamic performance design consideration for control valves. Figure 1-7 shows the extent of cavitation damage within the vicinity of a valve plug, and it can be observed that the valve plug is severely damaged and thus rendering it ineffective in providing any form of seal or fluid regulation.



Figure 1-7: Extent of Cavitation Damage Within the Vicinity of a Valve Plug (Flotech, 904-358-1849, 2020) [103]

Cavitation Measurement:

➤ Vibrations:

The extent of vibrations emanating from the imploding bubbles can be used to measure the intensity of cavitation, however, this technique requires specialised set up and process isolation conditions which are practical in a laboratory set up.

➤ Cavitation index:

The cavitation index defined as Sigma (σ), quantifies the extent of cavitation occurring within control valves. The cavitation index is defined as the ratio of the upstream pressure of a flow restriction minus the fluid vapour pressure to the differential pressure between the upstream and downstream pressure of the flow restriction.

$$\sigma = \left(\frac{P_1 - P_V}{P_1 - P_2} \right) \quad (1.1)$$

Where P_1 is the upstream pressure in (psia), P_2 is the downstream pressure, and P_V is the fluid vapour pressure at the given operating temperature.

The cavitation index was developed and quantified through extensive laboratory and field tests and can predict the potential for the onset of cavitation and its extent with reasonable accuracy. Hence, the cavitation index defines the extent of cavitation through specific numbers which generally range from 0 to 10.

The potential for differential pressure cavitating conditions is defined by the cavitation index as follows

- $\sigma \geq 2.0$. Indicates that there is no potential for cavitation to occur.
- $1.7 < \sigma < 2.0$. Indicates that there is no requirement for cavitation control.
- $1.5 < \sigma < 1.7$. Indicates that there is potential for some cavitation to occur.
- $1.0 < \sigma < 1.5$. Indicates that there is a potential for sever cavitation.
- $\sigma \leq 1.0$. indicates that flashing is occurring.

Flashing:

Flashing occurs when the local pressure within the vicinity of a restricted flow area falls below the vapour pressure of the fluid, and vapour bubbles form in the affected region, and here the pressure remains below the vapour pressure. Hence, in this case the vapour bubbles formed do not collapse and implode, and this results in a predominantly two-phase flow. Flashing can cause erosive damage to components within the vicinity of which it is occurring. Figure 1-8 depicts the pressure profile of cavitation and flashing of flow through a restriction along the control valve flow path.

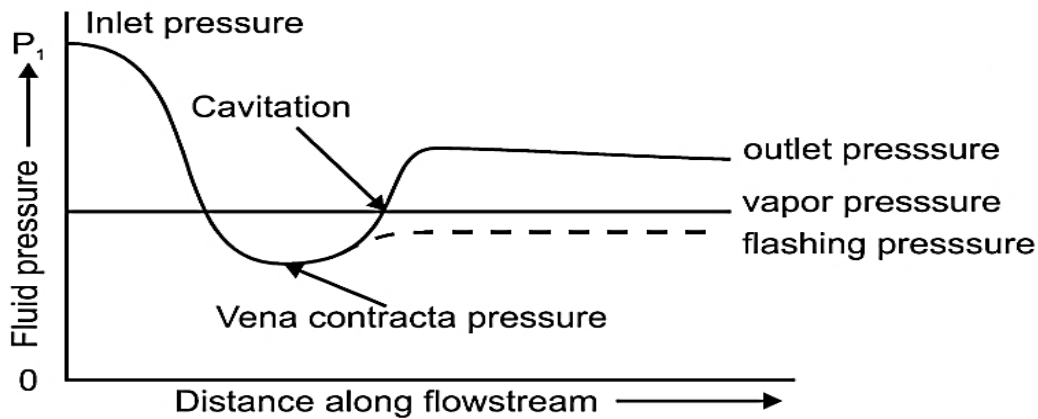


Figure 1-8: Cavitation and Flashing pressure profile within a control valve (Instrumentation Tools, 2020) [102])

1.5. Control Valve Hydrodynamic Performance Prediction Governing Principles

Fluid flow hydrodynamic flow and pressure characteristics calculations and predictions in control valves are governed by two main principles, and these governing principles have substantial bearing on the hydrodynamic characteristics design and process sizing considerations of control valves. The first category encompasses incompressible flow governed by standard hydrodynamic considerations and relevant equations for Newtonian incompressible flow fluids. And these specific equations are not applicable for non-Newtonian fluids and multiphase flows. Incompressibility of flow generally means that pressure effects on the fluid density are relatively small enough to be considered negligible such that there are no changes in the fluid density and specific volume of the flowing fluid. The second category encompasses compressible flow where compressibility effects in a fluid are of significance, such that the variations of pressure cause considerable change in the density and volume of the fluid. Hence this effect then requires that modifications be made to the standard Newtonian incompressible flow governing equations through relevant correction factors.

The compressible flow equations are only applicable for gas or vapour and are not applicable for heterogeneous multi-phase flows. The instrumentation Society of America (ISA) is the most widely referenced standard and has been over the past years for the sizing of control valves for process application specifically for valve capacity suitability for flow handling, and performance predictions with respect to maximum allowable flow rate, maximum global allowable differential pressure, and flow coefficient (CV).

The equations for incompressible and compressible Newtonian fluids control valve sizing have been populated in the standard ISA-75-01-01. The derivations and formulation of these equations is based on empirical data generated through exhaustive tests and measurements for standard specific general valve types and trim. From the context and scope through which the ISA standard sizing equations have been derived, the control valve performance is further categorised into two conditions of flow, and which are choked and non-choked turbulent flow. The Choked flow condition is considered as a control valve global and flow rate and pressure drop design and sizing limiting criteria at which full cavitation of an incompressible fluid that is a liquid is in effect. Choked flow in incompressible liquids is a phenomenon that occurs when the venturi effect on the liquid flowing through a restriction causes a reduction in the liquid pressure below the liquid vapour pressure at the operating temperature, and hence, at which bubbles form in the liquid and subsequently collapse causing cavitation. The extent of the bubble formation in the liquid at the flow restriction limits further increase in the flow with further increase in the differential pressure across the valve.

This phenomenon is governed by the mass continuity principle of fluid dynamics where the velocity of an incompressible fluid will increase as it flows through a constriction and its pressure will decrease to satisfy mass conservation of mechanical energy where an increase in the kinetic energy of the fluid resulting from a velocity increase as it flows through a restriction is compensated by a reduction in pressure. The general hypothesis of conservation of energy of an isolated system was introduced by a physicist called Daniel Bernoulli (1700 -1782 AD) which states that for steady, incompressible inviscid flows, an increase in the fluid velocity implies an increase in its kinetic energy with a simultaneous reduction in the sum of its potential energy inclusive of the static pressure and internal energy. And the Bernoulli principle is represented by the following expression:

$$P_1 - P_2 = \frac{\rho}{2} (v_2^2 - v_1^2) \quad (1.1)$$

where P_1 and P_2 is the upstream and downstream static pressure respectively, ρ is the density of the fluid, and v_1 and v_2 is the velocity at point of flow entrance and outlet, respectively.

1.6. ISA-75.01.01 Standard's Hydrodynamic Performance Predictions of a Control Valve:

This section presents detailed information on the published data on the considerations and methodology used in the prediction of the hydrodynamic performance of a control valve. The equations used to predict the hydrodynamic performance of a control valve for incompressible flow are governed by standard hydrodynamic equations for Newtonian fluids. Compressibility effects are accounted for with modifications to basic equations through introduction of correction factors, and these equations are explicitly for use with gas or vapour and are inapplicable with multiphase flow regimes. The standard scope confirms that, reasonable accuracy of the published equations can only be maintained for control valves if

$$\frac{C_V}{D^2} < 0.047 N_{18}, \quad (1.2)$$

where N_{18} is a numerical constant, and for (mm) units it is 1, and D is the diameter through which the fluid is flowing.

1.6.1. Piping Geometry Factor

The piping geometry factor F_p is used to account for the geometry associated with fittings attached upstream or downstream of a control valve. The piping geometry factor is described as the ratio of the global flow rate through a valve with attached fittings to the flow rate through a valve without attached fittings and determined through tests under identical conditions at which choked flow conditions will not occur. To satisfy a $\pm 5\%$ of the piping geometry factor, the F_p factor shall be determined through the test procedures as specified in the ANSI/ISA-75.0101 standard.

If the estimated values are satisfactory within the specified accuracy band the following expression shall be used to calculate the piping geometry factor.

$$F_p = \frac{1}{\sqrt{1 + \frac{\sum \zeta}{N_2} \left(\frac{C_i}{d^2} \right)^2}} \quad (1.3)$$

Where ζ is the effective velocity head loss coefficient of all fittings attached to the control valve. The velocity head loss of the valve and trim are not considered and accounted for. The sum of the head loss coefficients of all the fittings attached to a control valve are expressed as follows

$$\Sigma\zeta = \zeta_1 + \zeta_2 + \zeta_{B1} - \zeta_{B2} \quad (1.4)$$

For different inlet and outlet pipes connected to the control valve, the ζ_B coefficients are expressed as

$$\zeta_B = 1 - \left(\frac{d}{D}\right)^4 \quad (1.5)$$

For short length concentric reducers, ζ_1 and ζ_2 are approximated from the following expressions

➤ Inlet reducer:
$$\zeta_1 = 0.5 \left[1 - \left(\frac{d}{D_1}\right)^2 \right]^2 \quad (1.6)$$

➤ Outlet reducer (expander)
$$\zeta_2 = 1.0 \left[1 - \left(\frac{d}{D_2}\right)^2 \right]^2 \quad (1.7)$$

➤ Equal inlet and outlet reducers
$$\zeta_1 + \zeta_2 = 1.5 \left[1 - \left(\frac{d}{D}\right)^2 \right]^2 \quad (1.8)$$

The standard stipulates that, the piping geometry factor calculated from the above equations result in the selection of valve flow capacities slightly larger than required. The above calculation requires iteration.

1.6.2. Valve Style Modifier

The valve style modifier is defined in the standard as the ratio of the hydraulic diameter of a single flow passage to the diameter of a circular orifice, for which the area is equivalent to the sum of areas of all identical flow passages at a given travel, and it should be stated by the manufacturer as a function of travel.

$$F_d = \frac{N_{26} \nu F_L^2 F_R^2 (C/d^2)^2 \sqrt{CF_L}}{Q \left(\frac{F_L^2 C^2}{N_2 D^4} + 1 \right)^{1/4}} \quad (1.9)$$

Where F_L is the fluid pressure recovery factor of a valve without attached fittings, and it is stated that it accounts for influence of the valve internal geometry on the valve capacity at choked flow conditions. It is defined as the ratio of the actual maximum flow rate under choked flow conditions to a theoretical, non-choked flow rate which would be calculated if the differential pressure used is that of the valve inlet pressure and the apparent vena contracta pressure at choked flow conditions.

The fluid pressure recovery factor is calculated from the following expression.

$$F_L = \frac{Q_{\max}}{N_1 C} \times \sqrt{\frac{\frac{\rho_1}{\rho_0}}{P_1 - F_F P_V}} \quad (1.10)$$

Where F_F is the liquid critical pressure ratio factor, which is defined as the ratio of the apparent vena contracta pressure at choked flow conditions to the vapour of the liquid at inlet temperature. At vapour pressure near zero, the critical pressure ratio factor is 0.96.

$$F_F = 0.96 - 0.28 \sqrt{\frac{P_V}{P_C}} \quad (1.11)$$

The fluid pressure recovery factor for valves with attached fittings F_{LP} , and to satisfy the accuracy acceptance deviation $\pm 5\%$, it shall be determined by testing. When the estimated values satisfy the accuracy criteria, the fluid pressure recovery factor is then calculated from the following expression.

$$F_{LP} = \frac{F_L}{\sqrt{1 + \frac{F_L^2}{N_2} (\sum \zeta_1) \left(\frac{C}{d^2}\right)^2}} \quad (1.12)$$

1.6.3. Reynolds Number Factor

For low differential pressures, high viscosity, and small flow coefficients, or combined, the Reynolds number factor denoted F_R is the ratio of the flow rate under non turbulent conditions to the flow rate under turbulent conditions. The Reynolds number factor is calculated iteratively, and from the following expression.

$$Re_v = \frac{N_4 F_D Q}{v \sqrt{C_I F_L}} \left[\frac{F_L^2 C_I^2}{N_2 D^4} + 1 \right]^{\frac{1}{4}} \quad (1.13)$$

Where C_I is the assumed flow coefficient for iterative purposes, D is the internal diameter of the piping ν is the kinematic viscosity, N_4 is a numerical constant for flow rate unit conversion. N_2 is a numerical constant for diameter unit conversion, and F_D is the valve style modifier which can also be computed from the following expression

$$F_D = \frac{D_H}{d_o} \quad (1.14)$$

Where D_H , is the diameter of single flow passage and d_o , is the equivalent circular diameter of the total flow area, D_H is expressed as follows.

$$D_H = \frac{4 A_O}{I_W} \quad (1.15)$$

Where A_O is the area of the vena contracta of a single flow passage, and I_W , is the wetted perimeter of a single flow passage.

1.6.4. Non-Choked Turbulent Flow:

The flow coefficient for turbulent non-choked flow conditions for a control valve without attached fittings is calculated from the following expression.

$$C = \frac{Q}{N_1} \sqrt{\frac{\rho_1 / \rho_o}{\Delta P}} \quad (1.16)$$

The above expression is only applicable if the following expression is satisfied

$$\Delta P < F_L^2 (P_1 - F_F P_v) \quad (1.17)$$

The flow coefficient for turbulent non choked conditions for a control valve with attached fittings is calculated from the following expression

$$C = \frac{Q}{N_1 F_p} \sqrt{\frac{\rho_1 / \rho_o}{\Delta P}} \quad (1.18)$$

The above expression is only applicable if the following expression is satisfied

$$\Delta P < [(F_{LP} / F_p)^2 (P_1 - F_F P_v)] \quad (1.19)$$

1.6.5. Choked Turbulent Flow:

The flow coefficient for a control valve without attached fittings under turbulent choked flow conditions is calculated from the following expression

$$C = \frac{Q}{N_1 F_L} \sqrt{\frac{\rho_1 / \rho_o}{P_1 - F_F P_v}} \quad (1.20)$$

The above equation is applicable if the following expression is satisfied

$$\Delta P \geq (F_{LP} / F_p)^2 (P_1 - F_F P_v) \quad (1.21)$$

The flow coefficient for a control valve with attached fittings at choked flow conditions is calculated from the following expression

$$C = \frac{Q}{N_1 F_{LP}} \sqrt{\frac{\rho_1 / \rho_o}{P_1 - F_F P_v}} \quad (1.22)$$

The above expression is applicable if the following expression is satisfied

$$\Delta P \geq (F_{LP} / F_p)^2 (P_1 - F_F P_v) \quad (1.23)$$

The maximum allowable flow rate effective in producing choke flow conditions is calculated from the following expression

$$Q_{\max(L)} = N_1 F_L C \sqrt{\frac{P_1 - F_F P_v}{\frac{\rho}{\rho_o}}} \quad (1.24)$$

The maximum differential pressure that is effective in producing flow under choked flow condition is then calculated from the following expression

$$\Delta p_{\max(L)} = N_1 F_L^2 (P_1 - F_F P_v) \quad (1.25)$$

1.7. EN-60534-2-5 Standard's Hydrodynamic Performance Predictions for Fluid Flow Through Multistage Trim Control Valves with Interstage Recovery.

This section presents detailed information on the standards published data on the considerations and methodology used in the prediction of the hydrodynamic performance of multi passages or multistage control valves. The methodology and equations are only applicable for control valve designs of multistage multipath, and multistage single path trim configurations.

1.7.1. Multistage Multi-path Control Valves

As defined in the standard, a control valve with multiple flow paths and multiple flow passages with several stages separated by a gap, where the gap is the distance between adjacent stages, the gap should comply to the values calculated from the following expression with a tolerance of +15% -10%.

$$\text{Gap} = \text{total hole area of adjacent upstream stage at rated travel} \times \frac{1}{l} \times \frac{1,589}{\sqrt{D_s}} \quad (1.26)$$

Where area is in mm², l is the travel in mm, and D_s is the outside diameter of the adjacent upstream stage in mm. the gap limit is 4mm, and the maximum gap limit is 44mm. figure 1-9 shows an example of a multistage and multiple flow path control valve trim, and the configuration of the multistage gap specification where this standard is applicable.

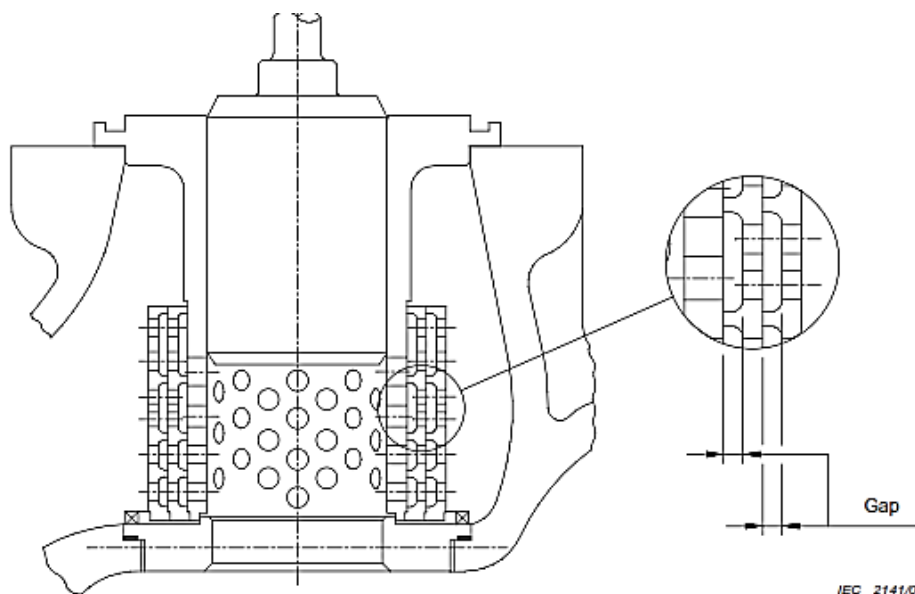


Figure 1-9: Example of a Multistage Multi Path Control Valve Trim (ISA 750101- EN 60534-2-5-2003-Page 6) [1].

1.7.2. Multistage Single-Path Control Valves

A control valve with a single flow path with several stages or flow passages that are separated by gap, where the minimum gap should be 0.6 times the seat diameter of the previous stage, and the maximum gap should be 1.10 times the seat diameter of the previous stage. Figure 1-10 shows the geometric configuration of a multistage single path control valve.

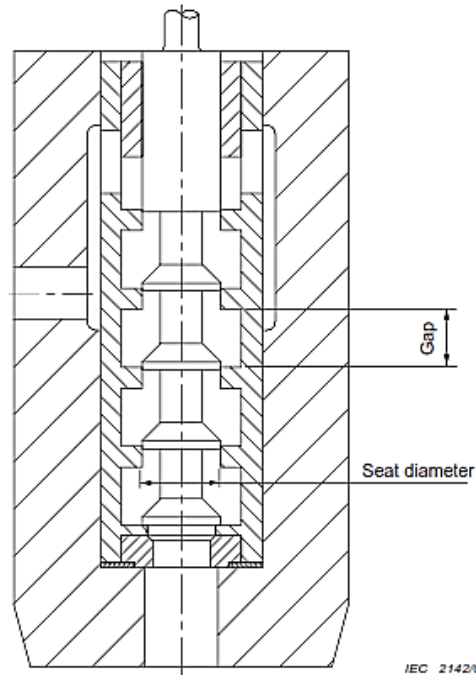


Figure 1-10: Example of a Multistage Single Path Control Valve (ISA 750101- EN 60534-2-5-2003Page 7) [1].

For a global control valve with a multistage trim with several stages separated by a gap, the applicability of the prescribed design or hydrodynamic performance predictions require that the apertures in all the stages or flow passages to be similar. The ratio of the second stage/flow passage flow coefficient (CV) to the first stage/ flow passage flow coefficient must not exceed 1.8. the ratio of the flow coefficient (CV) of the additional stages/flow passages to their upstream flow passages must not surpass 1.55 and must adhere to uniformity within a tolerance of $\pm 9\%$. Most significantly, the flow coefficients (CV) for incompressible flow are deemed to be approximately equal, and a slightly lower flow coefficient can be allocated to a particular stage/flow passage only if a higher-pressure drop is required at a particular stage/flow passage.

1.7.3. Empirical and Theoretical Considerations for Multistage Trims and Control Valves

➤ Incompressible Flow CV and Resistance Coefficient

In a control valve application terminology, the flow coefficient of an incompressible fluid flowing through a valve is described as the capacity of flow of water at 60 degrees Fahrenheit that can pass through a valve at 1 psi pressure drop. The ANSI/ISA 75.01.01 standard definition states the CV is the maximum flow rate in US gallons per minute that can flow through a valve at a pressure drop of 1 psi and is generally expressed as

$$CV = Q \sqrt{\frac{SG}{\Delta P}} \quad (1.27)$$

Where Q is the volumetric flow rate in US gallons per minute, ΔP is the pressure drop, and SG is the specific gravity of the fluid which is expressed as:

$$SG = \frac{\rho}{\rho_0} \quad (1.28)$$

Where ρ_0 is the reference density which is the density of water for liquids, and ρ is the density of the fluid flowing through the valve. The ISA standards utilize two sets of equations to calculate the flow coefficient which account for non-choked and choked flow condition. According to the standard ISA 75.01.01 non choked flow conditions are applicable if

$$\Delta P < F_L^2 (P_1 - F_F P_V) \quad (1.29)$$

Where P_1 is the inlet pressure, F_F is the fluid critical pressure ratio factor, P_V is the fluid vapour pressure, and F_L is the liquid pressure recovery factor. The liquid critical pressure ratio factor F_F is defined through the following expression:

$$F_F = 0.96 - 0.28 \sqrt{\frac{P_V}{P_C}} \quad (1.30)$$

Where P_V is the vapor pressure, and P_C is the fluid thermodynamic critical pressure. The fluid pressure recovery factor which is the ratio of the pressure drop across the control valve at choked flow conditions and the differential pressure between the inlet pressure and the fluid vapor pressure.

The fluid pressure recovery factor is determined experimentally and is specific for every valve type, and it can also be estimated from the following expression.

$$F_L = \sqrt{\frac{P_1 - P_2}{P_1 - P_{VC}}} \quad (1.31)$$

The flow coefficient (CV) for choked flow conditions is predicted from the following expression:

$$CV = \frac{Q}{N_1} \sqrt{\frac{SG}{F_L^2 (P_1 - F_F P_V)}} \quad (1.32)$$

The flow coefficient can be termed as an expression for the extent of flow resistance that is added to a pipeline. The empirical head loss coefficient is expressed as

$$H = K \frac{V^2}{2g} \quad (1.33)$$

And substituting the head loss for pressure drop the expression becomes:

$$\Delta P = K 0.5 \rho V^2 \quad (1.34)$$

Substitution into equation (1.16) and transposition yields the following Imperial relationship (established by crane)

$$CV = 29.9 \frac{d^2}{\sqrt{K}} \quad (1.35)$$

$$CV = \left(\frac{d}{4.654 \cdot K} \right)^2 \quad (1.36)$$

$$CV = 0.004634 \frac{d^2}{\sqrt{K}} \quad (1.37)$$

Further flow coefficient (CV) and resistance coefficient interrelation is expressed as:

$$K = 0.002148 \frac{d^4}{CV^2} \quad (1.38)$$

In the case of flow passages or stages in series, the total head loss coefficient is expressed as follows:

$$K_{TOTAL} = \sum_n^1 K_1 + K_2 + \dots \dots K_n \quad (1.39)$$

For multiple flow restrictions-passages in parallel the total head loss coefficient is expressed as follows

$$\frac{1}{K_{total}} = \sum_n^1 \frac{1}{K_n} = \frac{1}{K_1} + \frac{1}{K_2} + \dots \dots \frac{1}{K_n} \quad (1.40)$$

The total flow coefficient (CV) for flow restrictions-passages in series is expressed as:

$$\frac{1}{CV_{total}} = \sum_n^1 \frac{1}{CV_n} = \frac{1}{CV_1} + \frac{1}{CV_2} + \dots \dots \frac{1}{CV_n} \quad (1.41)$$

The total flow coefficient (CV) for flow restrictions-passages in parallel is expressed as:

$$CV_{total} = \sum_n^1 = CV_1 + CV_2 + \dots \dots CV_n \quad (1.42)$$

The control valve standard flow passages made up from the standard parts of the body, seat, cage, trim and plug can be considered individually with the overall flow coefficient being expressed as:

$$CV_{total} = \sum_n^1 = CV_{Body} + CV_{Cage} + CV_{Seat} + \dots \dots \quad (1.43)$$

➤ Derivations of Empirical Flow Equations

The Bernoulli's energy equation forms the benchmark from which most equations for incompressible and Newtonian flow are derived, and it is generally expressed as:

$$P_1 + \rho_1 \frac{1}{2} V^2 = P_2 + \rho_2 \frac{1}{2} V_2^2 \quad (1.44)$$

In terms of the differential pressure between two points along a streamline the expression becomes:

$$P_1 - P_2 = \rho_2 \frac{1}{2} V_2^2 - \rho_1 \frac{1}{2} V_1^2 \quad (1.45)$$

From mass conservation, the volumetric flow rate and effective flow area relations are derived as follows:

$$\begin{aligned}
Q &= A_1 V_1 = A_2 V_2 \\
V_1 &= \frac{Q}{A_1} \\
V_2 &= \frac{Q}{A_2} \\
P_1 - P_2 &= \frac{1}{2} \rho \left(\frac{Q}{A_2} \right)^2 - \frac{1}{2} \rho \left(\frac{Q}{A_1} \right)^2 \\
2(P_1 - P_2) \rho^{-1} &= \left[\left(\frac{Q}{A_2} \right)^2 - \left(\frac{Q}{A_1} \right)^2 \right] \\
2(P_1 - P_2) \rho^{-1} &= \left[\left(\frac{Q}{A_2} \right)^2 - \left(\frac{A_2}{A_1} \right) \left(\frac{Q}{A_1} \right)^2 \right] = \left(\frac{Q}{A_2} \right)^2 \left[1 - \left(\frac{A_2}{A_1} \right)^2 \right] \\
\left(\frac{Q}{A_2} \right)^2 &= \frac{2(P_1 - P_2) \rho^{-1}}{\left[1 - \left(\frac{A_2}{A_1} \right)^2 \right]} \\
Q &= A_2 \sqrt{\frac{2(P_1 - P_2) \rho^{-1}}{\left[1 - \left(\frac{A_2}{A_1} \right)^2 \right]}} \tag{1.47}
\end{aligned}$$

The effective flow area ratio can be re-written as:

$$\beta = \frac{A_2}{A_1} = \frac{0.25 \cdot \pi d_2^2}{0.25 \cdot \pi d_1^2} = \frac{d_2^2}{d_1^2} \tag{1.48}$$

The equation that finally characterizes the pressure, density, and volume flow of a fluid as a function of the effective flow area is expressed as follows:

$$Q = A_2 \frac{C_d}{\sqrt{1 - \beta^4}} \sqrt{\frac{2(P_1 - P_2)}{\rho}} \tag{1.49}$$

For compressible flow, the ANSI/ISA 75.01.01 [1] stipulates that choked flow conditions are in effect when the following conditions are satisfied

$$\frac{P_1 - P_2}{P_1} \geq F_{\gamma} X_t \tag{1.50}$$

The flow coefficient is expressed as

$$CV = \frac{\dot{m}}{N_6 0.677 \sqrt{F_\gamma x_t P_1 \rho_1}} \quad (1.51)$$

The flow through an effective flow diameter can be characterized with the discharge coefficient through the following expression:

$$C_d = \frac{\dot{m}}{Y N_6 \left(\frac{d}{4.654}\right)^2 \sqrt{F_\gamma x_t P_1 \rho_1}} \quad (1.52)$$

$$\dot{m} = C_d Y N_6 \left(\frac{d}{4.654}\right)^2 \sqrt{F_\gamma x_t P_1 \rho_1}$$

The control valve flow coefficient and the discharge coefficient relationship is thus expressed as:

$$CV Y N_6 \sqrt{F_\gamma x_t P_1 \rho_1} = C_d Y N_6 \left(\frac{d}{4.654}\right)^2 \sqrt{F_\gamma x_t P_1 \rho_1}$$

$$CV = C_d \left(\frac{d}{4.654}\right)^2 \quad (1.53)$$

$$Y = \left(1 - \left(\frac{P_1 - P_2}{P_1}\right) (3F_\gamma x_t)^{-1}\right) \quad (1.54)$$

Compressible non choked flow are considered when the following conditions are met

$$\frac{P_1 - P_2}{P_1} \leq F_\gamma x_t$$

$$CV = \frac{\dot{m}}{N_6 Y \sqrt{x P_1 \rho_1}}$$

$$C_d = \frac{\dot{m}}{Y N_6 \left(\frac{d}{4.654}\right)^2 \sqrt{(P_1 - P_2) \rho_1}}$$

$$\dot{m} = C_d Y N_6 \left(\frac{d}{4.654}\right)^2 \sqrt{(P_1 - P_2) \rho_1}$$

$$CV Y N_6 \sqrt{(P_1 - P_2) \rho_1} = C_d Y N_6 \left(\frac{d}{4.654}\right)^2 \sqrt{(P_1 - P_2) \rho_1}$$

$$CV = C_d \left(\frac{d}{4.654}\right)^2 \quad (1.55)$$

For incompressible choked flow effective flow diameter discharge coefficient and flow coefficient relations are derived as follows. For the ANSI/ISA 75.01.01.01 standard stipulation, choked flow parameters for calculating the CV are considered when the following conditions exist:

$$\Delta P \geq F_L^2 (P_1 - F_F P_V) \quad (1.56)$$

The corresponding CV under choked flow conditions is

$$CV = \frac{Q}{N_1} \sqrt{\frac{SG}{F_L^2 (P_1 - F_F P_V)}} \quad (1.57)$$

$$CV = \frac{Q}{N_1 F_L} \sqrt{\frac{SG}{(P_1 - F_F P_V)}}$$

$$Q = CV N_1 F_L \sqrt{\frac{P_1 - F_F P_V}{SG}} \quad (1.58)$$

Where N_1 is a unit conversion factor of 0.865, and SG is the specific gravity of the fluid.

The flow coefficient is then derived as a function of the effective flow diameter or flow restriction as follows.

$$C_d = \frac{Q}{Y N_1 \left(\frac{d}{4.654}\right)^2} \sqrt{\frac{SG}{(P_1 - F_F P_V)}}$$

$$Q = C_d Y N_1 \left(\frac{d}{4.654}\right)^2 \sqrt{\frac{P_1 - F_F P_V}{SG}}$$

$$CV N_1 F_L \sqrt{\frac{P_1 - F_F P_V}{SG}} = C_d Y N_1 \left(\frac{d}{4.654}\right)^2 \sqrt{\frac{P_1 - F_F P_V}{SG}}$$

$$CV = C_d \left(\frac{d}{4.654}\right)^2 \quad (1.59)$$

For non-choked incompressible flow, the CV and discharge coefficient relations are as derived for the following conditions:

$$\Delta P \leq F_L^2 (P_1 - F_F P_V)$$

$$CV = \frac{Q}{N_1} \sqrt{\frac{SG}{P_1 - P_2}}$$

$$Q = CV N_1 \sqrt{\frac{P_1 - P_2}{SG}}$$

$$C_d = \frac{Q}{N_1 \left(\frac{d}{4.654}\right)^2} \sqrt{\frac{P_1 - P_2}{SG}}$$

$$Q = C_d N_1 \left(\frac{d}{4.654}\right)^2 \sqrt{\frac{P_1 - P_2}{SG}}$$

$$CV N_1 \sqrt{\frac{P_1 - P_2}{SG}} = C_d N_1 \left(\frac{d}{4.654}\right)^2 \sqrt{\frac{P_1 - P_2}{SG}}$$

$$CV = C_d \left(\frac{d}{4.654}\right)^2 \quad (1.60)$$

From the relations revealed in the derivations, the flow coefficient is characteristic of the diameter and the discharge coefficient of the effective flow diameter, the flow coefficient is however a function of the fluid properties and rate of flow. With imperial units' considerations with conversion factors of 4.654 which converts the effective flow diameter from mm to inches, and 38 which converts imperial units of flow to metric, the following characteristics ensue:

$$\left(\frac{25.4}{4.654}\right)^2 \approx 29.8 \approx 38(0.25 \pi d^2) \approx 38 \frac{\pi d^2}{4} \quad (1.61)$$

Other derivations ensue from considerations of equations presented in the standards ISA 75.01.01 [1] and API 520 [4] which ensues in the following expression:

$$A = \frac{Q}{C_d} \sqrt{\frac{SG}{P_1 - P_2}} \quad (1.62)$$

Combination of equation (A-1.39) with the flow coefficient equation for non-choked flow yields the following expression for liquid flows:

$$38AC_d = CV = \frac{Q}{N} \sqrt{\frac{SG}{P_1 - P_2}} \quad (1.63)$$

For gaseous flows, the expression becomes:

$$CV = 27.66 A C_d \quad (1.64)$$

➤ Empirical Derivations of Multi-Stage-Flow Passages Flow and Pressure Characteristics as a Function of Effective Flow Diameter and Area.

For flow passages in series along a flow path, the relations, and interactions between the stages-flow passages w.r.t the effective flow areas is expressed as follows.

$$\left(\frac{1}{C_{deq}A_{eq}}\right)^2 = \left(\frac{1}{C_{dA_1}}\right)^2 + \left(\frac{1}{C_{dA_1}}\right)^2 + \dots \left(\frac{1}{C_{dn}A_n}\right)^2 \quad (1.65)$$

$$\left(\frac{1}{C_{deq}A_{eq}}\right)^2 = \sum_1^n \left(\frac{1}{C_{dn}A_n}\right)^2 \quad (1.66)$$

Then it is stipulated that the relationship between the effective flow areas is

$$A_2 = A_1\sqrt{s}$$

$$A_2 = A_1\sqrt{s}$$

$$A_n = A_{n-1}\sqrt{s} \quad (1.67)$$

Where s is the area ratio between the successive effective flow areas along a flow path in series.

This follows through that from the hypothesis, a reduction in the pressure drop across a stage-flow passage effective flow area by a factor of s , the effective flow area characteristic with the pressure drop should increase by a factor of the square root of s such that the conservation of mass is satisfied as follows:

$$Q_1 = A_1 \cdot C \sqrt{\frac{2\Delta P_1}{\rho}}$$

$$\begin{aligned}
Q_2 &= A_2 \cdot C \sqrt{\frac{2\Delta P_2}{\rho}} \\
A_2 &= A_1 \sqrt{s} \\
A_1 \cdot C \sqrt{\frac{2\Delta P_1}{\rho}} &= A_1 \cdot \sqrt{s} \cdot C \sqrt{\frac{2\Delta P_1 s^{-1}}{\rho}} \\
\left(\frac{1}{C_{deq} A_{eq}}\right)^2 &= \left(\frac{1}{C_d A_1}\right)^2 + \left(\frac{1}{C_d \sqrt{s} A_1}\right)^2 \\
&= \left[\frac{1}{C_d^2 A_1^2 s C_d^2 A_1^2}\right]^{0.5} \\
&= \left[\frac{C_d^2 A_1^2 + C_d^2 A_1^2}{C_d^4 A_1^4 s}\right]^{0.5} \\
C_d A_{eq} &= \left[\frac{1+s}{C_d^2 A_1^2 s}\right]^{-0.5} = C_d A_1 \sqrt{\frac{s}{s+1}} \tag{1.68}
\end{aligned}$$

A second successive stage in series along the flow path is expressed as follows.

$$\begin{aligned}
\left(\frac{1}{C_{deq} A_{eq}}\right)^2 &= \left(\frac{1}{C_d A_1 \sqrt{\frac{s^2}{s+1}}}\right)^2 + \left(\frac{1}{C_d A_1 s}\right)^2 \\
&= \left[\frac{C_d^2 A_1^2 \frac{s}{s+1} + C_d^2 A_1^2 s^2}{C_d^4 A_1^4 \frac{s^3}{s+1}}\right]^{-0.5} \\
&= \left[\frac{C_d^2 A_1^2 \left(\frac{s}{s+1} + s^2\right)}{C_d^4 A_1^4 \frac{s^3}{s+1}}\right]^{-0.5} \\
C_d A_1 &\sqrt{\frac{s^2}{s^2+s+1}} \tag{1.69}
\end{aligned}$$

For example, the equivalent area of a four stages-flow passages or particularly orifices in series can be derived as follows:

$$\left(\frac{1}{C_{deq}A_{eq}}\right)^2 = \left(\frac{1}{C_d A_1 \sqrt{\frac{s^2}{s^2+s+1}}}\right)^2 + \left(\frac{1}{C_d A_1 s^{1.5}}\right)^2$$

$$\left[\frac{C_d^2 A_1^2 \frac{s^2}{s^2+s+1} + C_d^2 A_1^2 s^3}{C_d^4 A_1^4 \frac{s^5}{s^2+s+1}} \right]^{-0.5}$$

$$C_d A_{eq} = C_d A_1 \sqrt{\frac{s^3}{(s^2+1)(s+1)}}$$

$$C_d A_{eq} = C_d A_1 \sqrt{\frac{s^3}{s^3+s^2+s+1}} \quad (1.70)$$

1.7. Motivation.

The hydrodynamic performance of a control valve is governed by infinite local and global geometric and flow parameter interdependence. Hence it is a futile effort to closely predict the hydrodynamic performance, and optimal design of a control valve without explicit and in-depth understanding of these parameters. Furthermore, the present existing state of the art assumes the local hydrodynamic behaviour within a valve through global parameters without explicit knowledge and accountability of the flow field's sensitivities on the local geometric profile along the flow path, and especially for valves with multiple flow passages along the flow path where the flow field is interdependent on the sequence of arrangement of the flow passages w.r.t the effective flow area sizes. These facts have motivated the author of the current research study to carry out a comprehensive research study on some critical features of the hydrodynamic characteristics of multistage trim control valves. Control valves are used in many critical applications where their ability to safely operate in severe services such as nuclear, medical, gas, oil, space travel, chemical processing, energy generation, and transportation, and where valve failure results in catastrophic consequences resulting in loss of life, irreversible environmental contamination and destruction, and financial loss.

Hence, it is essential to critically analyse the flow field hydrodynamic characteristics within a control valve. The hydrodynamic characteristics of the flow field mainly relates to the local pressure loss and recovery within a control valve due to geometric effects. The valve flow coefficient (CV) is a particularly important parameter that determines the suitability of a control valve to allow a given flow rate of a fluid through it without choking the flow and without excessive pumping power requirements which is the proportionality of the volumetric flow rate to the square root of the pressure drop. The valve flow coefficient is a dependent parameter of the geometry, flow rate and differential pressure, and hence in addition, the flow field analysis includes the contributions of these parameters on the hydrodynamic characteristics within a control valve. The unique and explicit combined contributions of multiple flow passages either in series or parallel sequence of arrangement along a flow path geometric and flow variable have facilitated the formulation and development of prediction models for allowable local and global differential pressure, allowable local and global flow rate, and rated flow coefficient (CV).

The optimal design of a control valve can thus be attained through the direct use of these prediction models. The sequence of arrangement of a control valve consisting of multiple local flow passages has significant effects on the flow field with regards to the flow passages effective flow area sizes pattern of arrangement in series along the flow path, and for which there exists unique interrelations between the local and global geometric parameters. The present published literature is limited in accounting for this phenomenon which is overly important in accurately predicting flow field behaviour within multiple flow passages or stages along a flow path. Hence, an in-depth understanding of the effects of multiple flow passages along a flow path within a control valve on the local flow and pressure structure is critical. Expressions need to be developed that characterise direct effective flow diameters or areas of flow passages with the flow and pressure structure, furthermore, there is need for these characterizations to be practical, easily interpretable, and scalable.

1.8. Research Aims.

Based on the motivation of this research study, the specific aims constructed for this study are as follows.

- 1 Empirically Based Valve Hydrodynamic Performance Diagnostics of a Control Valve
- 2 CFD based hydrodynamic performance diagnostics of a control valve
- 3 CFD based Parametric investigations

- 4 Development of an analytical tool for the optimum hydrodynamic performance design of multi-stage trim control valves.
- 5 Hydrodynamic Performance Optimization of a Multi-Stage Trim Control Valve

The aims of this research study encompass the pragmatic difficulties experienced at present in clearly and accurately determining critical hydrodynamic performance based on direct geometric reference for control valves with single or multiple flow passages or stages along the flow path. Hence, the specific aims are sufficient within the scope of this research study.

1.9. Thesis Structure:

From the information provided in the previous sections, the structure of work that has been carried out in thesis is as follows

Chapter 1: Presents a survey of the hydrodynamic characteristics of a control valve, the governing principles and parameter characterization are presented as applicable from current state of the art published literature. The motivation of undertaking this research work has culminated from this review and is described as such.

Chapter 2: Provides a comprehensive review of the extent and scope of work that has been undertaken on the hydrodynamic performance characteristics of control valves and multi-stage trim control valves. Published literature concerning the hydrodynamic characteristics of control valves and multi-stage trim control valves has been extensively reviewed. In addition, a review has been carried out on the available published literature regarding the optimization of control valves for hydrodynamic performance. The presented specific aims and objectives provide the detailed scope and extent of this research work.

Chapter 3: Presents the governing principles of the published literature and standards for the prediction of the hydrodynamic performance of a multi-stage trim control valve. The work carried out in this chapter includes the application of the published data to predict the allowable flow rate and allowable differential pressure drop, choked flow conditions and corresponding flow coefficient (CV) within a baseline control valve, here baseline refers to the original unaltered trim within the control valve under study. The predictions of the hydrodynamic performance of the baseline control valve with regards to the afore mentioned dependent parameters using the existing published data and current state of the art techniques is the highlight of this chapter. The information obtained in this chapter is especially important as it facilitated evaluations to be carried out in the next chapter through advanced computational fluid dynamics techniques for the evaluations of appropriateness of the published data in accurately predicting the hydrodynamic performance of a multi-stage trim control valve.

Chapter 4: Presents the governing principles of Computational Fluid Dynamics (CFD). This chapter presents CFD based modelling of single phase and multi-phase internal flow of fluid through a baseline control valve. Details of the solver settings and relevant boundary conditions have been presented. In addition, details of mesh that has been applied to the flow domain has been presented. In this chapter, simulations have been carried out to evaluate the appropriateness of the published data, where similar boundary conditions as those used through the published data hydrodynamic predictions have been used in the CFD based hydrodynamic prediction model in this chapter. Furthermore, this chapter includes qualitative and quantitative information on the local flow and pressure behaviour within the control valve. The qualitative information provided in this chapter provided visual observation of the local flow and pressure structure within the control valve, and together with the discrepancies between the published data CFD predictions of the maximum allowable flow rate, maximum allowable differential pressure and CV have been the highlight of this chapter. The local flow and pressure distribution observed in this study, and large discrepancies between the published data and CFD predictions have provided the impetus and justification to carry out parametric investigations to gain further insight into geometric and flow field correlations.

Chapter 5: elucidates the complex flow and pressure structure within a control valve, and the flow field's hydrodynamic characteristics sensitivities to the geometric and fluid interactions. A detailed and exhaustive parametric analysis has been carried out on the geometric pressure and flow field interrelations. The flow field characteristics have been analysed for various effective flow areas and sequence of arrangement along the flow path with regards to magnitude under various flow conditions. From the parametric studies carried out in this chapter, semi-empirical prediction models for local flow passage's pressure, global differential pressure, flow rate, potential for cavitation, pumping energy requirement, and local and global CV have been developed.

Chapter 6: Presents optimization models based on generalized reduced gradient non-linear method iterative based optimization . The optimization model is user friendly and consistent. The global and local differential pressure, flow rate, and CV form the input parameters for the optimization model, and the outputs of the optimization model are the optimal trim local flow passages effective flow area sizes and their sequence of arrangement as a function of magnitude along the entire flow path. The optimization model is unique in its capability in that it is scalable, it is simple to apply, and it can be implemented at industrial scale.

Chapter 7: Provides the conclusions of the investigations carried out in this study, the objectives and goals achieved in this study have been explicitly defined together with contributions to existing knowledge about the hydrodynamic design, flow and pressure mapping inside a control valve consisting of multiple flow passages along the entire flow path. In addition, recommendations for future studies have been detailed in this chapter

CHAPTER 2

LITERATURE REVIEW

From the detailed data gathered on the parameters influencing the design and performance characteristics of control valves and multi-stage trim control valves in the preceding chapter, a comprehensive literature review has been exhibited in this chapter that will highlight the gaps in the extant literature. It encompasses the published studies regarding control valves with multiple stages-flow passages along the control valve flow path, and includes literature on multi-stage trims such as anti-cavitation trims that are incorporated within a control valve flow path.

2.1. Control Valves, Multi-Stage/Flow Passage Trims and Singularities.

ISA-BS EN 605534-2-5 [1] This is a standard that is most referenced and used by many industrial institutions and companies. The standard provides the flow capacity-sizing equations for fluid flow through multistage control valves with interstage recovery. The standard's equations and methodology applicability is specified to be valid under the criterion where the multi-stages must be separated by a gap, the geometrical apertures in all stages must be similar, the ratio of the second stage flow coefficient C must not exceed 1.80, and the ratio of the flow coefficient C of the other stages to the previous stage must not exceed 1.55 and should be uniform within a tolerance of $\pm 9\%$. It is further stipulated by the standard that normally for incompressible fluids, the flow coefficients of the stages are approximately equal with a slightly smaller flow coefficient being allocated to a particular stage only if required to take a higher pressure drop.

For compressible flows, the stage interaction factor k is presented which is required to convert the valve pressure drop ratio x into the vena contracta pressure drop ratio and includes a correction factor for the difference between the pressure recovery between stages and at the exit of the final stage. A reheat factor r is also introduced which is a function of the expansion factor Y where the expansion factor accounts for the change in density as the fluid passes from the valve inlet to the vena contracta. This relationship is expressed as:

$$Y = \left[\frac{1 - \left(1 - k \frac{x}{x_T}\right)^{\frac{1}{n}}}{1.212 F_y} \right] \left(1 + r \frac{x^{\sqrt{n-1}}}{F_y} \right) \quad (2.1)$$

Table 2-1 shows the values of the stage interaction factor k and reheat factor r as applicable to a multi-stage trim.

Table 2-1: Values of the Stage Interaction Factor k and Reheat Factor r

Number of Stages	k	r
1	0,404	0
2	0,673	0,215
3	0,825	0,316
4	0,885	0,335
5	0,915	0,310

From the criteria stipulated for applicability of the methodology and equations for incompressible flows in multistage control valves, the methodology does not account for varying flow passage effective flow diameters and hence are severely limited in predicting the flow and pressure structure in varying trim geometric configurations. Furthermore, in the case of compressible flow considerations in multi-stage trim control valves there are no details presented on the derivations or methods through which the values presented in table 2-1 of the stage interaction factor k , and the reheat factors been have characterized with the geometry or how they have been established or computed.

Taimoor Asim, Rakesh Mishra et al. [2] carried out numerical studies of single-phase flow for an improved design of a multi-stage continuous resistance trim for minimum energy loss in control valves. The study focused on quantifying the effects of variations of the flow passages effective flow areas along the trim entire flow path on the hydrodynamic characteristics of the trim. It was found that significant non-uniformities in the local velocity and pressure structure are a result of the local geometric/design features, and in addition, it was observed that the position and size of the flow passage affects the local flow field. The local pressure losses along a multistage flow path were quantified as a function of a length scale reference in the form of radial distance unique only to the geometric feature of the specific type of trim. The parameter developed to quantify the pressure drop within the trim has been defined as:

$$D_{pr} = \frac{p_I - P_{I+1}}{r_I - r_{i+1}} \quad (2.2)$$

Where p_I is the local average static pressure upstream of the i th flow passage, and where r_I is the radius (in m), from the centre of the trim, to the location where p_I is measured.

Figure 2.1 shows (a) the trim geometric parameter definitions, and (b) a plot of pressure loss variations across rows as a function of the row radius and outer radius of trim ratio. The hydrodynamic performance has not been explicitly expressed as a function of the actual effective flow area sizes but has been characterised with geometry through which the flow path is formed within, hence there is no direct relationship between the effective flow areas of the flow passages along the flow path to the local trim hydrodynamic performance of the trim and valve. Hence, the results obtained in this study are unique only to this type of trim geometric configuration and are non-scalable.

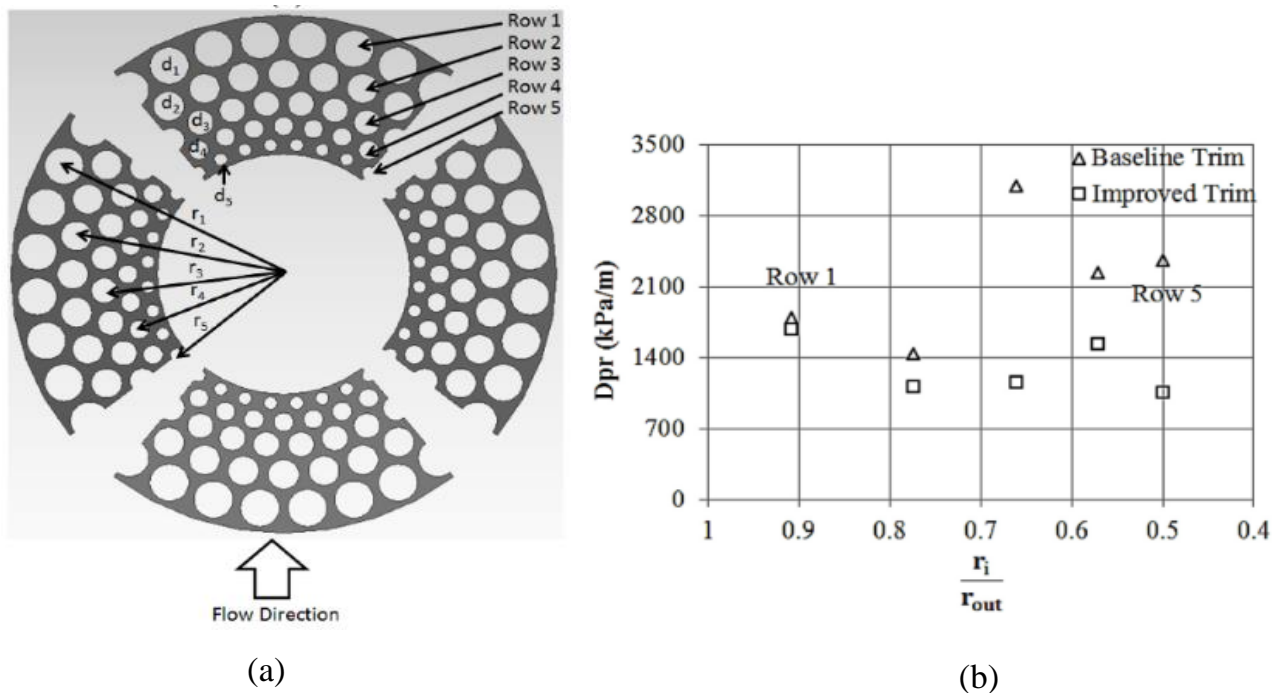


Figure 2-1 (a) Trim Geometry (b) Pressure Loss Variations Across Rows Across the Flow Path

Seungbin Ko [3] carried out numerical studies on the effects of design parameters on cavitation in a solenoid valve. It was found that severe cavitation occurred at the smallest gap between the seat and the ball seal, and they characterised the extent of cavitation as a function of vapour volume fraction with the ratio of the narrowest seat flow passage gap area to the inlet area. No analysis on the flow field w.r.t local and global velocity and pressure drop within the valve has been considered in the study. Furthermore, no expression for the prediction of the local and global flow rate and pressure drop as a function of geometry has been developed.

A.S Tabrizi [4] carried out experimental and numerical studies on the pressure loss across a ball valve flow passage under varying ball opening angles as a function of the cavitation index expressed as

$$C_{cs} = \frac{\Delta P}{P_{in} - P_v} \tag{2.2}$$

Figure 2-2 shows the plot of experimental and numerical cavitation index variations as a function of variations in the ball valve opening angles at different velocities. Furthermore, the ball valve opening angles were characterized with the pressure loss coefficient K expressed as

$$K = \frac{\Delta P}{0.5 \rho U_i^2} \tag{2.3}$$

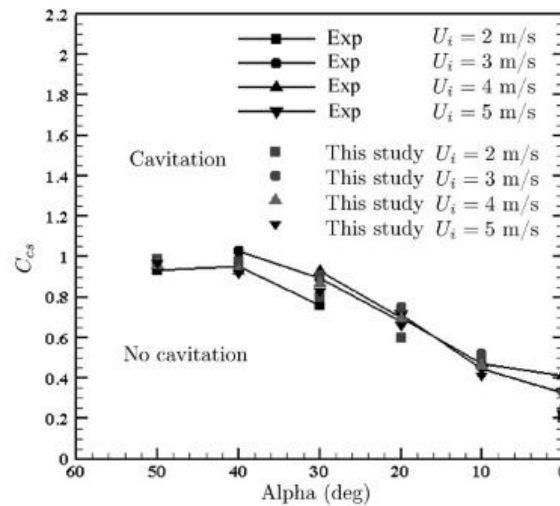


Figure 2-2: Experimental and numerical Variations of the cavitation index w.r.t variations of the ball valve opening angle.

Figure 2-3 shows the experimental and numerical variations of the head loss coefficient w.r.t the variations of ball valve opening angle.

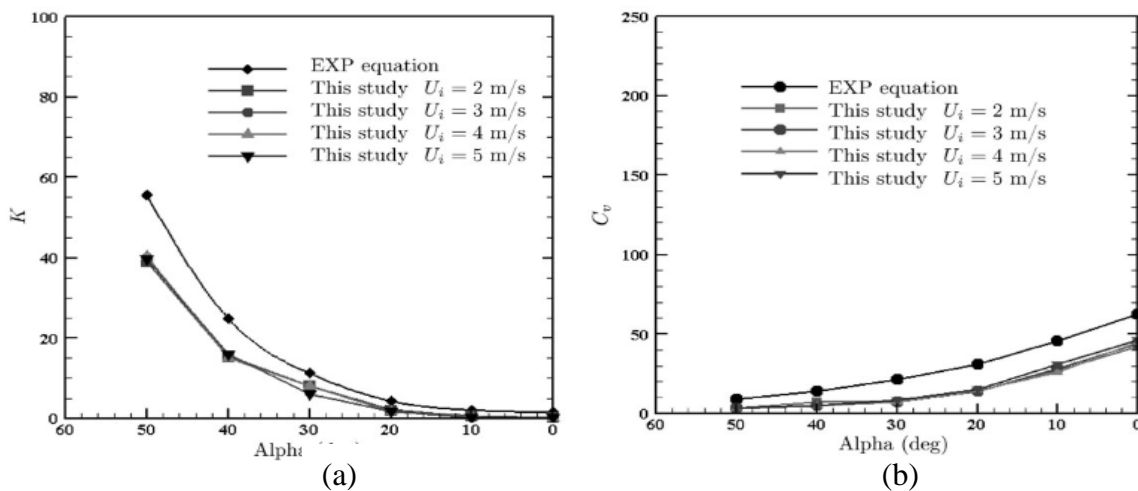


Figure 2-3: Experimental and Numerical Variations of (a), the Head Loss Coefficient, and (b), the flow coefficient (CV) w.r.t Variations of the Ball Valve Opening Angle.

It can be seen from figures 2-2 and 2-3 that the cavitation index, pressure loss coefficient, and flow coefficient (CV) have been independently characterised as a function of the ball valve opening angles. The study does not include the local flow and pressure structure within the valve. Furthermore, the effective flow areas of the valve opening angles have not been accounted for w.r.t their effects on the local and global flow and pressure structure, and hence the findings are only unique to the specific valve they studied.

LI BEIBEI et al. [5] carried out numerical studies for cavitation characteristics in a throttle valve consisting of 3 flow passages. They developed an expression derived from mass conservation and the energy, (equation (2.4, 2.5, 2.6)) to predict the downstream pressure at each of the flow passage along the flow path.

$$P_1 = P_0 + \frac{\rho Q^2}{2} \left(\frac{1}{A_0^2} - \frac{1}{A_1^2} \right) \quad (2.4)$$

$$P_2 = P_0 + \frac{\rho Q^2}{2} \left(\frac{1}{A_0^2} - \frac{1}{A_2^2} \right) \quad (2.5)$$

$$P_3 = P_0 + \frac{\rho Q^2}{2} \left(\frac{1}{A_0^2} - \frac{1}{A_3^2} \right) \quad (2.6)$$

Figure 2-4 shows the arrangement of the multiple flow passages within the throttle valve

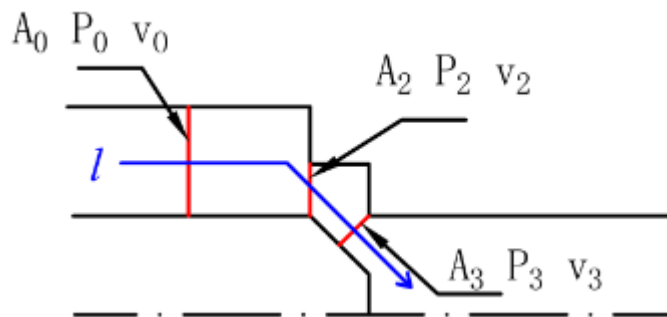


Figure 2-4: Throttle Valve Multi Flow Passages Arrangement

The developed expressions for predicting the downstream pressure at each flow passage are only valid for the first flow passage downstream of the inlet flow passage, such that the second flow passage pressure calculation does not account for the pressure and flow structure of the upstream flow passage. The pressure and flow structure for all the flow passages are calculated as a function of the inlet effective flow area where the effective area of intermediate flow passages has been ignored resulting in inconsistencies and large discrepancies between the predicted pressure and flow structure and actual verified and validated pressure and flow structure.

Hence, the developed expressions do not represent the actual and correct pressure and flow structure due to the neglect of the flow passages effective flow area's interactions and interdependence of the pressure and flow structure in between flow passages with the upstream and downstream flow passages effective flow areas.

Hojin Ha et al. [6] carried out numerical analysis and 4D flow magnetic resonance imaging (MRI) to investigate and estimate the irreversible pressure drop across a stenosis through characterisation and quantifying turbulent production of the flow. It was demonstrated that the pressure drop estimations based on the turbulent production robustly predicted the irreversible pressure drop, respective of stenosis severity. CFD with large eddy simulation turbulent model was used to obtain time averaged velocity fields, laminar viscous stresses, and Reynolds stresses. Qualitative comparison with 4D MRI showed good agreement with velocity and Reynolds stress tensor primary components. The investigations, quantification and characterization of the irreversible pressure drop with turbulent production was based on 14.6mm diameter pipe with a 75° area reduction stenosis. The proposed model does not require corrective terms, and geometric descriptions, and was reported to allow for robust irreversible pressure drop estimation even for complex geometry. Even though pressure recovery has been generally discussed in this work, it is limited to generalized characterization and single geometric flow path. There has been no detailed information reported by the Authors on the local pressure recovery dynamics and their interrelations with global parameters.

Claudio Alimonti et al. [7] carried out experimental investigations on the hydrodynamic characteristics of two- phase flow through a multiple orifice valve with considerations of frictional pressure drop and void fraction. Based on the hypothesis that in single phase flows the contraction causes a convergence of flow lines that accelerate the fluid with corresponding reduction in pressure and forming a vena contracta downstream of the contraction. When the length of the orifice is less than the expansion zone, the orifice is defined as thin, and if the expansion zone is shorter than the expansion zone, it is defined as thick. The reference for these characteristics is defined by the ration of the throat thickness and diameter S_t/d_t where a ratio above 0.5 defines a thick edged orifice. Figure 2-5 shows the flow profile across a thin and thick orifice.

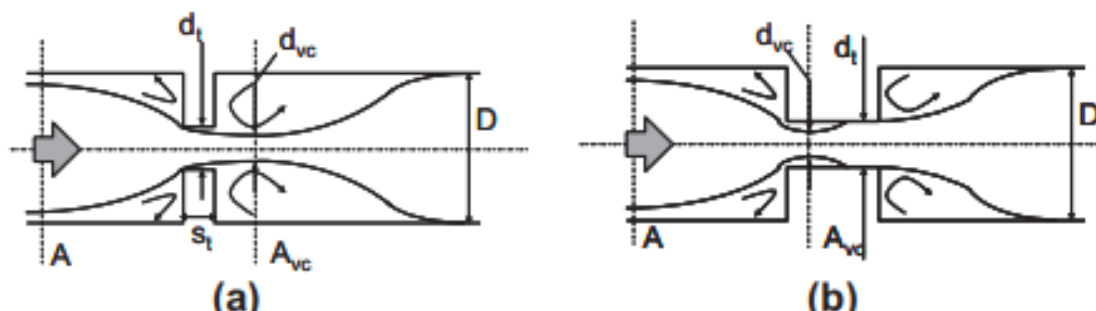


Figure 2-5: Depiction of Fluid Flow Across (a) Thin Orifice, and (b) Thick Orifice

With the assumption that the fluid expansion is irreversible, and the fluid is incompressible, the pressure drop for single phase flow is thus defined as

$$\Delta p_{sp} = \frac{\rho u^2}{2} \left(\left(\frac{1}{\sigma \sigma_c} - 1 \right) \right)^2 \quad (2.7)$$

Where $\sigma = \left(\frac{d_t}{D} \right)^2$, and σ_{vc} is the contraction coefficient $\left(\frac{d_{vc}}{D} \right)^2$

Following on that for thick orifices, the energy loss due to a double expansion is expressed as

$$\Delta P_{sp} = \frac{\rho_1 u_1^2}{2} \left[\left(\frac{1}{\sigma \sigma_{vc}} \right)^2 - 1 - \frac{2}{\sigma^2} \left(\frac{1}{\sigma_{vc}} - 1 \right) - 2 \left(\frac{1}{\sigma_{vc}} - 1 \right) \right] \quad (2.8)$$

From the results of this study there has been no discussions on the effects of the multiple orifices or flow passages effective flow diameter or area magnitudes and sequence of arrangement on the pressure structure within the valve.

Furthermore, no expressions have been developed to advance the energy loss equation (2.8) to integrate a direct geometric function that accounts for the combined effects of the multiple orifices or flow passages on the local and global flow and pressure structure.

Raul Sanchez et al. [8] carried out experimental investigations for cavitation effects in a sharp-edged orifice and reported theoretical scalability to valves and transitions through characterization of two non-dimensional coefficients of local head losses and minimum value of the cavitation number in order to verify the local effects under cavitation flow conditions. They quantified the influence of cavitation on head losses in singularities. They reported that the cavitation index can be used to determine the maximum flow for a known singularity head loss not affected by cavitation. The authors reported discrepancies in head losses between sharp edged orifices and a butterfly valve with a similar head loss coefficient, thus ruling out scalability as objectively proposed as basis of study. Furthermore, the work is limited to investigations of head losses within asymmetric singularities, and as subjectively within the scope of the study. No expressions for the geometric and flow field relations have been developed in this study.

H.R. Yaghoubi, et al. [9] carried out numerical analysis of cavitation phenomenon in a globe valve with different numbers of anti-cavitation trims. Their investigations were severely limited to only describing the flow and pressure structure sensitivities with respect to the characteristics of a valve with a trim or without a trim. From the results, no discussions were made on the geometric effects w.r.t the effective flow diameters and their sequence of arrangement along the flow path, and hence, no expressions for the flow and pressure structure characteristics as a function of the geometry have been developed in this study.

Behrouz Ebrahimi et al. [9] carried out theoretical, numerical, and experimental investigations of high-pressure cavitation flow through a thick orifice plates with sudden contraction and sudden expansion geometry in a constant cross section pipe. They characterised the energy loss between the upstream location of the orifice flow passage A_1 and the vena contracta A_{VC} through the following expression:

$$P_1 - P_{VC} = \frac{\rho_1 u_1^2}{2} \left[\left(\frac{1}{\sigma \sigma_c} \right)^2 - 1 \right] \quad (2.7)$$

Where P_{VC} is the vena contracta pressure, ρ_1 is the fluid density, u_1 is the area averaged flow velocity upstream of the orifice at A_1 , σ is the flow area ratio $\frac{A_O}{A_I} = \left(\frac{d_o}{d_i} \right)^2$ and σ_c is the contraction coefficient $\frac{A_{VC}}{A_O}$.

Advancing through with the contraction coefficient theory hypothesis, the contraction coefficient is a function of the flow area through the expression:

$$\sigma_c = \frac{1}{0.639 (1 - \sigma)^{0.5} + 1} \quad (2.8)$$

The expansion from the vena contracta A_{VC} to the downstream location A_2 is expressed through the momentum equation for a thick orifice as follows.

$$P_{VC} - P_2 = \frac{\rho_1 u_1^2}{2} \left[\frac{2}{\sigma^2} \left(\frac{1}{\sigma_c} - 1 \right)^2 - 2 \left(\frac{1}{\sigma} - 1 \right) \right] \quad (2.9)$$

the overall pressure drop across the pipe is expressed as

$$\Delta P = P_1 - P_2 = \frac{\rho_1 u_1^2}{2} \left[\left(\frac{1}{\sigma \sigma_c} \right)^2 - 1 - \frac{2}{\sigma^2} \left(\frac{1}{\sigma_c} - 1 \right) - 2 \left(\frac{1}{\sigma} - 1 \right) \right] \quad (2.10)$$

The volume flow rate is then defined through the following expression:

$$Q = \frac{C_d A_1}{\sqrt{\frac{1}{\sigma^2} - 1}} \sqrt{\frac{2\Delta P}{\rho_1}} \quad (2.11)$$

Where C_d is the discharge coefficient defined as:

$$C_d = \sqrt{\frac{(1 - \sigma^2)}{\left(\frac{1}{\sigma_c} - 1\right)^2 + (1 - \sigma)^2}} \quad (2.12)$$

The maximum flow rate is thus defined as

$$Q = \frac{C_d A_1}{\sqrt{\frac{1}{\sigma^2} - 1}} \sqrt{\frac{2\Delta P_{\max}}{\rho_1}} \quad (2.13)$$

Where ΔP_{\max} is the maximum allowable sizing pressure drop defined as

$$\Delta P_{\max} = F_L^2 (P_1 - F_F P_V)$$

Where F_L is the liquid pressure recovery factor, and F_F is the liquid critical pressure ratio factor, for both factors are expressed as:

$$F_L = \sqrt{\frac{P_1 - P_2}{P_1 - P_{VC}}} \quad (2.14)$$

$$F_F = \sqrt{\frac{P_1 - P_2}{P_1 - P_{VC}}} \quad (2.15)$$

The work carried out in this study has presented detailed flow and pressure characteristics as a function of the single orifice-flow passage geometric parameters in terms of the effective flow diameter, however, geometric considerations of the theoretical contraction coefficient has been integrated in the local flow and pressure structure characteristics. This presents substantial uncertainties in the true vena contracta area which is based on unquantified assumptions, and these assumptions progressively lead to ambiguity in the predictions of the local and global flow and pressure structure.

V.K. Singh et al. [10] carried out CFD based numerical investigations and experimental investigations of the flow and pressure characteristics for multi hole orifice flow meters for varying Reynolds number magnitudes. The multiple holes considered in this study were arranged on a single plate where they characterised the hydrodynamic performance of flow rate, pressure drop and pressure recovery to determine the discharge coefficient as a function of the multiple holes configurations on a single plate w.r.t their pitch circle diameter arrangements. No expressions for the effects of the equivalent multiple hole effective flow areas or diameters on the pressure drop, pressure recovery and discharge coefficient have been developed.

Ma Haoyuan et al. [11] carried out numerical and experimental studies of cavitation flow characteristics in diesel a fuel injector control valve. They characterised the extent of cavitation through the vapour volume fraction as a function of valve seat lift. The study carried out here is substantially limited in its geometric and cavitation extents characterization, for which expressions for the geometric effective or equivalent flow area on diameter and relations with the flow and pressure structure have not been developed.

Yang Ye et al. [12] carried out experimental and numerical investigations on the suppression of cavitation through introduction of multiple check valves within the flow path of a diaphragm pump. Figure 2-6 shows the working principles of their diaphragm pump on which the investigations were carried out.

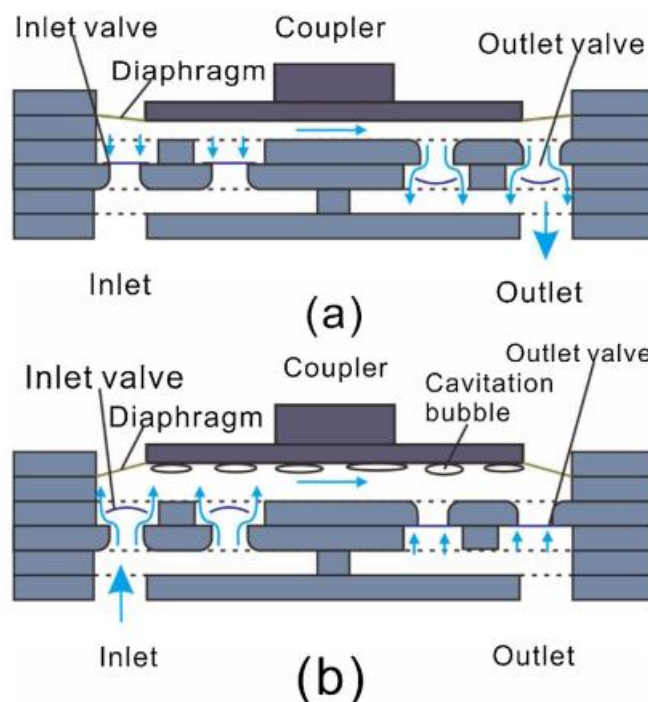


Figure 2-6: Working Principle of Diaphragm Pump With 3 Inlets and 4 Outlets

They characterized the pressure and flow structure within the diaphragm pump with the cavitation number expressed as

$$Ca = \frac{P - P_v}{0.5 \times \rho V^2} \quad (2.7)$$

The study does not present any insight into the geometric effects on the pressure and flow structure within the pump flow passages, and in addition, the investigation does not present any details on the combined effects of the multiple flow passages and their sequence of arrangement on the pressure and flow structure within the diaphragm pump.

Abdulrazaq A. Araoye et al. [13] carried out numerical studies of the flow and pressure characteristics through a serial arrangement of two similar bevel edged orifice plates fitted in a 25.4 mm horizontal pipe. They characterized the flow through a double orifice through w.r.t the pressure drop (Δp) as a function of density, viscosity, mean flow velocity, orifice diameter ratio, pipe diameter, surface roughness, axial distance and orifice spacing with the parameter characterization being expressed as follows:

$$\Delta p = f\left(\rho, \mu, U_{av}, D, D_r, \frac{k_s}{D}, \frac{x}{D}, \frac{S}{D}\right) \quad (2.8)$$

Where μ is the dynamic viscosity, f is the friction factor, Re is the Reynolds number, U_{av} is the average flow velocity, k_s is the surface roughness, x axial distance, and S is the spacing for the double arrangement orifices.

The expression was further expressed in the non-dimensional format through the Buckingham pi theorem as follows

$$\frac{\Delta p}{0.5 \times \rho V^2} = f\left(Re, D_r, \frac{k_s}{D}, \frac{x}{D}, \frac{S}{D}\right) \quad (2.9)$$

Comparisons of the pressure drop, and hydraulic losses where made between single and double orifice geometric arrangements in series within a pipe of similar internal diameter. they reported findings related to the spacing between two orifices arranged in series where they established that the orifices with 2D spacing resulted in a substantially higher total pressure drop than the orifices with a 1D spacing arrangement. In addition, they established that double orifices with 1D spacing resulted in the least pressure drop, while the double orifices with 2D spacing yielded the highest pressure drop.

They concluded that, the pressure distribution and characteristics attributed to the 1D spacing in the double orifice arrangement is that the spacing creates a shorter deceleration zone downstream of the second orifice causing a decrease in the resulting pressure drop. Their closing statement on this phenomenon were recommendations on the importance of further studies on establishing characteristic relations between the orifice spacing and total pressure drop. Figure 2-7 shows the variations of pressure drop for the double orifice arrangements of 1D spacing and 2D spacing w.r.t the normalised axial distance as a function of the ratio of the orifices effective flow diameters. The depiction of the pressure distribution in figure 2-7 (a) for the 1D spacing shows a high pressure recovery as compared to (b) 2D spacing between the orifices which shows a low pressure recovery. This substantiates their findings stated earlier on the effects of the spacing between the orifices-flow passages on the pressure distribution.

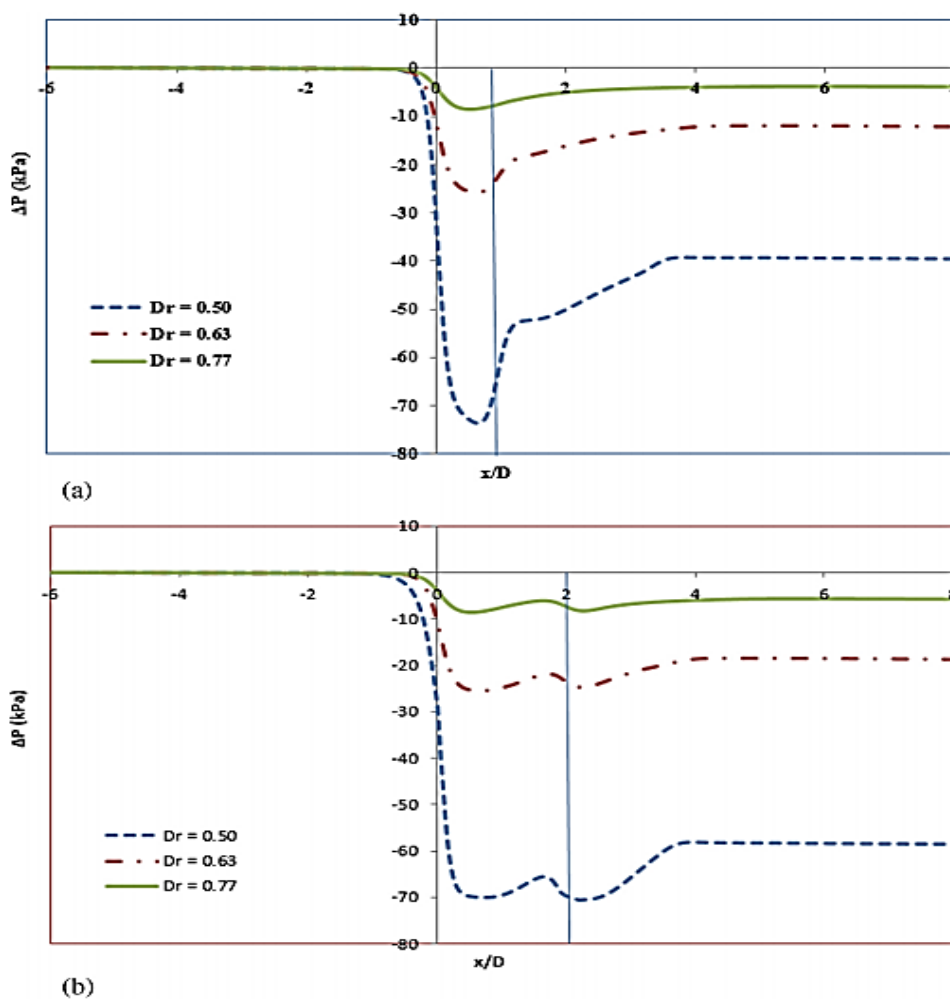


Figure 2-7: Variations of Pressure Drop for (a) Double Orifice- 1D Spacing and (b) Double Orifice 2D Spacing.

Regardless of some unique revelations of the effects of the spacing between flow passages-orifices along a flow path on the pressure structure distribution, no expressions have been developed to account for more than two flow passages-orifices along the flow path w.r.t pressure drop characteristics. Furthermore, the effects of the combined geometric configuration and interaction on the flow and pressure structure w.r.t the ratios of the effective flow diameters-areas is limited to two orifices- flow passages has not been reported. In addition, the effects of the local flow and pressure structure on the global parameters and vice-versa have not been reported. It can be stated that the limitations in the study they carried out are confined within the scope of their study, and the stated limitations in the investigations they carried out are characteristic of most of the published literature and is a major impetus for the work carried out in this Thesis.

Chaitanya R. Mali et al. [14] carried out CFD numerical investigations on the effects of various geometric parameters of honeycomb type orifices on the local hydrodynamic characteristics of pressure drop and cavitation. They investigated the geometric effects of honey combed shaped orifices w.r.t the effective flow area magnitudes, spacing between the stages-plates, number of plates-stages, and the orientation of the plates w.r.t inline or offset along the flow path. They noted the difficulty and challenging prospects faced by present technology of determining, predicting, and measuring the local hydrodynamic pressure and flow structure and cavitation performance. Within the scope of this study, the analysis has been limited to considerations of each of the stages within the multiple stages-flow passages having similar effective or equivalent flow areas along the trim flow path, where the extents of cavitation have been characterised as a function of varying number of stages for a given single flow area for all the stages. They characterised the flow behaviour and pressure losses within the orifice trim assembly through the discharge coefficient, for which it was defined as

$$C_D = \frac{u_o \sqrt{1-\beta^2}}{\sqrt{\frac{(P_1 - P_2)}{\rho_1}}} \quad (2.11)$$

Where u_o is the throat velocity (m/sec), P_1 and P_2 are the inlet and outlet pressure of the single or multi-stage trim assembly, β is the equivalent diameter ratio of the multi-stage total equivalent diameter to the main supply pipe flow diameter. Figure 2-8 shows the variations of the discharge coefficient as a function of the Reynolds number for the different geometric configurations

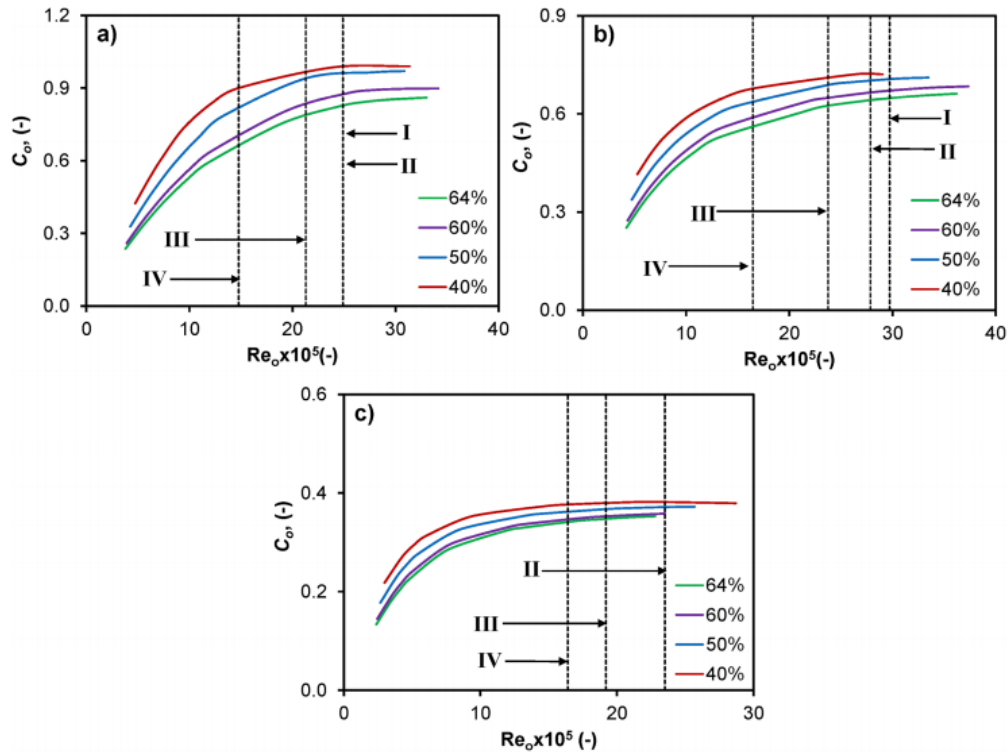


Figure 2-8: Variations of the Flow Passages Equivalent Discharge Coefficient as a function of the Reynolds Number for (a) Single Plate-Stage, (b) Six Plate-Stages Inline Conditions, (c) 14 Plate Offset Conditions at Various Flow Area Ratios.

Hence, from the results of this study, there have been no detailed discussions on the direct effects of the flow passages-stages effective flow areas or diameters on the local flow and pressure structure within the vicinity of the flow passages. Furthermore, expressions for the global and local flow and pressure structure relations with the trim geometric configuration in terms of effective flow areas of diameters or sequence of arrangement of the stages-flow passages have not been developed.

Testud et al. (2007) [15] carried out experimental investigations on cavitation characteristics in single and multiple hole orifices in series and parallel arrangements along the flow path, and their effects acoustic characteristics. They developed hydrodynamic models for global and local flow and pressure drop characteristics as a function of the orifice's geometric configurations along the flow path. They characterized the extents of cavitation through the cavitation number expressed as:

$$\Sigma = \frac{P_2 - P_v}{\Delta P} \quad (2.10)$$

Where $\Delta P = P_1 - P_2$ which is the pressure drop across the orifice with P_1 being the static pressure upstream of the orifice, and P_2 which is the orifice downstream pressure, and P_v is the fluid vapour pressure.

Through their experiments, they established the cavitation regime's benchmark's where in good agreement with Tullis' formulars, where for a single hole orifice, incipient cavitation was characterized by the criteria $\sigma_i \geq 0.93$, and cavitation extent to induce choked flow was characterized by the criteria $\sigma_i \leq 0.74$. With focus on the hydrodynamic performance aspect and scope of the work they carried out, the hydrodynamic performance characteristics for pressure drop across a single hole orifice was developed as follows, where the ratio between the free jet cross section S_j and the pipe cross section S was considered as fixed.

Hence, mass conservation is satisfied through the expression

$$S_j U_j = S U \quad (2.11)$$

The upstream jet flow assumed inviscid steady potential flow and expressed as

$$P_1 + 0.5 \rho_w U^2 = P_j + 0.5 \rho_w U_j^2 \quad (2.12)$$

Where P_j and S_j are the jet pressure and velocity respectively, the cavitation model developed as a function of pressure drop across the orifice was expressed as follows:

$$\frac{\Delta P_{measured}}{0.5 \rho_w U^2} = \left[\left(\frac{S}{S_j} \right)^2 - 1 \right] + \left[2 - 2 \frac{S}{S_j} \right] \quad (2.13)$$

The hydrodynamic model for pressure drop across multi-hole orifice was specified as follows:

$$\frac{\Delta P_{measured}}{0.5 \rho_w U^2} = \left[\left(\frac{S}{S_j} \right)^2 - 1 \right] + \left[2 \left(1 - \frac{S}{S_d} \right) + 2 \left(\frac{S}{S_d} \right)^2 \left(1 - \frac{S_d}{S_j} \right) \right] \quad (2.14)$$

$$\frac{\Delta P_{measured}}{0.5 \rho_w U^2} = 1 - 2 \left(\frac{D}{d} \right)^2 + 2 \left(\frac{D}{d} \right)^4 \left(\frac{1}{\alpha} + \frac{1}{2 \alpha^2} \right) \quad (2.15)$$

Where α is the contraction coefficient which is $\frac{S_j}{S_d}$

Haimin et al. (2013) [16] carried out experimental investigations to determine the pressure drop characteristics of a 6 stage-flow passages let down orifice tube containing 6 orifices in series. The geometric effects on the pressure drop was characterised with the cavitation index as a design criterion to establish the extent of cavitation in the varying geometry under study. There have been no specific detailed discussions on the combined effects of the flow passages-orifices on the local pressure and flow structure within the vicinity of the orifices, and the effects on the global parameters w.r.t to their effective flow area magnitudes and sequence of arrangement along the flow path.

(Rani et al., [17] Carried out numerical investigations of energy and Reynolds stress distribution of turbulent flow in an orifice. They reported that flow through an orifice is characterized by complex flows, and where the nature of the complex nature of the flow through an orifice is further aggravated when passing through multiple orifices located close to each other. They reported that the aggressive nature of the flow through multiple combinations of flow passages resulted in failures in many energy and oil & gas transportation systems due to variety of degradation mechanisms such as cavitation erosion. The discussions on the results obtained for the pressure and flow characteristics have been limited to the development of the turbulent kinetic energy TKE, shear and normal stresses within the vicinity of the orifice flow passage for which was characterised with the extent of flow accelerated corrosion (FAC) with as a function of the Reynolds number. No discussions on the actual effects of the geometry in terms of effective flow area magnitude and sequence of arrangement of the flow passages- orifices have been presented.

Sanchez et al. [18] carried out experimental investigations with the objective of estimating the extent of cavitation from the head loss coefficient. They developed expressions to determine the cavitation limit for choked flow from local head loss coefficients for sharp edge orifice plate and valves where geometrical transitions are more complex. In addition, they developed the relationship between choking cavitation limit and head loss coefficient based on the amplitude of pressure fluctuations as a function of velocity head in the vena contracta section in order to characterise the local effects under cavitating flow conditions.

They characterized the head loss coefficient with the cavitation index through the following expressions:

$$K \begin{cases} 0 \leq \sigma_2 \leq \sigma_{2v} \rightarrow K = \frac{P_1 - P_2}{\rho \frac{U^2}{2}} = \frac{P_1 - P_v - (P_2 - P_v)}{\rho \frac{U^2}{2}} = \sigma_{1m} - \sigma_2 \geq K_m \\ \sigma_2 > \sigma_{2v} \rightarrow K = K_m \end{cases} \quad (2.16)$$

$$K \begin{cases} 0 \leq \sigma_{p2} \leq \sigma_{p2v} \rightarrow K = \frac{P_1 - P_2}{\rho \frac{U^2}{2}} = \frac{P_1 - P_v - (P_2 - P_v)}{P_1 - P_2} = \sigma_{1m} = \frac{\sigma_{1m}}{1 + \sigma_{p2}} \geq K_m \\ \sigma_{p2} > \sigma_{p2v} \rightarrow K = K_m \end{cases} \quad (2.17)$$

The work they carried out was detailed and it revealed useful information with regards to the relations between the head loss coefficient with the cavitation index, however no expressions have been developed that characterise the orifice effective flow diameter directly with the flow and pressure structure within the local vicinity of the orifice flow passage. Furthermore, the developed parameters that characterise the head loss under cavitating flow conditions in sudden transitions such as valves are severely limited in that they must be determined experimentally. Hence the developed methodology in this study is not scalable and applicable without information obtained by carrying out initial experiments for specific valve trim geometric configurations.

Pandey et al. (2013) [19] carried out experimental investigations for multi-stage honey-comb orifices arranged in series in a prototype fast breeder reactor (PFBR) operating as permanent pressure drop devices in the foot of the (PFBR) subassembly. The performance of these staged honey-comb orifices is critical in achieving the required pressure drop without cavitating, where the pressure drop across the multi-stage honey-comb flow passages is dependent on the geometrical factors and Reynolds number. (Re). Hence, experimental tests were carried out to determine the incipient cavitation index and compare it with the operating cavitation index to determine the extent of cavitation. They characterised the pressure drop across the multi-stage assembly with the flow rate, and head loss coefficient with the Reynolds number and the cavitation index as calculated at nominal flow condition. From the extensive investigations within the scope of their work, there have been no discussions with regards to the actual geometric effects on the flow and pressure structure w.r.t the effective flow areas or diameters of the flow passages. In addition, no expressions have been developed for the effects of the effective and equivalent flow areas of stages on the local flow and pressure drop within the multi-stage assembly, and the overall pressure drop across the multi-stage flow passage assembly. Furthermore, no expressions have been developed for the effects of the combined interactions of the multi-stage flow passage assemblies assembled in series with respect to their

sequence of arrangement as a function of their effective-equivalent flow area or diameter magnitudes.

AI Wan-Zheng et al. (2014) [20] carried out numerical investigations with theoretical and experimental verification and validation on the cavitation characteristics in a multi-stage orifice plate as a function of orifice plate spacing and arrangement of the flow passages w.r.t the effective flow diameters. their theoretical considerations were based on their stated principle of equal cavitation characteristics for which their principle defined that if cavitation should occur in one orifice in a multistage orifice arrangement, then cavitation if occurring in other flow passages-orifice plates should occur at the same time. They presented an expression to meet this criterion as

$$\sigma_j - \sigma_j^c = \sigma_{j+1} - \sigma_{j+1}^c \quad (2.18)$$

Where σ_j is the cavitation number of the j th orifice plate or flow passage, and σ^c is the critical cavitation number, and from the above characterization the cavitation number σ_j and critical cavitation number was expressed as follows:

$$\sigma_j = \frac{P_j - P_v}{0.5\rho u^2} \quad (2.19)$$

$$\sigma_j^c = \frac{P_j - P_j^{min}}{0.5\rho u^2} \quad (2.20)$$

Where P_j is the average pressure taken at position $0.5D$ upstream of the j th orifice plate, and P_j^{min} is the lowest pressure of the j th orifice plate. The governing principle of equal cavitation characteristics that they defined presents significant limitations and validity in the applicability of the principle with regards to the objective. From the results obtained from the investigations, there has been no detailed discussions on the effects of the orifice's-flow passages effective flow diameters on the local flow and pressure structure within the vicinity of the orifice plates. No expressions for pressure drop, flow rate, energy loss coefficient and cavitation number as a function of the orifice-flow passage effective flow diameters, spacing, and their sequence of arrangement along the flow path have been developed.

2.2. Summary of Literature Regarding Multi-Flow Passages and Singularities Within Flow Control Valves.

The methodologies presented in the literature review on the local hydrodynamic flow and pressure characteristics of multi-flow passage trims or geometric singularities within control valves are based on approximations of the local flow field from coefficients and calculations derived from empirical global parameter considerations. The current available standard's for the hydrodynamic prediction of multi-stage trims stipulate that the methodology is only valid for similar apertures and arrangement. There is comprehensive published literature on local flow and pressure structure within the vicinity of flow restrictions and singularities such as orifices, which are not geometrically universal, scalable and applicable outside the scope of their specific configurations and flow physics. There are severe limitations in local flow field experimental measurement capabilities, and in addition, the interaction and combined effects of local multiple flow passages or singularities within control valves on the local and global hydrodynamic characteristics is presently unknown and has not been reported. Based on the presented literature review, it can be concluded that there is currently no known local geometric, and hydrodynamic characterisation methodology that is geometrically universal, and that accounts for varying aperture configurations, and is accurately applicable in predicting the local multiple flow passages pressure drop, exit pressure, CV, velocity, cavitation potential, and pumping energy requirement, and as well as their interrelations with global parameters. Hence, an encompassing hydrodynamic characterisation methodology and relative parameter prediction models are necessary in order to accurately design and optimize multi-flow passage trims and singularities within control valves. .

2.3. Scope of Research.

The current knowledge on the complex local flow phenomenon within multi-stage or multi-flow passages and singularities is extremely limited. The main contributions that have facilitated the gap in the knowledge are as follows:

- Primarily most studies being conducted are based on global parameters from which empirical derivations are developed to roughly approximate the local flow and pressure characteristics.
- There is currently no reliable means to monitor and measure the local flow and pressure characteristics within the vicinity of flow singularities and trims, where probes will inadvertently interfere with the flow field sensitivities resulting in ambiguity in the flow field characteristics.

The advent of numerical computational tools that can analyse complex flows and physics, it is now possible to carry out diagnostics of complex local flow and pressure characteristics within control valves. From the published literature review, important areas presenting knowledge gaps have been established, and on that basis, the main key areas of this present study are as follows:

1. Application of existing designated standards methodologies, relevant empirical and theoretical equations to predict the hydrodynamic flow and pressure structure within a multi-flow passage trim control valve. To evaluate the appropriateness and applicability of the existing control valve hydrodynamic performance prediction tools, the hydrodynamic performance of the control valve needs to be predicted using the current methods.
2. This second key area of this study is the diagnostics and evaluation of the control valve hydrodynamic performance characteristic predictions of the standards and empirical methodologies using numerical CFD techniques and models. This area is focused on evaluations of the local flow and pressure structure and their relations to the critical global limiting flow rate and pressure drop as a function of cavitation extents as predicted by the standards and empirical methodologies.
3. Diagnostics of geometric, flow and pressure characteristics through parametric studies to establish key interrelations of local and global geometric, flow and pressure parameters must be studied comprehensively. Furthermore, the interactions between the multi-flow passages or singularities with the flow field, and their effects on the local flow and pressure structure need to be analysed extensively. Scalable characterization of geometry as a function of flow, and pressure parameters must be developed, and from which prediction models for the flow field hydrodynamic structure must be developed in order to encompass a wide scope of local trim geometric configurations.
4. Based on the findings of the above key research areas, this key area of this study is dedicated to the optimization of multi-flow passages and singularities within control valves. The optimization is key at the design level where the hydrodynamic performance can be accurately and precisely tuned as a function of the geometric configuration within the control valve for optimum efficient and safe operating characteristics.

2.4. Research Objectives:

- Hydrodynamic performance determination of a baseline valve using standard methodologies.
- CFD based control valve performance evaluation
- To determine the effects of local trim geometry flow areas on the velocity and pressure variations within the valve
- To determine the effects of local trim geometry on the local CV and overall global CV
- To determine the combined effects of flow passages pattern of arrangement with regards to the effective flow area sizes on the pressure, pressure drop, flow, CV, cavitation potential, and pumping energy requirements.
- To formulate the effects of trim local flow passage and inherent flow variations on local velocity and pressure variations
- To formulate relationships on pressure loss and recovery downstream of the valve seat entrance.
- Development of semi-empirical mathematical relations for geometry with , pressure, pressure drop, pressure recovery, flow, cavitation potential, pumping energy requirement, and flow coefficient (CV) in multi-stage trim valves.
- Development of a prediction tool for the hydrodynamic performance and design of a multi-stage control valve.
- Development of a robust and scalable optimization model for the hydrodynamic performance and design of a multi-stage trim control valve.

CHAPTER 3

EMPIRICALLY BASED HYDRODYNAMIC PERFORMANCE PREDICTIONS OF A MULTI- STAGE TRIM CONTROL VALVE

Based on the identified research objectives of this work, the hydrodynamic performance prediction of a baseline valve has been determined using the widely referenced and industry acknowledged standards (ISA-75.01.01). This has been carried out as a benchmark calculation to facilitate evaluations further on in this study to establish the appropriateness of the published standard methodology and relevant data in predicting the hydrodynamic performance of a control valve. The valve performance predictions have been carried out for Newtonian incompressible fluids, and hydrodynamic performance characteristics of maximum allowable flow rate, maximum pressure drop, and rated CV have been calculated for the benchmark baseline valve. The equations that have been used for the calculations have been derived from standard Newtonian incompressible fluid flow under process flow conditions that the valve is expected to operate in.

3.1. Hydrodynamic Performance of a Control Valve

The standard calculations follow a defined sequence to determine the hydrodynamic performance of a control valve. The valve flow coefficient (CV) is an integral parameter in control valve performance, as it determines the amount of flow that flows through the valve with a one psi pressure drop across the valve at 60° Fahrenheit temperature. The hydrodynamic performance of a valve within the scope of the standards is benchmarked on choked flow. With regards to incompressible liquid flow, the choked flow term is described as the condition of a fluid where the volumetric flow rate will not increase any further regardless of further increase in the differential pressure across the valve. It is from the choked flow conditions, that critical calculations of maximum flow rate and maximum differential pressure are derived. The two flow conditions considered with regards to how the flow coefficient is calculated are as follows, for non-choked flow, the valve flow coefficient is calculated as

$$CV = \frac{Q}{N_1} \times \sqrt{\frac{\frac{\rho_1}{\rho_0}}{\Delta P}} \quad \text{m}^3/\text{hr. Bar} \quad (3.1)$$

The flow coefficient for choked flow conditions is calculated as

$$C = \frac{Q}{N_1 F_L} \times \sqrt{\frac{\frac{\rho_1}{\rho_0}}{P_1 - F_F P_V}} \quad \text{m}^3/\text{hr. Bar} \quad (3.2)$$

Where N_1 is a numerical pressure unit conversion factor, F_L is the fluid pressure recovery factor which will be discussed in detail in this section, $\frac{\rho_1}{\rho_0}$ represents the specific gravity, P_1 is the inlet pressure, and P_V is the fluid vapour pressure. Table 3-1 shows the boundary conditions at which the hydrodynamic performance of the valve was calculated based on the traditional standard methodology. The process media was water at ambient temperature conditions, and in this investigation, cavitation and choked flow conditions are the focal parameters for the hydrodynamic performance prediction capability evaluations of the standard's model. Hence the inlet and pressure boundary conditions have been specified with a substantial differential pressure between them at which extensive cavitation is expected to occur.

Table 3-1: Valve Operating Process Conditions.

Fluid:	Water
Inlet Temperature:	$T_1 = 363\text{K}$
Saturation pressure:	$P_V = 70 \times 10^3 \frac{\text{N}}{\text{m}^2}$
Thermodynamic fluid critical pressure:	$P_C = 22100 \times 10^3 \frac{\text{N}}{\text{m}^2}$
Kinematic viscosity:	$\nu = 3.3 \times 10^{-7} \frac{\text{m}^2}{\text{s}}$
Inlet absolute pressure:	$P_1 = 3194.236 \times 10^3 \frac{\text{N}}{\text{m}^2}$
Outlet absolute pressure:	$P_2 = 790.8 \times 10^3 \frac{\text{N}}{\text{m}^2}$
Flow rate	$Q = 34 \frac{\text{m}^3}{\text{hr}}$
Pipe size:	$D_1 = D_2 = 50.8 \text{ mm (2 inches)}$

3.1.1. Valve Type Classification and Reference Criteria:

Valve Style.

The valve style describes the valve trim geometric configuration, and selection of the appropriate style is carried out with reference to the standard published geometric configurations for which hydrodynamic performance data for specific valve types has been determined through extensive experimental tests within the scope and context of the standards considerations. From reference table 2 of ISA – 75.01.01-2007 (IEC 60534-2-1 Mod), the baseline valve closely resembles the Globe small trim type (flat seat short travel), and on this criterion, the determination of the hydrodynamic performance is based on the experimentally derived coefficients for the selected valve type.

Fluid Pressure Recovery Factor.

The fluid pressure recovery factor is an important parameter that predicts the amount of pressure recovery that will take place between the vena contracta and the valve outlet. The pressure recovery factor is determined experimentally through a test procedure as stipulated in the ISA standard EN 60534, and most importantly it is used to account for the effects and influence of a valve's internal geometry on the maximum capacity of the valve. The calculation of the fluid pressure recovery factor requires global parameters of maximum flow rate (referred to as choked flow), the inlet and outlet pressure, and the fluid inlet temperature. Hence, in effect, the fluid pressure recovery factor is used to determine the effects of the local trim geometry flow passages on the critical hydrodynamic performance of the valve with respect to maximum allowable flow rate, maximum allowable pressure drop for local non cavitating conditions, and corresponding rated flow coefficient (CV).

The fluid pressure recovery factor is also generally described as the ratio of the pressure drop that occurs between the vena contracta and the upstream pressure, and can be computed from the following expression

$$F_L = \frac{Q_{\max}}{N_1 C} \times \sqrt{\frac{\rho_1 \rho_0}{P_1 - F_F P_v}} \quad (3.3)$$

From the parameters determined in the tests carried out on the baseline valve for inlet velocities ranging from 2 to 4m/sec, the pressure recovery factor was determined from equation (3.3) as

$$\text{Pressure recovery factor } F_L = 0.85.$$

As stated earlier, the standards provide a table of geometric characteristics of fluid pressure recovery factor and valve geometric style modifier. These tabulated characteristics are based only on specific valve types covered within the scope of the standards for which the type of control valves accounted for are those known to be in industrial service at the time of print. Having identified that the baseline valve closely resembles the Globe small trim type (flat seat short travel), the fluid pressure recovery factor specified by the standard and presented in table 2 of ISA – 75.01.01-2007 (IEC 60534-2-1 Mod) is

$$\text{Fluid pressure recovery factor (Standards reference) } F_L = 0.84.$$

However, having taken geometric reference from the standards through arbitral similarities, it is interesting to note that the fluid pressure recovery factor calculated from parameters determined in the experimental tests has not been calculated at maximum flow rate and choked flow conditions for which it is stipulated in the standard's methodology. However, the value of the fluid recovery factor arbitrarily selected from a valve that closely resembles the baseline valve in this study is similar to the calculated fluid recovery factor from test data at non-choked conditions. Since the determination of the fluid pressure recovery factor requires maximum flow rate and inlet pressure parameters at critical flow conditions, and the fact that the calculated fluid pressure recovery factor was determined from non-critical parameters and yet is similar to the fluid pressure recovery factor obtained from the listed values for a valve that closely resembles the baseline valve indicates that it does not represent the true hydrodynamic characteristics of the valve. Hence, this and other uncertainties will be highlighted in the following sections.

Valve Style Modifier:

To predict the hydrodynamic performance of a control valve, it must be established if the type flow is turbulent or non- turbulent, and this criterion utilises the valve style modifier to determine the type of flow. The valve style modifier is defined as the ratio of the hydraulic diameter of a single flow passage to the diameter of a circular orifice, of which the area is equivalent to the sum of areas of all identical flow passages at a given travel.

The valve style modifier can be computed from equation (6) as

$$F_D = \frac{D_H}{d_o} \quad (3.4)$$

Where D_H , is the diameter of single flow passage and d_o , is the equivalent circular diameter of the total flow area, D_H is expressed as follows.

$$D_H = \frac{4 A_O}{I_W} \quad (3.5)$$

Where A_O is the area of the vena contracta of a single flow passage, and I_W , is the wetted perimeter of a single flow passage.

The area of the vena contracta of a single flow passage is determined as

$$A_O = \frac{N_{23} C F_L}{N_O} = 114.6 \text{ mm}^2 \quad (3.6)$$

Where C is the valve flow coefficient, N_O is the number of independent and identical valve closure flow passages of a trim, and in this case N_O is 1 as only one valve closure flow passage is available, N_{23} is a numerical unit conversion constant.

$$D_o = \sqrt{\frac{4 N_{23} C F_L}{\pi}} = 12.08 \text{ mm} \quad (3.7)$$

$$D_H = \frac{4 N_{23} C F_L}{\pi (D_o + d_I)} = 4.87 \text{ mm} \quad (3.8)$$

The valve style modifier F_D is then calculated to be 0.4, the valve style modifier as stated previously is a parameter that will be used to calculate the valve Reynolds number for which

the result will determine whether the laminar or turbulent flow coefficient calculation will be applicable.

3.2. Empirically Based Hydrodynamic Performance Calculations:

Proceeding on with the stipulated standard sequence of calculations to determine the hydrodynamic performance of the baseline valve, the fluid critical pressure ratio factor must be determined. The fluid critical pressure ratio factor (F_F) is calculated from the following expression

$$F_F = 0.96 - 0.28 \sqrt{\frac{P_V}{P_C}} = 0.94 \quad (3.9)$$

Following on, the type of flow must be determined with respect to whether the flow is choked or non-choked. The type of flow is calculated as

$$F_L^2 \times (P_1 - F_F \times P_V) = 2261 \times 10^3 \frac{N}{m^2} \quad (3.10)$$

This value is less than the differential pressure of 2404.4 KN/m² across the valve, hence the type of flow is characterised as choked flow as per standard criterion, and the valve flow coefficient is calculated as

$$C = \frac{Q}{N_1 F_L} \times \sqrt{\frac{\rho_1 \rho_0}{P_1 - F_F P_V}} = 7.16 \text{ m}^3/\text{hr. bar} \quad (3.11)$$

Where ρ_1/ρ_0 is the specific gravity, and N_1 is a unit correction factor presented in the ISA-75-01-01 standard tables 1, and it is given as 1×10^{-1} . After determining the flow coefficient with the relevant prescribed equation for non-choked flow, the Reynolds number must be calculated to determine whether the flow is laminar or turbulent, and if the flow is laminar further correction factors will be introduced in the flow coefficient equation. However, in the case of this baseline valve it can be confidently deduced that the flow within the control valve is turbulent. Even if it is known that the flow is turbulent, the standard procedure requires that the Reynolds number be calculated, and it is calculated as follows.

$$\text{Re}_v = \frac{N_4 F_D Q}{v \sqrt{C_1 F_L}} \left[\frac{F_L^2 C_1^2}{N_2 D^4} + 1 \right]^{\frac{1}{4}} = 1354209 \quad (3.12)$$

The above equation confirms that the flow is turbulent, and based on the standards criteria, the valve Reynolds number is greater than 10000, and hence no further corrections are necessary, and for the given flow conditions, the valve CV has been calculated appropriately w.r.t the standards methodology. Following on from the determination of the valve flow coefficient CV, the critical valve performance limitations of the maximum allowable global flow rate and pressure drop across the valve must be determined. For a control valve installed without attached fittings as in this case, the maximum flow rate is calculated as

$$Q_{\max(L)} = N_1 F_L C \sqrt{\frac{P_1 - F_F P_v}{\frac{\rho}{\rho_0}}} = 30.7 \text{ m}^3/\text{hr} \quad (3.13)$$

The maximum differential pressure that is effective in producing flow under choked flow condition is then calculated as follows

$$\Delta p_{\max(L)} = N_1 F_L^2 (P_1 - F_F P_v) = 2260.9 \text{ KN/m}^2 \quad (3.14)$$

Figure 3.1 Presents the ISA ISA-75.01.01- (60534-2-1 standard hydrodynamic performance control valve sizing process flow chart that has been followed for this present study. From the results obtained through this standard process, detailed CFD based evaluations and discussions are presented in the proceeding chapters.

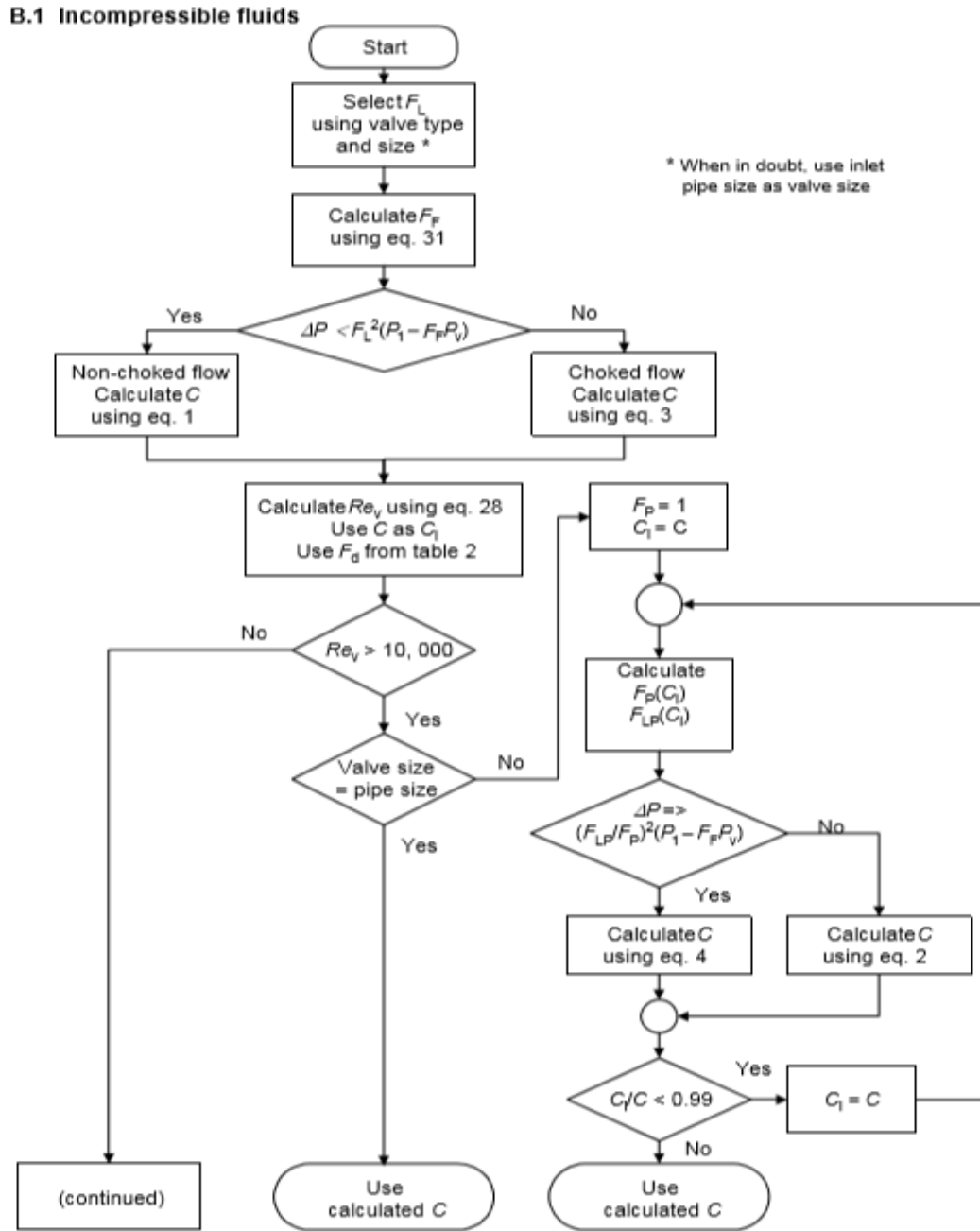


Figure 3-1 Control Valve Hydrodynamic Sizing Flow Chart

CHAPTER 4

CFD BASED HYDRODYNAMIC PERFORMANCE EVALUATIONS OF A MULTI-STAGE CONTROL VALVE

Based on the research objectives set out in this study, the previous section determined the control valve hydrodynamic performance based on the current published data and standards methodology, and It has been observed that selection of a valve type from the standards tables that closely resembles the baseline valve used in this study or any other valve type outside of the scope of the standards is an ambiguous effort. This gives rise to uncertainties with the accuracy of the hydrodynamic performance calculations. Hence, advanced CFD techniques have been used to quantitatively evaluate the hydrodynamic performance of the control valve through computational simulations.

The application of these techniques has been presented in this section. Applicable solver settings and boundary conditions in the current study have been stated. Computational fluid dynamics governing equations are formulated based on continuum mechanics, and literature on these equations is widely accessible on the wide web and relative CFD books. The ANSYS CFD version 17.0 package was used at the time this study was carried out to achieve the specified objectives in this thesis through simulations and analysis.

4.1. Pre – Processing Set Up of CFD Model:

CFD simulation pre-processing constitutes of creation of geometry and meshing of the fluid flow domain. This section outlines in detail, the modelling of the geometry and meshing of the control valve geometry.

4.1.1. Configuration of Control Valve Geometry:

The control valve geometry was created using the 3D modelling software Solid Works. The flow domain geometry was created with consideration of the Standard ISA-75-01-01 test piping requirements with respect to the distances of the pressure measurement taps upstream and downstream of the valve. The length of the inlet is required to be 2 x the nominal pipe diameter of 2” (50.8mm), and is 101.6mm, and the inlet boundary conditions in the solver are prescribed at the entrance of the inlet pipe. The length of the outlet pipe is required to be 6 x the pipe nominal diameter, and the outlet boundary conditions are prescribed at the exit of the outlet pipe. The inlet pipe, test section valve, and the outlet pipe which constitute the flow domain was prescribed with a roughness height of 0 which corresponds to smooth walls, and a roughness constant of 0.5 was also prescribed in the solver, which represents a uniform sand grain roughness, and as described in the ANSYS documentation, the default roughness constant of 0.5 reproduces Nikuradse’s resistance data for pipes roughened with tightly packed, uniform sand-grain roughness. The geometry flow domain of the inlet pipe, test section (valve), and outlet pipe is shown in figure 4.1 below.

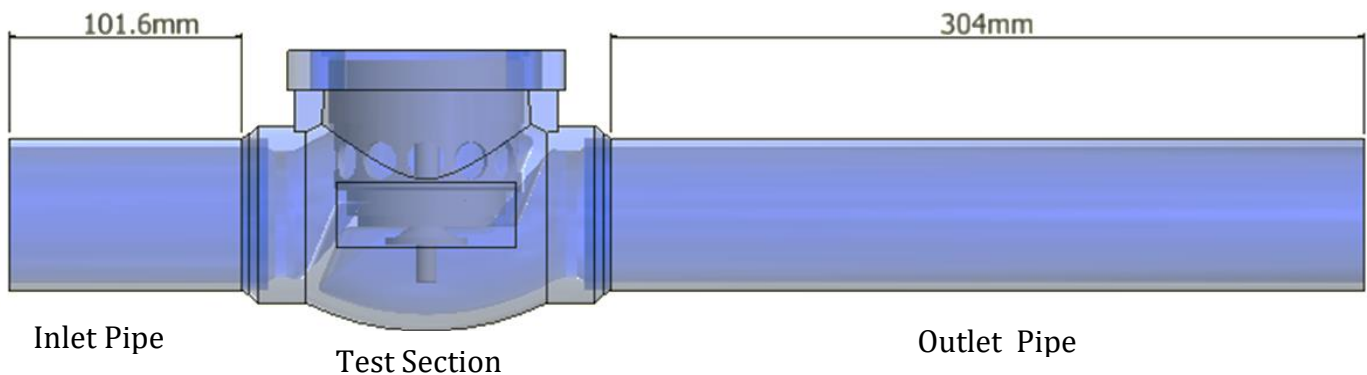


Figure 4-1 Valve Geometric Flow Domain

Figure 4.2 shows the baseline valve trim flow passages along the flow path, in the control valve under investigation in this current study there are 3 flow passages arranged in series and these have been defined as (FP1), (FP2), and (FP3) respectively. The local geometric contributions to the flow structure will be discussed in detail in the proceeding chapters.

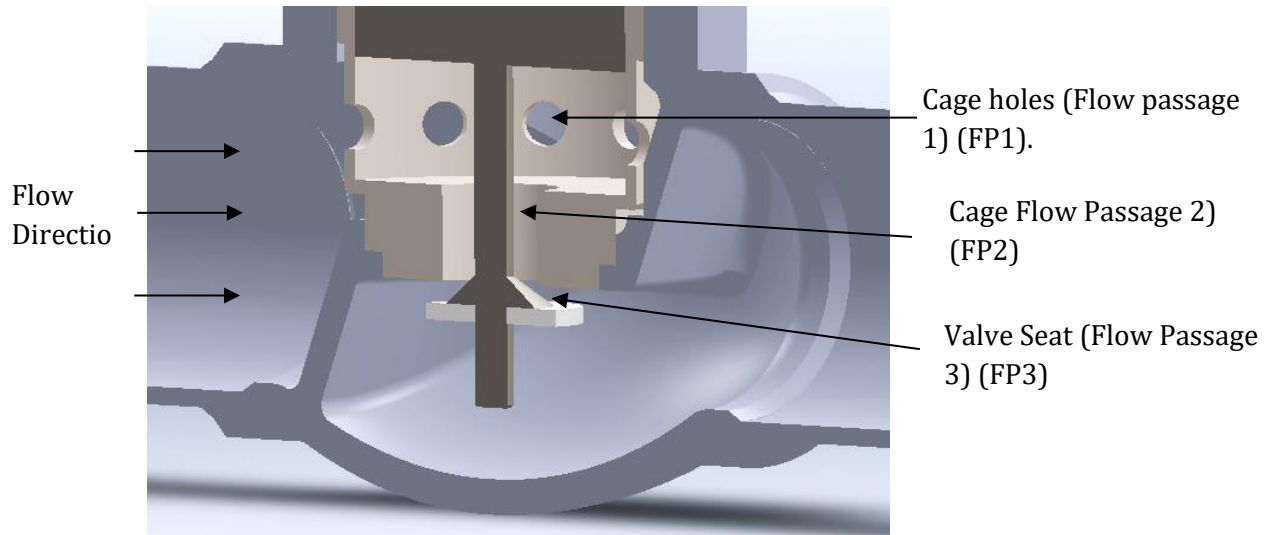


Figure 4-2 Valve Trim Flow Passages Along the Flow Path

4.1.2. Meshing the Flow Domain:

One type of mesh has been used to mesh the entire flow domain, meaning that one type of mesh has been created in the domain. The mesh for the entire flow domain has been generated using the Cut-Cell method, the Cut-Cell mesh converts a volume mesh into a prominently Cartesian mesh, meaning that the mesh is constituted mostly of hexahedral elements. This mesh type has been used in this study for reasons stated below

- The predominant Hexahedral mesh elements in the cut cell mesh produce more accurate results due to low numerical diffusion.
- Cut-Cell mesh can be generated in significantly reduced time for complex geometry.

Mesh Independence Tests:

A reliable solution requires it to be independent of the mesh, and to assert this, a mesh independence test must be carried out. In this test, the static pressure at the valve plug entrance, defined in this current study as flow passage 3 (FP3) has been used as a parameter of reference. Two different mesh sizes of 1017442 and 1235942 elements were used for the mesh independence test. The analysis in this work was carried out on a 64 bit i9-10900 2.8 GHz, and 32GB RAM CPU.

Table 4.1 shows the results of the mesh independence test with a 12% and 0.02% difference in the valve plug entrance (FP3) local static pressure for 0.95 million mesh elements and 1.02 mesh elements respectively as compared to the results for 1.24 million elements. Qualitatively, a difference close to zero is optimal and reduces cumulative mesh related errors to the flow field solver where at the given mesh element number there is minimal change in the results to the order of the % difference. Thus, on the qualitative basis of this test, it can be affirmed that the mesh with 1.02 million elements can accurately predict the complex local flow field and has been used for further analysis of the hydrodynamic characteristics of the valve under this current study.

Table 4-1: Mesh Independence Test Results

Number of Mesh Elements	Pressure at Valve Plug Entrance	Difference in Pressure with 1.24 million elements mesh
	(N/m ²)	
0.95 million	1978952.32	12%
1.02 million	2249187.22	0.02%
1.24 million	2248755.47	

4.1.3. Solver Execution:

The Fluent solver has been used in this current study, and it is a part of the CFD package Ansys 17.0. The solver settings implemented in this study are discussed in detail in this section.

Physical Model Selection:

Based on the global process conditions as discussed earlier, the low flow velocities within the control valve flow domain render compressibility effects negligible, and hence incompressible conditions have been specified in the solver through selection of the pressure-based solver. The pressure-based solver holds the density and fluid dynamic viscosity constant.

Valves are generally designed for fluid flows under steady state conditions, however unsteady conditions do occur where the fluid properties change through varying process conditions that will not have been accounted for at the design stage. Based on the objectives set out in this chapter, simulations have been carried out under non cavitating and cavitating choked flow conditions, and hence property changes in the fluid is expected. Therefore, an unsteady state time dependent solver has been used in this current work for the hydrodynamic performance evaluation of a baseline valve. The implicit mixture multi-phase model with slip velocity, and dispersed flow interface has been used to model choked flow under cavitating conditions. The number of mass transfer mechanisms has been set to 1 with phase 1 of water and phase 2 of air.

A relevant turbulent model must be prescribed that corresponds with the type of flow within the valve. Based on the valve sizing and hydrodynamic performance calculation standards ISA-75-01-01(IEC60534), the criterion for turbulent flow requires that the Reynolds number be greater than 10000. The process flow rates in which the valve in this study is operating range from 2m/sec to 4m/sec with corresponding Reynolds numbers of 10000 – 35000. Hence, the flow in the valve is turbulent. The CFD package that has been used in this study offers a variety of turbulent models each with different advantages and disadvantages. With regards to internal flow in control valves with complex local geometry where flow separation, swirling flow, severe velocity, and adverse pressure gradients are expected to occur. The 2 equations k- ω turbulent model has been used in this study. The k- ω turbulent model is renowned for its superiority to accurately model the aforementioned flow conditions that are known to occur within the complex internal geometry of this valve.

Many experimentally validated CFD based studies have shown that the shear stress transport (SST) k- ω model is able to closely predict the variations in the local flow and pressure distribution, and furthermore, it has been shown that the SST k- ω model type under-predicts the static gauge pressure at the inlet by 5.2%, and whereas the standard k- ω model overpredicted the inlet static gauge pressure by 18.7%. This is a significant difference because a good agreement between a real experiment result and CFD model validates the model, such that a satisfactory discrepancy is below 5%, and 5.2% here, is acceptable.

The k- ω is a two-equation model which has 2 model types available in the solver, which are the standard k- ω model, and the shear stress Transport SST k- ω model. The shear stress model has been selected for use in this current study, and the specific reason for this selection is that

- The SST k- ω model encompasses a blending function for near wall treatment, and further modifies the turbulent viscosity to account for the turbulent shear stress transport.
- The SST k- ω equation includes further modifications with addition of a cross diffusion term, and a blending function o ensure stability and appropriate behaviour of the equations in both the near-wall and far field zones.

Based on the characteristics mentioned above, the SST k- ω model is more accurate and can reliably model a wide scope of flows such as flow separation, and adverse pressure gradient flows.

Material Properties and Operating Conditions:

The fluid medium within the valve flow domain has been specified as liquid water, with a density of 998 Kg/m³, and the dynamic viscosity of 0.00103 Kg/m-sec. The solver has been executed under operating conditions of operating pressure at 101325 N/m² atmospheric pressure, and gravitational acceleration was not considered so was turned off.

Boundary Conditions:

Table 4.2 shows the boundary conditions that have been specified for the solver for the global conditions at which the flow through the control valve was solved, where the inlet pipe boundary type is a pressure inlet where a static pressure magnitude has specified at the inlet pipe section flow entrance. The outlet pipe section is a pressure outlet boundary type where a static pressure magnitude has been prescribed at the exit to the outlet pipe section. The internal walls of the entire valve have been prescribed as a stationary wall with no slip conditions,

Table 4-2. Solver Boundary conditions

Boundary Name	Boundary Type
Inlet Pipe	Pressure inlet
Outlet Pipe	Pressure outlet
Walls of The Pipe and Valve	Stationary

Based on the flow conditions used earlier in this chapter to calculate the hydrodynamic performance of the baseline valve using the Standards methodology, in this study, similar flow conditions have been prescribed in the solver through boundary conditions shown in table 4.2. The inlet pressure was prescribed as 3088.2KN/m^2 , and the outlet pressure was prescribed as 337.843KN/m^2 . The temperature was based on the ambient temperature of 25°Celsius at which the empirical calculations were carried out. In this study, temperature variations within fluid single phase properties were accounted for through the specific gravity as a function of density changes.

As articulated earlier the valve flow domain inclusive of the inlet and outlet pipe has been prescribed with the default roughness constant of 0.5, which considers the flow domain walls to roughened with tightly packed, uniform sand-grain consistent with a surface finish attained from standard pipe manufacturing processes. Global experimentally derived coefficients such as the fluid pressure recovery factor, piping geometry factor, valve style modifier, and Reynolds number factor are widely published and presented in the ISA standards. The data published in the standards is specific to standard valve types covered within the scope of the standard as discussed in chapter 2.

Based on the test procedure set out in the standard EN 60534-2-3, for liquid pressure recovery factor F_L , the maximum flow rate for which choked flow occurs must be determined. The test is carried out at fixed inlet conditions, and choked flow is evidenced to be occurring by failure of increasing the pressure differential to produce further increase in the flow rate. The criterion for failure of further increase in the flow rate stated to be satisfactory when there is at least 2% difference in the flow rate as the differential pressure is increased further. This test was replicated using CFD techniques in this current work, where the inlet pressure was held constant at 3103 KN/m², and the outlet pressure was varied from 2068 KN/m² to 206.843 KN/m². Data from this present study has been acquired and used to determine the hydrodynamic performance of the baseline valve. Furthermore, the data from this present study was used to highlight the valve local hydrodynamic performance within the complex flow path consisting of multiple flow passages.

Solver Settings:

Solver settings based on the application are required to accurately predict the fluid flow behaviour in the flow domain. The settings in the solver consist of:

- Pressure – Velocity Coupling
- Gradient
- Spatial Discretization

The Navier Stokes equations form the governing equations of the solver, the equations are solved in the discretised form. In this form, the velocity and pressure are linearly dependent on each other. Thus, pressure – velocity is required to predict the pressure distribution in the flow domain with relatively close accuracy. The pressure- velocity coupling has been discretised using the SIMPLE algorithm because of its known accuracy for flows within complex geometry, and its fast convergence. The velocity and pressure field estimation are acquired by solving the momentum equation through the coupled pressure velocity algorithm. The pressure gradient is calculated explicitly using the pressure distribution from the previous iteration or a prior estimate. To obtain the new state of the pressure distribution, the pressure equation is formulated and solved where velocity values are corrected, and calculations of the conservative fluxes at that new state are calculated.

The construction of values of a scalar at the cell faces require gradients to compute secondary diffusion terms and derivatives of velocity. The Green- Gauss Node based gradient evaluation has been implemented in this current study. Through this gradient interpolation method, exact values of a linear function at a node are reconstructed from the surrounding cell. Spatial discretization provides approximation on the local conservation of quantities instead of on the entire flow domain, and this is necessary to account for the limited memory of computers. Discrete values of the scalars are stored at cell centres, the convection terms require face values, and they are interpolated from the values at the cell centres. The 2nd order upwind spatial discretization scheme has been used for pressure, momentum, turbulent kinetic energy, and turbulent dissipation rate interpolation in this study. Through the upwind scheme the values at the cell faces are derived from upstream cell values in the direction relative to the normal velocity.

Convergence Criteria:

Convergence of a solution implies that conservation of mass and momentum has been achieved locally and globally throughout the flow domain with no further variations in the flow parameters. Hence reliable predictions of the flow field are taken from a converged solution.

The Ansys 17 default convergence criteria for 3-dimensional continuity, velocity and turbulent parameters is 0.001. when the change in the continuity, velocity, and turbulent parameters reduces to 1×10^{-4} , the solution is taken as converged. It is practical to monitor convergence with respect to a global parameter e.g. pressure, mass flow rate, instead of benchmarking the convergence solely on the default criteria. The local minimum static pressure downstream of the valve opening has been monitored in this current study at every time step for the complete iterative process. A stable, non-fluctuating minimum static pressure has been taken as criterion to render the solution to have converged.

4.2. Results of Single-Phase Flow in a Control Valve:

The single-phase Global flow structure of water flowing through the valve must be understood and validated with the CFD model set out as described in the previous section. The static pressure distribution within the valve is shown in figure 4.3. Pressure variations are depicted within the vicinity of every flow passage along the flow path, and as shown in the figure, varying magnitudes of local static pressure are seen to occur across each flow passage along the flow path with respect to the diametric size of each of the flow passages.

The flow coefficient CV, was determined through experimental tests carried out on the baseline valve, and the baseline overall valve CV was calculated from equation (3.1)

$$CV = 5.1 \text{ m}^3/\text{hr. bar}$$

The differential pressure across the valve, and flow rate predicted by the CFD model used in this study were used in equation (3.1) to calculate the valve CV as

$$CV_{\text{CFD}} = 5.2 \text{ m}^3/\text{hr. bar}$$

The CFD predictions of the valve flow coefficient for single phase flow is in excellent agreement, and the predictions are within admissible accuracy of less than 2% as compared to the experimental results carried out under similar conditions.

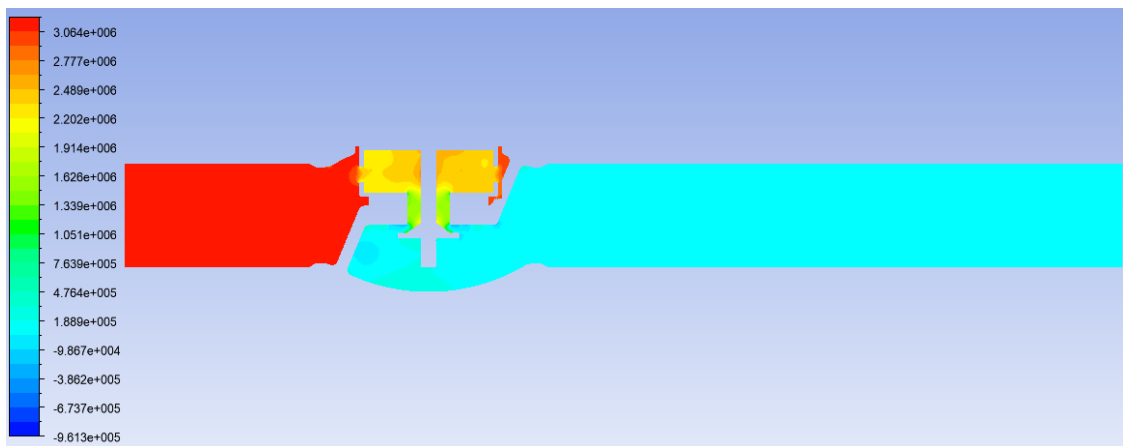


Figure 4-3 Variations of Static Pressure (N/m^2) Within the Valve.

Figure 4.4 shows the static pressure variations within the valve along the mid-section of cage holes flow passage. In this current study, the cage holes flow passage has been defined as (FP1) which stands for flow passage 1. The plots of static pressure variations as show in figure 4.3, and 4.4 provide details of the scales of pressure distribution in terms of pressure loss and differential pressure across each of the 3 flow passages along the control valve flow path. On that premise, the significant effects of the flow areas of each flow passage on the global flow coefficient CV, and pressure variations downstream of the valve plug will be discussed in detail later in this section. Furthermore, the local flow coefficients CVs of each flow passage and their combined contribution to the global overall CV across the valve will be discussed.

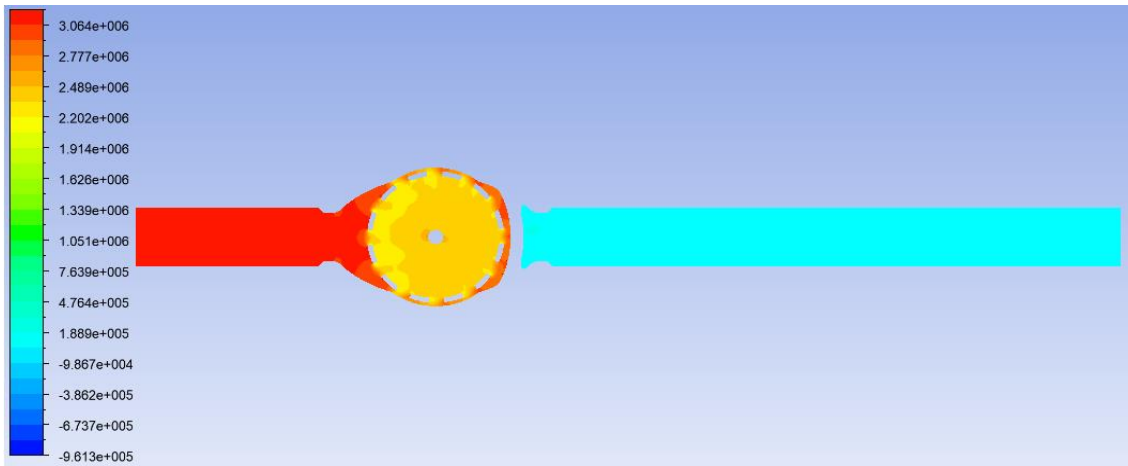


Figure 4-4 Variations of Static Pressure (N/m^2) Within the Valve Along the Mid Section of the Cage Holes Flow Passages. The Flow Section Holes are Defined as (FP1) In This Study.

Figure 4.5 and 4.6 show the variations of velocity within the valve, the inlet pipe velocity varies with respect to the differential pressure across the valve. The velocity is seen to increase significantly as the flow passes through the restrictions of the flow passages. The velocity at the wall of the inlet pipe, outlet pipe, and valve is zero, and this consistent with the no slip boundary condition prescribed on the flow domain walls.

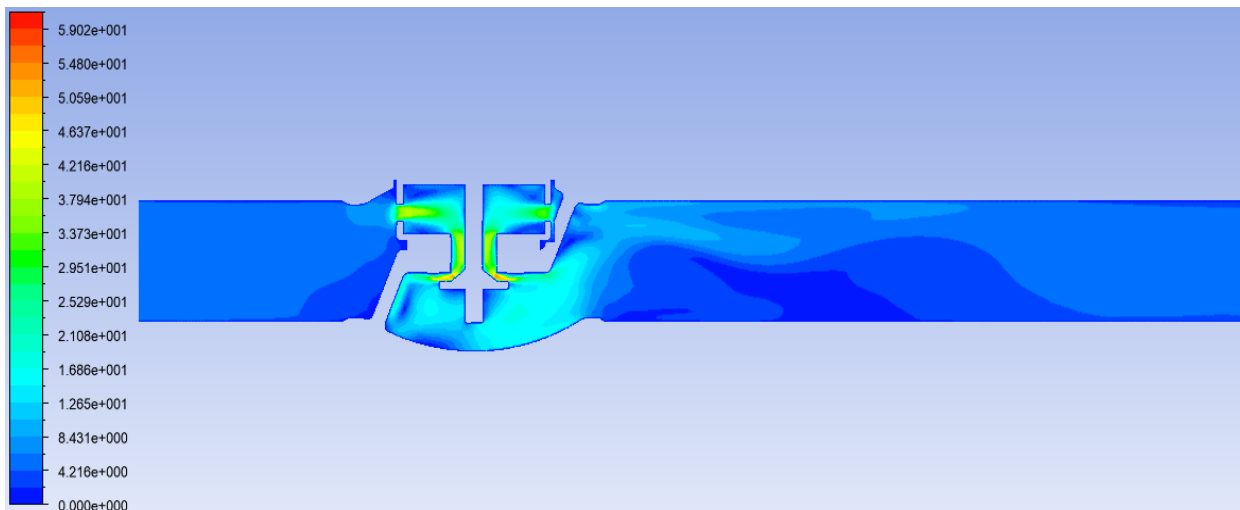


Figure 4-5. Variations of Velocity (m/sec) with-in the Valve

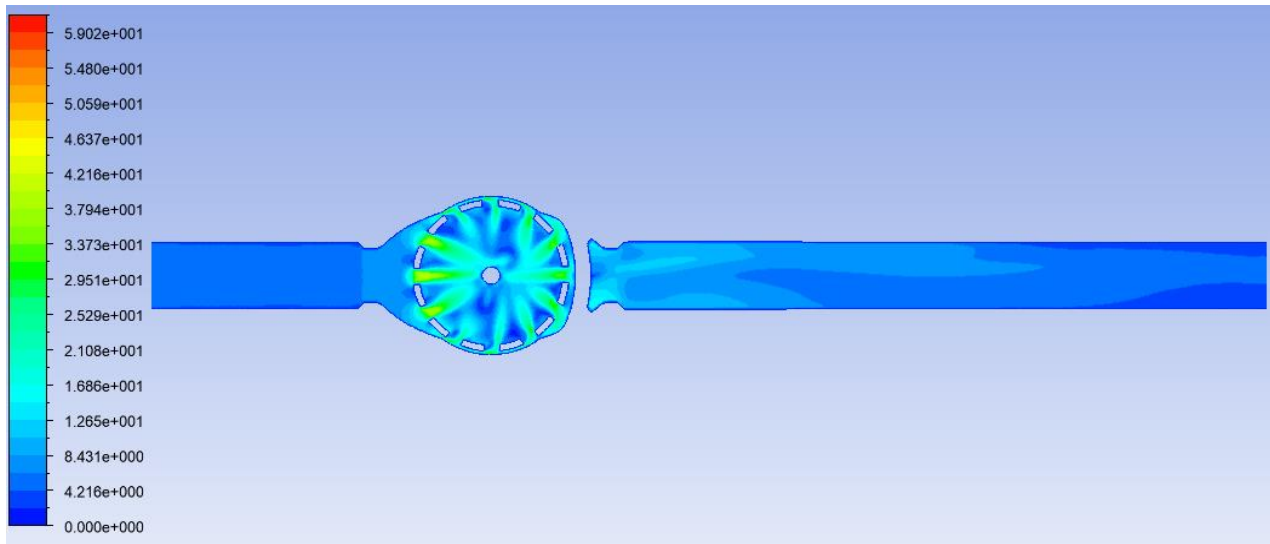


Figure 4-6 Variations Of Velocity (m/sec) Within The Valve Along The Mid Section of the Cage Holes Flow Passages (FP1).

4.2.1. Pressure Loss and Pressure Recovery Downstream of the Valve Plug:

In order to evaluate the pressure loss and pressure recovery dynamics, the variation of pressure downstream of the valve plug have been analysed locally in the form of pressure loss and pressure recovery. Detailed information on the local pressure structure downstream of the valve plug has been determined. As discussed earlier, the analysis has been carried out with the inlet pressure boundary condition held constant at 3103 KN/m^2 , and with varying outlet pressure values of 2068.410 KN/m^2 , 1378.940 KN/m^2 , 689.470 KN/m^2 , 344.735 KN/m^2 , and. The pressure variations downstream of the valve plug has been plotted at each of the outlet pressure values. Figure 4-7 shows the variations of static pressure downstream of the valve plug along the centreline flow path streamline across the valve opening over a length (x) taken from the valve plug exit and up to the outlet boundary as a ratio of the valve opening effective flow diameter (D). It can be seen from figure 4-7 that the pressure structure typifies the expected pressure variations downstream of a flow restriction and satisfies continuity with regards to the pressure loss and recovery, where there is pressure reduction immediately downstream of the valve plug exit corresponding to high velocity and followed by the pressure recovering as the velocity reduces with reconversion of kinetic energy into pressure energy. In can be seen that the valve

plug entrance pressure reduces as the differential pressure across the valve increases, and with a corresponding relative decrease in the minimum pressure downstream of the valve plug.

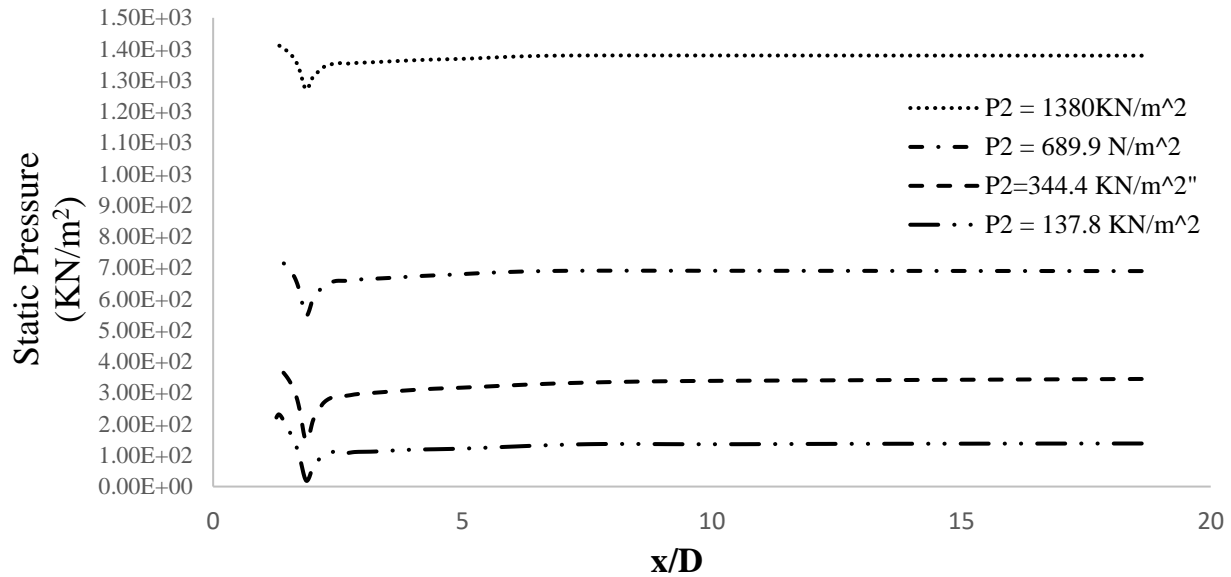


Figure 4-7. Pressure Variations Downstream of the Valve Opening at Varying Outlet Pressure.

4.3. Choked Flow Analysis in a Control Valve with Multiphase Flow Model.

In order to evaluate the standard based predictions presented in chapter 3 of choked flow conditions of the maximum allowable global pressure drop and flow rate, where the maximum allowable flow rate is predicted from equation (3.13) from the following expression

$$Q_{\max(L)} = N_1 F_L C \sqrt{\frac{P_1 - F_F P_V}{\frac{\rho}{\rho_o}}}$$

The maximum differential pressure that is effective in producing flow under choked flow condition is then estimated from equation (3.14) from the following expression

$$\Delta p_{\max(L)} = N_1 F_L^2 (P_1 - F_F P_V)$$

As defined in chapter 1, the fluid pressure recovery factor F_L characterises choked flow conditions in a control valve, and it is determined experimentally for specific valve types, where the global differential pressure is increased gradually by holding the inlet pressure constant and varying the outlet pressure until there is no further increase in the volume flow rate. Fluid pressure recovery factors for standard specific valve types are published in the ISA -75-01.01 (ICE 60534-2-1) standards, however the fluid pressure recovery factors cannot be accurately referenced for control valve geometric configurations outside the scope of those covered by the standards. Hence, this presents a crucial gap in the knowledge with regards to the unavailability of overall hydrodynamic performance prediction tools for control valve local geometric configurations outside the scope of the standards and other relevant published literature.

In the previous chapter, the standards methodology was used to determine the maximum allowable global flow rate and differential pressure across a baseline control valve under investigation in this study, where a published fluid pressure recovery factor for a valve type trim that closely resembles the baseline valve trim geometric configuration was used. Hence, the objective of this CFD based study is to determine the global maximum allowable flow rate and differential pressure at which choked flow conditions occur and determine the local fluid properties and their contributions to choked flow conditions. Furthermore, and most importantly, the results of the CFD analysis will then be compared with the results from the standards methodology, and from which evaluations of appropriateness and applicability will be carried out.

The multi-phase mixture cavitation model has been used to account for the local fluid phase change from liquid to vapor at the valve seat opening, where the extent of vapour and liquid mixture within the vicinity of the valve seat opening is characterized through the phase percentage volume fraction.

4.3.1. Physical Model Selection:

- The implicit multi-phase mixture model with slip velocity and dispersed interface model with cavitation mass transfer has been used in this study.
- The 2 equations SST $k-\omega$ turbulent model has been used in this study.
- The pressure- velocity coupling has been discretised using the SIMPLE algorithm
- The least squares cell based gradient evaluation has been implemented in this current study.

- The 2nd order upwind spatial discretization scheme has been used for pressure, momentum, turbulent kinetic energy, and turbulent dissipations rate interpolation in this study.

4.3.2. Choked Flow Characteristics Within a Control Valve

To quantify choked flow conditions within the valve, the volumetric flow rates have been plotted against the varying global differential pressures across the control valve. Figure 4-8 shows the plot of the volumetric flow rates at varying differential pressure boundary conditions set out in this study as stated in the previous section. The volumetric flow rate can be seen to increase linearly as the differential pressure increases, further increase in the volumetric flow rate is seen to stop at a differential pressure of 2748 KN/m². Based on the criterion set out in the ISA standards, fully choked flow is occurring when there is at least 2% difference in the volumetric flow rate as the differential pressure is increased further. At a differential pressure of 2886KN/m², the volumetric flow rate increased by 0.19%, and at a further increase in the differential pressure to 2954KN/m², the volume flow rate increased by 0.17%, and this satisfies the criterion of fully choked flow as specified in the standard ISA EN 60534-2-3.

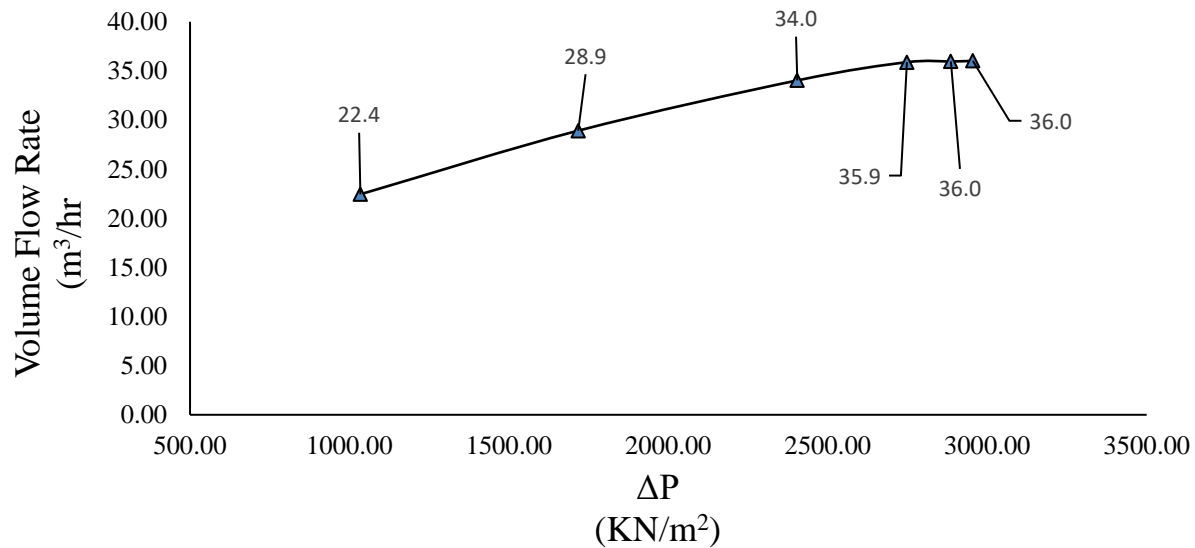


Figure 4-8. Variations of Volumetric Flow Rate as a function of Global Differential Pressure Across the Valve

In order to portray the extent local fluid property characteristics at which choked flow conditions are occurring, contours of volume fraction have been plotted downstream of the valve opening at a differential pressure of 2748 KN/m² and volume flow rate of 35.89 m³/hr. Figure 4-9 depicts the vapour volume fraction downstream of the valve opening at which the volume flow rate does not increase any further as shown in figure 4-8 above, where it remains constant onwards at 35.9 kg/hr from a differential pressure 2748 KN/m² and above. It can be seen that the entire flow path is almost fully covered with vapour at varying scales with an average volume fraction of about 0.7.

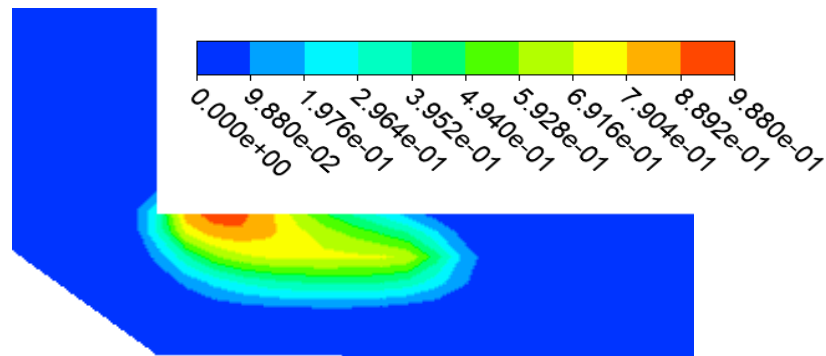


Figure 4-9: Variations of Vapour Volume Fraction downstream of the Valve Plug

From the results obtained in the CFD based analysis of the choked flow conditions of maximum global flow rate differential pressure, evaluations can be then be carried out through comparison with the results from the standards methodology predictions of choked flow conditions of the same control valve geometric configuration as presented in chapter 3. While adhering to the standards tolerance stipulations that if the flow rate in the first test is within 2% of the flow rate in the second test then the flow rate in the first test may be taken as Q_{\max} . hence, based on that criterion, the maximum flow rate which occurs at a differential pressure of 2757 KN/m² is

$$Q_{\max} = 35.89 \text{ m}^3/\text{hr}$$

The overall global flow coefficient $CV = K_v$ (m³/hr. bar) for flow under choked flow can then be determined from the above parameters from equation 3.2 as

$$K_v = 7.5 \text{ m}^3/\text{hr. bar}$$

The maximum differential pressure that is effective in producing flow under choked flow conditions across the valve is

$$\Delta P_{\max(L)} = 2757 \text{ KN/m}^2$$

The fluid pressure recovery factor specific for the baseline valve can be determined semi-empirically as

$$F_L = \frac{Q_{\max}}{N_1 C} \times \sqrt{\frac{\rho_1 \rho_0}{P_1 - F_F P_V}} = 0.85$$

From the CFD model used in this study, the hydrodynamic performance of the maximum flow rate and maximum differential pressure effective for producing choked flow in the baseline valve has been determined directly from the CFD results under similar conditions as those used in the standards methodology. Based on the objective of this current study, evaluations of appropriateness of the standards methodology for predicting the hydrodynamic performance of the baseline valve can thus be scrutinised, and the results are presented in table 4-3 bellow.

Table 4-3 shows the results of the CFD numerical model and the ISA-75.01.01 based methodologies predicted results of the maximum allowable overall flow rate, the maximum allowable overall pressure drop, the fluid pressure recovery factor and the flow coefficient (CV).

Table 4-3: Valve Hydrodynamic Performance Comparison

Parameter	Standard Methodology	CFD Model	% Difference
Maximum Global Flow Rate (Q_{\max}) (m^3/hr)	30.7	35.89	14.4%
Maximum Global Pressure Drop $\Delta P_{\max(L)}$ (KN/m^2)	2260	2757	18.1%
Fluid Pressure Recovery Factor (F_L)	0.85	0.84	1%
Flow Coefficient (Kv)	7.16	7.54	5.3 %

From the results presented in table 4.3, the CFD model has over predicted the maximum flow rate by 14.4% as compared to the maximum flow rate predicted by the standards methodology, and the corresponding differential pressure at which the maximum flow rate occurs has been overpredicted by 18.1%. The fluid pressure recovery factors are in good agreement, but however it is evident from the CFD results that the representation of the local geometric and hydrodynamic characteristics through the fluid pressure recovery factor yields inconsistent results. The inconsistencies are attributed to the unavailability of specific published data for a trim that matches the baseline multi-flow passage trim used in this study, and most importantly, the unaccountability of the local trim effects. Hence, a characterisation methodology is needed that explicitly accounts for the effects of local flow passages or singularities within a valve on the local and global hydrodynamic state. The small variation of 5.3% in the flow coefficient (CV) may seem to indicate good agreement between the standard and CFD model, and these closely similar values of CV should be expected at relatively similar global differential pressures across the valve for both the CFD and empirical results. However, this is not the case as there is a large discrepancy in the CFD and empirical differential pressure results of 18.1%, and this is attributed to the local effects being explicitly accounted for in the CFD model.

4.4. Summary of the Hydrodynamic Performance Analysis of The Baseline Valve:

An analysis of the hydrodynamic performance of a baseline valve has produced the following results:

- The maximum flow rate effective for producing choked flow within the valve has been over predicted by 14.4% by the CFD model as compared to the standard methodology.
- The maximum differential pressure effective for producing choked flow has been over predicted by 18.1% by the CFD model as compared to the standard methodology. This indicates that the CFD technique is more competitive because, based on the standards prediction of the significantly lower maximum differential pressure effective to cause choked flow conditions, a larger valve size with a higher flow coefficient would have been selected with higher cost implications, and risk of oversizing for the process.
- The valve flow coefficient (Kv) has been over predicted by 5.3% by the CFD model.

- The fluid pressure recovery factor predicted by the CFD model is in good agreement with the standard model, but its application yields significant under prediction of maximum allowable flow rate, maximum allowable pressure drop and flow coefficient (CV).

From the information procured in this chapter with regards to the predictions of the hydrodynamic performance of a baseline control valve based on the published data and ISA-75-01-01(IEC60534) standard's methodology, and CFD based evaluations of the standards methodology predictions. The current published data and standards do not provide a full picture of the hydrodynamic performance of a control valve whereas CFD does provide a full local and global picture. The current published data and standards do not provide a full picture of the hydrodynamic performance of a control valve hydrodynamic performance mainly because there are no details on and explicit considerations of direct local geometric configuration interactions with the flow field and effects on the local and overall hydrodynamic characteristics. Hence, the use of the current published data and standards for overly complex trims will amplify the uncertainties and differences in the correct hydrodynamic performance of flow and pressure characteristics highlighted earlier. Furthermore, the standards may need to be improved by providing additional equations so that the inaccuracies can be minimized. Hence it is because of these significant differences and critical uncertainties that further thorough investigations must be carried out on local geometric interactions with the flow field and effects on the hydrodynamic performance characteristics of a control valve.

CHAPTER 5

PARAMETRIC INVESTIGATIONS

The results obtained from the CFD evaluations of the hydrodynamic performance of a baseline valve in accordance to relevant published data and standard's criterion highlighted major inconsistencies with respect to characterization of the local geometry through the pressure recovery factor to predict a multi-stage trim control valve hydrodynamic performance in terms of limits of maximum differential pressure and maximum flow rate effective for producing choked flow. For control valve trim geometry outside the scope of the standards, it is inappropriate to match the geometry based on close resemblance with trims covered in the standards as the predictions of the hydrodynamic performance will be invalid. Furthermore, there is need to explore beyond the globally predicted fluid pressure recovery factor to accurately characterise the local geometric effects on the overall hydrodynamic performance of a control valve. Hence, a detailed investigation has been carried out to understand the current inscrutable local geometric effects on the flow structure within a multi flow passage trim control valve, and the Computational Fluid Dynamics model used in the study is able to predict the local flow and pressure structure with reasonable accuracy. Effects of various local geometric and global flow and pressure independent parameters on the local flow and pressure structure with regards to pressure drop, exit pressure and cavitation extents across multiple flow passages within a control valve have been investigated. Furthermore, the effects of the sequence of arrangement of multiple flow passages within a control as a function of effective flow area magnitudes on the flow field have been investigated. Most importantly, from the results of the investigations in this study, novel scalable geometric and flow field characterisations have been developed, and from which important local and global flow field prediction models have been developed.

5.1. Analysis of Single-Phase Flow in a Control Valve:

Prior to the flow analysis in a control valve, the flow structure of single-phase flow in a control valve must be understood and validated with the single phase CFD model created in the previous chapter. Hence the static pressure at flow passage 1 (FP1), and the pressure drop across the inlet and flow passage 1 (FP1) has been validated through the Bernoulli's energy equation.

Figure 5.1 depicts the contours of area averaged static pressure distribution within the multi-stage baseline control valve geometric configuration taken across a mid-section plane with water flowing through the valve. The area averaged static pressure at flow passage 1 (FP1) represented by the 12 cage holes taken at the exit region of the flow passage as shown in figure 5.1 is 768741.6 N/m², and with a corresponding inlet pressure (P1) of 929405.6 N/m².

Applying the Bernoulli's energy loss principle which is expressed as

$$P_1 - P_2 = 0.5\rho (V_2^2 - V_1^2) \quad (5.1)$$

Where V_1 is the inlet velocity and V_2 is the first flow passage (FP1) velocity, by calculating the velocities based on the effective flow areas at the inlet and flow passage 1 (FP1) through continuity, and inserting the corresponding velocities into equation 4.1 while neglecting the minor friction losses, the static pressure at the first flow passage after the inlet (FP1) along the flow path is calculated is:

$$(P_{FP1}) = 763113.8 \text{ N/m}^2$$

The corresponding differential pressure between the inlet and flow passage 1 (FP1) predicted through the energy equation is:

$$(P_{Pin} - P_{FP1}) = 166291.8 \text{ N/m}^2$$

The static pressure at flow passage 1 (FP1) predicted by the Computational Fluid Dynamics model is:

$$(P_{FP1 (CFD)}) = 768741.6 \text{ N/m}^2$$

and the differential pressure between the inlet and flow passage 1 (FP1) predicted by the CFD model is:

$$(P_{Pin} - P_{FP1}) \text{ (CFD)} = 170988.6 \text{ N/m}^2$$

The discrepancy between the Bernoulli principle-based calculation of the differential pressure and the CFD predicted differential pressure is 2.7%, and from this minimal discrepancy, it can be concluded in principle that the Computational Fluid Dynamics model can accurately predict the local pressure drop and pressure structure for single phase flow of water within a control valve within reasonable accuracy.

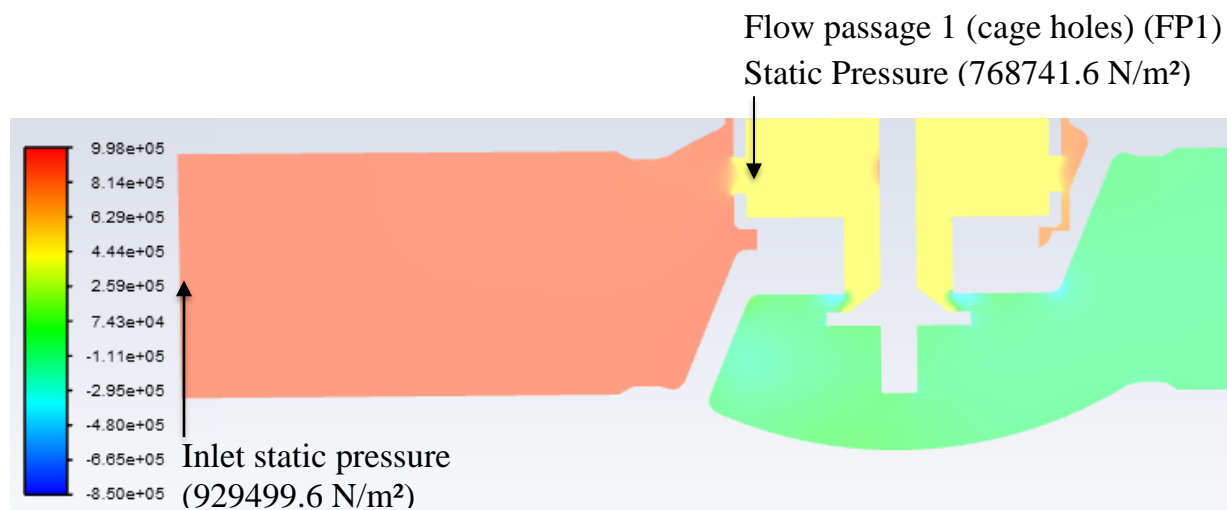


Figure 5-1. Variations of Water Flow Pressure in the Baseline Control Valve

5.2. Analysis of local trim geometric Effects on local and Global CV

The results of the local geometric effects on the global overall flow coefficient for varying flow passages area sizes mentioned in the previous section have been presented here. The complex fluid flow characteristics within the vicinity of the trim flow passages has been qualitatively and quantitatively analysed. Figure 5.2 shows a mid section cut plane of the valve flow passages along the flow path, and the points at which the local flow parameters of pressure and velocity have been measured.

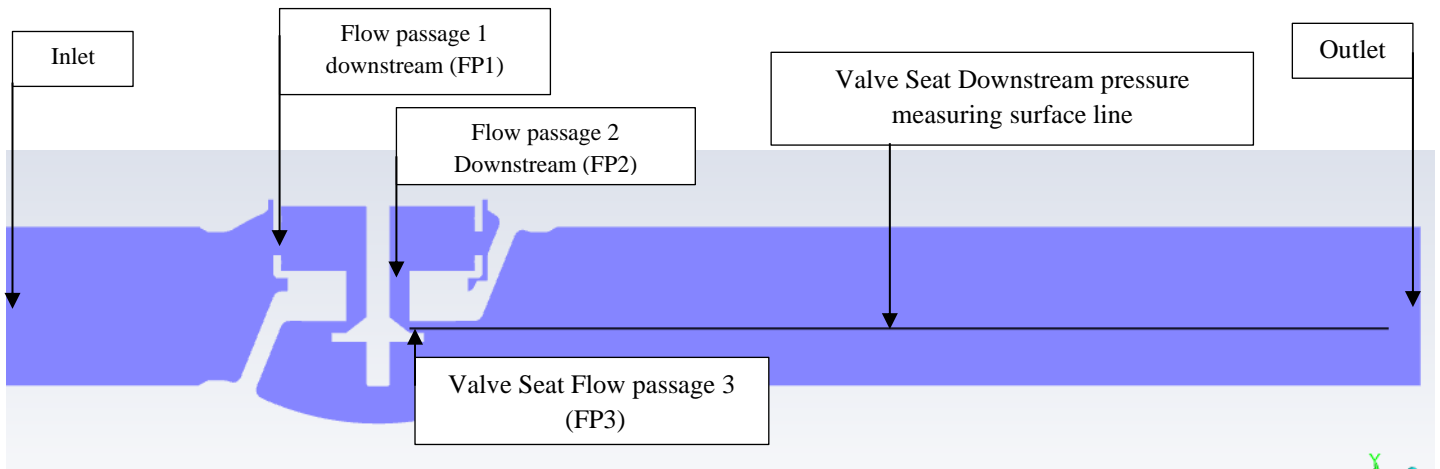


Figure 5-2. Positions of stages-flow passages along the valve flow path Flow passage positions and flow parameter measuring points.

As discussed in the previous chapter, the valve plug seat forms the controlling point of the fluid, and current performance deterministic methodologies are only focused on the flow field characteristics downstream of the valve plug. Figure 5-3 shows the variations of static pressure downstream of the valve seat. It can be seen that the pressure structure forms a typical structure that is synonymous with flow passing through a constriction, where there is pressure loss at some point downstream of the restriction as the velocity increases and satisfying mass conservation. Furthermore, the pressure can be seen to recover and stabilise to a non fluctuating constant pressure that is dependent on the outlet pressure conditions. However later on in this section the pressure profile characteristics along the entire flow path will be presented.

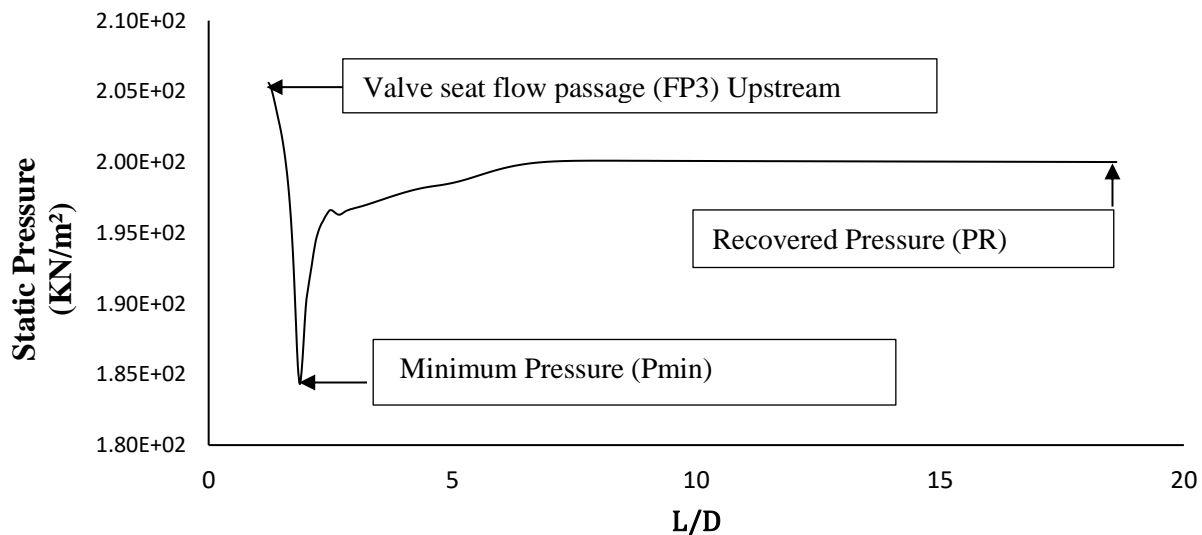


Figure 5-3. Variations of Static Pressure Upstream and Downstream of The Valve Seat

5.2.1. Mesh Independence Tests

From the discussions carried out in chapter 4, the optimal mesh elements number of 1.02 million elements were qualitatively acknowledged that they can predict the flow features with reasonable accuracy were used for this and further analysis in this work.

5.2.2. Benchmark Tests

A critical step that is particularly important when undertaking numerical investigations is the benchmarking of the results. Effective benchmarking requires direct comparison of results obtained from the numerical model with experimental results under similar flow conditions to confidently authorise that the numerical model accurately represents the physical model. Figure 5-4 shows the schematic diagram of the experimental test loop and physical test rig arrangement under which the experimental tests were carried out. The flow loop consists of a test section of 2inch (50mm bore diameter pipeline and fittings made from stainless steel with a maximum operating pressure of 68 Bar. A centrifugal pump is installed for positive suction and connected to a water tank of 1m x 2m x 1m. The centrifugal pump's maximum operating pressure is 10 Bar (145 PSI), with an operating fluid temperature ranging from 10° C, to 120° C, and maximum flow rate of 570 USGPM. The centrifugal pump motor has a rating of 7.5 KW at 2950 RPM with an efficiency of 79%. The centrifugal pump outlet is connected to a DC powered electro – magnetic flow meter with a maximum working pressure of 10 Bar (150 PSI), with a maximum operating temperature of 50° C, and an operating flow rate ranging from 1.9 – 18.9 L/sec. There are two pressure tapings downstream and upstream of the valve connected to a differential pressure gauge with a measuring range of 0-1000 psi, and an accuracy of $\pm 0.5\%$. The flow rate is regulated through an integrated control system that varies the RPM of the centrifugal pump, and there is a flow throttling valve upstream of the flow meter and downstream of the test valve to finitely control the flow rate and for flow isolation purposes.

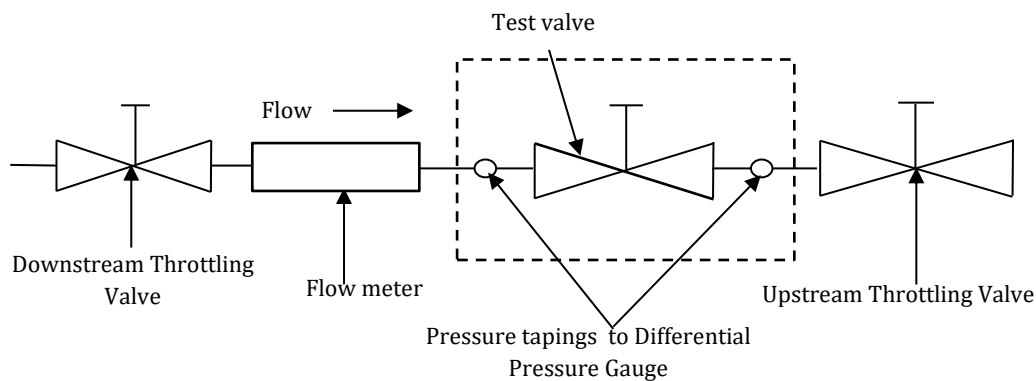
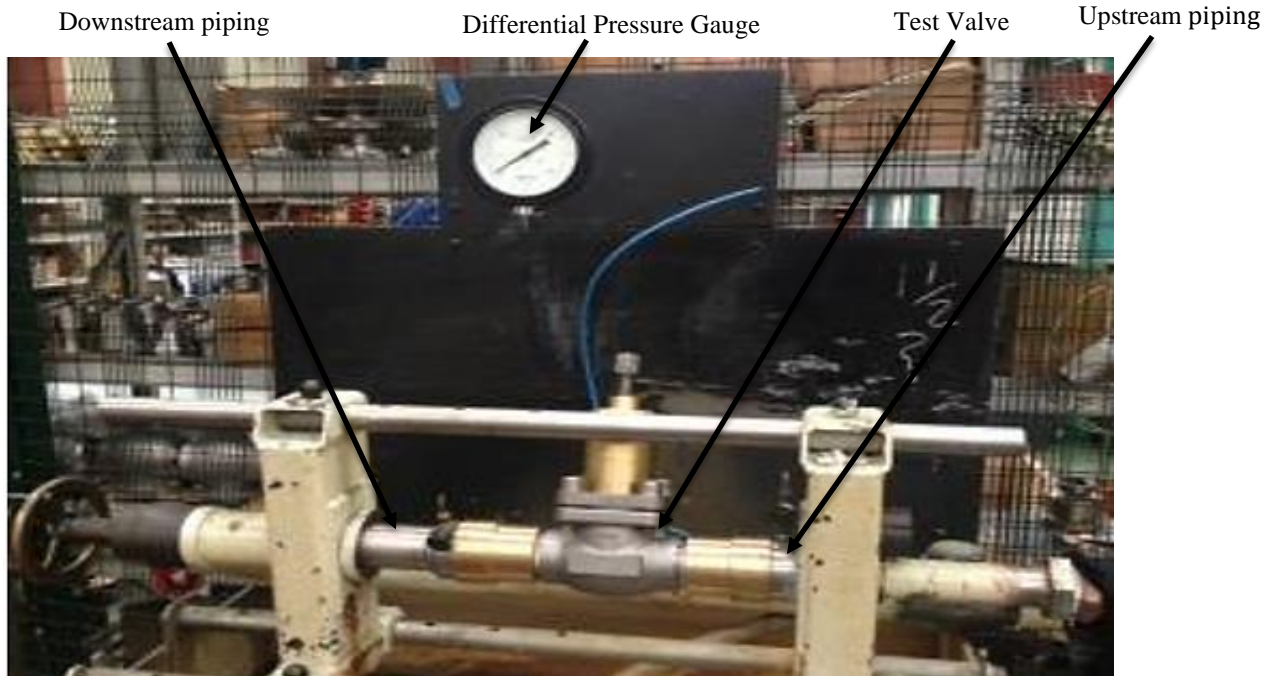


Figure 5-4: Actual Test Rig Arrangement and Schematic Representative Diagram of Test Loop.

In this current study, the numerical model has been validated against the experimental results for global pressure drop, flow rate, and flow coefficient. Table 5.1 shows the conditions that have been set for the numerical model. Furthermore, and it can be seen from the results presented, the results of the flow rate and valve coefficient (CV) are in good agreement with an average variation of less than 5%. Furthermore, figure 5.5 depicts the variations of overall pressure drop across the control valve for both CFD and experimental results. The results are in good agreement, and on that basis, the CFD model has been confidently deemed a valid and appropriate model that

accurately represents the physical model of the control valve. This model has thus been used for further analysis throughout this study.

Table 5-1. Experimental and CFD Results Comparison

INLET PRESSURE	OUTLET PRESSURE	PRESSURE DROP	CV (CFD)	CV (EXPERIMENT)	% DIFFERENCE (CV)	FLOW RATE (CFD)	FLOW RATE (EXPERIMENT)	% DIFFERENCE (FLOW RATE)
(PSI)	(PSI)	(PSI)				(USGPM)	(USGPM)	
25	15	10	12.96	12.9	0.5	41	40.9	0.2
50	25	25	12.4	13	4.8	62	64.8	4.3
75	25	50	12.6	13	3	88.9	91.8	4.1

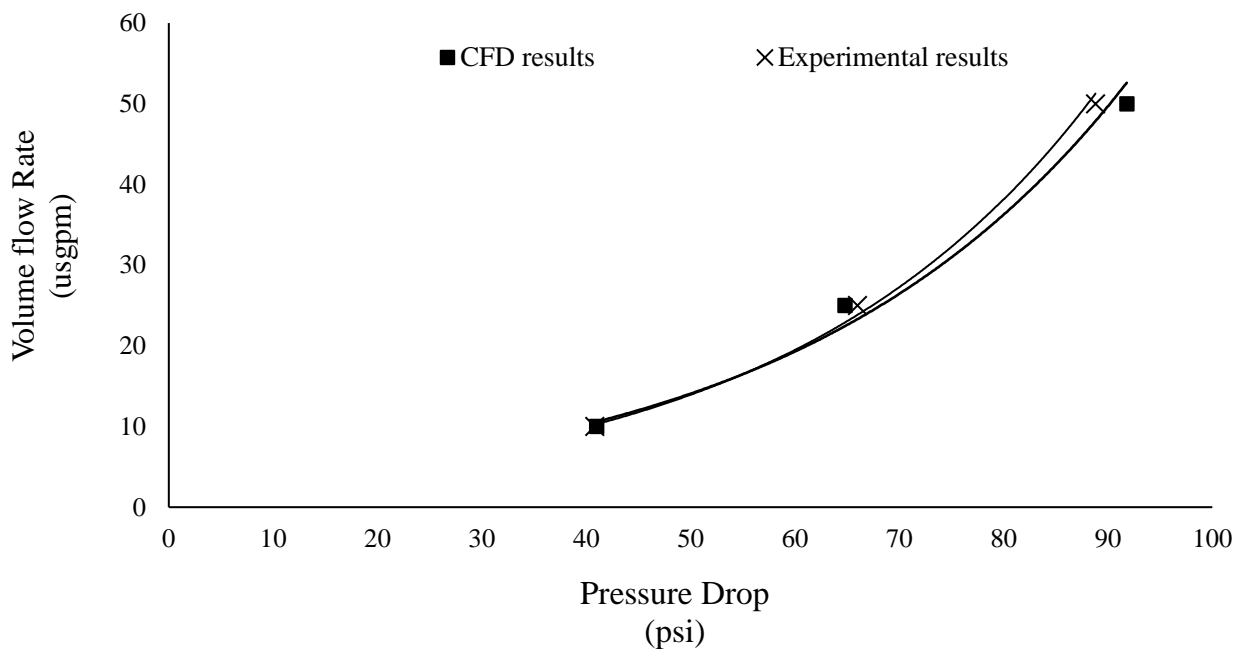


Figure 5-5: Validation of CFD Results and Experimental Results for Pressure Drop Across the Control Valve at Various Volumetric Flow Rates.

5.2.3. Valve Trim Geometric Effects on Local and Global CV

In order to understand the local geometric effects on the overall global pressure drop across the valve and CV, the local CV needs to be calculated at each flow path, and as discussed in the previous sections, the flow passages are presented in series along the flow path. The flow capacity of the trim consisting of 3 flow passages in series can be calculated as:

$$CV_{\text{Trim}} = \frac{1}{\sqrt{\left(\frac{1}{CV_{\text{FP}_1}^2}\right) + \left(\frac{1}{CV_{\text{FP}_2}^2}\right) + \left(\frac{1}{CV_{\text{FP}_3}^2}\right)}} \quad (5.2)$$

The control valve in this current study consists of 3 flow passage in the trim along the entire flow path from inlet to outlet. Hence it is anticipated that varying local flow passages sizes will exhibit varying flow behaviour and effects on the critical valve plug downstream velocity and pressure structure, and overall global pressure drop across the valve, and flow coefficient.

In order to understand the geometric effects on the flow structure, the flow areas of the trim flow passages must be analysed in detail. Hence it was seen fit to initially explore sensitivities of multiple flow passage areas along the entire flow path by means of the ratio of effective flow area passages as a function of their sequence of arrangement. Hence in order to investigate and quantify the geometric flow passage effective area effects on the flow and pressure structure within the vicinity of the flow passages as a function of the area ratios, a parameter has been developed (Flow Area Ratio (F_{AR}), which is defined as

$$F_{\text{AR}} = \frac{FA_i}{FA_{i+1}} \quad (5.3)$$

Where FA_i is the available flow area (in m^2) in the i th flow passage in the trim along the flow path. Hence, the flow area ratio F_{AR} is the ratio of the successive flow passages along the flow path. F_{AR} defines flow geometry and it may be used as a geometric parameter in the design process if we can establish how F_{AR} affects the local flow and pressure characteristics, and aid in the development of scalable hydrodynamic performance prediction models for multi flow passage trims through hydraulic or effective area representation for geometric similarities and corresponding hydrodynamic similarities on that basis.

In this current study, the flow areas of the flow passages have been varied within a minimum and maximum range that is manufacturable and maximum values that would not compromise the structural integrity of the components. The flow passage sizes have been varied at random intervals within the minimum and maximum range, specific values of intervals of size variations are not important, as any value of variation within the minimum and maximum range will yield similar proportionality.

Table 5-2 shows the variations of the flow passages effective flow areas at which this investigation was carried out. Where 4 different sizes of effective flow areas have been specified at random intervals within the maximum and minimum possible size constraints with respect to practical manufacturability and limiting stress integrity requirements. The specified effective flow area variations and sequence of arrangement with respect to size have been deemed sufficient to capture the sensitivities of the flow field.

Table 5-2. Variations of Flow Passages Effective Flow Areas, Flow Area Ratios, and Combined Flow Area Ratios Along the Flow Path

Flow Passage 1 (FP1) Effective Flow Area (m ²) (CONSTANT)	0.0006	0.000603	0.000603	0.000603
Flow passage 2 (FP2) Effective Flow Area (m ²)	0.00032	0.0004	0.00048	0.00066
Flow Area Ratio (FAR) ₁ (FA _i /FA _{i+1}) =(FP2/FP1)	0.52	0.43	0.8	0.92
Flow passage 3 (FP3) Effective Flow Area (m ²)	0.00027	0.00030	0.00033	0.000377
Flow Area Ratio (FAR) ₂ (FA _i /FA _{i+1}) =(FP3/FP2)	0.86	0.75	0.68	0.57
Outlet (Similar to Inlet) Effective Flow Area (m ²)	0.002255	0.002255	0.002255	0.002255
Flow Area Ratio (FAR) ₂ (FA _i /FA _{i+1}) =(Outlet/FP3)	0.12	0.13	0.14	0.17
Combined Flow Area Ratio (C _{FAR}) =[(FAR) ₁ × (FAR) ₂ × (FAR) ₃]	0.0555	0.0668	0.0784	0.104

Figure 5.6 Depicts the graphical representation of the 3 flow passage’s effective flow areas and flow area ratio variations as presented in table 5-2 at which this investigation was conducted.

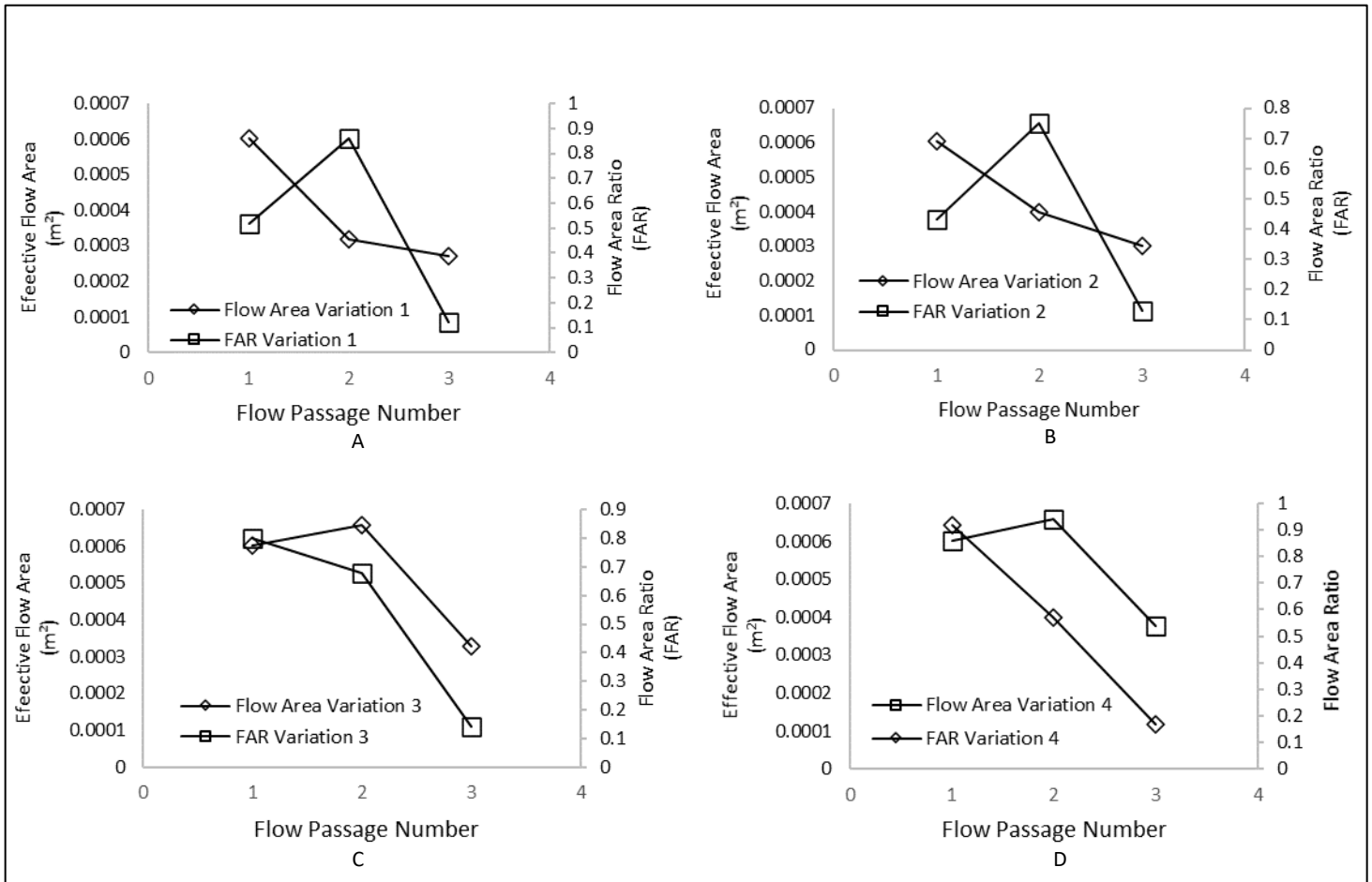


Figure 5-6-Depiction of Flow Passage’s Effective Flow Areas and Flow Area Ratio Variations.

Due to the multiple number of flow passages, the combined effects of the different flow area sizes on the flow and pressure structure must be understood, hence, a parameter that encompasses the multiple flow area ratios along the flow path has been developed (Combined Flow Area Ratio (CFAR), and it is shown in table 5-2 above and is defined as

$$C_{FAR} = AR_i \times AR_{i+1} \tag{5.4}$$

Figure 5.7 shows the variations of the global pressure drop across the valve as a function of the combined flow area ratios of the three flow passages at 4 different combined flow area ratios along the entire flow path at a mean velocity of 3m/sec flowing through the valve. Through multiple regression, It can be seen that the differential pressure drop across the valve varies linearly with the combined flow area ratio (CFAR). It can be seen that a low combined flow area ratio (CFAR) corresponds to a low differential pressure across the valve and vice versa. The results of this parameter characterization indicates the significant effects of the pattern of multiple flow passage arrangement along the entire flow path on the global differential pressure. The results obtained of these characteristics are very important finding as they will be used to develop the prediction and optimization tools as will be presented in the following chapters

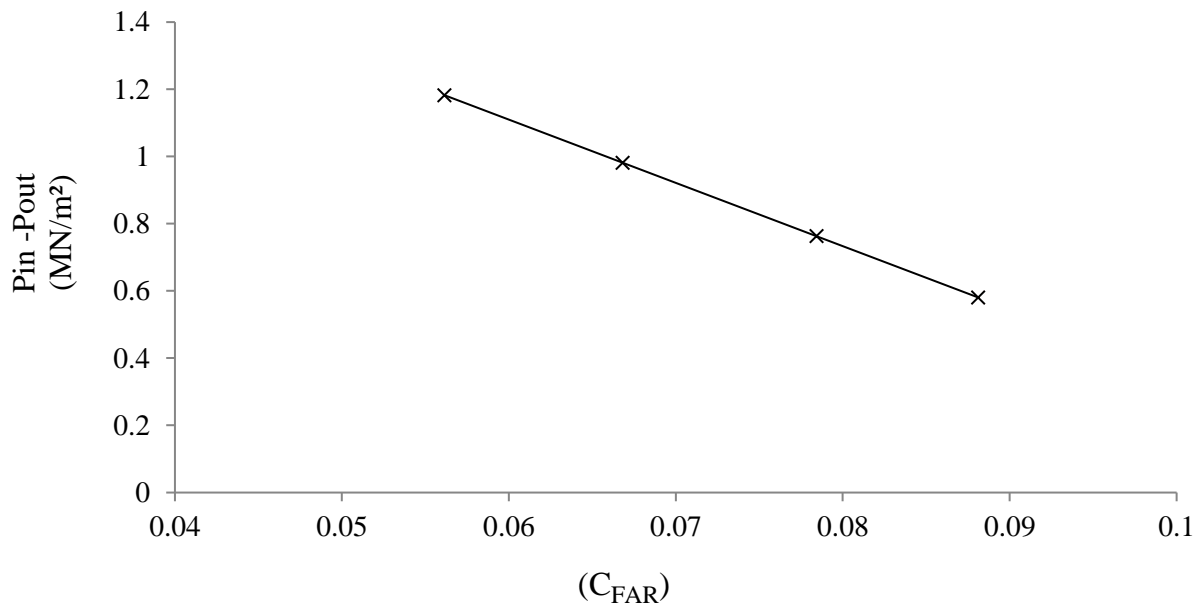


Figure 5-7. Variations of Global Pressure Drop Across the valve for Various Sequential Flow Passage Area Ratios.

Figure 5.8 shows the variations of the trim flow capacity with respect to variations of the trim flow passages combined flow area ratio (CFAR) with a mean velocity of 3m/sec flowing through the valve. It can be seen that the flow capacity varies linearly as a function of the combined flow area ratio (CFAR). Furthermore, the flow capacity of the trim increases as the combined flow area ratio increases, and this is attributed to larger flow passage areas being presented to the flow. Computational Fluid Dynamics thus predicts the local trim pressure drop and flow capacity and the inherent global overall flow capacity of the control valve with 95% accuracy as determined in the benchmark tests.

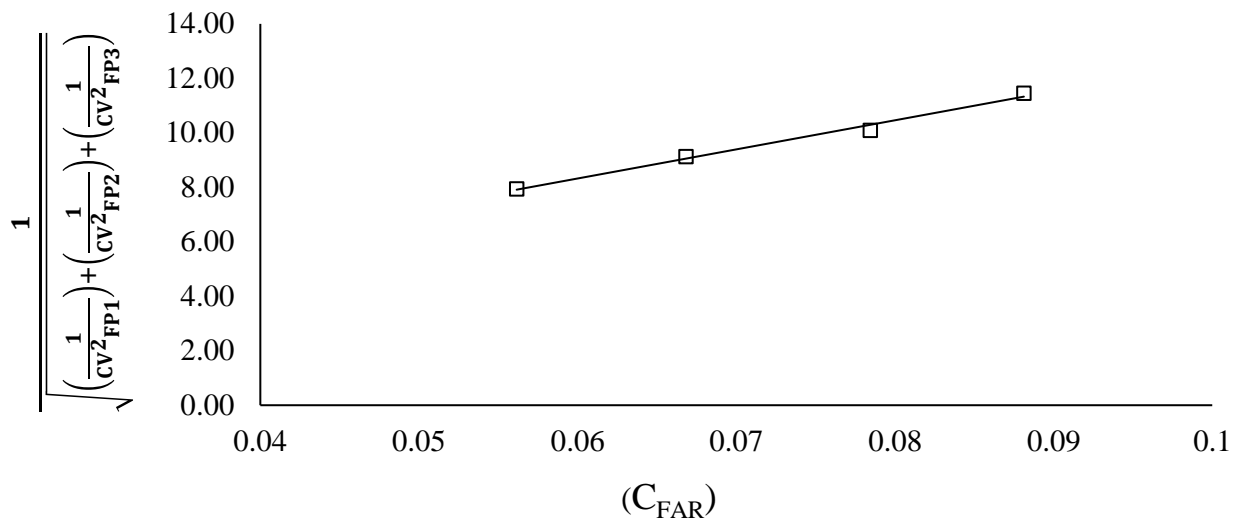


Figure 5-8 Variations of Trim Flow Capacity for Various Sequential Flow Area Ratios (C_{FAR})

Having established the local flow passages combined flow area effects on the global CV where the local combined flow passage area is indicative of significant effects on the global CV. However, the effects of an individual flow passage flow area on the local flow and pressure structure upstream and downstream of the flow passage must be known to deduce quantifiable relations for which the flow and pressure structure at each flow passage can be substantiated as a function of the individual flow passages effective flow areas. Hence, to quantify the effects of a single flow passage effective flow area on the local CV of that flow passage, CFD simulations were carried out for 10 different effective flow areas and the CV was calculated based on the resulting pressure drop at a constant inlet velocity of 2m/sec.

5.3. Analysis of Local and Global Geometric and Flow Parameter Correlations

In order to understand the complex effects of geometric flow area interaction on the flow structure within the vicinity of the trim and their global contributions, the geometric and flow correlations must be determined and understood in detail. The significance and importance of the trim flow passage effective area sizes and their combined influence on the local and global flow structure and pressure structure has been discussed in the previous sections. As discussed in the previous section, the pressure structure downstream of the valve seat forms the reference on which a control valve's hydrodynamic performance is measured. Hence, in order to quantify the extent of the pressure structure within the vicinity of the valve seat flow passage, a new parameter has been developed which is the differential pressure ratio (DPR) which is defined as follows

$$D_{PR} = \left(\frac{P_{i+1}}{P_i} \right) \quad (5.5)$$

Where P_i is the local average static pressure upstream of the i th flow passage along the valve flow path, and $(P_i + 1)$ is the average static pressure downstream of the i th flow passage, respectively. The developed parameters of (differential pressure ratio (D_{PR}), (flow area ratio (F_{AR}), and (combined flow area ratio (C_{FAR}) have been discussed in detail in this section. Furthermore, the parameters stated above have effectively only quantified the significant effects of the combined flow areas for which a discrete value has been characterised with the system CV, and global pressure. The parameter characterization and results from the previous sections have provided important information on which basis further investigations have been carried out in this section. Hence, investigations have been carried out in this section to determine explicit effects of the individual flow passages geometric flow areas on the flow and pressure structure at each flow passage, and culminative effects on the valve seat upstream and downstream flow and pressure structure.

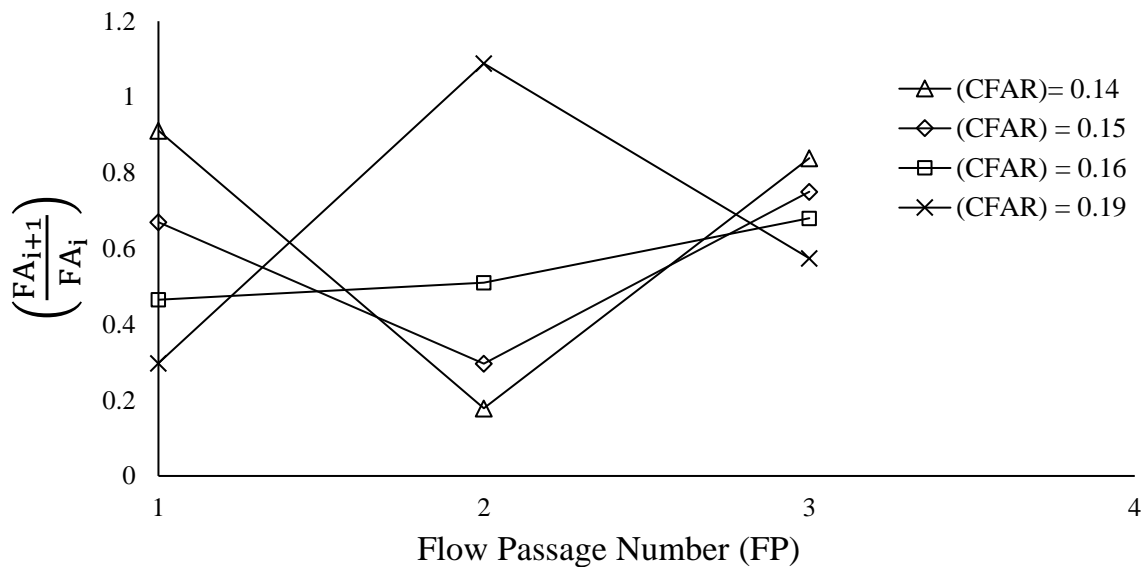
5.3.1. Effects of Flow Passage Areas on Local Pressure Structure

To analyse the effects of the flow passage areas on the pressure structure downstream of the valve seat entrance, a mean inlet velocity of 3m/sec has been prescribed for this investigation. Table 5.3 shows the range of the flow passages effective flow diameters from which the flow areas have been determined, and as discussed in the previous chapter, the range of flow diameter variations has been constrained by the valve size, manufacturability, and stress structural integrity. However geometric and dynamic scalability has been made possible through the developed hydrodynamic flow characteristic interrelations.

Table 5-3. Variations of Flow Passages Diameters

	Effective Flow Diameter (mm)			
	8	10	12	14
Cage Holes (FP1)	8	10	12	14
Cage/Stem Flow passage (FP2)	20	23	25	29
Valve Seat Flow passage (FP3)	18.8	19.5	20	22

As discussed in the previous sections, the control valve in this study consists of 3 flow passages within the trim, the valve inlet is the first point of flow entry into the valve, and hence it forms the first flow area ratio with the trim first flow passage (FP1). Figure 5.9 shows the variations of the flow passage area ratios along the valve flow path, and for reference purposes the flow area ratios are characterized by the combined flow area ratio (CFAR). It can be seen in Figure 5.9 that the flow area ratios form a wide range of combinations providing an exhaustive scope through which quantitative and qualitative investigations can be carried out.

Figure 5-9: Flow Area Ratio (F_{AR}) Variations Along the Valve Flow Path

5.3.2. Effects of Effective Flow Passage Areas on Local Flow Passage Differential Pressure:

The pressure structure downstream of the valve seat in the direction of flow with regards to pressure magnitude at the vena contracta is the reference parameter on which the hydrodynamic performance of a control valve is measured. In this current study the effects of the flow areas along the flow path on the vena contracta pressure have been quantitatively investigated. To quantify the effects of the local geometric flow passage areas on the vena contracta pressure, simulations have been carried out for 4 different flow path configurations of flow areas along the flow path at a constant velocity of 3m/sec.

Table 5.4 shows how the flow passage effective flow areas have been varied with regards to variations in the flow diameters, in this current study flow passage 1 (FP1) diameter has been held constant at 12mm while flow passage 2, and 3 have been varied as shown.

Table 5-4: Variations of Flow Passages Diameters

	Effective Flow Diameter (mm)			
Flow Passage 1 (FP1)	12	12	12	12
Flow passage 2 (FP2)	22	24	26	30
Flow passage 3 (FP3)	18.8	19.6	20.4	22

To quantitatively analyse the local flow passage geometric effects on the local pressure structure and vena contracta pressure, a parameter of area ratio has been used to define the changes in the flow passages area along the flow path and is defined as

$$F_{AR} = \left(\frac{FA_i}{FA_{i+1}} \right) \quad (5.6)$$

Where FA_i is the available effective flow passage area (in m^2) upstream of the i th flow passage along the flow path, and (FA_{i+1}) is the available effective flow passage area downstream of the i th flow passage along the flow path, respectively.

Hence, to analyse the effects of the flow passage area magnitudes and their pattern of size arrangement along the flow path on the differential pressure variations and ultimate effect on the vena contracta pressure magnitude downstream of the valve seat. Figure 5-10 shows the variations of local differential pressure ratios $\left(\frac{P_{i+1}}{P_i}\right)$ along the valve flow path at each flow passage as a function of the respective flow passage area ratios $\left(\frac{A_i}{A_{i+1}}\right)$ along the flow path for 4 different sequences of flow passages area sizes arrangements. It can be observed that the pattern and sequence of the flow area ratios along the flow path has a significant effect on the vena contracta pressure magnitude, it can be seen that a flow area ratio $\left(\frac{A_i}{A_{i+1}}\right)$ of 1.2 at flow passage 3 (FP3), with a corresponding differential pressure ratio $\left(\frac{P_{i+1}}{P_i}\right)$ of 0.4 results in a differential pressure ratio $\left(\frac{P_{i+1}}{P_i}\right)$ of 0.026 at the vena contracta. On a scale of 0 to 1, a differential pressure ratio close to 0 indicates a significantly low pressure at the vena contracta and a differential pressure ratio close to 1 signifies a higher pressure at the vena contracta. It can also be seen that a flow area ratio $\left(\frac{A_i}{A_{i+1}}\right)$ of 1.74 at flow passage 3 (FP3), with a corresponding differential pressure ratio $\left(\frac{P_{i+1}}{P_i}\right)$ of 0.53 results in a differential pressure ratio $\left(\frac{P_{i+1}}{P_i}\right)$ of 0.6 at the vena contracta which signifies a high pressure at the vena contracta. The desirable operating region is also shown in figure 5-10 with regards to the effective flow area ratios and arrangement of the flow passages, which are conducive in resulting in a desirable pressure at the valve seat that is higher than the fluid vapour pressure. This characterisation method is very useful for the designer in that it provides an explicit local map of the pressure structure along the flow path of a multi-stage trim in a valve as a function of the flow passages effective flow area magnitudes and their sequence of arrangement.

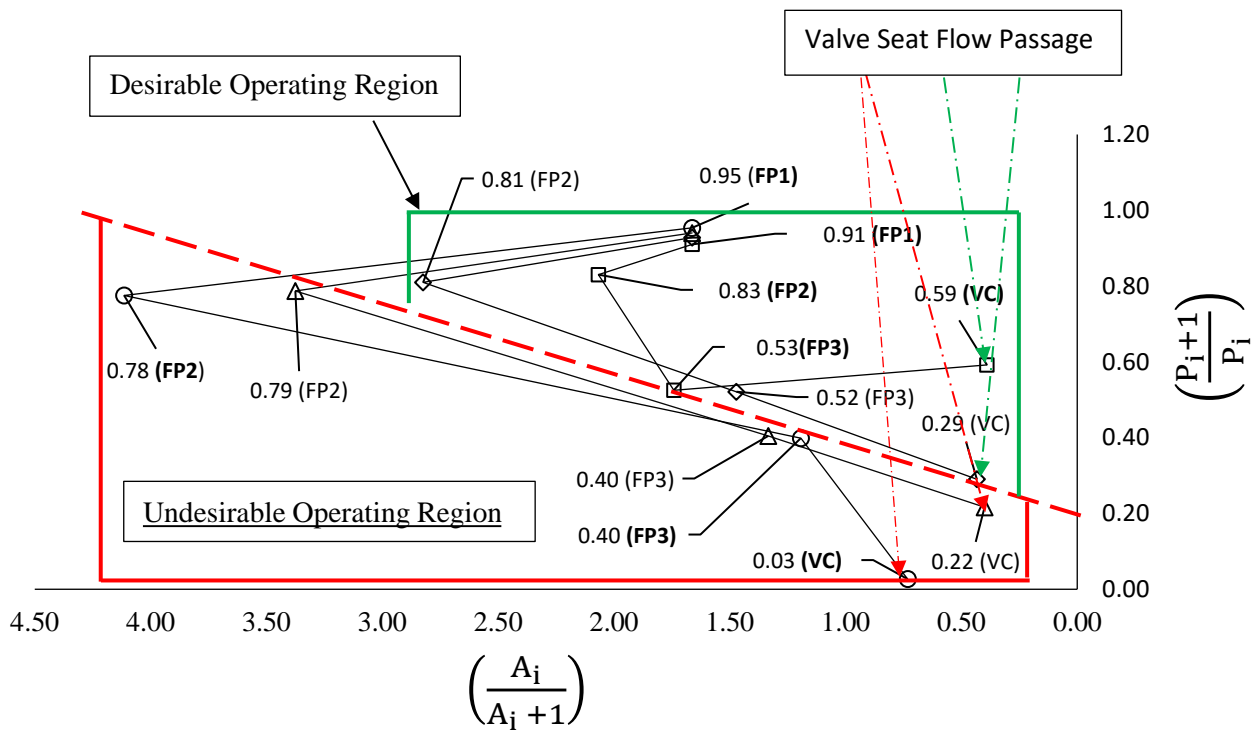


Figure 5-10. Differential Pressure Ratio Variations Along the Flow Path w.r.t Flow Passage Area Ratio Variations.

5.3.3. Effects of The Global Pressure on the Extent of Cavitation within The Vicinity of the Multiple Flow Passages Along the Flow Path

As discussed in the previous sections, the valve plug and seat flow passage at which the fluid is regulated is the reference flow passage at which the hydrodynamic performance of a control valve is determined. To further understand the pressure structure downstream of the valve seat, the effects of the global differential pressure must be understood. As discussed in detail in Chapter 3, The ISA-75-01-01 Standards methodology of predicting the hydrodynamic flow conditions of maximum allowable flow rate, and maximum allowable differential pressure relates the critical pressure ratio factor (F_F) multiplied by a constant vapour pressure (P_v) subtracted from the inlet pressure as a function of the pressure recovery factor (F_L) which accounts for the differential pressure at critical choked flow conditions. However, as discussed in chapter 3, the fluid pressure recovery factor is determined experimentally for specific valve type trims for which the data is currently published.

The fluid pressure recovery factor is not geometrically scalable, and hence it is not valid for control valve trims outside the scope of the specific trims published in the present available literature. Hence the effects of the differential pressure needs to be investigated to facilitate the development of a scalable prediction model.

The outlet pressure has substantial contributions to the pressure structure downstream of the valve seat and plug flow passage, and hence it is prudent to investigate the effects of the outlet pressure on the hydrodynamic performance of the control valve.

The global differential pressure across a control valve is simply the outlet pressure subtracted from the inlet pressure ($P_{in} - P_{out}$) where a similar differential pressure is possible for a finite combination of inlet and outlet pressures. This is of significance because it has been observed that the outlet pressure has significant effects on the pressure structure downstream of the valve seat flow passage or the flow passage upstream of the outlet, in this current work, a global differential pressure ratio parameter (G_{DPR}) has been developed, and which is defined as

$$G_{DPR} = \left(\frac{P_{OUT}}{P_{IN}} \right) \quad (5.7)$$

Where (P_{OUT}) is the pressure at the valve outlet, and (P_{IN}) is the inlet pressure. To quantify the global differential pressure and local pressure structure characteristics, the cavitation number at each local flow passage was characterized with the global differential pressure ratio. The cavitation index σ is expressed as

$$\sigma = \left(\frac{P - P_v}{0.5 \rho v^2} \right) \quad (5.8)$$

Where P is the inlet pressure to the flow passage, P_v is the fluid vapour pressure, and v is the mean velocity at the given flow passage. Figure 5.11 shows the variations of the cavitation number at all the local flow passages (FP1), (FP2), and (FP3) along the entire valve flow path as a function of variations of the global differential pressure ratio (G_{DPR}). The analysis was carried out at a constant global flow rate 250 USGPM, and at varying outlet pressures of 20, 40, 80, 110, and 150 PSI, with a corresponding similar global differential pressure of 259.7 at all outlet pressure variations. It can be seen in figure 5-11 that that local pressure structure significantly varies w.r.t the global differential pressure ratio as expected. At flow passage 3, which is the valve plug and

seat flow passage, for a global differential pressure across the valve of 259.7 and with a differential pressure ratio of 0.07, the cavitation number at flow passage 3 is 1.23, which indicates that substantial cavitation is taking place downstream of flow passage 3, and at the same flow passage 3 a global differential pressure of 259.7 with a differential pressure ratio of 0.13 the cavitation number is 1.38 which indicates that there is a potential of cavitation to take place with minimum severity. It is also observed that at flow passage 2 and 3, the cavitation number varies with variations of the global differential pressure ratio as a function of outlet pressure variations with a similar global pressure drop across the valve. Hence this characteristic is overly important, and specific consideration must be taken on how the differential pressure across the valve is referenced, such that the outlet pressure must be explicitly accounted for in the prediction of the local and global hydrodynamic performance of a control valve.

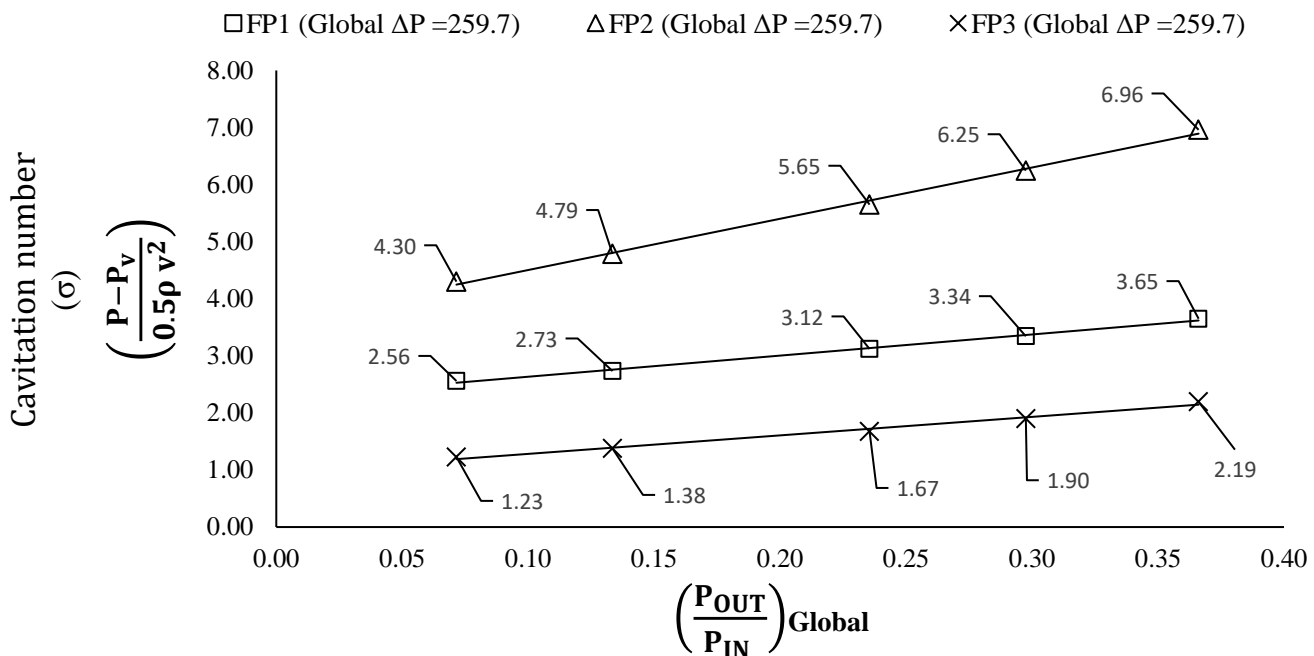


Figure 5-11: Variations of Local flow Passages Cavitation Number at Variations of Global differential pressure Ratio.

Furthermore, to qualitatively analyse the effects of the global pressure drop ratio as a function of the outlet pressure, the pressure structure within the vicinity of the valve plug and seat flow passage has been numerically analysed. The valve seat and plug presents the smallest flow restriction along the entire control valve flow path, and hence it was prudent to focus this analysis on this region. A numerical multiphase based mixture, cavitation model has been used to analyse the cavitation characteristics within the vicinity of the valve seat flow passage at the parameters presented in figure 5-10. The analysis was carried out at a constant flow rate of 250 USgpm to determine the extent of cavitation at the valve seat flow passage (FP3) for 2 different outlet pressure conditions of, (a) global pressure drop ratio of 0.07, where the inlet static pressure is 279.7 PSI, and outlet static pressure is 20 PSI with a global pressure drop of 259.7 PSI, and (b), at a global pressure drop ratio of 0.13, where the inlet static pressure is 309.7 PSI, and the outlet static pressure is 40 PSI with a global pressure drop of 259.7 PSI.

Figure 5-12 (a) shows the extent of cavitation within the vicinity of the valve seat and plug flow passage as a function of vapour volume fraction at a global differential pressure ratio of 0.07, with an inlet pressure of 279.7 PSI, and outlet pressure of 20 PSI, and where the cavitation index is 1.23 at a pressure drop of 259.7 PSI. It can be seen in that at (a) a vapour volume fraction forms a gradient ranging from area weighted average values of 0.8 to 0.3 from the upper wall of the flow passage with the vapour volume fraction gradient developing up to the mid-section of the flow passage. This indicates that there is substantial fluid phase change occurring at different extents through the vapour volume fraction gradient within the region shown. Within this region there will be subsequent formation of bubbles which will then implode as the pressure recovers above the fluid vapour pressure at the given temperature and causing cavitation to occur. With reference to the choked flow analysis carried in chapter 4, and as presented in figure 4-9, the extent of the vapour fraction distribution shown in figure 5-12 (a) is characteristic of choked flow conditions. Figure 5-12 (b) depicts the vapor volume fraction distribution at a global differential ratio of 0.13, with an inlet pressure of 309.76 PSI and an outlet pressure of 40 PSI, and where the cavitation index is 1.38 at a pressure drop of 259.7 PSI. the vapour volume fraction here, again forms a gradient ranging from 0.4 to 0.2 from the upper wall of valve seal flow passage with the volume fraction gradient extending only a short distance from the upper wall towards the mid-section of the flow passage.

This indicates that there will be bubble formation but within an exceedingly small region as compared to conditions depicted in figure 5-12 (a), and hence here the extent of cavitation is confined to a smaller region. The extent of cavitation with regards to intensity as a function of bubble characteristics, distribution and intensity has not been considered here. With reference again to the choked flow analysis carried in chapter 4, and as presented in figure 4-9, the extent of the vapour fraction distribution shown in figure 5-12 (a) is not characteristic of choked flow conditions, and it has been quantified that at this extent of vapor volume fraction distribution, choked flow will not be occurring.

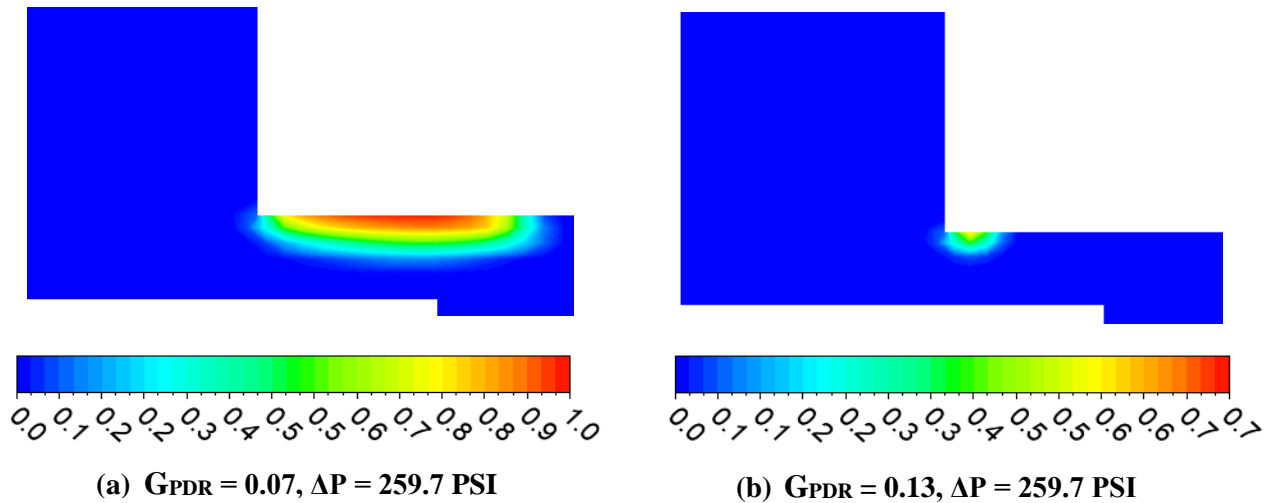


Figure 5-12: Variations of Vapour Volume Fraction at the Valve Seat Flow Passage at (a) 20 PSI Outlet Pressure, and at (b) 40 PSI Outlet Pressure.

5.4. Summary of Global Pressure Drop Effects and Outlet Pressure on Extent of Cavitation Within the Vicinity of the Multiple Flow Passages.

A detailed CFD based diagnostics of the global pressure drop effects on the local pressure structure and extent of cavitation within the vicinity of the multi-flow passage trim within a control valve. This study was carried out to highlight the significant differences in the extent of cavitation at a similar global pressure drop at a constant flow rate, where a similar global pressure drop occurs at a constant inlet flow rate and at any outlet pressure magnitude for which the inlet pressure magnitude is inherent of the constant inlet flow rate at a given outlet pressure magnitude. The diagnostics carried out in this study have revealed the following results:

- For given local trim geometric flow passages effective flow areas, a decrease in the outlet pressure at a constant flow rate for a similar inherent global pressure drop sees a reduction the flow passages cavitation index, meaning an increase in the potential for cavitation to take place.
- The vapour volume fraction and the region of occurrence within the vicinity of the valve seat flow passage which presents the smallest effective flow area along the flow path increases with reduction of the outlet pressure at a constant flow rate over a similar inherent global pressure drop. This means that the extent of cavitation and the region of occurrence increases, respectively.
- This study has highlighted that different local pressure characteristics can occur at a similar global pressure drop across the control valve at a given constant flow rate and varying outlet pressure magnitudes for a given geometric configuration. Hence, at a constant inlet flow rate and at various outlet pressure magnitudes, the global pressure drop remains the same, and this highlight the fact that the hydrodynamic performance of allowable pressure drop across the valve should be determined as a function of the outlet pressure magnitude. Hence, the limiting global pressure drop should not be generally based on a global pressure drop figure for which the local pressure characteristics will differ at different outlet pressure magnitudes given the inlet flow rate remains constant.

An example that further showcases the uncertainties that are related to the facts stated above is presented here. Based on the standards ISA -75.01.01 (60534-2-5), criteria, choked flow is occurring in a control valve when the following expression is satisfied as presented in in chapter 1 from the following expression:

$$\Delta P < F_L^2 (P_1 - F_F P_V) \quad (5.9)$$

Where F_L is the fluid pressure recovery factor, which is 0.85 as determined in chapter 3, P_1 is the inlet pressure, F_F is the critical pressure ratio factor, which is 0.943 for water, and P_V is the vapor pressure for water which is 2.45 KN/m² at the given operating temperature. Hence for the conditions represented by figure 5-11 (a) for an inlet pressure of 279.7 PSI, and where the outlet pressure is 20 PSI, the calculated pressure drop from equation (5.9) is 189 PSI, and this is lower than the actual pressure drop of 259.6 PSI, and hence the flow is choked as defined by the criteria

set out in equation 5.9. The prediction of choked flow from the criteria set out in equation (5.9) agrees to the local conditions depicted in figure 5-11 (a) where the vapor fraction structure has been verified numerically in chapter 4, to be characteristic of choked flow.

For the conditions presented in figure 5-12 (b), for an inlet pressure of 309.7 PSI, and with an outlet pressure of 40 PSI, the calculated pressure drop from equation (5.9) is 218 PSI, which is again less than the actual pressure drop of 259.7 PSI. From the criteria set out in equation (5.9), this indicates that the flow is choked. With reference to figure 5-12 (b), the vapour fraction distribution and extent is not characteristic of choked flow at the given pressure and flow conditions. Hence the choked flow prediction is not in agreement with the non-choking conditions depicted in figure 5-12 (b),

Hence, these inconsistencies present critical uncertainties in the accurate application and predictions of hydrodynamic performance characterises through existing standards, which do not explicitly account for the outlet pressure and its effects on the local flow and pressure structure. These findings have been used in the development of a prediction tool for the hydrodynamic performance of a multi-flow passage control valve.

5.4.1. Inlet Average Flow Velocity Effects on the Pressure Drop Ratio at the Valve Seat Flow Passage

To investigate the effects of the average global velocity on the pressure drop ratio at the local valve seat flow passage at varying upstream flow passage area ratios as discussed in the previous section. Varying mean flow velocities of 1, 2, 3, and 4 m/sec were chosen for the flow diagnostics. Figure 5-13 shows that a velocity of 1m/sec exhibits a pressure drop ratio ranging from 0.82 to 0.95 within the given combined flow passage area ratios (CFAR), and this indicates that the difference between the valve seat entrance pressure and the minimum pressure downstream of the valve seat is close to being similar and is substantially above the fluid vapour pressure. At a mean flow velocity of 4m/sec within similar combined flow passage area ratios (CFAR), the pressure drop ratio ranges from 0.02 to 0.6, with lowest pressure loss ratio of 0.02 indicating a minimum pressure close to the fluid vapour pressure. The results of the flow characteristic and relationships obtained in this section will form the basis on which the geometric, flow and pressure structure characterization will be formulated, and from which prediction models will be developed in the following section.

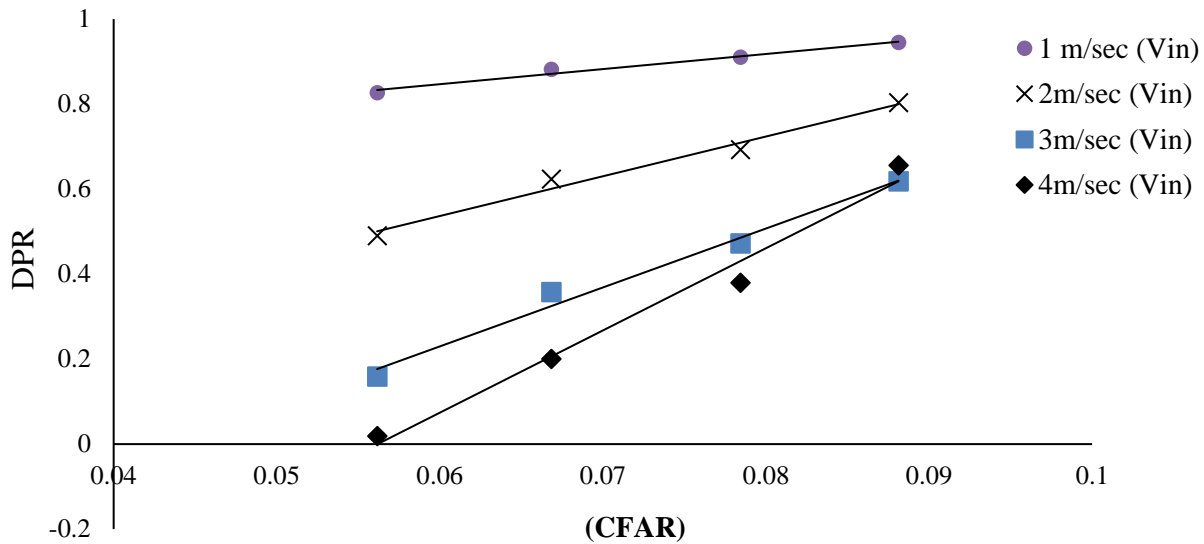


Figure 5-13: Variations of Differential Pressure Ratio at Varying Combined Flow Area Ratios (CFAR)

5.4.2. Effects of Flow Passage Effective Area Sizes and Sequence of Arrangement

From the information obtained in the previous section, it has been established that the flow passages along the flow path have a substantial effect on the flow and pressure structure within the valve. In the previous section the geometric flow passage area effects have been defined through the flow passages effective area ratios and their sequence of arrangement along the flow path. Furthermore, flow field inherent characteristics have been defined in the form of pressure ratios, however it is prudent to further scrutinize the geometric and flow field characteristics with regards to the actual pressure and velocity magnitudes within the vicinity of each flow passage along the entire flow path. Deterministic characteristics of independent geometric parameters and dependant pressure have been established in this section at a subjective flow rate of 135 Usqpm, and at arbitrary flow passages effective flow area magnitudes. To determine and quantify the effects of the flow passages effective flow area magnitudes and pattern of arrangement along the flow path on the local and global pressure structure, the resulting static pressure downstream of each flow passage has been plotted together with the corresponding flow coefficient at each flow passage.

Figure 5-14 (a) shows the velocity and pressure distribution within the vicinity of the valve flow passages at flow passage 1 (FP1) total effective flow diameter = 38.1mm, (FP2) effective flow diameter = 30.5mm, and (FP3) effective flow diameter = 25.4mm with water flowing through the valve at 148 Usgpm. The velocity distribution depicts a velocity magnitude of 19m/sec at flow passage 1 (FP1), and 12m/sec at flow passage 2 (FP2), and a velocity of 17m/sec is seen to occur downstream of the valve plug/seat here defined as flow passage 3 (FP3). Figure 5-14 (b) depicts the corresponding pressure distribution downstream of the flow passages along the flow path, where a static pressure of 41.2 psi is seen to occur downstream of flow passage 1 (FP1), and a static pressure of 33.2 PSI is seen to occur downstream of flow passage 2 (FP2), and a static pressure of 9.7 psi is seen to occur downstream of flow passage 3 (FP3) respectively.

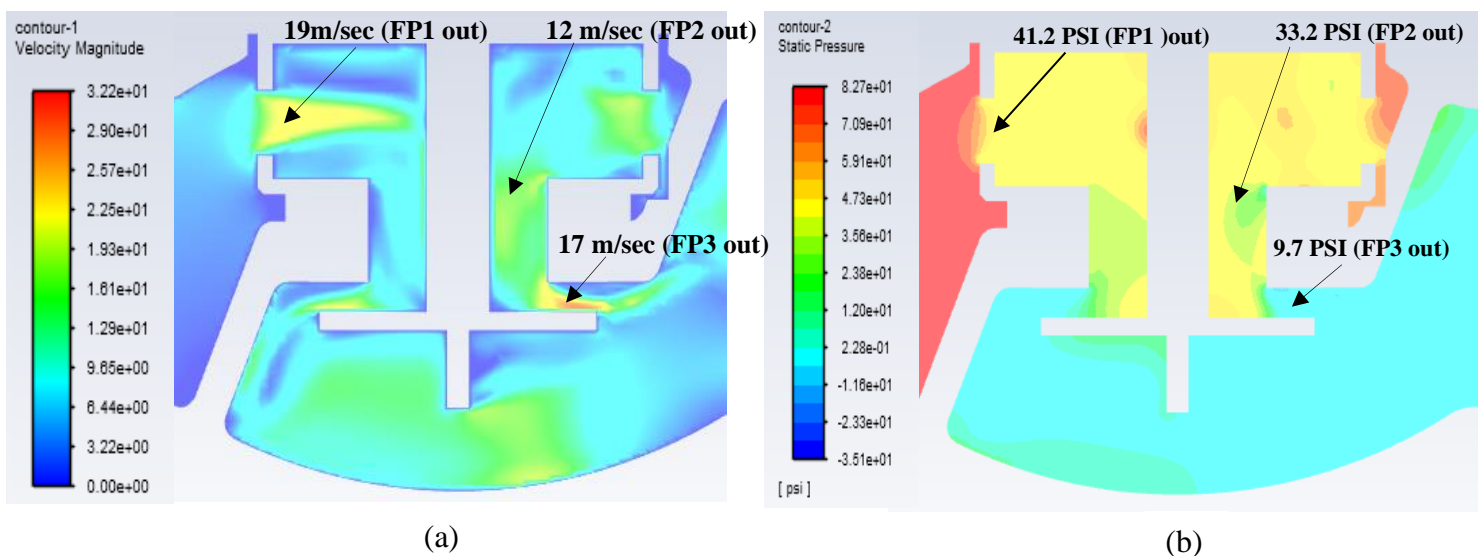


Figure 5-4: Variations of (a) Velocity and (b) Pressure, for Flow Passages Diameter FP1 = 38.1mm, FP2 = 30.5mm, FP3 = 25.4mm at flow rate of 148 Usgpm.

Figure 5-15 shows the velocity and pressure distribution within the vicinity of flow passage 1 (FP1) 12 holes on section plane normal to the direction of flow, it is much clearer to observe the complex flow field of velocity and pressure distribution where varying velocity and pressure magnitudes are experienced immediately downstream of each hole where the measurements of the velocity and pressure have been taken. The velocity distribution shows that the velocity is much higher in the 3 holes directly exposed to the flow in the inlet pipe chamber, with a velocity magnitude of

19m/sec, and a much lower velocity of 16.2m/sec is observed to occur in the holes confined to the narrow channel around the cage that exposes them to the flow. However, the average velocities for all the holes equate to the expected velocity for the total equivalent effective diameter of 38.1mm for 12 holes at 11mm diameters each. However, despite this phenomenon of slightly different velocities in similar hole size diameters, the average velocity for all the holes equates to the calculated velocity for the total effective area of the holes with excellent agreement when verified with the mass conservation expression:

$$P_1 A_1 V_1 = \rho_2 A_2 V_2 = \text{constant} \quad (5-10)$$

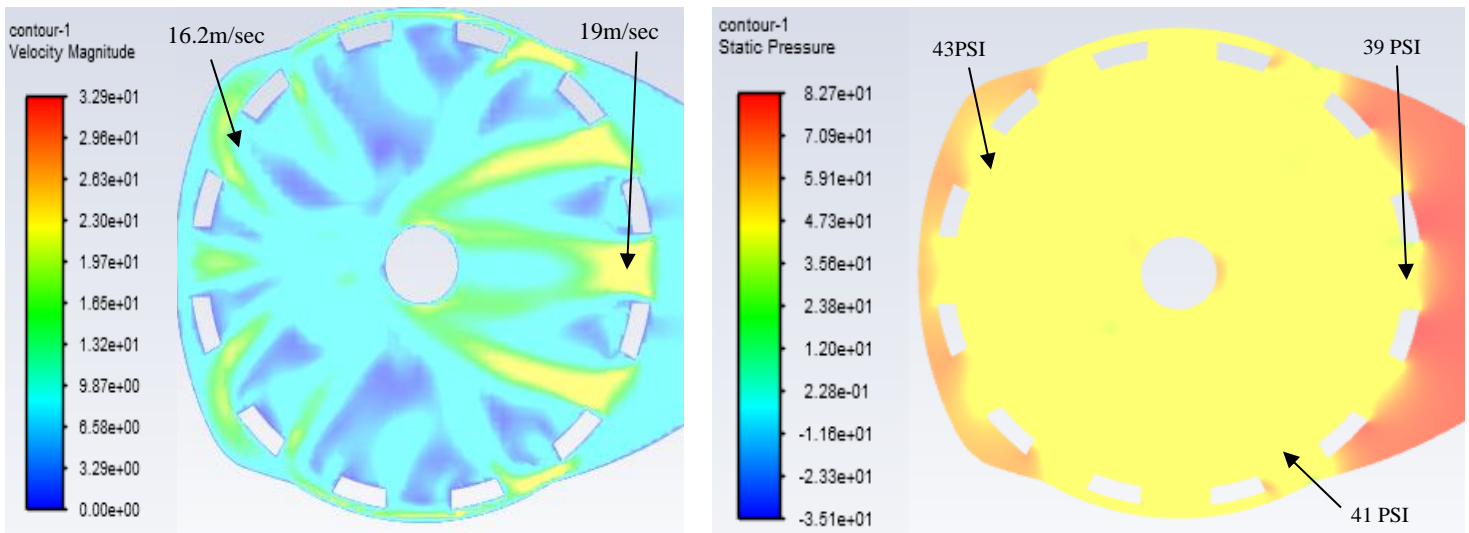


Figure 5-15: Variations of (a) Velocity and (b) Exit Pressure, for Flow passage 1 (FP1) 12 Holes of 11mm Diameter with Total Effective Diameter of 38.1mm at a Global Flow Rate of 148 Usgpm.

From the information obtained from the CFD analysis from which qualitative contour plots of pressure and flow variations have been represented in figures 5-14, and 5-15, there is need for quantitative representation of the data from the CFD study. To extract further detailed information on the complex flow field sensitivities to variations in the local passages effective flow areas along the entire flow path, the local differential pressure across each flow passage has been characterised with a local cavitation index (σ). The local cavitation index will provide information on the extent of the pressure structure with regards to whether there is potential for cavitating or non cavitating conditions within the local vicinity of the flow passages along the flow path.

Figure 5-16 depicts the variations of the differential pressure across each of the flow passages along the entire flow path, and the corresponding CV at each flow passage respectively, at flow passage 1 (FP1) total effective diameter = 38.1mm, (FP2) effective diameter = 30.5mm, and (FP3) effective diameter = 25.4mm with water flowing through the valve at 135 Usgpm.

The differential pressure profile along the flow path is the inverse profile of the actual pressure map downstream of each flow passage along the flow path. The differential pressure from the inlet and flow passage 1 (FP1) is 30.4 PSI, and with a corresponding CV of 24.7, and here the cavitation index is 2.88, which means there is no risk of potential cavitation, and this is verified from the static pressure contour plot in figure 5-14, where the average static pressure downstream of flow passage 1 (FP1) is 42 PSI, which is evidently above the fluid saturation pressure at the given operating temperature conditions. The differential pressure across flow passage 1 (FP1) and flow passage 2 (FP2) is 8.8 PSI, and with a corresponding CV of 45.9, and here the cavitation index is 6.5, and where the static pressure downstream of flow passage 2 (FP2) as presented in figure (5.14 b) is 33.2 PSI. The differential pressure at the valve seat/flow passage 3 (FP3) is 19.5, and the corresponding CV is 30.8, and with a corresponding cavitation index of 2.5, and where the corresponding downstream pressure is 9.7 PSI.

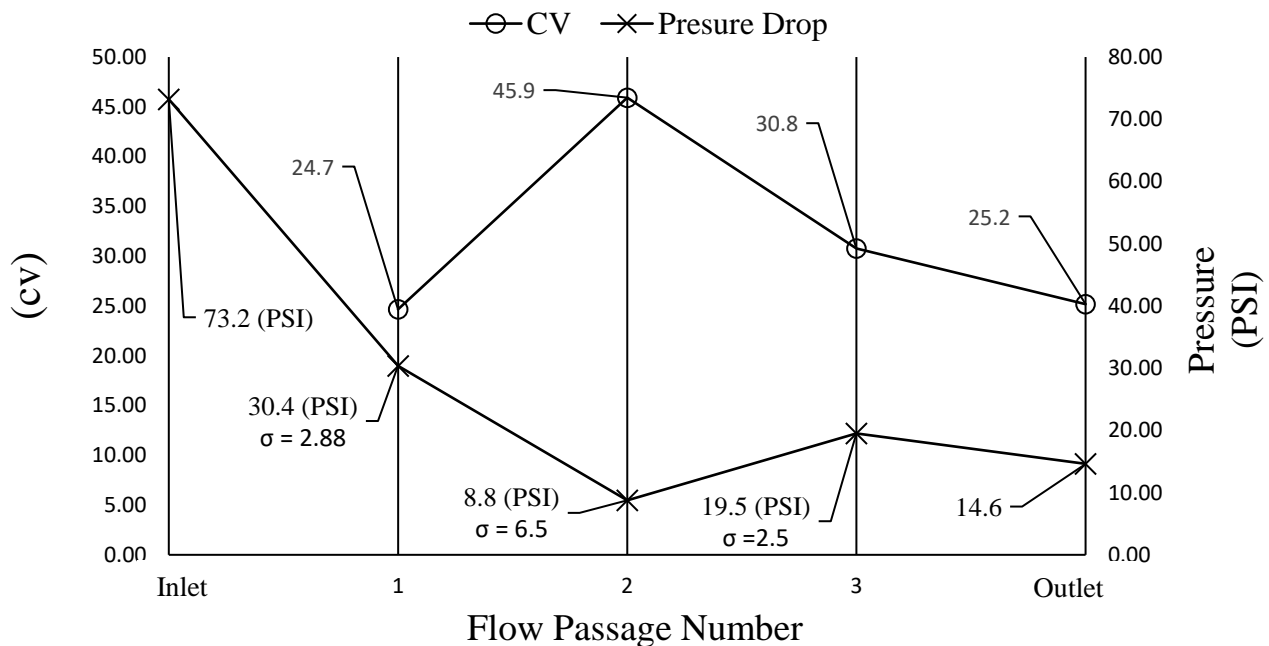


Figure 5-16: Variations of Differential Pressure across each Flow Passage and respective Local CV at for Flow Passages Diameter FP1 = 38.1mm, FP2 = 30.5mm, FP3 = 25.4mm at flow rate of 148 Usgpm.

To further evaluate the flow field sensitivities as a function of flow passages effective flow area magnitudes and sequence of arrangement along the flow path, figure 5-17 shows the variations of the differential pressure across each of the flow passages along the flow path and the respective CV at each flow passage. The results of the differential pressure at each flow passage and respective CV have been plotted at different flow passages effective flow areas and sequence of arrangement along the flow path that have been randomly selected. The total effective flow diameter of the 12 holes in the guide cage at flow passage 1 (FP1) is 26.4mm, the effective flow diameter of flow passage 2 (FP2) is 20.3mm, and the effective flow diameter of flow passage 3

(FP3) is 20.3mm. The differential pressure and CV variations have been plotted at constant flow rate of 148 Usgpm, similar to the flow rate at which differential pressure and CV variations have been plotted as show in figure 5-15 above. From figure 5-16, It can be observed that differential pressure from the inlet and across flow passage 1 (FP1) is 76.7 PSI, and with a corresponding CV of 15.52, and relative to the inlet pressure of 191.5 PSI, the inherent cavitation index is 2.68.

The differential pressure from flow passage 1 (FP1) and across flow passage 2 (FP2) is 50.1 PSI, and with a corresponding CV of 19.2, and relative to flow passage 1 (FP1) exit pressure of 76.7 psi, the cavitation index is 2.57. The differential pressure from flow passage 2 (FP2) and across flow passage 3 (FP3) is 50.1, and this is similar to (FP2) attributed to a similar effective flow diameter, the corresponding CV at flow passage 3 (FP3) is again similar to that at (FP2) at 19.2, and relative to flow passage 2 (FP2) exit pressure of 64.7 PSI, the inherent cavitation index is 1.57. The cavitation index of 1.57 at flow passage 3 (FP3) indicates that there is potential for the onset of, and severe cavitation occurring downstream of flow passage 3 (FP3) which in this case is the valve seat.

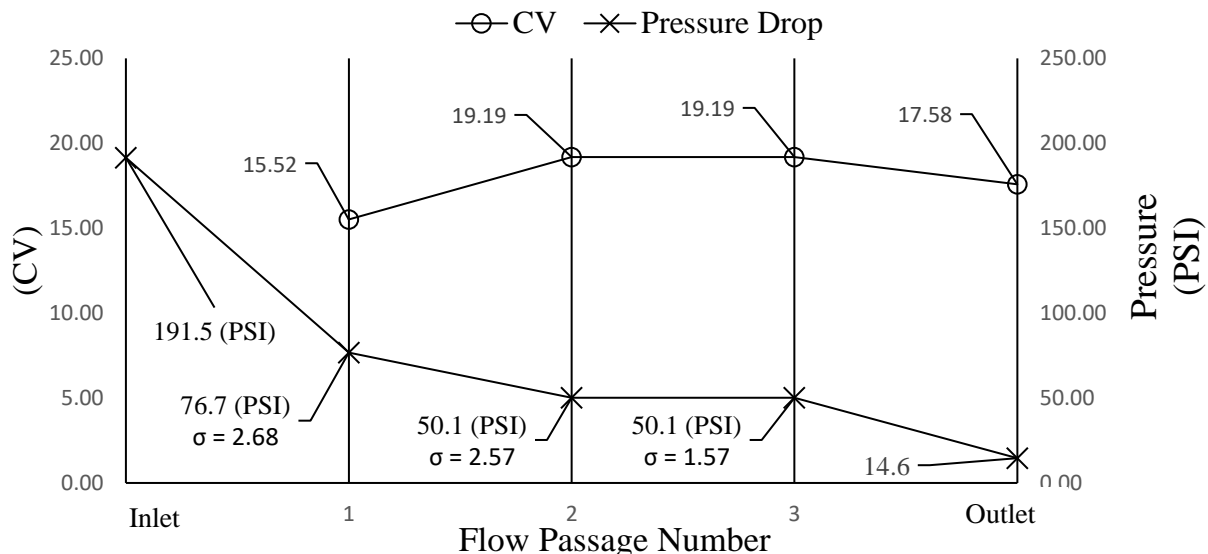


Figure 5-17: Variations of Differential Pressure across each Flow Passage and Respective CV for Flow Passages Diameter FP1 = 26.4mm, FP2 = 20.3 mm, FP3 = 20.3 mm at flow rate of 148 Usgpm.

To further explore the extent of the pressure structure downstream of the valve seat flow passage (FP3) that corresponds to a cavitation index of 1.57 and for which a value below 2 is a conservative indication of the potential for the onset of cavitation occurring. A CFD multiphase cavitation physical model similar to that implemented for the multiphase analysis presented in chapter 3 has been used in this study. Figure 5-18 depicts extent of the vapour volume fraction distribution within the vicinity of the valve trim, and an average volume fraction of 0.8 is seen to occur at the upper wall surface downstream of valve seat/plug flow passage entrance, which is defined as flow passage 3 (FP3) in this study, and the vapour volume fraction is seen to reduce gradually up to 0.2 at the mid-section of the flow passage. The vapour fraction distribution indicates areas where cavitation is taking place within the vicinity of the valve trim, and where the extent of cavitation is attributed to flow separation and scale of convective acceleration of the fluid as it enters the valve seat/plug flow passage.

The results in this study suggest that the cavitation index can be reliably referenced to determine the potential of cavitating or non-cavitating conditions.

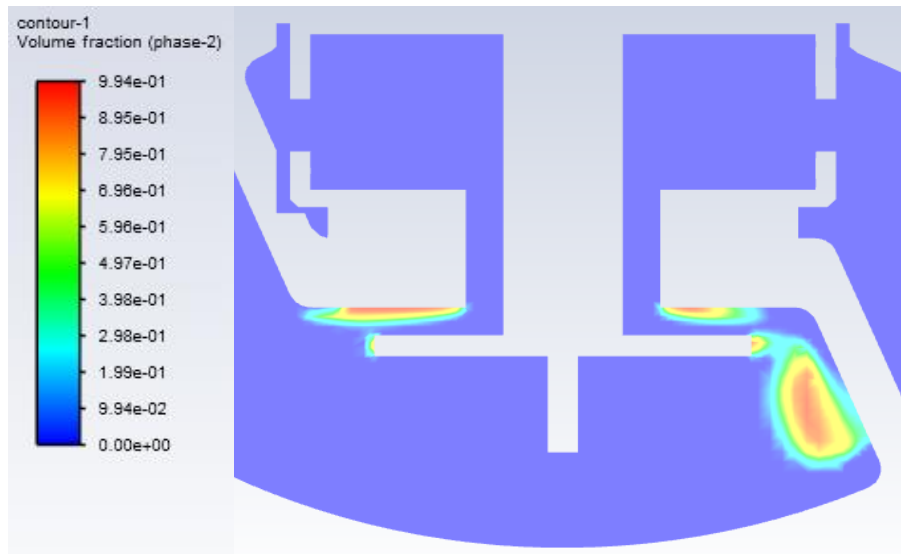


Figure 5-18: Variation of Vapour Volume Fraction Within the Vicinity of The Flow Passages, at Flow Passages Diameter FP1 = 26.4mm, FP2 = 20.3 mm, FP3 = 20.3 mm at flow rate of 148 Us/gpm.

From the information obtained from the investigations carried out in this study where the flow field sensitivities to the variations in the flow passages effective flow areas and their sequence of arrangement along the flow path. It is evident that there is a complex geometric and flow

interaction that is significantly non-linear with explicit interdependence of the flow and pressure structure on the pattern of arrangement of the flow passages effective flow areas as a function of magnitude. The flow passages effective flow areas along the entire flow path have a unified effect on the local and global flow and pressure structure within the valve. Hence, from the results in this study, it is only comprehensible within the scope of this work to map the entire flow path's flow and pressure structure. by initially defining desired global parameters of flow rate, CV, or differential pressure, and then varying the local flow passages effective flow areas to satisfy the known or desired global flow and pressure conditions. Furthermore, desired flow and pressure conditions can be specified locally, and from which global parameters that inherently satisfy these conditions can be predicted. The detailed information presented in this section has been used to develop prediction models as presented in the following section.

5.5. Prediction Models

Based on the geometric and flow parameter characterization results in this chapter, prediction models can be developed. Semi empirical prediction models of the following parameters have been developed

- For multiple stages or flow passages in series along a trim flow path, the local pressure drop across a single flow passage has been developed as follows:

From the definition of the flow coefficient CV which states that it is the rate of flow in gpm at 60 degrees Fahrenheit at a pressure drop of 1 PSI across the valve.

The definition of CV can be extended to account for a flow restriction or flow passage as the rate of flow of water in gpm at 60 degrees Fahrenheit at a pressure drop of 1 PSI across a flow restriction or flow passage with an effective area A and currently defined pressure loss coefficient K, which is expressed as follows

$$C_v = Q \sqrt{\frac{\rho}{\Delta P(62.4)}} = \frac{29.9d^2}{\sqrt{fL/D}} = \frac{29.9d^2}{\sqrt{K}} \quad (5.11)$$

Where 62.4 is water density in lb/ft³, and hence the effective flow area must be accounted as follows

$$29.9 d^2 = 38.08 \frac{\pi}{4} d^2 = 38.08A \quad (5.12)$$

Hence, the flow coefficient (CV) can be expressed as

$$CV = \frac{38.08 A}{\sqrt{K}} \quad (5.13)$$

The flow coefficient can also be expressed as follows

$$CV = \frac{Q}{\sqrt{\frac{\Delta P_{Net}}{SG}}} \quad (5.14)$$

Where Q is the volumetric flow rate, ΔP is the differential pressure across the valve, and SG is the specific gravity.

The Current local pressure loss coefficient defined as K accounting for the pressure loss or head loss across a flow restriction is expressed as

$$K = \frac{\Delta P}{0.5 \rho v^2} \quad (5.15)$$

The pressure drop across a flow restriction along a streamline is defined from the energy loss equation as follows

$$\Delta P = 0.5 \rho (V_1^2 - V_2^2) \quad (5.16)$$

By combining equation (5.15) and equation (5.16), the local pressure loss coefficient K can then be extended as follows

$$K = \frac{0.5 \rho (V_1^2 - V_2^2)}{0.5 \rho V_2^2} = \frac{(V_1^2 - V_2^2)}{V_2^2} \quad (5.17)$$

The local pressure loss coefficient can then be redefined as K_L in terms of losses associated with geometric flow restriction effective flow area as follows

$$K_L = \frac{0.5 \rho \left[\left(\frac{Q}{A} \right)_1^2 - \left(\frac{Q}{A} \right)_2^2 \right]}{0.5 \rho \left(\frac{Q}{A} \right)_1^2} = \left[\frac{A_1^2 - A_2^2}{A_1^2} \right] \quad (5.18)$$

Hence, combining equations 5-13 and (5.18), and integrating equation (5.14) the local pressure drop across a flow restriction within a multi-stage trim can be accurately predicted from the following developed expression:

$$\Delta P_{FP} = \left[\left(15852 Q_{FP} \left((SG) 38 A_{FP} \sqrt{\left(\frac{A_{Inlet}^2 - A_{FP}^2}{A_{Inlet}^2} \right)} \right)^{-1} \right) \right]^2 \quad (5.19)$$

Where ΔP_{FP} is the pressure drop (psi) across a flow passage (FP), (A_{INLET}) is the effective flow area of the control valve inlet, (A_{FP}) is the effective flow area at a given flow passage in (inch^2), (Q_{FP}) is the volumetric flow rate at the given flow passage in (m^3/sec). The number 15852 is a unit conversion factor from (m^3/sec) to (USgpm).

- The flow rate can be calculated with regards the specified pressure drop across a flow passage as a function of effective flow area by transposition of equation (5.19) from the following expression.

$$Q_{FP} = 0.0000631 \left[\sqrt{\Delta P_{FP}} \left((SG) 38 A_{FP} \sqrt{\left(\frac{A_{Inlet}^2 - A_{FP}^2}{A_{Inlet}^2} \right)} \right)^{-1} \right] \quad (5.20)$$

Where Q_{FP} is the volumetric flow rate in m^3/sec , 0.0000631 is the unit conversion factor from (USgpm) to (m^3/sec).

- The local flow passage flow coefficient (CV) can be calculated from the following expression

$$CV_{FP} = \left(\frac{1}{\left((SG) 38 A_{FP} \sqrt{\left(\frac{A_{Inlet}^2 - A_{FP}^2}{A_{Inlet}^2} \right)} \right)^2} \right) \quad (5.21)$$

- For a given number of flow passages along the flow path, and in this work the valve has 3 flow passages, and for a known flow rate and outlet pressure, and as a function of flow passages effective flow areas, the sequential pressure drop and upstream pressures at each flow passage along the flow path up to the inlet can be defined from the following expression.

$$P_{IN} = \left(\frac{(15852 (Q_{FP1}))}{(SG) 38 A_{FP1} \left(\sqrt{\frac{(A_{Inlet}^2 - A_{FP1}^2)}{A_{Inlet}^2}} \right)^{-1}} \right)^2 + \left(\frac{(15852 (Q_{FP2}))}{(SG) 38 A_{FP2} \left(\sqrt{\frac{(A_{Inlet}^2 - A_{FP2}^2)}{A_{Inlet}^2}} \right)^{-1}} \right)^2 + \left(\frac{(15852 (Q_{FP3}))}{(SG) 38 A_{FP3} \left(\sqrt{\frac{(A_{Inlet}^2 - A_{FP3}^2)}{A_{Inlet}^2}} \right)^{-1}} \right)^2 + \dots + P_{out} \quad (5.22)$$

- The valve overall global flow coefficient (CV) for the given number of flow passages and their effective flow areas can be defined from the following expression.

$$\left(\frac{1}{\sqrt{(CV^2) - 1}} \right) = \frac{1}{\left(\frac{(SG) 38 A_{FP1}}{\sqrt{\left(\frac{(A_{Inlet}^2 - A_{FP1}^2)}{A_{Inlet}^2} \right)}} \right)^2} + \frac{1}{\left(\frac{(SG) 38 A_{FP2}}{\sqrt{\left(\frac{(A_{Inlet}^2 - A_{FP2}^2)}{A_{Inlet}^2} \right)}} \right)^2} + \frac{1}{\left(\frac{(SG) 38 A_{FP3}}{\sqrt{\left(\frac{(A_{Inlet}^2 - A_{FP3}^2)}{A_{Inlet}^2} \right)}} \right)^2} + \dots \quad (5.23)$$

Figure 5-19 shows the disparity between the downstream pressure at each flow passage along the flow path calculated from the expression presented in equation (5.11), and the downstream pressure at each flow passage along the flow path obtained from the CFD results to approbate the applicability and adequacy of these semi-empirical geometric and flow parameter characterisation and relationships. It can be observed from figure 5-19 that the maximum discrepancy in the prediction model calculated static pressure results and the CFD static pressure results is 5%, where for example, the exit static pressure at flow passage 1 (FP1) calculated from the static pressure prediction equation (5.11) is 36 PSI, and the CFD exit static pressure prediction at flow passage 1 (FP1) is 34.4 PSI. Hence, the prediction models developed in this study emblemize the pressure and flow structure within a control valve as a function of the local geometric parameters discussed in the previous sections with assuasive accuracy, and this applies to the other developed prediction models. The unique and novel homogeneous characterisation of the geometric and flow parameters facilitate the mapping of the pressure distribution along the entire flow path for any given geometric and flow parameters. Furthermore, and most importantly, dynamic, and geometric scalability is applicable and valid through the prediction models.

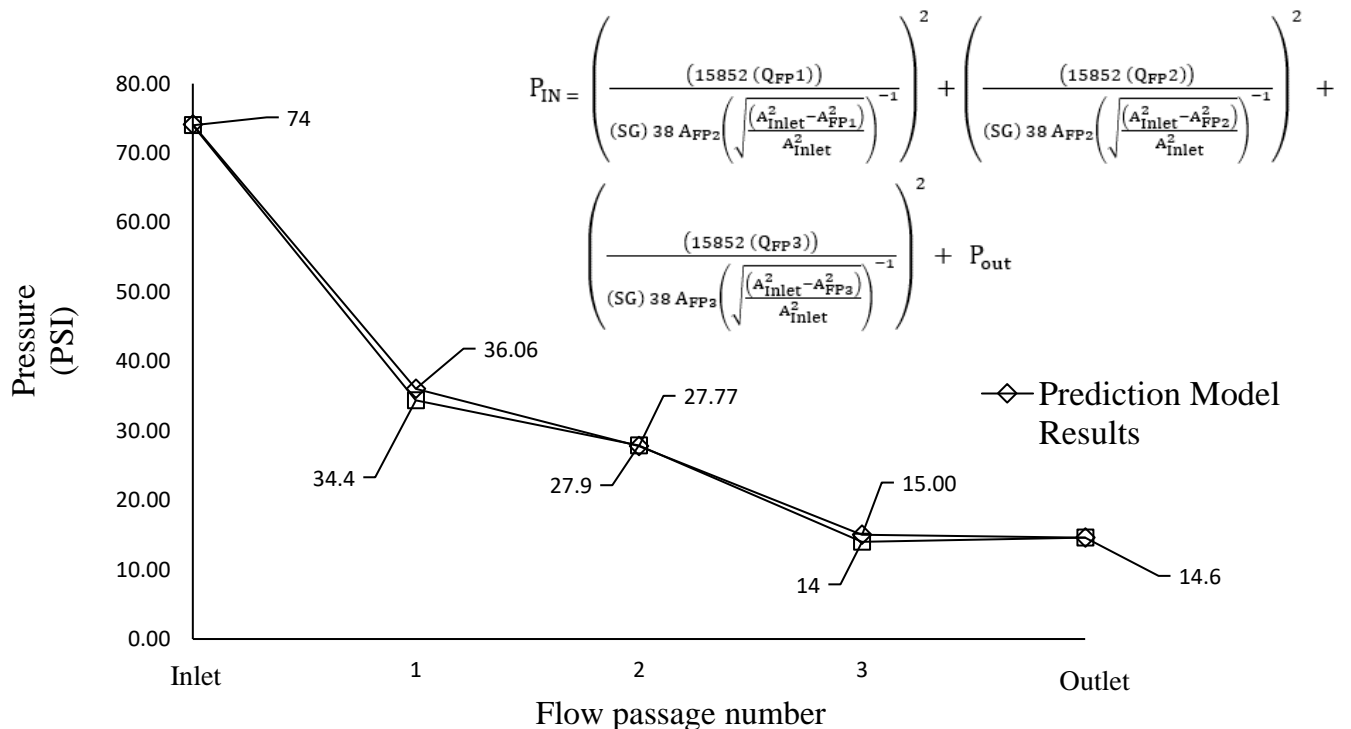


Figure 5-19: Variations of Prediction Model and CFD Results of The Flow Passages Downstream Exit Static Pressure.

5.6. Summary of the Control Valve Analysis

A comprehensive analysis of flow inside a control valve has divulged the following results:

- For a control valve with multiple flow passages, the local pressure and flow distribution is substantially sensitive to the sequence of arrangement of the flow passages along the flow path w.r.t the effective flow area magnitudes. The flow field pressure and flow structure is unique to the combined effects of the given flow passage's sequence of arrangement along the entire flow path with regards to their effective flow area sizes.
- The local pressure and flow structure within the vicinity of a flow passage can be closely predicted as a function of the flow passages effective flow areas.
- The unique parameter characterization allows for geometric and dynamic scalability through the developed pressure loss coefficient.
- Maximum allowable local and global flow rate and overall pressure drop can be computed directly from the flow passage effective flow areas along the entire flow path.

The details provided in this chapter with regards to the flow of water in a control valve and the developed prediction models provide a significant contribution to how control valves with single to multiple flow paths can be designed solely as a function of direct effective flow area. This eliminates ambiguity which can be introduced through selection and reference to geometric and flow parameter coefficients presented in current control valve design standards for which the empirical data is for a specific trim and will not be valid for any trim outside the scope of the available standards empirical data. Furthermore, there is inexhaustible published data on internal flow through restrictions where the burden of discernment of applicability is extremely difficult. Based on the information obtained in this chapter, the next chapter provides the details of the optimal design of a multi-stage trim control valve.

CHAPTER 6

OPTIMIZATION OF A MULTI-STAGE TRIM CONTROL VALVE

Optimization of a control valve hydrodynamic performance characteristic is critical with regards to accurate sizing for given process conditions. Furthermore, optimization is essential in providing accurate information on the local pressure and flow distribution inside the valve, and hence, reliably predicting safe allowable conditions for which a control valve can operate with regards to the extent of cavitation occurrence. The parameter characterization and correlations developed for pressure, and CV in the previous chapters, have been used to develop a methodology to predict an optimal design for any given local flow passage effective flow area with the optimality based on desired flow passage inherent downstream pressure, and CV,

6.1. Introduction

The information provided in the literature review discloses the extent of the current state of the art with regards to deterministic methodologies for the hydrodynamic performance, and it must be reservedly declared by the author the current published literature is exceptionally limited with regards to the design optimisation of multi-flow passage trim control valves. Current state of the art methodologies are sufficiently equipped to predict a control valve size requirement for a given process condition within the scope of published specific empirical data for known valve types covered within that scope.

The optimization model encompasses only the parameters that have been considered in this study which form the basis of the current hydrodynamic performance objectives which are mainly benchmarked by the flow coefficient CV as a function of global differential pressure limits and flow rate limits for which a control valve can operate without inducing local cavitation and flashing. The way the parameter characterization has been formulated and developed allows for direct iterative optimization for local objective functions as a function of pressure and flow distribution along the entire flow path as basis of a global objective function or vice-versa.

6.2. Optimization of a Multiple Flow Passage Control Valve

Application of an optimization tool for the hydrodynamic performance of a control valve that accounts for the local flow field behaviour as a function of direct local geometric parameters is critical. It is overly important to clearly understand the operational safety limits of multistage control valves and account for all the flow singularities along a control valve flow path with regards to flow and pressure fluctuations, flashing and cavitation to prevent catastrophic failures and consequential detrimental effects on life, the environment, and financial costs.

6.3. Pressure and Flow Output Objective Functions

The pressure drop across a single flow passage can be calculated from the following expression

$$\Delta P_{FP} = \left[\left(15852 Q_{FP} \left((SG) 38 A_{FP} \sqrt{\left(\frac{A_{Inlet}^2 - A_{FP}^2}{A_{Inlet}^2} \right)} \right)^{-1} \right) \right]^2 \quad (6.1)$$

Where ΔP_{FP} is the pressure drop (psi) across a flow passage, (A_{FP}) is the effective flow area at a given flow passage in (inch^2) along the flow path at which the differential pressure across it is being calculated, (Q_{FP}) is the volumetric flow rate at the given flow passage in (m^3/sec), and (A_{Inlet}) is the effective flow area of the control valve inlet which can be extended to account for an inlet reducer or expander. The number 15852 is a unit conversion factor from (m^3/sec) to (USgpm).

Where the flow rate across a single flow passage can be expressed as follows in a control valve.

$$Q_{FP} = 0.0000631 \left[\sqrt{\Delta P_{FP}} \left((SG) 38 A_{FP} \sqrt{\left(\frac{A_{Inlet}^2 - A_{FP}^2}{A_{Inlet}^2} \right)} \right)^{-1} \right] \quad (6.2)$$

The flow coefficient (CV) of a local flow passage or flow restriction at position along the control valve flow path can be calculated from the following expression.

$$CV_{FP} = \left(\frac{1}{\sqrt{\left((SG)38A_{FP} \left(\sqrt{\frac{(A_{Inlet}^2 - A_{FP}^2)}{A_{Inlet}^2}} \right)^{-1} \right)^2}} \right) \quad (6.3)$$

The pressure distribution along a flow path consisting of multiple flow passages in series can be calculated iteratively from the following expression

$$P_{IN} = \left(\frac{(15852 (Q_{FP1}))}{(SG)38A_{FP1} \left(\sqrt{\frac{(A_{Inlet}^2 - A_{FP1}^2)}{A_{Inlet}^2}} \right)^{-1}} \right)^2 + \left(\frac{(15852 (Q_{FP2}))}{(SG)38A_{FP2} \left(\sqrt{\frac{(A_{Inlet}^2 - A_{FP2}^2)}{A_{Inlet}^2}} \right)^{-1}} \right)^2 \quad (6.4)$$

$$+ \left(\frac{(15852 (Q_{FP3}))}{(SG)38A_{FP3} \left(\sqrt{\frac{(A_{Inlet}^2 - A_{FP3}^2)}{A_{Inlet}^2}} \right)^{-1}} \right)^2 + \dots + P_{Out}$$

The global flow coefficient (CV) can be expressed as a function of the local flow passage CVs and as a direct function of local geometric and flow variables from the following expression.

$$\left(\frac{1}{\sqrt{(CV^2)^{-1}}}\right)_{(G)} = \frac{1}{\left(\frac{(SG)_{38} A_{FP1}}{\sqrt{\left(\frac{A_{Inlet}^2 - A_{FP1}^2}{A_{Inlet}^2}\right)}}\right)^2}^{-1} + \frac{1}{\left(\frac{(SG)_{38} A_{FP2}}{\sqrt{\left(\frac{A_{Inlet}^2 - A_{FP2}^2}{A_{Inlet}^2}\right)}}\right)^2}^{-1} + \frac{1}{\left(\frac{(SG)_{38} A_{FP3}}{\sqrt{\left(\frac{A_{Inlet}^2 - A_{FP3}^2}{A_{Inlet}^2}\right)}}\right)^2}^{-1} + \dots \quad (6.5)$$

The cavitation index can be calculated from the following expression

$$\sigma = \left(\frac{P - P_v}{0.5 \rho v^2}\right) \quad (6.6)$$

As derived in previous chapter, the redefined geometric local pressure loss coefficient K_L can be calculated from the following expression:

$$K_L = \left[\frac{A_{Inlet}^2 - A_{FP}^2}{A_{Inlet}^2}\right] \quad (6.7)$$

6.4. Operation of The Optimization Model

Based on the presented optimization models, the local flow field within a control valve can be optimized for multiple desired objective function outputs of flow and pressure structure along the flow path, global differential pressure, and global flow coefficient (CV). Hence, the optimization model for an objective function output is run as follows.

6.4.1. Optimal Available Flow Coefficient (CV)

To run the optimization for the available CV for a given flow rate within the geometric minimum and maximum effective flow area constraints, the following steps should be followed.

1. The global flow rate Q is known from process conditions
2. Prescribe the outlet pressure of the process which can be the absolute atmospheric pressure.
3. Calculate the effective flow areas at each of the flow passages
4. Calculate the geometric pressure loss factor K_L value at each of the flow passages equation (6.7).
5. Calculate the local CV at flow passage 3 (FP3), (FP2) and (FP1) in that order from equation (6.3).
6. Calculate (FP3) pressure drop and cavitation index from equations (6.1) and (6.6) respectively.
7. Calculate (FP2) pressure drop, exit static pressure and cavitation index from equations (6.4) and (6.6) respectively.
8. Calculate (FP1) pressure drop, exit pressure, and cavitation index from equations (6.4), and (6.6) respectively.
9. Calculate the inlet pressure from equation (6.4), which is outlet pressure + (FP3) pressure drop + (FP2) pressure drop + (FP1) Pressure drop
10. Calculate the overall global CV from equation (6.5).
11. Repeat steps 3 to 10 for various flow passages effective flow areas while maintaining the condition (cavitation index $(\sigma) \geq 2$) at all flow passages until the rated maximum CV is achieved at the resulting global pressure drop and flow rate.

Figure 6.1 shows the flow chart of the optimization model presented here, it must be noted that the same sequence of the optimization model can be followed where the know desired global parameter is either the flow coefficient (CV), the global differential pressure, the differential pressure across any of the flow passages along the flow path, and any desired magnitude of pressure downstream of any flow passage along the flow path

The tool can be preferably set up in an excel spreadsheet and takes approximately 30 minutes to set up and solve.

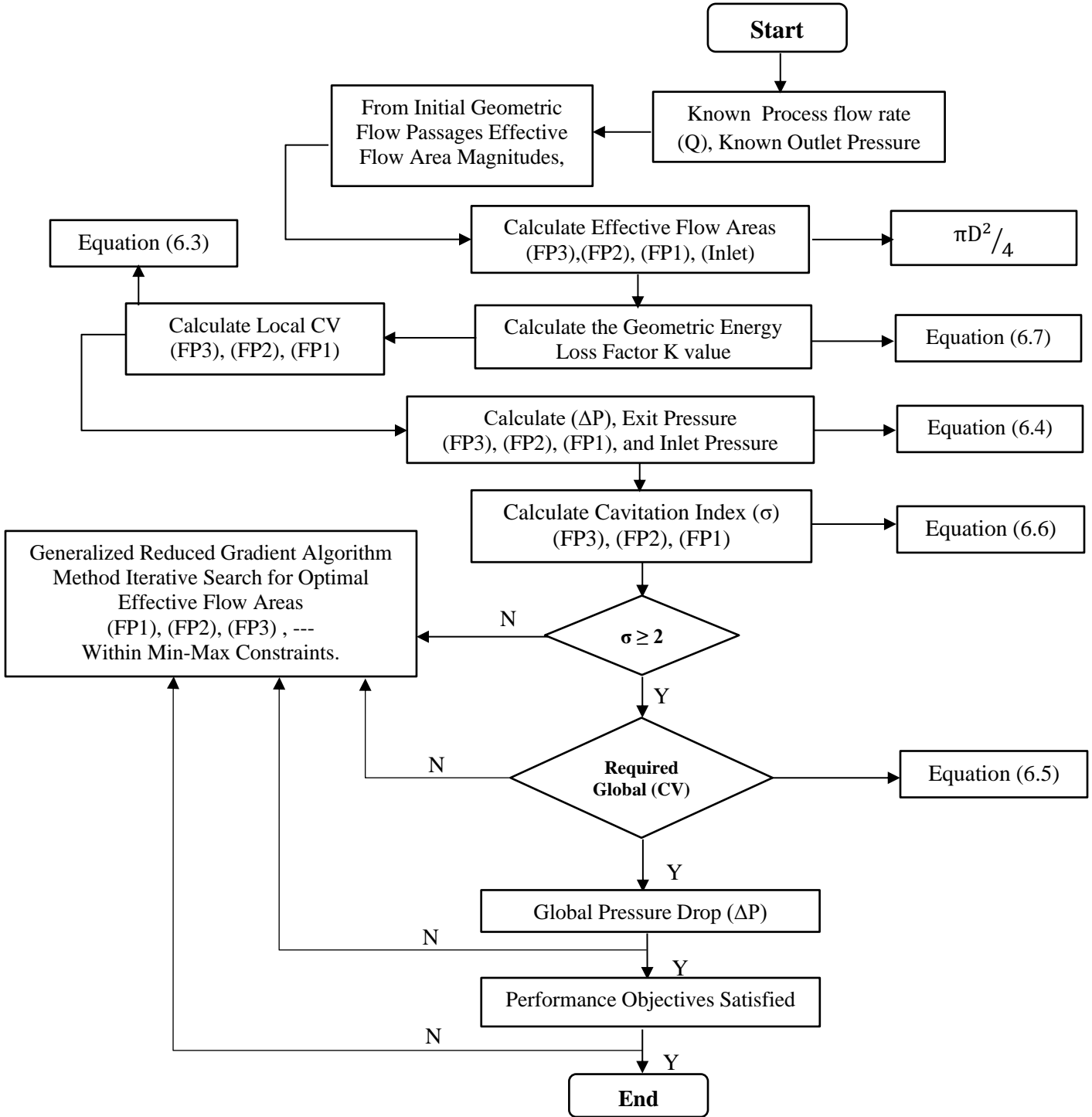


Figure 6-1: Flow Chart of the Targeted Optimization Methodology

6.5. Optimization Model Limitations

The model developed in this study is focused on the hydrodynamic performance of the control valve, and this is the major limitation of this optimization model. Furthermore, additional limitations and assumptions are listed below:

- The developed prediction models are only valid and applicable for single phase fluids.
- The prediction models for local flow and pressure structure have only been validated through CFD and proven Newtonian and continuum physics macroscopic equations with excellent agreement, but they have not been validated against experimental data, and hence could result in a degree of inconsistencies in the design process.

6.6. Design Example 1, Multiple Flow Passage Control Valve

A control valve is required to be installed in a process loop with a flow rate of water at 130 Usgpm. For a control valve consisting of 3 flow passages in series along the entire flow path. Find the optimal flow passages effective flow areas and corresponding differential pressure across each flow passage complying to the condition (cavitation index (σ) ≥ 2), and the corresponding optimal global CV.

Solution: As discovered in this work, the flow field is uniquely sensitive to the magnitude of the flow passages effective flow areas and their sequence of arrangement along the flow path. There is a unique combined effect of the flow passages effective flow area sequence of arrangement for which a solution for specific multiple objective function outputs requires solving through iterations.

From the provided information of the process flow rate, and the design condition to maintain the Cavitation index above 2. Here the cavitation index is the ratio of potential resistance for vapour bubble formation to the potential for causing the formation of vapour bubbles which is defined from equation (6.6).

Table 6-1 shows the geometric configuration with regards to the effective flow diameters of the flow passages along the control valve flow path at flow passage 1 (FP1), flow passage 2 (FP2), and flow passage 3 (FP3), and included is the resulting pressure drop, cavitation index, flow coefficients (CV's) across each flow passages, and the resulting global pressure drop at the given global flow rate as calculated from the prediction equations.

Table 6-1. Variations of flow parameters w.r.t flow passage effective flow diameters for the baseline valve

	FP1	FP2	FP3	Global	Prediction Equation
Effective flow Diameter (D) (inches)	1.1	0.7	0.9		
(ΔP) (PSI)	62.45	72.4	25.93	165.4	(6.4)
Cavitation Index (σ)	2.9	1.9	2.12		(6.6)
Q (Usgpm)				130	Known Process Parameter
CV	15.8	14.7	24.6	9.9	(6.3) and (6.5)

Table 6-1 depicts the local pressure drop and CV at the flow passages along the flow path with respect to the baseline/original effective flow diameters at each flow passage with 130 Usgpm of water flowing through the valve. At (FP1), the cavitation index is 2.9 which satisfies the specified design criteria of (cavitation index (σ) ≥ 2). The cavitation index at (FP2) is 1.9, which indicates the potential of some cavitation occurring, and it falls below the cavitation index design criteria, and cavitation index at (FP3) satisfies the design criteria with a value of 2.12. For this geometric configuration, the overall global pressure drop across the valve is 165.4 PSI, and the flow coefficient is 9.9, it is prudent to note that the global pressure drop is significantly high, and it is desirable to have a low pressure drop with regards to pumping energy requirements where the pumping energy increases proportionally with an increase in the overall global differential pressure across the control valve through the expression

$$E = \Delta P_{\text{Perm}} \times Q \quad (6.8)$$

where E is the pumping energy, in Watts, ΔP_{Perm} is the permanent pressure drop in N/m^2 , and Q is the volumetric flow rate in m^3/sec . Further depiction of the flow path pressure distribution and the cavitation index at the given effective flow area sizes and sequence of arrangement of

the baseline valve is hydrodynamic characteristics of local flow passages pressure drop and cavitation index is graphically represented in figure 6-2. Flow passage 2 (FP2) with an effective flow diameter of 0.7 inches, has the lowest cavitation index of 1.9 at a corresponding differential pressure of 72.4 PSI. Flow passages 1 (FP1) and (FP3) have a cavitation index of 2.9 and 2.12, respectively. The resulting cavitation index of 1.9 at flow passage 2 (FP2) which is below 2, indicates that there is potential for cavitation to occur within the vicinity and downstream of flow passage 2 (FP2).

Further details of the unique sensitivities of the flow field on the flow. passages sequence of arrangement along the flow path are provided in the following optimization first iteration results

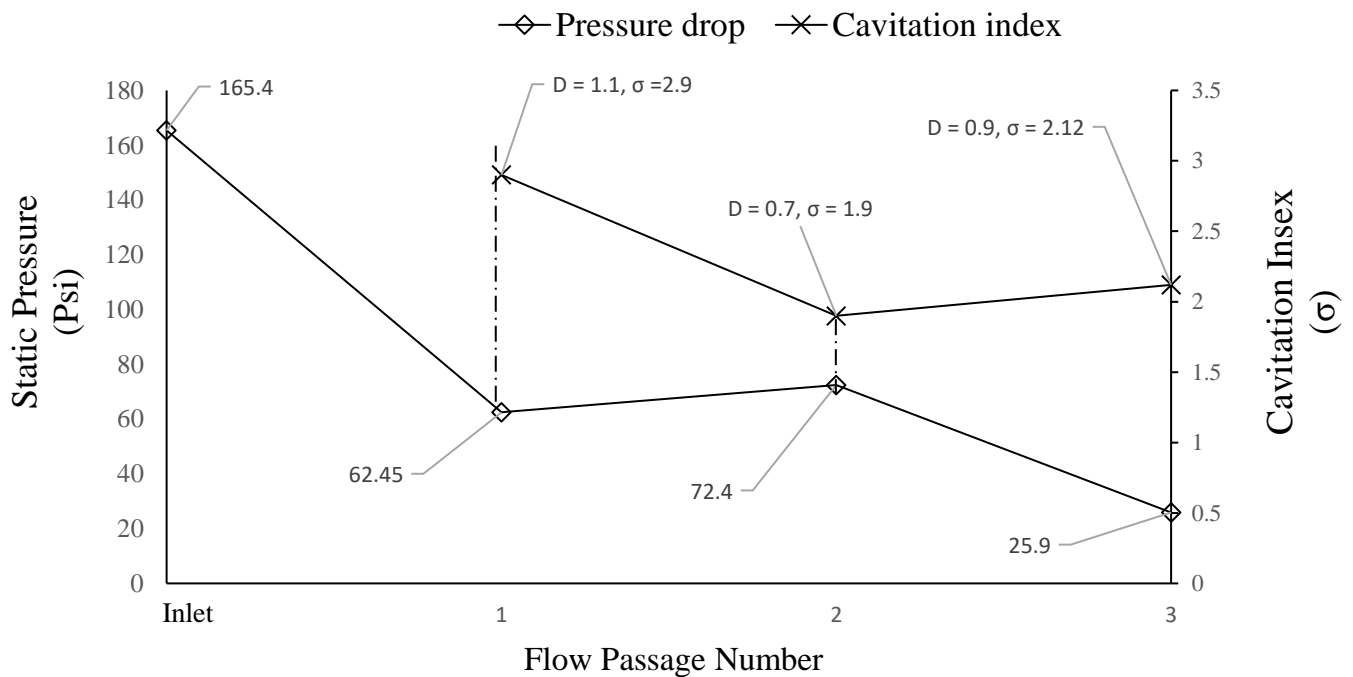


Figure 6-2: Variations of pressure drop and cavitation index at each flow passage along the flow path for the Baseline Geometric Configuration at the Given flow and Pressure Conditions Presented in Table 6.1.

Table 6-2 shows the variations of the pressure drop, cavitation index, and CV along the flow path for the first iteration of the objective function output optimization, and here (FP1) diameter has been changed from 1.1 to 1.2 inches, and (FP2) has been changed from 0.7 to 1.3 inches, and (FP3) from 0.9 to 1.2, respectively. The changes in the effective flow diameters is seen to have a substantial effect on the pressure drop across each flow passage where the pressure drop at (FP1) has seen reduced by 29.9% as compared to the baseline valve, (FP2) has seen a reduction of 92.7%, and (FP3) has increased by 70.6%.

The highest decrease in the pressure drop is at flow passage 2, (FP2) with a 92.7% decrease in the pressure drop, but it is interesting to note that the cavitation index is 1.83 a further decrease from the baseline valve cavitation index of 1.9, and remains below the cavitation index design criteria of ($\sigma \geq 2$). The overall global differential pressure across the valve has seen a reduction of 33.3% which is attributed to the increase in the flow passages effective flow diameters, and the overall global CV has increased by 33.2 % respectively from 9.9 to 14.8.

Table 6-2: Variations of Flow Parameters for Varied Effective Flow Passage Diameters For Optimization iteration 1.

	FP1	FP2	FP3	Global
D (Inches)	1.2	1.3	1.2	
ΔP (PSI)	43.8	5.3	7.6	110
Σ	2.83	1.83	4.82	1.29
Q (USgpm)				130
CV	18.9	54.5	45.4	14.8

To visualise the pressure distribution results of the first iteration as presented in table 6-2, figure 6-3 shows the variations of pressure drop, and cavitation index at each flow passage along the flow path for the iteration 1 of the optimization model. There is need to carry out further iterations to get the cavitation index at (FP2) above 2, and hence the following section provides information on the second iteration of the optimization model. It must be noted that the iteration process is exhaustive and numerous acceptable solutions are possible that fit the design criteria, hence, the optimization model is not limited to global independent parameters but can be implemented through the novel developed homogeneous equations for specific local objective functions.

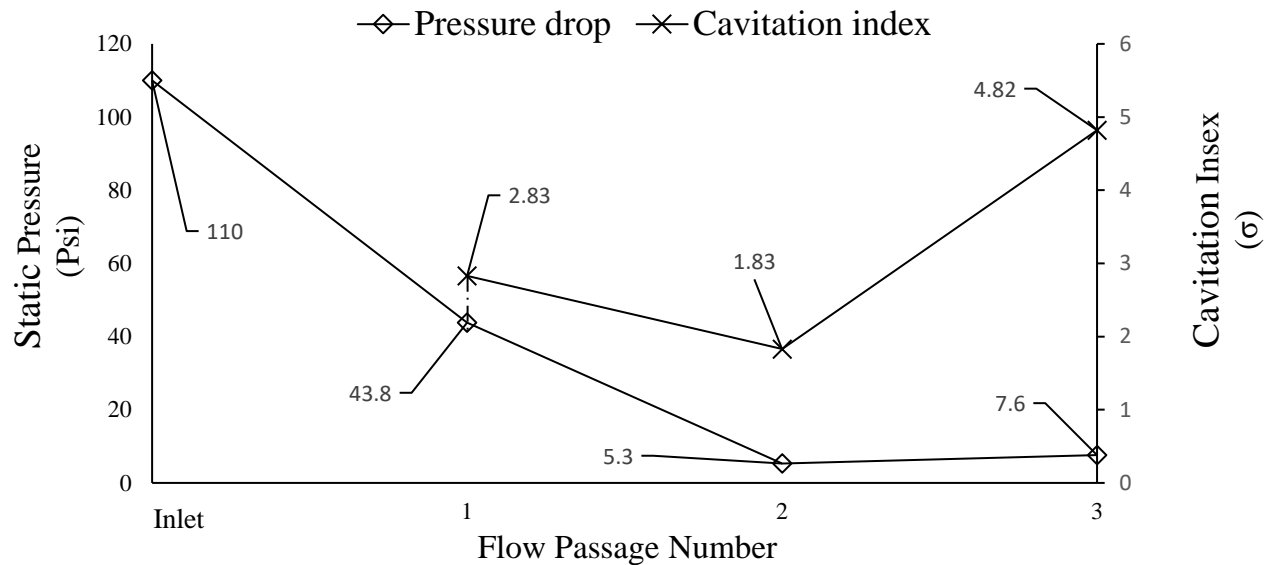


Figure 6-3: Variations of Pressure Drop and Cavitation Index at Each Flow Passage Along the Flow Path for Iteration 1 of the Optimization Process.

Table 6-3 shows the variations of pressure drop, cavitation index, and CV for the optimization iteration 2. Here it can be seen that the cavitation index at all the flow passages is above 2, which satisfies the cavitation index design criteria, the pressure drop at (FP1) has dropped by a further 42.9%, while (FP2) and (FP3) have seen an increase of 55.8% and 72.9% respectively. It is key to note that the sequence of arrangement of the flow passages effective flow diameters are reducing along the flow path from the inlet to the last flow passage (FP3) and expanding again to the outlet diameter which is similar to the inlet diameter. The lowest cavitation index is seen to occur at (FP3) with a value of 2.04, however this above the cavitation design criteria of ($\sigma \geq 2$).

Table 6-3: Variations of Flow and Pressure Parameters for Varied Effective Flow Passage Diameters for Optimization Iteration 2.

	FP1	FP2	FP3	Global
D (inches)	1.5	1.1	0.9	
ΔP (Psi)	18.8	12	28	80.3
Σ	5	4	2.04	1.44
Q (USgpm)				130
CV	30	37.5	24.6	15.2

Furthermore, figure 6-4 explicitly depicts the pressure drop distribution across each flow passage along the flow path together with the respective corresponding cavitation index at each flow passage. This is the optimal hydrodynamic performance with regards to the specific objective function of this optimization criterion.

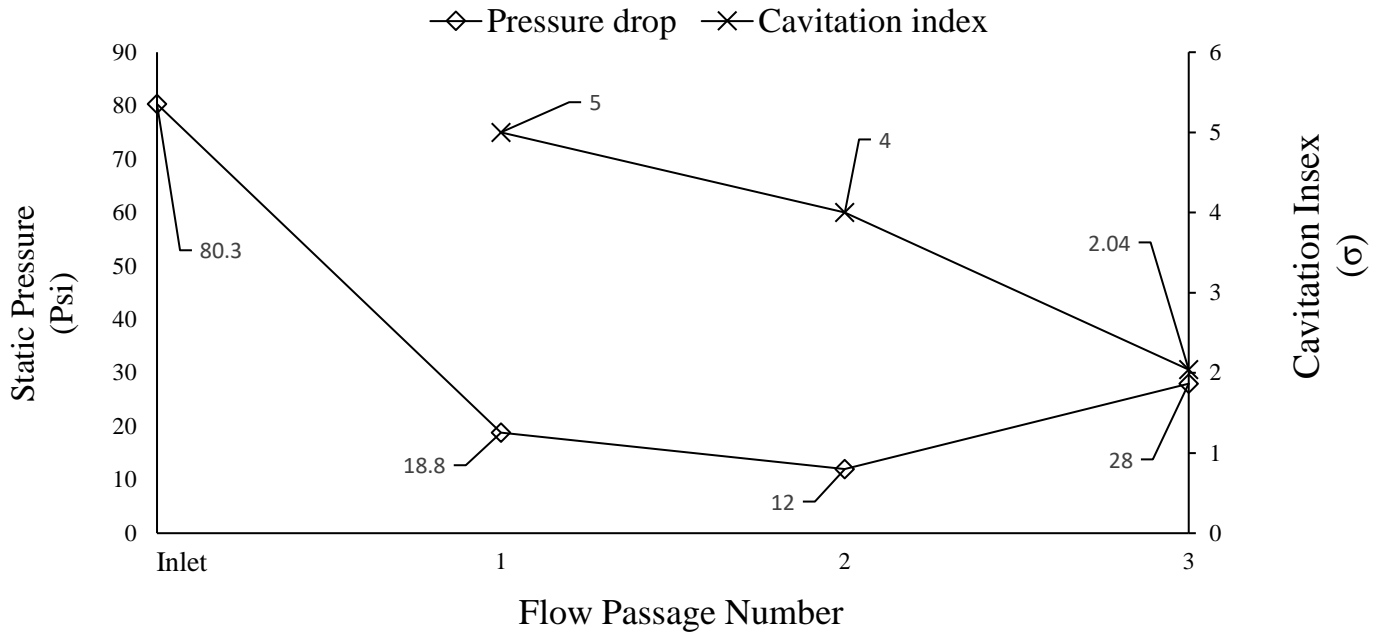


Figure 6-4: Variations of Pressure Drop and Cavitation Index at Each Flow Passage Along the Flow Path for the Optimal Local Geometric Configuration.

The design examples presented in this chapter represent a portion of the optimization model which can be exhaustive with regards to specific local or global objective function outputs. The optimization model presented in this study is simple in use and robust, the novel and unique geometric and flow characterization implemented in the optimization study allows its application in any valve or flow handling device if the flow passage or passages effective flow areas are known. The optimization model can be used for industrial applications with satisfactorily accurate results.

6.6.1. Summary of a Multi-Stage Trim Control Valve Optimization

From the extensive investigations carried out in this work on the hydrodynamic performance of a control valve, the following results have been disclosed.

- The sequence of arrangement of the flow passage effective flow diameters along the flow path has significant effect on the pressure distribution along the flow path. Hence, the specific combinations of geometric effective flow passages areas along the flow path can be determined iteratively through the generalised non-linear reduced gradient algorithm method, while accounting for multiple geometric input effective flow area variables, and objective output function constraint of cavitation index $\sigma \geq 2$ across each of the given flow passages along the flow path for the optimal global CV, allowable flow rate, and allowable pressure drop.
- The local flow field can be specifically altered to any prescribed or desired pressure, pressure drop, flow, CV, and pumping energy requirement within the local flow passages effective flow area size design constraints. This is achieved as a function of the multi-stages or singularities effective flow area sizes and sequence of arrangement along the entire flow path.
- The optimization model allows for geometric and dynamic scalability.

6.7. Design Example 2 for Water Flow in a 4 Stage-Passage Trim Control Valve

To determine the application viability of the prediction model for different control valve trim geometric configurations, the prediction tool has been used to predict and optimise the hydrodynamic performance of global and local pressure drop, cavitation index, and CV along the flow path of a 4 stage- passage trim control valve with water as the flow media. A globally experimentally validated CFD model implemented in chapter 3 has been used at similar global flow rate of 130 USgpm as that used for the geometric configuration presented in the previous section. Here again, the baseline trim geometric configuration consists of randomly specified flow passages effective flow area magnitudes where the maximum and minimum available sizes are limited within structural stress integrity and manufacturability constraints. Figure 6-5 (a) shows the geometric configuration of the multi-hole double cage trim within the control valve, and (b) shows the velocity contours through a section across cage 1 and 2 flow holes normal to the direction of flow.

Figure 6-5 (b) shows the extent flow distribution within the trim flow passages where equal velocity magnitudes are observed to be occurring at each of the holes around a cage, and higher velocities are seen to be occurring at the smaller effective flow diameter in stage 2 as expected. The significance of similar velocities occurring at each of the holes around a cage is that all the holes around a cage can be characterized as a single effective flow area.

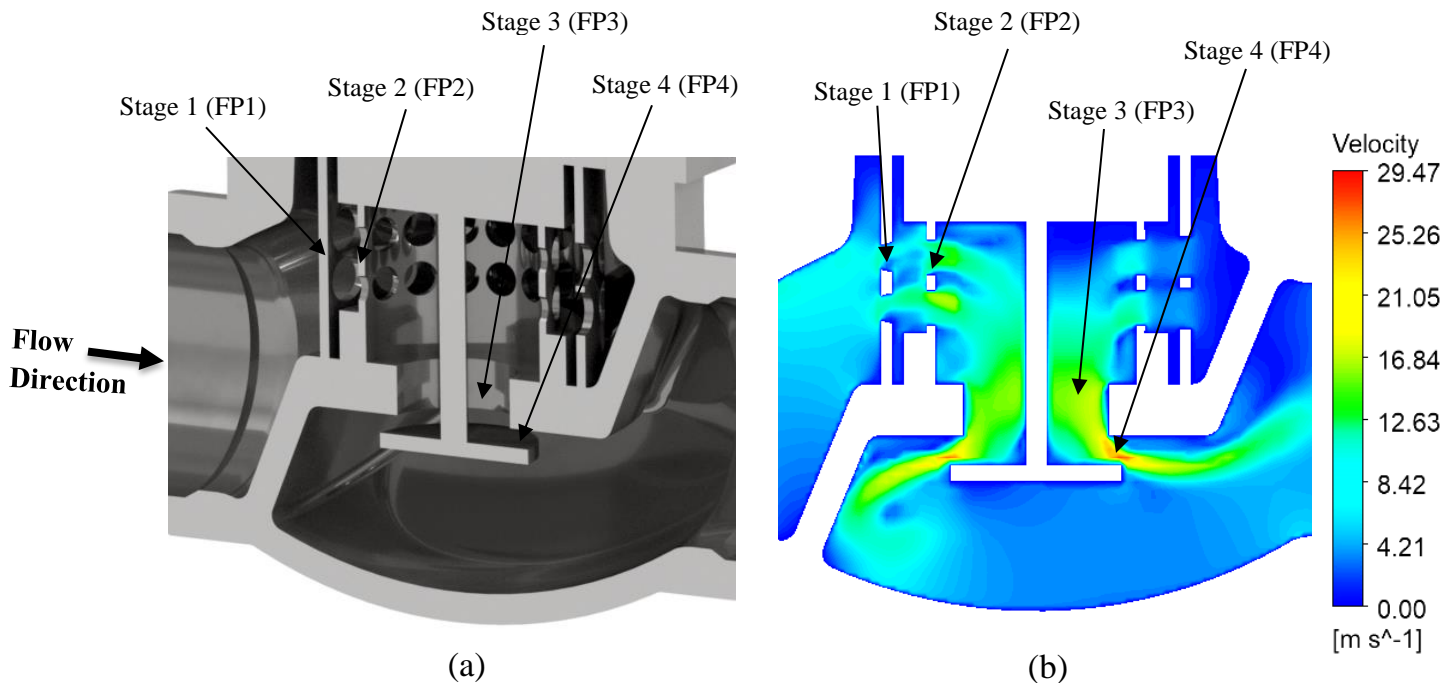


Figure 6-5: Geometric Configuration for a Multi Hole Double Cage Trim Within a Control Valve (a) and velocity contours within cage trim flow passages. (b).

Table 6-4 shows the control valve trim geometric configuration and variations of local and global flow parameters, the study was carried out at global flow rate of 130 Usqpm with an outlet pressure of 30 PSI. The trim in this study consists of 4 flow passages along the control valve flow path where each flow passage has been characterized as an effective flow area. The effective flow area of a cage is the total area of all the holes around the cage, and which represents an effective single flow passage along the flow path. The local pressure drop at flow passage 1 denoted (FP1) is the differential pressure between the inlet pressure and exit pressure at flow passage 1 (FP1), the pressure drop at flow passage 2 (FP2) is the differential pressure between the exit pressure at flow passage 1 (FP1) and exit pressure at flow passage 2 (FP2), the pressure drop at flow passage 3 (FP3) is the differential pressure between the exit pressure at flow passage 2 (FP2) and exit pressure at flow passage 3 (FP3), the pressure drop at flow passage 4 (FP4) is the differential pressure between the exit pressure at flow passage 4 (FP4)

and the outlet pressure, and the global pressure drop is the differential pressure between the inherent inlet pressure and the outlet pressure. Variations of the prediction model and CFD predicted geometric energy loss factor (K), cavitation coefficient (σ), and flow coefficient (CV) are also presented.

Table 6-4: Control Valve Trim Geometric Parameter Configuration and Variations of Prediction Tool and CFD Results of Local and Global Flow Parameters.

	Inlet	FP1	FP2	FP3	FP4	Outlet	Global
Effective flow area (m ²)	0.002255	0.000477	0.000288	0.0002638	0.000251		
Static Pressure (PSI)	252.3					30	
Pressure Drop Prediction Model (ΔP) (PSI)		20.4	57.3	68.8	75.9		222.3
Pressure Drop CFD (ΔP) (PSI)		21.4	60	67	72		222.4
Loss coefficient Prediction Model (K)		0.954	0.983	0.986	0.987		3.91
Loss coefficient CFD (K)		0.96	0.986	0.988	0.989		3.93
Cavitation Index Prediction Model (σ)		13.1	4.3	2.75	1.58		
Cavitation Index CFD (σ)		12.5	4.02	2.71	1.61		
Q (Usgpm)							130
CV Prediction Model		28.8	17.2	15.7	14.9		8.7
CV CFD		28.1	16.8	15.9	15.3		8.73
Pumping Energy (P) (KW)		15.4	43.2	51.84	57.24		168

In order to quantify the validity of the prediction model, the CFD and prediction model predicted results of the control valve trim local pressure drop across each of the flow passages, has been plotted against the ratio of the inlet diameter to the diameter of the respective flow passage along the entire trim flow path. Figure 6-6 shows the results of the global pressure drop and local pressure drop across each of the flow passages along the flow path, where the global pressure drop is the sum of the local differential pressures across each flow passage along the entire flow path. The results show that the prediction tool results are in excellent agreement with the CFD results within an accuracy of $\pm 5\%$, and most importantly, the prediction tool here, has been applied to a completely different and much complex control valve trim geometric

configuration, and the results as show in figure 6-6 demonstrate the viability, accuracy and scalability of the prediction model.

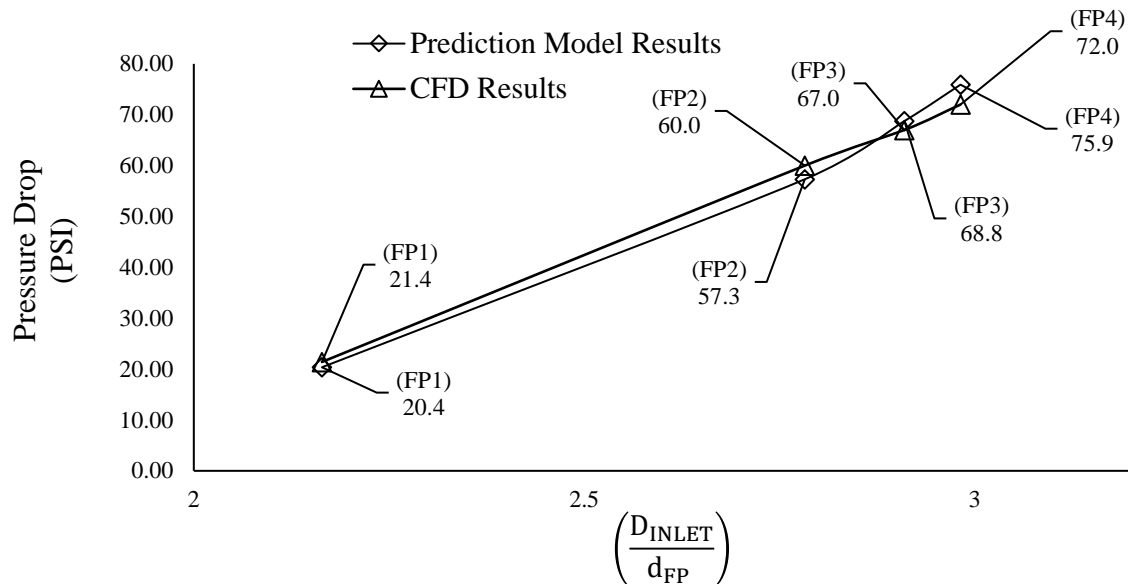


Figure 6-6: Prediction Model and CFD Results of Pressure Drop Variations Across the Trim Flow Passages Along the Control Valve Flow Path for the Baseline Valve Trim.

As reported in the previous chapters, the parameters that have been considered in this study to classify the hydrodynamic performance of a control valve trim are the global and local pressure drop, cavitation index, velocity, and flow coefficient (CV). Figure 6-7 shows the variations of pressure drop and cavitation index across each flow passage along the trim flow path as a function of the ratio of the inlet diameter and respective flow passage effective flow passage diameter along the flow passage. The trim in this study effectively consists of 4 flow passages along the flow path within the control valve, and at the given global flow and pressure conditions and local geometric configurations presented in table 6-4. It can be observed in figure 6-7 that at flow passage 1(FP1), the cavitation index is 13.10 at an effective flow diametric ratio with the inlet of 2.2 with a corresponding pressure drop of 20.4 PSI.

This indicates that the pressure magnitude within the vicinity and downstream of flow passage is substantially above the fluid saturation pressure, and this is quantified against the conditions at which the potential of the fluid to cavitate which is characterized by a cavitation index below 2. The cavitation index at flow passage 2 (FP2) is 4.3 at an effective flow diametric ratio with

the inlet of 2.8 with a corresponding pressure drop of 57.3 PSI, and here again cavitation is not expected to occur since the cavitation index is substantially above 2.

At flow passage 3 (FP3), the cavitation index is 2.7 at an effective flow diametric ratio with the inlet of 2.9, and with a corresponding pressure drop of 68.8 PSI. At the last flow passage 4 (FP4) along the control valve flow path, the cavitation index is 1.60 at an effective flow diametric ratio of 3, and with a corresponding pressure drop of 75.9 PSI. Relative to flow passages 1 (FP1), 2 (FP2), and 3 (FP3), the pressure drop across flow passage 4 (FP4) is substantially higher and with a corresponding lower cavitation index of 1.60 which is below 2.00, and this indicates that there is potential for the fluid to cavitate at the current flow conditions and geometric configuration combination with regards to the arrangement of the flow passages along the flow path as a function of effective flow area magnitudes.

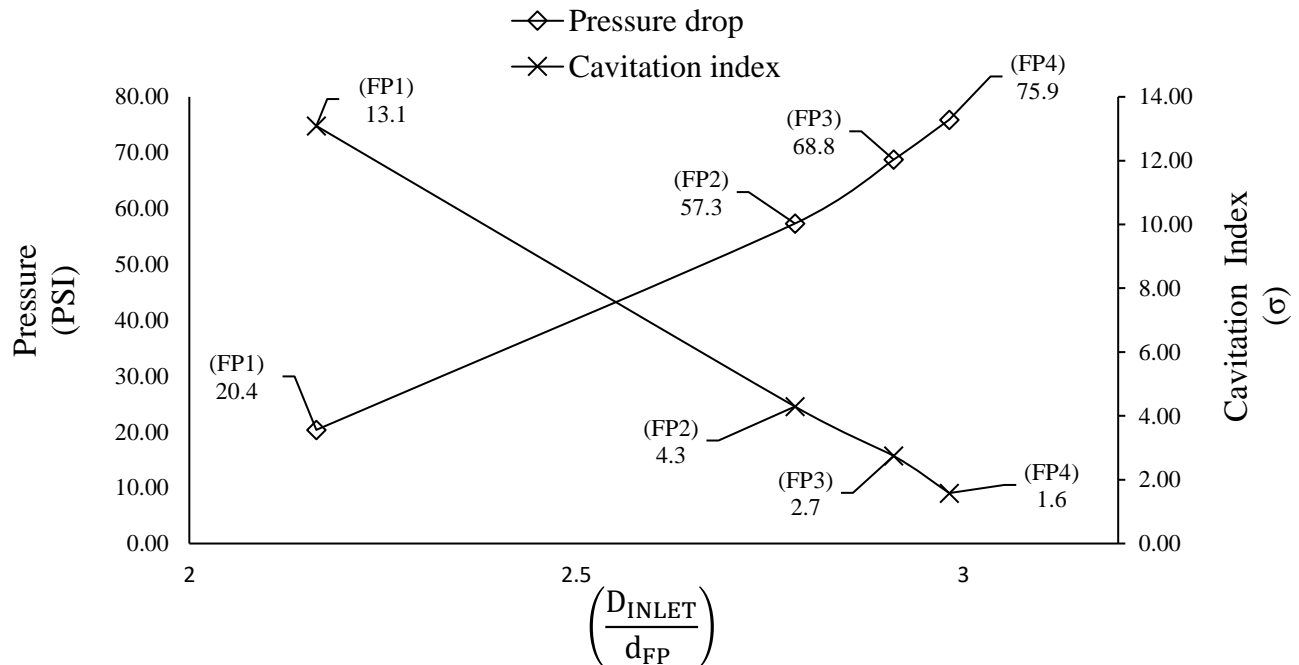


Figure 6-7: Variations of Local Pressure Drop at Each of the Flow Passages and Corresponding Cavitation Index as a Function of the Ratio of Effective Inlet Flow Diameter and Respective Effective Flow Passage Diameter Along the Flow Path for the baseline Valve Trim Geometric Configuration.

To further quantify the defined hydrodynamic performance of the control valve trim in this study through the developed prediction models, variations of local pressure drop across the trim flow passages along the flow have been plotted against the ratio of the inlet effective flow diameter to the respective effective flow passage diameter along the control valve flow path. Figure 6-8 depicts the local pressure and flow structure within the control valve trim in terms of the pressure drop across each of the 4 flow passages along the flow path, and corresponding flow coefficient (CV) at each flow passage w.r.t the area ratio of the inlet diameter to the respective flow passage effective diameter along the flow path. As the pressure drop across the flow passage increases the flow coefficient decreases as expected, and this is characteristic to an increase in the inlet and flow passage diameter ratio. With reference to the previous figure 6-7, an increase in the ratio of the inlet diameter to a flow passage diameter is also characteristic with a decrease in the cavitation index. In addition, it must be noted that the pattern of arrangement of the flow passages flow area magnitudes along the flow path has direct effects on the local pressure and flow structure. Subsequently there is a combined geometric interdependence on the inherence of the local pressure and flow structure along the control valve flow path. The prediction model developed in this work explicitly accounts for global and local geometric flow passages effective flow areas interdependence to predict the local or global flow and pressure structure.

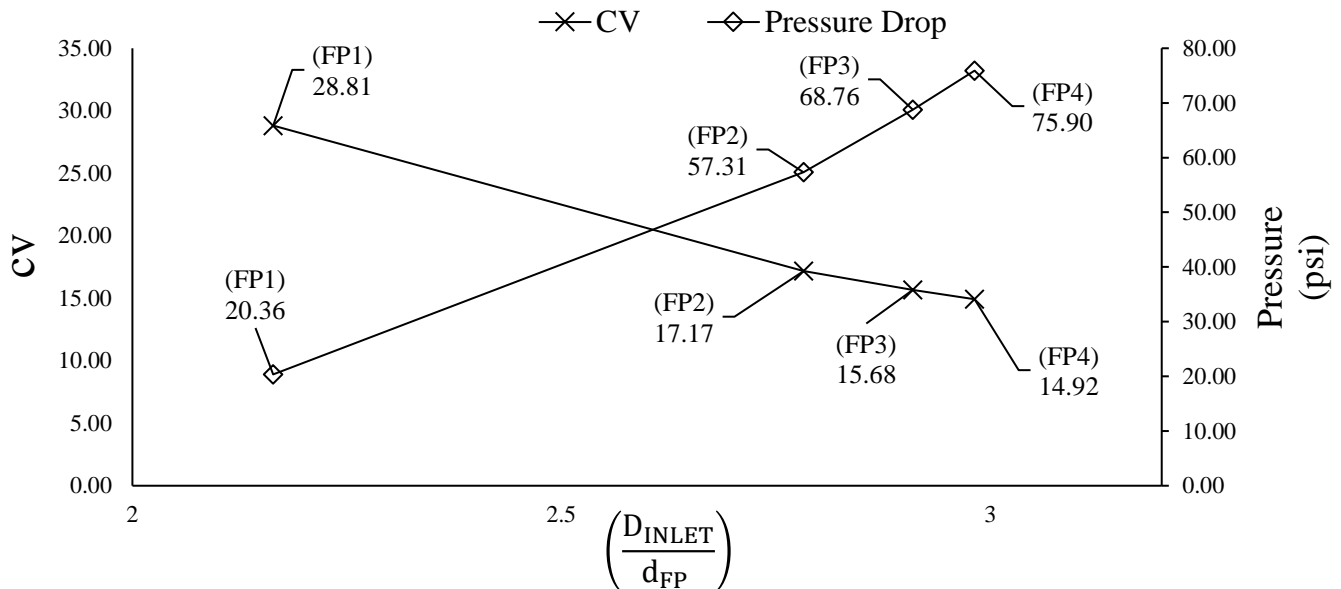


Figure 6-8: Variations of Local Pressure Drop and CV Across the Trim Flow Passages Along the Flow Path, w.r.t the Ratio of Effective Inlet Flow Diameter and Respective Effective Flow Passage Diameter Along the Control Valve Flow Path.

The accuracy and applicability of the prediction model has been validated through the prediction of the hydrodynamic performance of a different control valve trim configuration to that at which the prediction model was developed through the unique flow and geometric parameter characterization of the baseline valve trim as presented in chapter 3.

Having established the viability and scalability of the prediction model, the optimal hydrodynamic performance of the control valve trim can be determined. It must be noted that the scope of the optimal hydrodynamic performance of a control valve considered in this study include cavitation, flashing, flow rate, flow coefficient (CV), and pumping energy requirements. The optimal global and local hydrodynamic performance of the control valve is confined within the local geometric constraints of the flow passages w.r.t to the maximum possible available flow passages effective flow area sizes. The optimal local flow passages effective flow area sizes and sequence of arrangement along the control valve flow path with regards to sizes can be determined for an optimal global and local pressure drop, maximum flow rate, flow coefficient (CV), and pumping energy requirement.

6.7.1. Specific Hydrodynamic Performance Optimization of a 4 Stage-Flow Passage Control Valve Trim.

Determine the optimal trim geometric configuration of effective flow area sizes and arrangement along the flow path to achieve the maximum overall flow rate, CV, and minimum pumping energy requirement. The cavitation index σ at each of the flow passages along the flow path should satisfy the constraints of $\sigma \geq 2.00$. Table 6-5 presents the variations of the local trim pressure drop, geometric energy loss factor (K), cavitation index (σ), CV, and pumping energy requirement at each flow passage along the flow path as a function of the optimal flow passages effective flow areas and sequence of arrangement along the flow path . In addition, the global flow rate, inlet and outlet pressure, and pumping power are also presented.

Table 6-5. Variations of The Control Valve Global and Local Trim Pressure and Flow Parameters for the Optimal Trim Flow Passages Effective Flow Area Sizes and Sequence of Arrangement Along the Flow Path.

	Inlet	FP1	FP2	FP3	FP4	Outlet	Global
Effective flow area (m²)	0.002255	0.00191	0.00150	0.00063	0.000546		
Effective flow diameter (mm)	53.7	49.3	43.8	28.4	26.4	53.7	
Static Pressure (PSI)	96.5					30	
Pressure Drop (ΔP) (PSI)		0.9	2.8	26.5	36.2		66.4
Loss coefficient (K)		0.27	0.54	0.92	0.94		3.91
Cavitation Index (σ)		133.6	41.13	4.18	2.32		
Flow Rate Q (Usgpm)							200
CV		209	119.2	38.8	33.2		24.5
Pumping Energy (KW)		1.1	3.3	30.8	42		77

From the results presented in table 6-5, it can be observed that the optimal sequence of arrangement of the flow passage along the control valve flow path is where the effective flow diameter at flow passage 1 (FP1) is 49.3mm, 43.8mm at flow passage 2 (FP2), 28.4mm at flow passage 3 (FP3), and 26.8mm at flow passage 4 (FP4). In this case, flow passage 4 (FP4) is the valve seat which presents the smallest effective flow diameter along the flow path, hence this optimal flow passages effective flow diameter sequence of arrangement along the flow path is at which a maximum flow rate of 200 Usgpm is achievable while maintaining the cavitation index at flow passage 1 above 2 at 2.32 with a corresponding optimal CV of 24.5. Furthermore, the optimal pumping power is 77 KW, which is 54.2% lower than the baseline geometric configuration presented in the previous section in table 5-4 of 168 KW. Due to the nonlinear interdependent effects of the flow passage effective flow area magnitudes and sequence of arrangement on the local flow and pressure structure along the entire control valve flow path, a specific optimal objective is determined iteratively. The optimal global pressure drop is 66.4 PSI for this optimal flow passages geometric configuration and is substantially lower than the baseline pressure drop of 222 PSI, and the low-pressure drop is attributes to the low pumping power requirement.

Figure 6-9 characterises the variations of pressure drop and cavitation index at the flow passages along the flow path as a function of the optimal flow passage effective flow diameter magnitudes and sequence of arrangement along the flow path. As expected, it can be observed that as the ratio of the inlet diameter to a flow passage effective flow diameter increases the pressure drop across a flow passage increases, and as the pressure drop across a flow passage increases, the cavitation index decreases relatively at a constant flow rate. As mentioned earlier, the overall complex interdependent and combined effects of the flow passages effective flow diameters and sequence of arrangement along the flow path cannot be simply characterised with the flow and pressure structure through a polynomial, exponential, power, or logarithmic relationship. Hence, the optimal flow passages geometric configuration for the specified objective flow and pressure characteristics have been determine iteratively through the generalised reduced gradient algorithm method implemented through the developed prediction model.

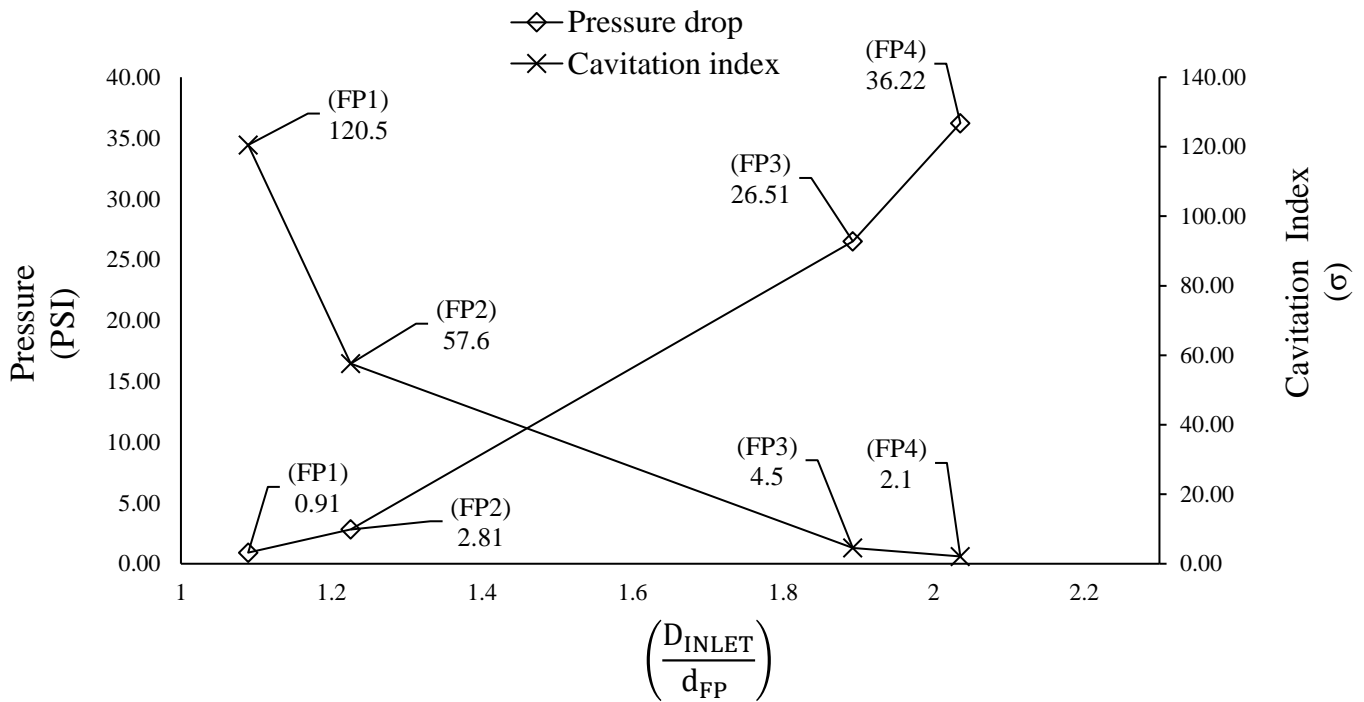


Figure 6-9. Variations of Pressure Drop and Cavitation Index at the Flow Passages Along the Flow Path Within the Control Valve w.r.t the Optimal Flow Passages Effective Flow Area Magnitudes and Sequence of Arrangement Along the Control Valve Flow Path.

Figure 6-10 characterizes the variations of the local pumping power requirements with the flow ratio of the inlet diameter to the ratio of the respective effective flow passage diameter along the flow path for the baseline model and the optimal model for the specific output function objectives. The total global pumping power is also presented for the baseline and optimal model, and it can be observed that the lower the ratio of the inlet to a respective flow passage along the path the lower the pumping power requirement. This lower the ratio of the inlet diameter to a respective flow passage effective flow diameter means that there is less resistance to flow due to the lower differences in the inlet diameter to a flow passage effective flow diameter. The pumping power requirement is seen to increase with an increase in the ratio of the inlet diameter to a respective flow passage effective flow diameter, and as presented in figure 5-9, this is characteristic with an increase in the pressure drop across a flow passage and a decrease in the cavitation index. The global pumping power requirement for the baseline geometric configuration is 168 KW and 77 KW for the optimal geometric configuration which is 59.5% less than the baseline geometric configuration as presented in table 6-4.

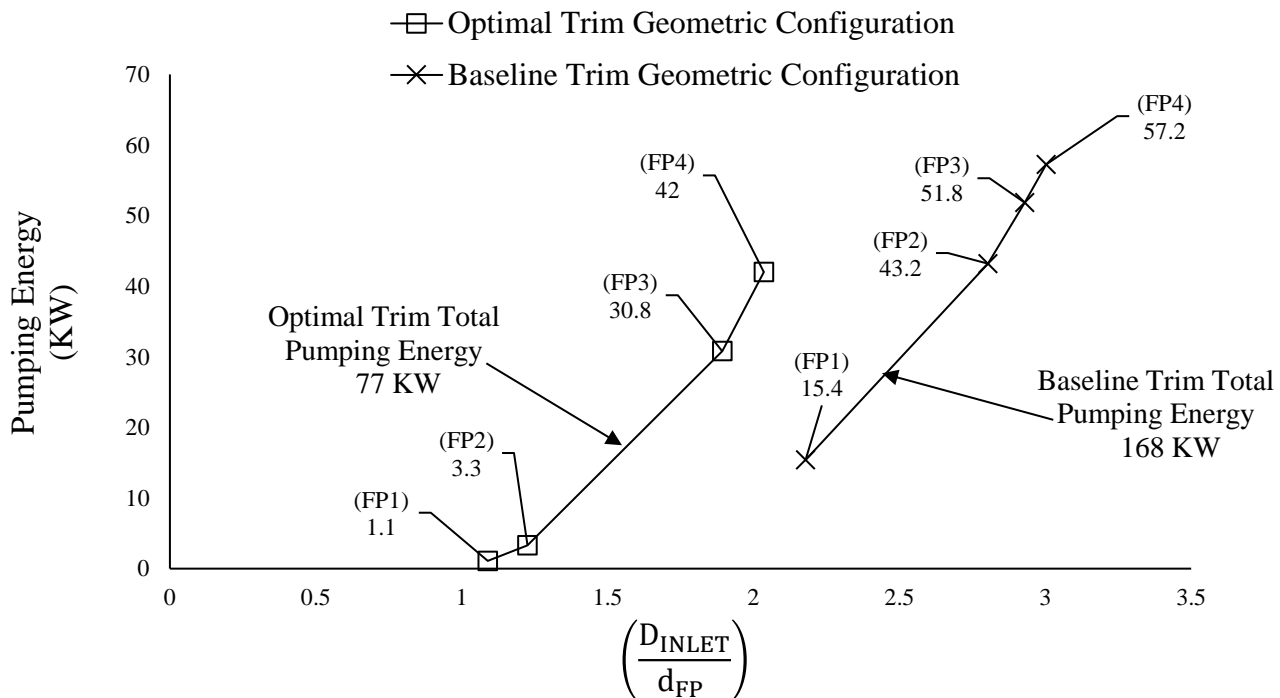


Figure 6-10: Variations of Pumping Energy Requirements w.r.t the Ratio of the Inlet Diameter to The Effective Flow Diameter at a Respective Flow Passage Along the Flow Path for the Baseline and Optimal Geometric Configuration.

Figure 6-11 depicts the variations of the pressure drop and flow coefficient (CV) As a function of the ratio of the inlet diameter to a respective flow passage effective flow diameter along the control valve flow path for the optimal trim geometric configuration. The optimum geometric configuration here satisfies the specified optimal output objective functions of maximum allowable flow rate, minimum pressure drop, and minimum pumping power requirements within the geometric constraints w.r.t the maximum and minimum available flow passages effective flow areas. The local CV at each of the flow passages is substantially higher, which is attributed to the respective low pressure drop across each flow passage as compared to the baseline geometric configuration as presented in figure 6-8. The local flow coefficient can be observed to reduce as the ratio of the inlet diameter to the respective flow passage effective flow diameter increases, and relatively the pressure drop is seen to increase.

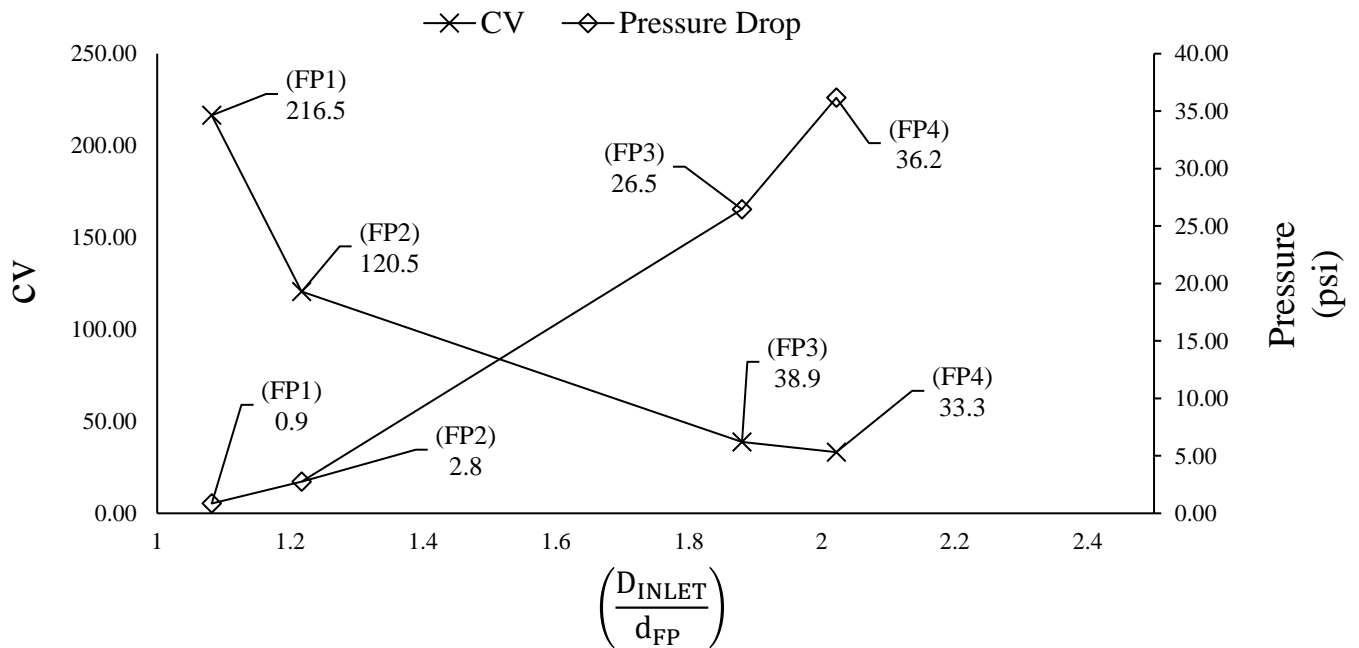


Figure 6-11: Variations of Flow Coefficient (CV) and Pressure Drop w.r.t the Ratio of the Inlet Diameter to the Respective Flow Passage Effective Flow Diameter along the Control Valve flow path for the Optimal Geometric Configuration.

6.8. Design Example of a Five Stage Continuous Resistance Trim with Liquid Helium Flow Media.

The hydrodynamic performance of 5 stage continuous trim of the flow and pressure structure with liquid helium flowing through it must be established to determine the optimal geometric configuration of the 5-stage continuous resistance trim in terms of the trim maximum allowable flow rate where an exit pressure of 40 psi is required at the last stage 5 along the trim flow path. In addition, determine the corresponding optimal trim local and overall pressure drop, velocity and CV, and the optimal trim local and overall pumping energy requirement. Following a similar technique as that implemented in the previous section, the multi-stage trim design is a completely different geometric configuration to that at which the prediction tool was developed.

Hence, before the specific optimization can be carried out, the hydrodynamic performance of the baseline multi-stage trim configuration must be determined and quantitatively authenticated against a globally experimentally validated CFD model for single phase flow that has been used in this thesis study. Figure 6-12 (a) shows the geometric configuration of the baseline 5 stage multi-hole continuous resistance trim, and (b) shows the distribution of flow velocity distribution within the trim flow passages. Similar to the flow velocity distribution phenomenon observed in the previous section, Figure 6-12 (b) shows the extent of flow distribution within the trim flow passages where again equal velocity magnitudes are observed to be occurring at each of the holes around a single stage, and higher velocities are seen to be occurring across stages with smaller effective flow diameters as expected. Again, as stated in the previous section, the significance of similar velocities occurring at each of the holes around a stage is that all the holes around a single cage can be characterized as a single effective flow area or diameter, and as mass is conserved the volumetric flow rates are similar across all the holes in a single stage.

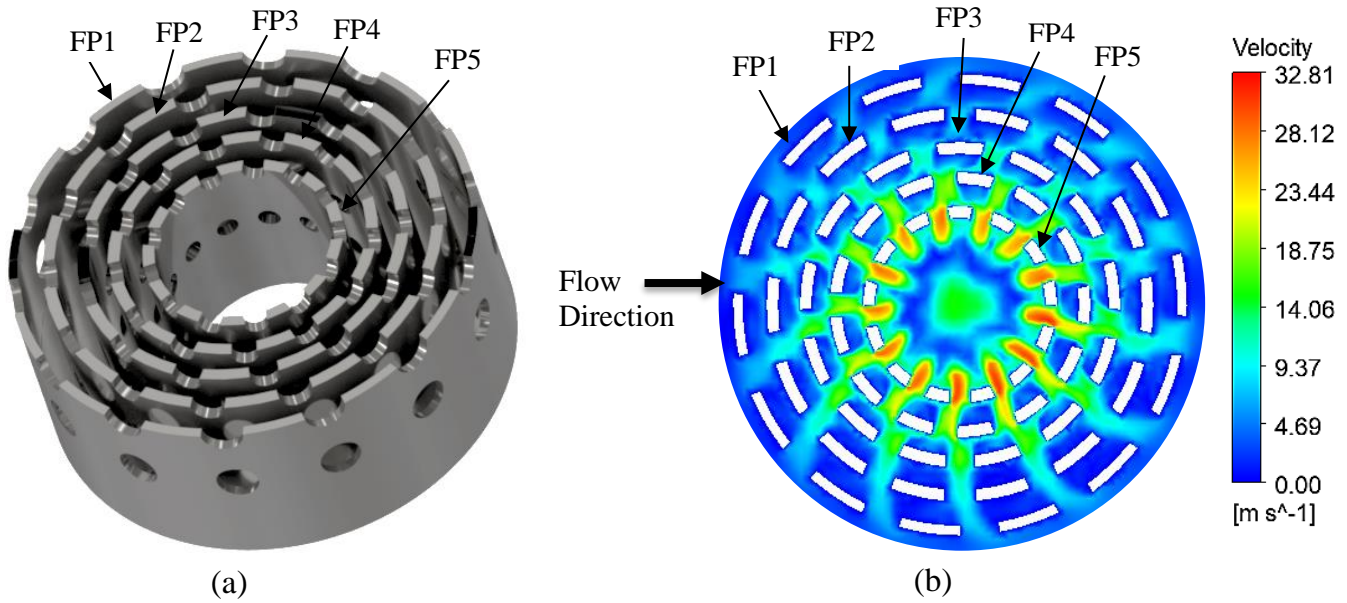


Figure 6-12: (a) Multi-Stage Trim Geometric Configuration and (b) Distribution of Flow Velocity Within the Trim.

Equation (6.9) represents the local pressure drop across each of the 5 flow passages along the trim flow path as a function of flow rate, flow passages effective flow areas, and outlet pressure. As discussed in detail in chapter 4, the operation of the prediction tool allows initial local known or desirable boundary conditions of pressure and flow parameters to be specified at any single given effective flow passage, and from which the entire local trim and global pressure and flow structure can be predicted. As characterized in equation (6.9), the global inlet pressure (P_{IN}) is then computed from the parameter summation across the 5 flow passages that constitutes the trim flow path, and the overall pressure drop is the inherent inlet pressure subtracted from the outlet pressure.

$$\begin{aligned}
 P_{IN} = & \left(\frac{(15852 (Q_{FP1}))}{SG(38A_{FP1}) \left(\sqrt{\frac{(A_{Inlet}^2 - A_{FP1}^2)}{A_{Inlet}^2}} \right)^{-1}} \right)^2 + \left(\frac{(15852 (Q_{FP2}))}{SG(38A_{FP2}) \left(\sqrt{\frac{(A_{Inlet}^2 - A_{FP2}^2)}{A_{Inlet}^2}} \right)^{-1}} \right)^2 + \left(\frac{(15852 (Q_{FP3}))}{SG(38A_{FP3}) \left(\sqrt{\frac{(A_{Inlet}^2 - A_{FP3}^2)}{A_{Inlet}^2}} \right)^{-1}} \right)^2 + \\
 & \left(\frac{(15852 (Q_{FP4}))}{SG(38A_{FP4}) \left(\sqrt{\frac{(A_{Inlet}^2 - A_{FP4}^2)}{A_{Inlet}^2}} \right)^{-1}} \right)^2 + \left(\frac{(15852 (Q_{FP5}))}{SG(38A_{FP5}) \left(\sqrt{\frac{(A_{Inlet}^2 - A_{FP5}^2)}{A_{Inlet}^2}} \right)^{-1}} \right)^2 + P_{Out} \quad (6.9)
 \end{aligned}$$

Table 6-6 presents the results of the specified hydrodynamic performance of the multi-stage trim computed by the prediction model as defined in equation (6.9), and the results of the same specific hydrodynamic performance predicted by the CFD model.

Table 6-6: Stage Trim Geometric Parameter Configuration and Results of Local and Global Pressure and Flow Parameters for the Prediction Model and CFD Model.

	Inlet	FP1	FP2	FP3	FP4	FP5	Outlet	Global
Effective flow area (m²)	0.00226	0.000665	0.000445	0.000327	0.00025	0.000184		
Effective Flow Diameter (mm)	53.7	29.1	23.8	20.4	17.85	15.3		
Static Pressure	103.4						40	
Flow rate (Q) Usgpm								43.9
Prediction Tool Flow Passage Exit Static Pressure (psi)		101.3	96.3	86.8	70.4	40		
CFD Model Flow Passage Exit Static Pressure (psi)		101.1	95.6	86.4	69.3	43		
Prediction Model Pressure Drop (ΔP) (psi)		2.14	5	9.5	16.3	30.4		63.34
CFD Model Pressure Drop (ΔP) (PSI)		2.1	5.2	9.2	17.1	29.3		63.3
Prediction Model Normalised Pressure Difference (psi)		26.96	90.25	210	416.1	800		
CFD Model Normalised Pressure Difference (psi)		27.8	94.6	209	418	805		
Prediction Model CV		30	19.6	14.3	10.9	7.96		5.51
CFD Model CV		29	18.9	14.5	10.6	8.1		5.52
Prediction Model Pumping Power (P) (KW)		0.55	1.28	2.4	4.2	8.0		18.43
CFD Model Pumping Power (P) (KW)		0.61	1.5	2.8	4.8	8.5		18.2

As shown previously in figure 6-12, each of the stages in the multi-stage trim consist of holes equally spaced around a cage for which the sum of the areas of the holes of a stage have been characterised as an effective flow area of the respective stage. The sequence and pattern of arrangement of the flow passages effective flow areas or diameters have been arranged in a manner such that the effective flow diameters of the stages or flow passages are continually reducing up to the trim exit, and where the factor of reduction has been randomly specified. The effective flow diameters have also been randomly selected within the minimum and maximum allowable hole size constraints on the basis that this is the baseline trim from which a measured optimal geometric configuration will be determined from a random geometric configuration, and in addition, reassert the versatility and viability of the prediction models developed in this work.

From the results presented in table 6-6 it can be observed that the effective flow diameter at stage 1 (flow passage 1 (FP1) is 53.7mm, stage 2 (flow passage 2 (FP2) diameter = 29.1mm, stage 3 (flow passage 3 (FP3) diameter = 23.8, stage 4 (flow passage 4 (FP4) diameter = 17.85mm, and stage 5 (flow passage 5 (FP5) diameter = 15.3mm. The global input flow rate at which the hydrodynamic performance was predicted is 43.9 Usgpm, and as stated in the previous section, the exit pressure at flow passage 5 has been specified as 40 psi. Hence, the pressure drop, exit pressure, normalised pressure difference, pumping energy requirement, and flow coefficient (CV) across each of the flow passages and the inlet pressure have been explicitly predicted from the specified exit pressure at flow passage 5. For the initial boundary flow rate of 43 Usgpm, at the given baseline geometric configuration the overall pressure drop is 222.3 psi, the overall CV is 5.51, and the overall pumping energy requirements is 18.6 KW. There are negligible discrepancies in the results of the prediction tool and the CFD model, and this substantiates the integrity of the developed prediction tool. It must be reiterated for the benefit of the reader that this validation process does not form the optimization procedure, but a means of highlighting the confidence factor and robustness of the prediction tool for the purpose of the objectives and deliverables of this Thesis. Contrast of the hydrodynamic performance results w.r.t comparison of pressure drop across the 5 stages (flow passages) along the trim flow path for the prediction tool and the CFD model is further quantitatively depicted in figure 6-13 where the pressure drop across each of the stages/flow passages has been characterised with the ratio of the control valve inlet diameter to a respective trim stage/flow

passage effective flow diameter along the trim flow path. The prediction tool and CFD model results are in excellent agreement within a maximum discrepancy margin of 4.5%.

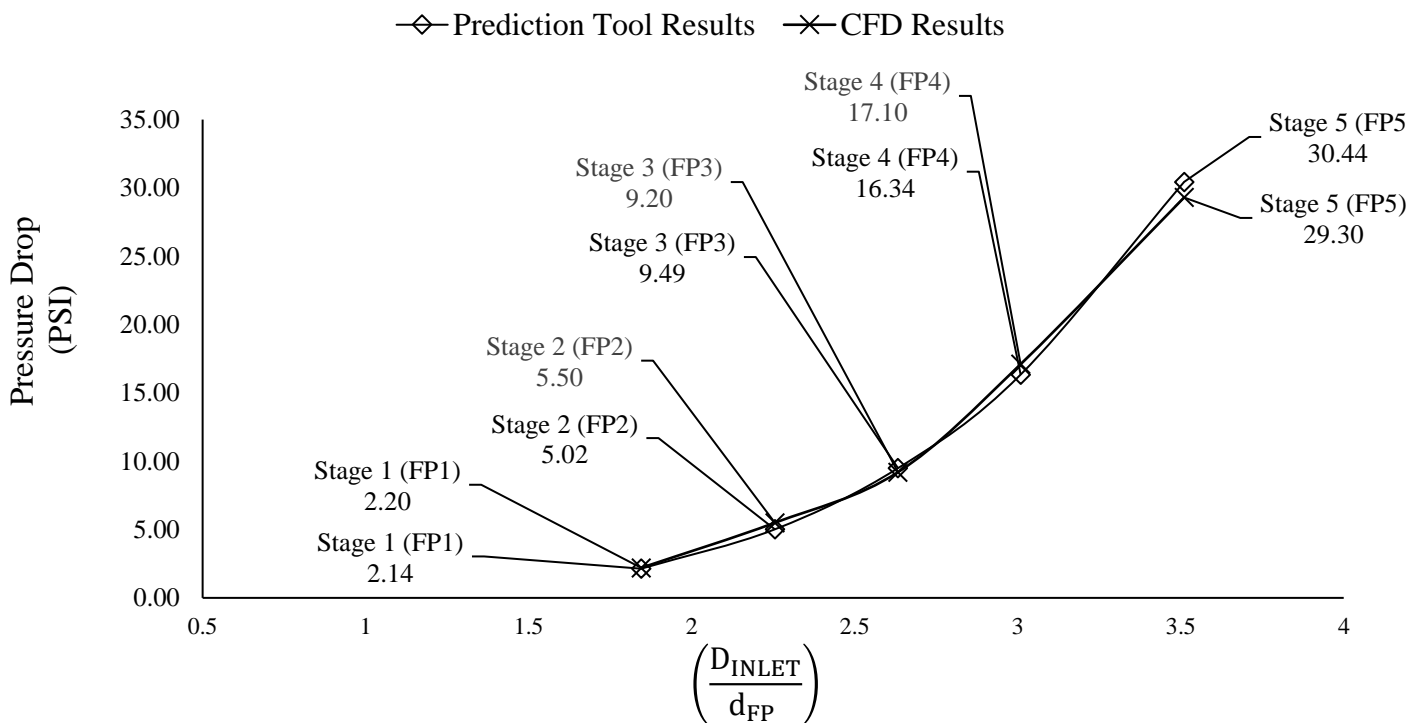


Figure 6-13: Prediction Model and CFD Results of Variations of Local Static Pressure Drop Across The 5 Flow Passages Along the Trim Flow Path for the Baseline Valve Trim.

In order to quantify the local trim hydrodynamic pressure structure characteristics, the normalised pressure difference and corresponding exit pressure across each of the trim stages/flow passages, has been plotted against the ratio of the inlet diameter to a respective stage/flow passage effective flow diameter along the trim flow path. Figure 6-14 depicts the variations of the normalised pressure difference and the local exit pressure characterized by the ratio of the inlet diameter to the effective flow diameter of a respective stage/flow passage along the trim flow path. It can be observed that the higher the ratio of the inlet diameter to a stage/flow passage effective flow diameter along the trim flow path the higher the normalised pressure difference and with corresponding decrease in the respective flow passage exit pressure. This characterization is particularly useful it relates local and global pressure and flow parameters as a function of geometry, and hence the extent of a flow passage exit pressure can be determined.

At stage 5 (flow passage 5 (FP5)), the differential pressure ratio is 800.1 and the exit pressure is 40 PSI, however it must be noted that this pressure has been specified as a desired specific exit pressure. Hence, at the given baseline trim geometric configuration and global input flow rate, the pressure and flow structure has been predicted at each stage-(flow passage) upstream of stage/flow passage 5 as a function of stage 5-(flow passage exit pressure) 40 PSI, and flow rate.

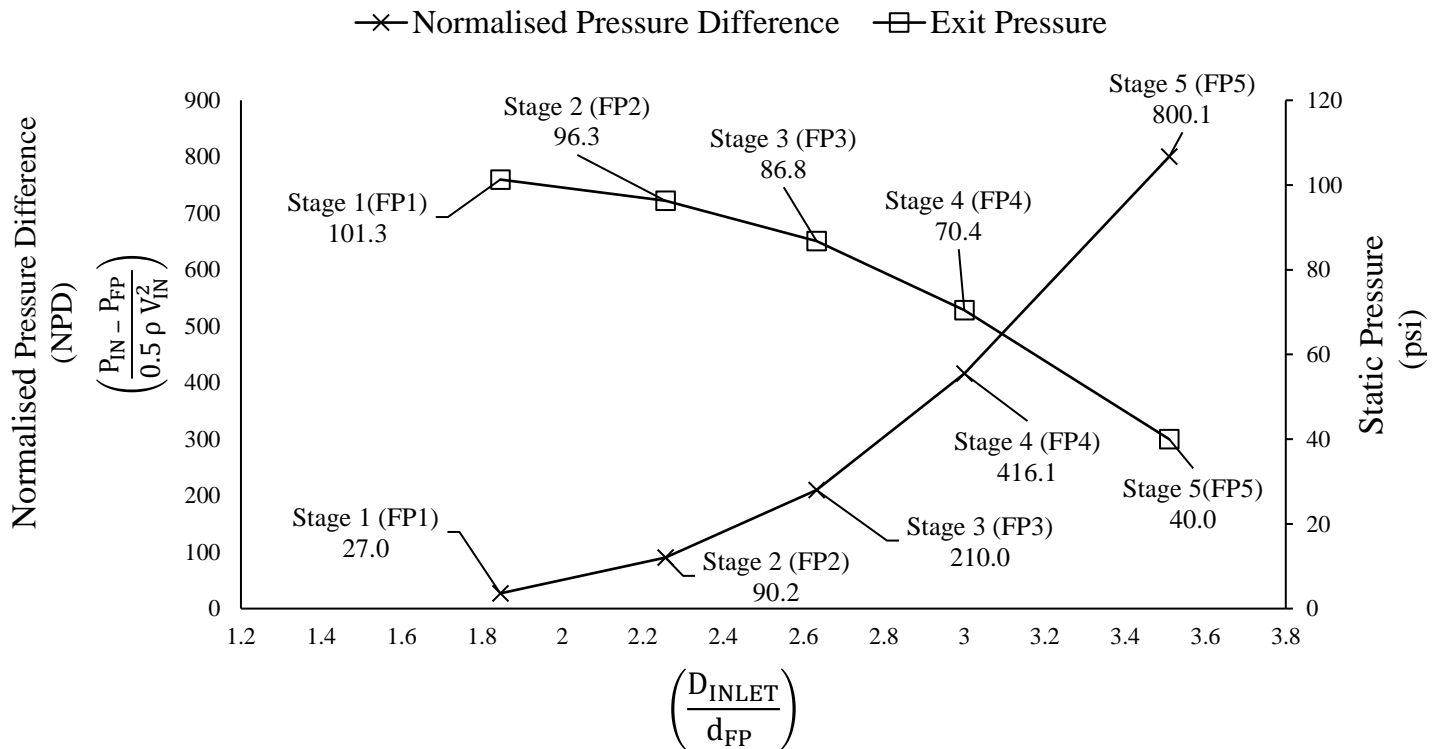


Figure 6-14: Variations of Normalised Pressure Difference and Stage/ Flow Passage Exit Static Pressure w.r.t the Ratio of The Inlet Diameter to The Effective Flow Diameter of a Respective Stage/Flow Passage Along the Trim Flow Path.

Further characteristics of the hydrodynamic performance for the given baseline geometric configuration have been quantitatively depicted by plotting the pressure drop and flow coefficient (CV) across each of the stages/flow passages along the trim flow path as a function of the ratio of the inlet diameter to the effective flow diameter of a respective stage/flow passage along the trim flow path. Figure 6-15 depicts the variation of pressure drop and CV as a function of the ratio of the inlet diameter to the effective flow diameter of a respective stage/flow passage along the trim flow path. It can be seen that the pressure drop increases as the CV decreases and as the ratio of the inlet diameter to the effective flow diameter of respective stage/flow passage increases.

This phenomenon is as expected, such that an increase in the ratio of the inlet to a stage-flow passage effective flow diameter means a decrease in the respective stage-flow passage effective flow diameter, which then results in a decrease in the local CV at the flow passage, and an increase in the pressure drop as the flow is subjected to increasing flow resistance. However, notwithstanding of how the phenomenon is expected to occur through continuity, the distinctive parameter characterization as depicted in figure 6-15 allow for explicit mapping of the trim flow path for local CV and pressure drop as a direct function of initial known flow rate and geometric configuration.

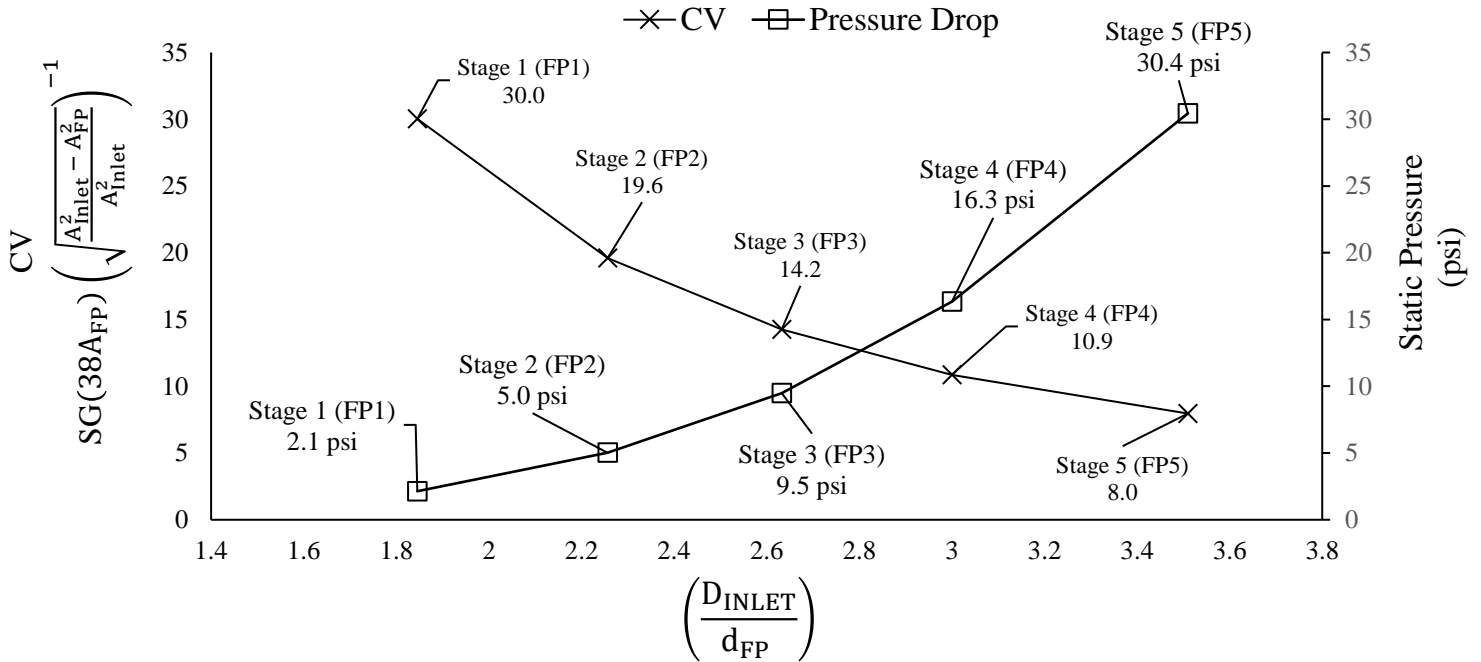


Figure 6-15: Variations of Pressure Drop and Flow Coefficient (CV) at Each of the Stages-Flow Passages Along the Trim Flow Path w.r.t the Ratio of the Inlet Diameter to the Respective Stage-Flow Passage Effective Flow Diameter Along the Trim Flow Path.

For the specific hydrodynamic performance parameters considered for the multi-stage trim, and in addition to the characteristics presented in figures 6-14 and 6.15, the pumping energy requirement at each of the stages/flow passages along the trim flow path has been characterized as a function of the CV at a respective stage/flow path along the trim flow path. The pumping energy has been computed based on a general pump efficiency of 65%, however this can vary with respect to the user's specific pump efficiency.

Figure 6-16 shows the variation of the pumping energy requirement across each of the 5 stages/flow passages along the trim flow path as a function of the respective stage/flow passage flow coefficient (CV) along the trim flow path. The flow coefficient (CV) has been characterized in a novel method directly accounts for and correlates the fluid specific gravity, flow rate and stage/flow path effective flow area. The pumping power is observed to increase as the CV decreases, and this is expected as the CV relationship of effective flow area and flow rate defines that the reduction of the CV is directly proportional to the decrease in the effective flow area of a flow passage. At flow passage 5 (FP5), the pumping energy requirement is 8 KW, for a CV of 7.8 at a ratio of the inlet diameter to the effective flow diameter of 3.51, and the pumping energy requirement at stage 1-flow passage 1 (FP1) is 0.5 KW, with a CV of 30, and at a ratio of the inlet to the effective flow diameter of 1.85. which again as expected, indicates that as the ratio of the inlet diameter to the effective flow diameter of a respective stage flow passage increases there is a proportional increase in the CV and decrease in the pumping energy requirement, and vice-versa.

These hydrodynamic characteristics of pumping energy requirements and flow coefficients (CV) at all the stages- flow passages as a function of the geometric effective flow diameter magnitudes and sequence of arrangement along the trim flow path are overly important. The unique parameter characterization directly correlates global and local trim pressure and flow structure with global and local geometric parameters, and accounts for the complex dependence of the pressure and flow structure on the interaction of multiple flow passages in series as a function of their magnitudes and sequence of arrangement along the trim flow path as a function of their effective flow diameter magnitudes. The construction of the prediction tool developed in this work accounts for all the numerous specific hydrodynamic performance parameters defined in this study.

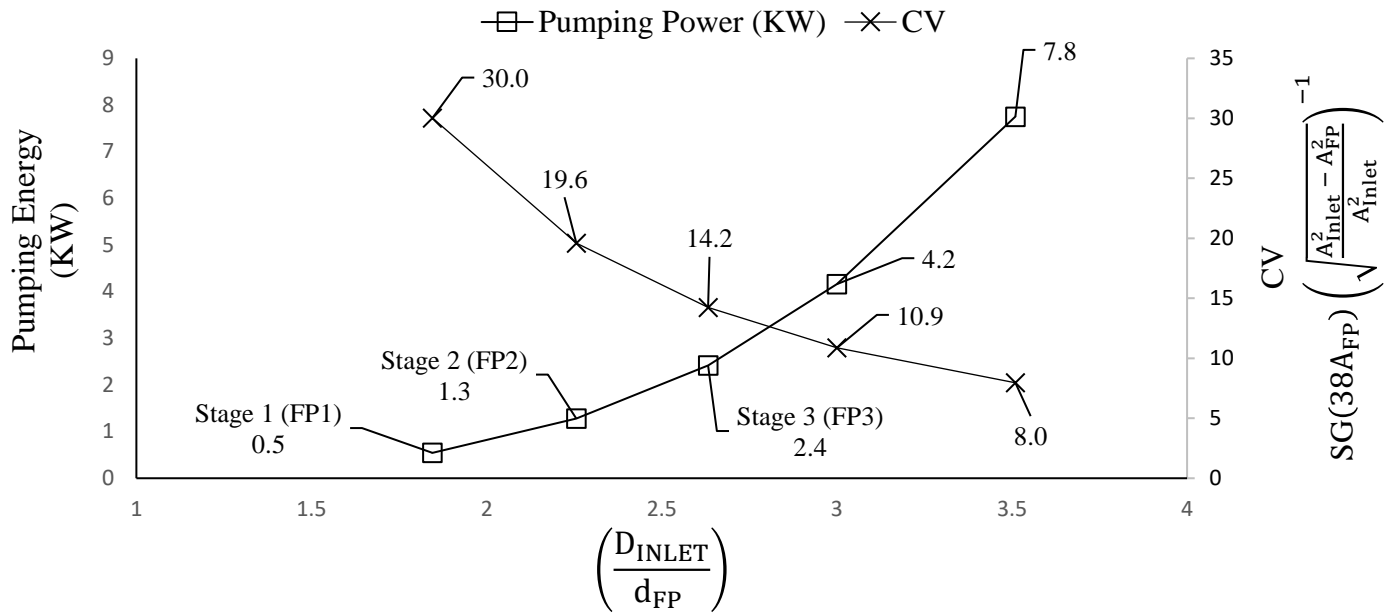


Figure 6-16: Variations of Pumping Power Requirements Across the Stages/Flow Passages Along the Trim Flow Path w.r.t the Flow Coefficient (CV) Across a Respective Stage-Flow Passage Along the Trim Flow Path.

6.8.1. Optimal Trim Local and Overall Pressure Drop, CV and Pumping Energy Requirement.

The specific hydrodynamic performance of 5 stage continuous trim of the flow and pressure structure with liquid helium flowing through the valve is to be established. Determine the optimal geometric configuration of the 5-stage continuous resistance trim at similar flow conditions as those for the baseline trim geometric configuration in terms of the optimal trim local and global pressure drop, CV, and pumping energy requirement. Table 6-7 presents the trim stages/flow passages optimal geometric configuration in terms of effective flow diameter magnitudes and sequence of arrangement along the trim flow path for the specific optimal design hydrodynamic performance requirements as presented.

Table 6-7: Variations of the Specific Optimal Hydrodynamic Performance Characteristic of the Optimal Trim Geometric Configuration.

	Inlet	FP1	FP2	FP3	FP4	FP5	Outlet	Overall
Effective flow area (m²)	0.002264	0.001294	0.00103	0.000893	0.000735	0.00062		
Effective flow diameter (mm)	53.7	40.6	36.2	33.7	30.6	28.1	53.7	
$\left(\frac{D_{\text{INLET}}}{d_{\text{FP}}}\right)$		1.32	1.48	1.59	1.75	1.9		
Static Pressure (psi)	46.5						40	
Flow Rate (USgpm)								44
Pressure drop (psi)		0.42	0.78	1.1	1.72	2.5		3.91
Normalised Pressure Difference (psi)		5.25	15	28.8	50.4	109.2		
Exit Pressure (psi)		48.3	47.5	46.4	44.7	40		
Cavitation Index (σ)		116	61.9	43	26.9	9.31		2.68
CV		68.1	49.9	41.94	33.6	27.8		17.2
Pumping Energy (KW)		0.1	0.23	0.32	0.51	0.74		1.92

From the results presented in table 6-7, it can be seen that the overall pressured drop across the trim is 3.91 psi as compared to the baseline trim pressure drop of 63.4 psi at the same initial volumetric flow rate of $0.0028 \frac{\text{m}^3}{\text{sec}}$. The overall trim flow coefficient is 24.5, and pumping energy requirement is 1.92 KW as compared to 5.51 and 18.2 (KW) respectively. At a business rate average power cost of £15/kWh, the annual pumping power cost for the baseline trim valve is £1572, and £165 for the optimal trim valve, which is a 90% reduction from the baseline cost, and is an exceptionally large reduction. The optimal stages (flow passages sequence of arrangement along the trim flow path in terms of the ratio of the inlet flow diameter to the effective flow diameter of a stage (flow passage) is arranged such that it is 1.32, 1.48, 1.59, 1.75, and 1.9 at stage-flow passage 1 (FP1), stage-flow passage 2 (FP2), stage -flow passage 3 (FP3), stage/flow passage 4 (FP4), and stage 5-flow passage 5 (FP5) respectively.

Figure 6-17 depicts the variations of the exit pressure downstream of the trim 5 stages-flow passages along the trim flow path, and the corresponding normalised pressure difference as a function of the ratio of the inlet diameter to the effective flow diameter of a respective stage-flow passage along the trim flow path. In this design example, the exit pressure at flow passage 5 has been specified as a design condition at 40 psi where the normalised pressure difference is seen to be 109.2, and the sequence of arrangement of the stages-flow paths in terms of effective flow diameter along the trim flow path is optimal in achieving this condition at the given global input flow rate of $0.0028 \frac{\text{m}^3}{\text{sec}}$. It can be observed that the exit pressure at stage-flow passage 4 is 44.7psi with a normalised pressure difference of 50.4, at stage-flow passage 3(FP3) the exit pressure is 46.4psi with a normalised pressure difference of 28.9, at stage-flow passage 2 (FP2) the exit pressure is 47.5 psi with a normalised pressure difference of 15, and at flow passage 1(FP1) the exit pressure is 48.2 psi with a normalised pressure difference of 5.3.

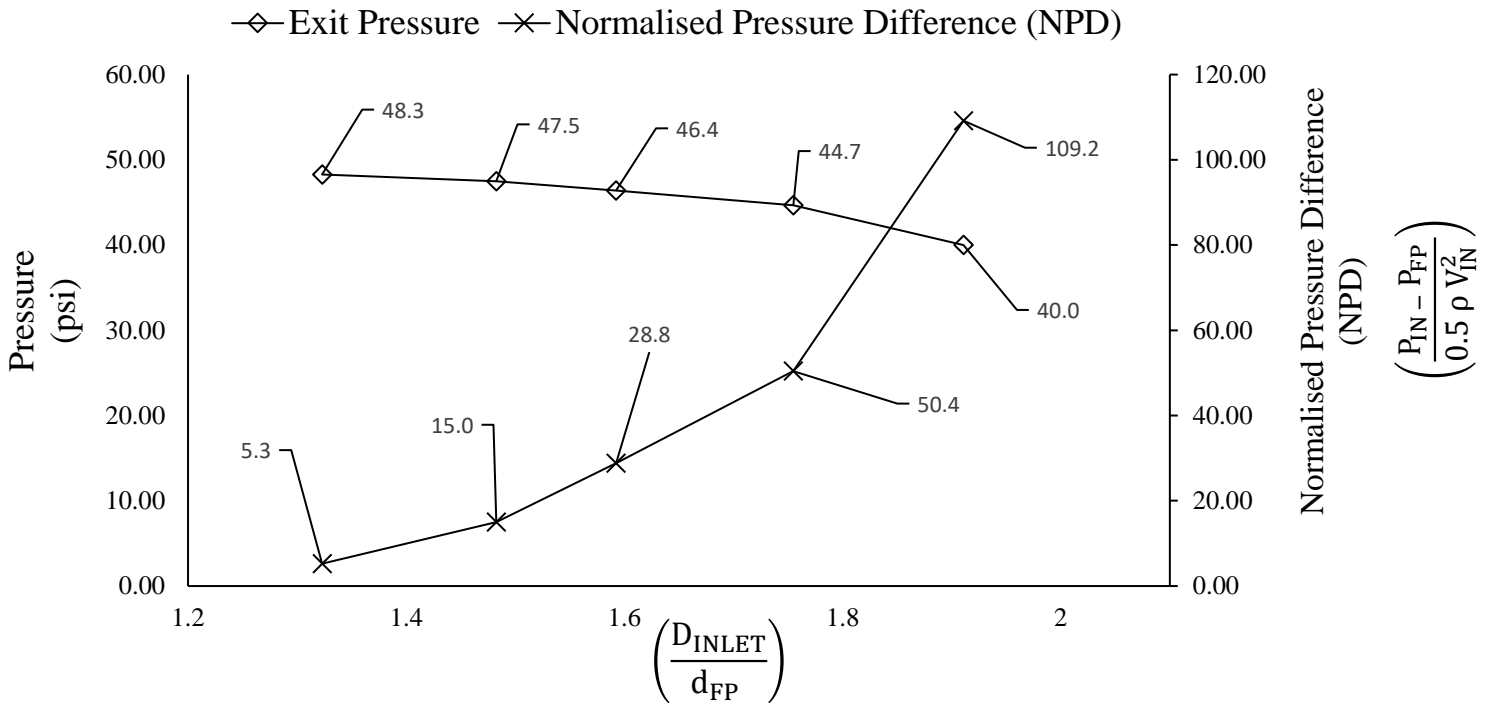


Figure 6-17: Variations of Exit Pressure at Each Stage-Flow Passage Along the Trim Flow Path and Normalised Pressure Difference w.r.t the Optimal Ratio of the Inlet Diameter to the Effective Flow Diameter of a Respective Stage Flow Passage Along the Trim Flow Path.

The specific hydrodynamic performance parameters of the trim are further accentuated in figure 6-18 which depicts the variations of the flow coefficient and pressure drop at each of the stages-flow passages along the trim flow path with respect to the optimal trim flow passages effective flow diameter magnitudes and sequence of arrangement along the trim flow path. The geometric configuration and sequence of arrangement of the effective flow diameters of the stages-flow passages along the trim flow path is characterized with significantly low differential pressures across the flow passages and corresponding high local flow coefficients (CV). The local trim flow passages CV and pressure structure are the inherent characteristics of the optimal geometric configuration for the prescribed desired exit pressure at stage-flow passage 5 (FP5) and the specific optimal objectives of minimal possible local and overall trim pressure drop, and pumping energy requirements at the given global flow rate.

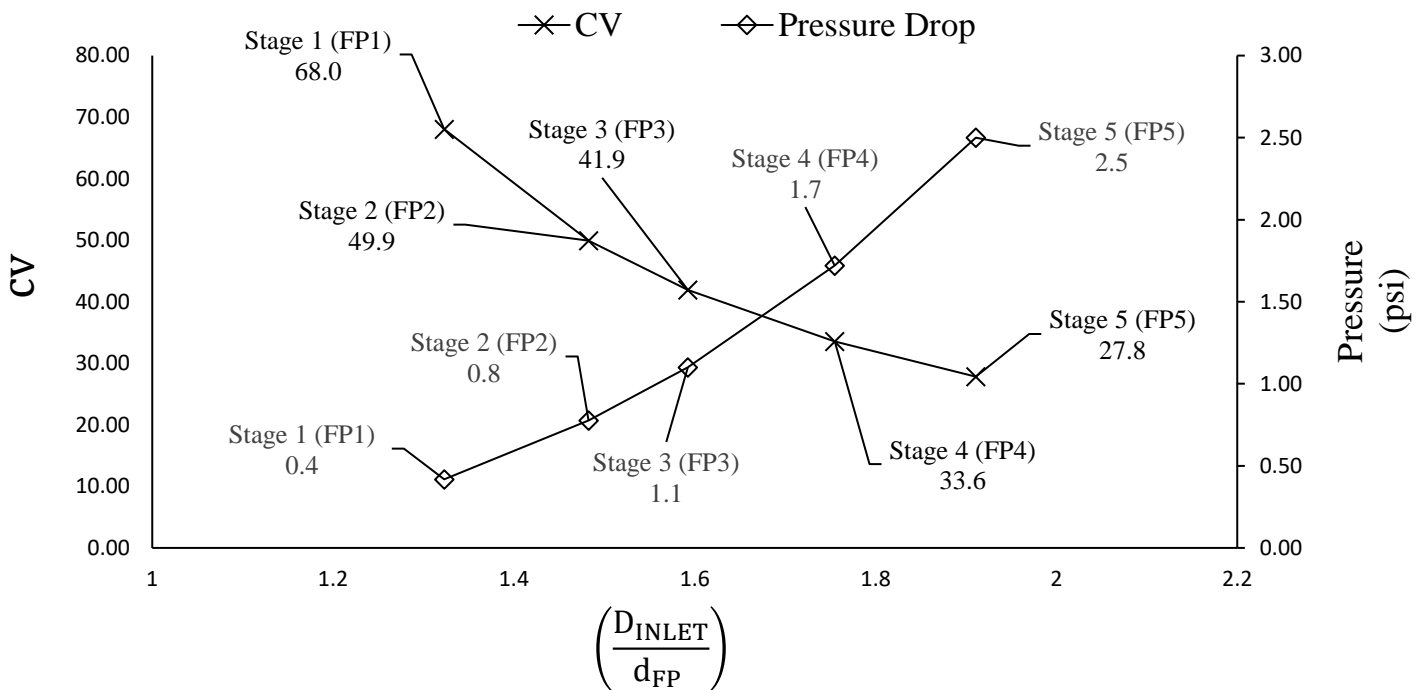


Figure 6-18: Variations of Optimal CV and Pressure Drop Across the Trim Stages-Flow Passages Along the Flow Path w.r.t the Optimal Ratio of the Inlet Diameter to the Effective Flow Diameter of a Respective Stage-Flow Passage Along the Trim Flow Path.

Figure 6-19 depicts the variations of pressure drop across each of the trim stages-flow passages along the trim flow path for the optimal geometric configuration and the baseline geometric configuration w.r.t the sequence of arrangement of the stages-flow passages effective flow diameters along the trim flow path. The geometric configuration of the sequence arrangement along the trim flow path has been characterized through the ratio of the inlet diameter to the effective diameter of a respective stage-flow passage along the trim flow path. It can be observed that for the optimal geometric configuration, at stage-flow passage 1 (FP1) the pressure drop is 0.42 psi at a ratio of the inlet diameter to effective flow diameter of 1.32, and for the baseline geometric configuration, at stage-flow passage 1 (FP1), the pressure drop is 2.1 psi at a ratio of the inlet diameter to the stage-flow passage effective flow diameter of 1.85. At the final stage-flow passage 5 of the trim, it is further observed that the pressure drop for the optimal geometric configuration is 2.5 psi at a ratio of the inlet diameter to the stage-flow passage effective flow diameter of 1.91, and the pressure drop for the baseline geometric configuration at the final stage-flow passage 5 of the trim is 30.4 psi at a ratio of the inlet diameter to stage-flow passage effective flow diameter of 3.5.

The overall pressure drop for the optimal trim geometric configuration is 3.9 psi, and the overall pressure drop for the baseline trim is 63.3 psi which is a substantial reduction in the optimal trim geometric configuration overall pressure drop as compared to the baseline geometric configuration at the same global flow rate of $0.0028 \frac{\text{m}^3}{\text{sec}}$.

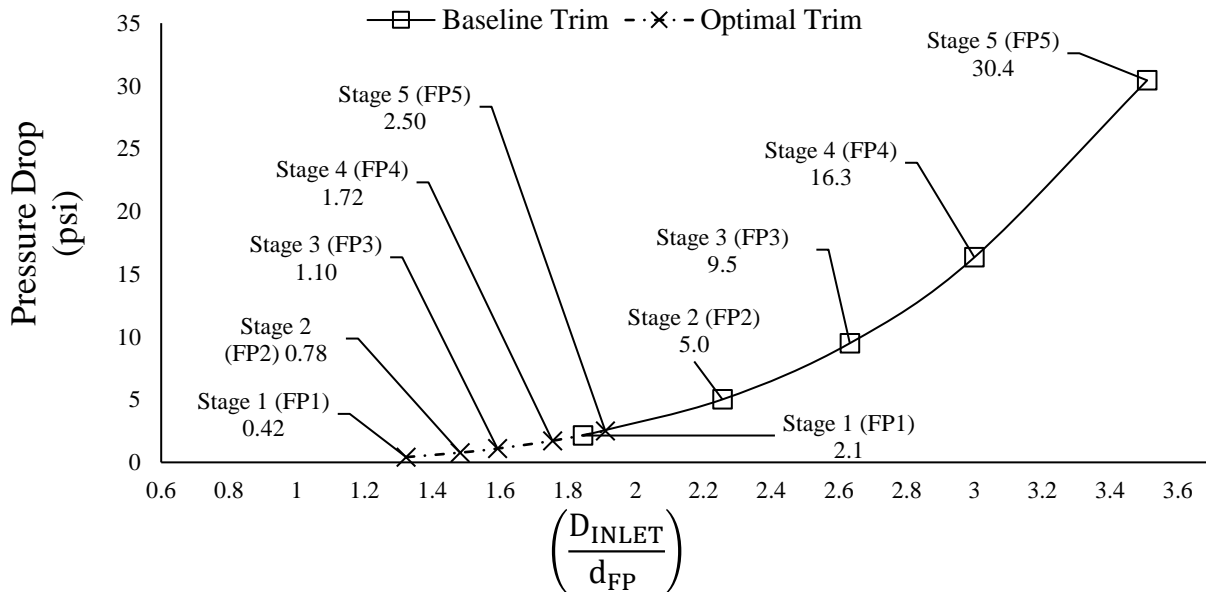


Figure 6-19: Variations of Pressure Drop Across the Flow Passages for the Optimal and Baseline Trim as a Function of the Ratio of the Inlet Diameter to the Effective Flow Diameter of a Flow Passage Along the Trim Flow Path.

The contrast between the optimal and baseline trim geometric configuration's specific hydrodynamic performance is further depicted in figure 6-20 which shows variations of the normalised pressure difference for the optimal and baseline trim w.r.t the geometric configurations characterized by the ratio of the inlet diameter to the effective flow diameter of a respective stage-flow passage along the trim flow path. The optimal geometric configuration in terms of the ratios of the control valve inlet diameter to the trim flow passages effective flow diameters along the trim flow path are substantially lower than the baseline model. As depicted, low ratios of the inlet diameter to the effective diameter of a respective flow passage are characteristic of a lower normalised pressure difference which in retrospect is the ratio of the difference between the control valve inlet pressure and the exit pressure of a respective stage-flow passage along the flow path to the inlet dynamic pressure, and this is characteristic of a low difference between the inlet pressure and a stage-flow passage exit pressure.

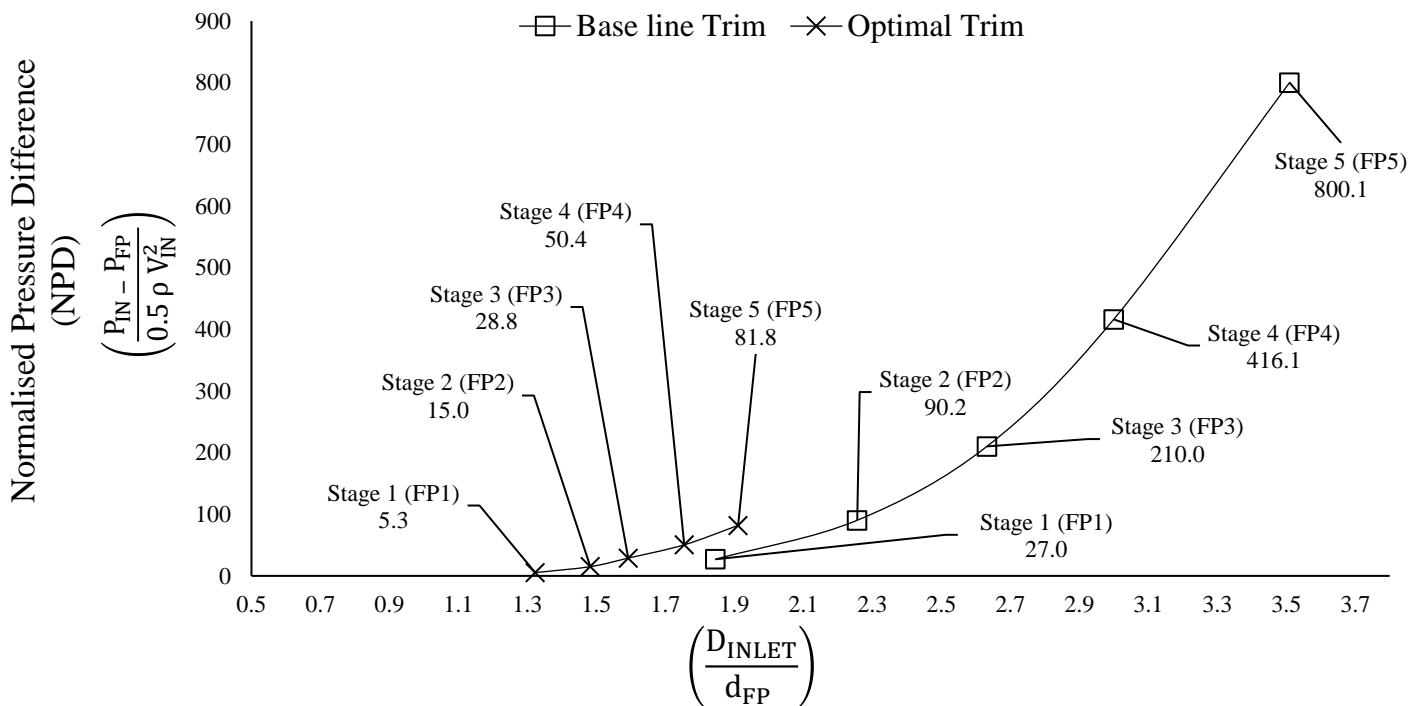


Figure 6-20: Variations of Normalised Pressure Difference for The Optimal and Baseline Trim Geometric Configuration.

Figure 6-21 depicts the variations of the exit pressure at the trim 5 stages-flow passages along the trim flow path for the optimal and baseline geometric configurations, where the geometric configuration is characterised by the ratio of the inlet diameter to the effective diameter of a respective stage-flow passage along the trim flow path. Exit pressures for the baseline geometric configuration stages-flow passages along the trim flow path are substantially larger as compared to the optimal geometric configuration. Furthermore, the differential pressures between the stages-flow passages exit pressures is larger which means that the pressure drop between the respective stages-flow passages is higher than it is for the baseline geometric configuration. For example, the exit pressure at stage-flow passage 1 for the optimal geometric configuration is 46.1 psi and 44.2 psi at stage-flow passage 2 with a differential pressure of 0.8psi, and for the baseline geometric configuration, the exit pressure at stage-flow passage 1 is 103 psi and 96.3 psi at stage-flow passage 2 with a differential pressure of 5 psi. what is more significant in the hydrodynamic characteristics of the optimal and baseline geometric configuration is the pressure structure at the trim exit stage-flow passage, it can be seen that the differential pressure between stage-flow passage 4 and stage-flow passage 5 is 30.4 psi with a prescribed exit pressure of 40 psi at stage-flow passage 5.

The differential pressure at stage-flow passage 4 and stage-flow passage 5 for the optimal trim geometric configuration is 2.2 psi with the prescribed exit pressure of 40 psi at stage-flow passage 5. The optimal geometric configuration yields substantially lower differential pressures across the stages-flow passages at the same global flow rate and prescribed exit pressure at flow passage 5.

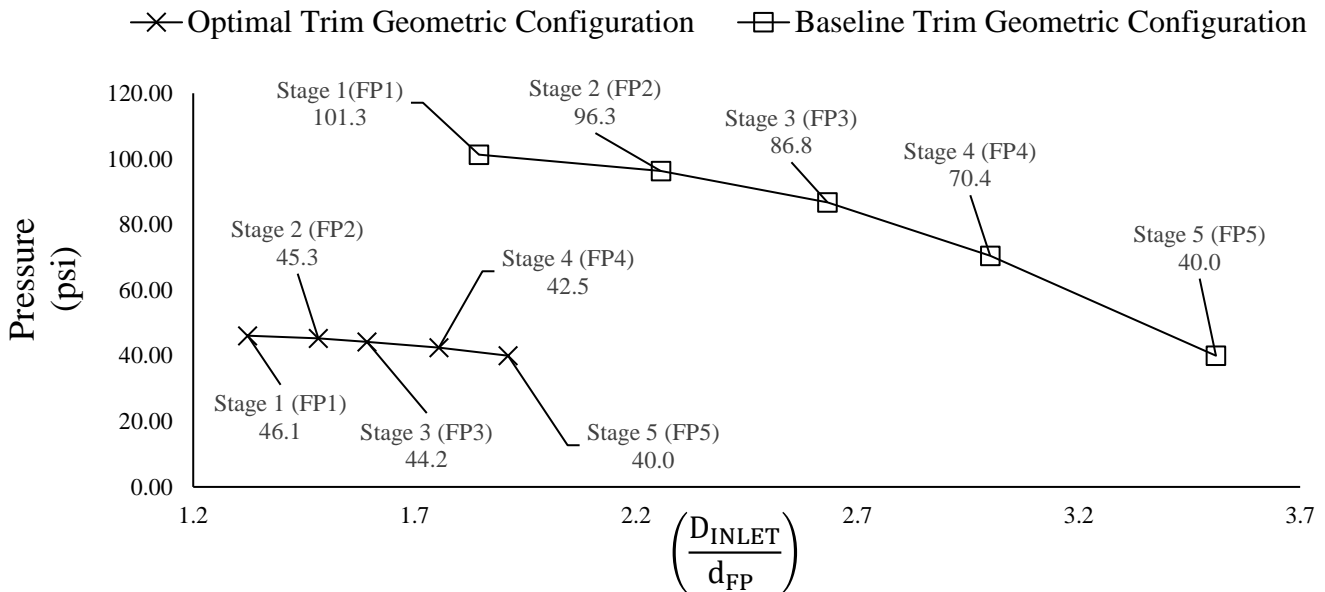


Figure 6-21: Variations of Exit Static Pressure of the Trim Stages-Flow Passages Along the Trim Flow Path for the Optimal and Baseline Trim Geometric Configuration.

Further hydrodynamic characteristics of the pumping energy requirements for the optimal and baseline and optimal trim geometric configuration have been presented in figure 6-22 which depicts the pumping energy requirements at each of the stages- flow passages along the trim flow path for the baseline and optimal geometric configuration. It can be observed that the pumping energy requirements at the optimal trim stages-flow paths is substantially low as compared to the baseline trim, and the low pumping energy requirements are seen to decrease with the reduction in the ratio of the control valve inlet diameter to the effective flow diameter of a respective stage-flow passage along the trim flow path.

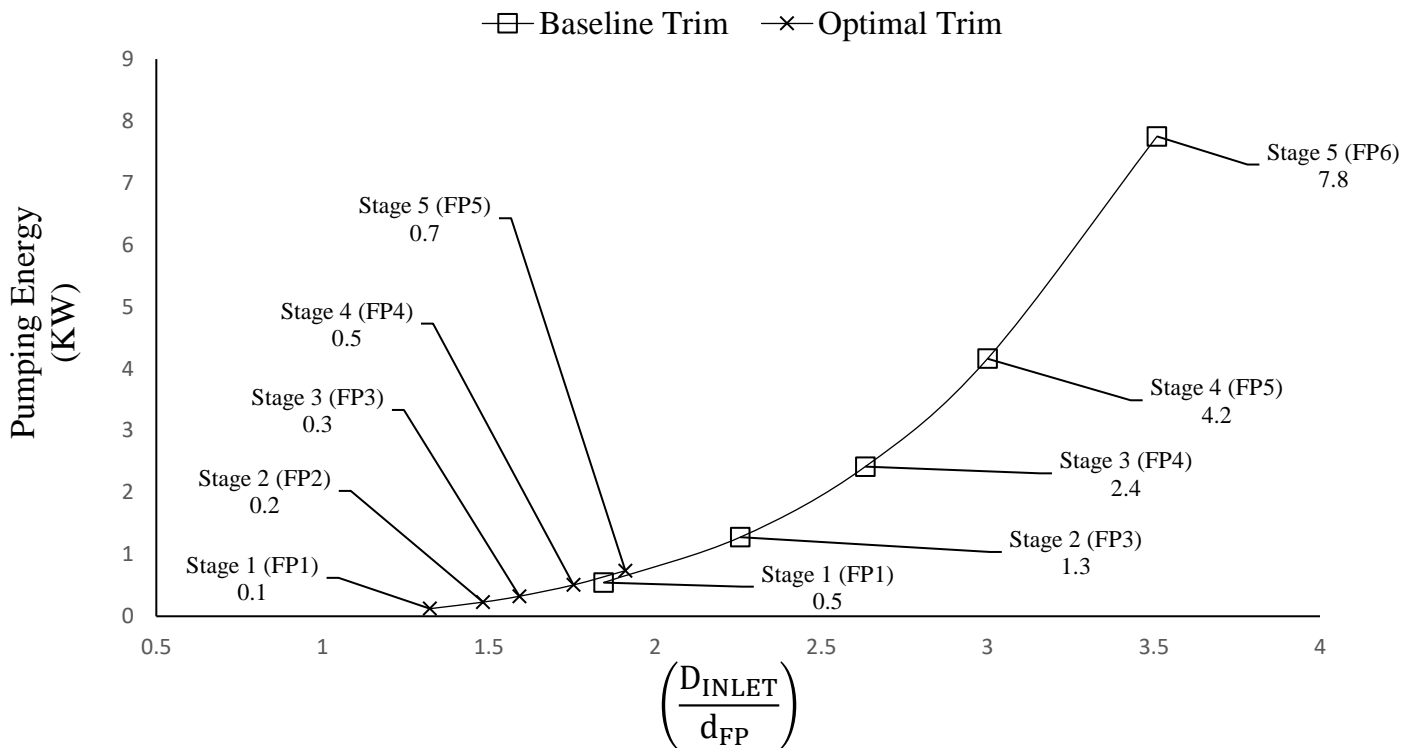


Figure 6-22: Variations of Pumping Energy Requirements for the Optimal and Baseline Trim w.r.t the Ratio of the Inlet Diameter to the Effective Flow Diameter of a Flow Passage Along the Trim Flow Path.

6.8.2. Effects of Trim Geometric Configuration on the Trim Overall Maximum Allowable Flow Rate and Pressure Drop.

In order to analyze the effects of the trim stages-flow passages geometric configuration on the global allowable flow rate and corresponding pressure drop, the optimal and baseline geometric trim geometric examples in the previous section have been analysed at a high global flow rate of $0.007 \text{ m}^3/\text{sec}$ (110 Usgpm). The flow rate was varied from the original benchmark flow rate of $0.0028 \frac{\text{m}^3}{\text{sec}}$ (44 Usgpm) for the optimal trim geometric configuration with design constraints of maintaining the cavitation index across each of the stages-flow passages above 3. The limiting flow rate established iteratively for the optimal trim geometric configuration was then subjected to the baseline trim geometric configuration to facilitate comparison of the hydrodynamic performance between the two trim geometric configurations.

Figure 6-23 depicts the variations of the cavitation index for the optimal and baseline geometric configuration, where the geometric configuration is characterised as the ratio of the control valve inlet to the effective flow diameter of a respective stage flow passage along the trim flow path. At the final stage-flow passage of the baseline trim the cavitation index is 1.2, and this indicates that there is potential for severe cavitation to occur within the vicinity of the stage-flow passage. The cavitation index at stage-flow passage 5 of the optimal trim geometric configurations is 3.55 which is satisfactorily above the threshold of being above the reference threshold of 2 at which either incipient or full cavitation is not expected to occur.

It can be seen that the cavitation indexes at stages-flow passages 1 to 4 for the optimal and baseline trim geometric configurations are not substantially different and yet the baseline geometric configurations yields a pressure structure at which the trim will experience severe cavitation across the final stage-flow passage 5. This critical pressure structure characteristic is not experienced by the optimal trim geometric configuration due to attribution of the sequence of arrangement of the stages-flow passages along the trim flow path w.r.t to effective flow diameter magnitudes.

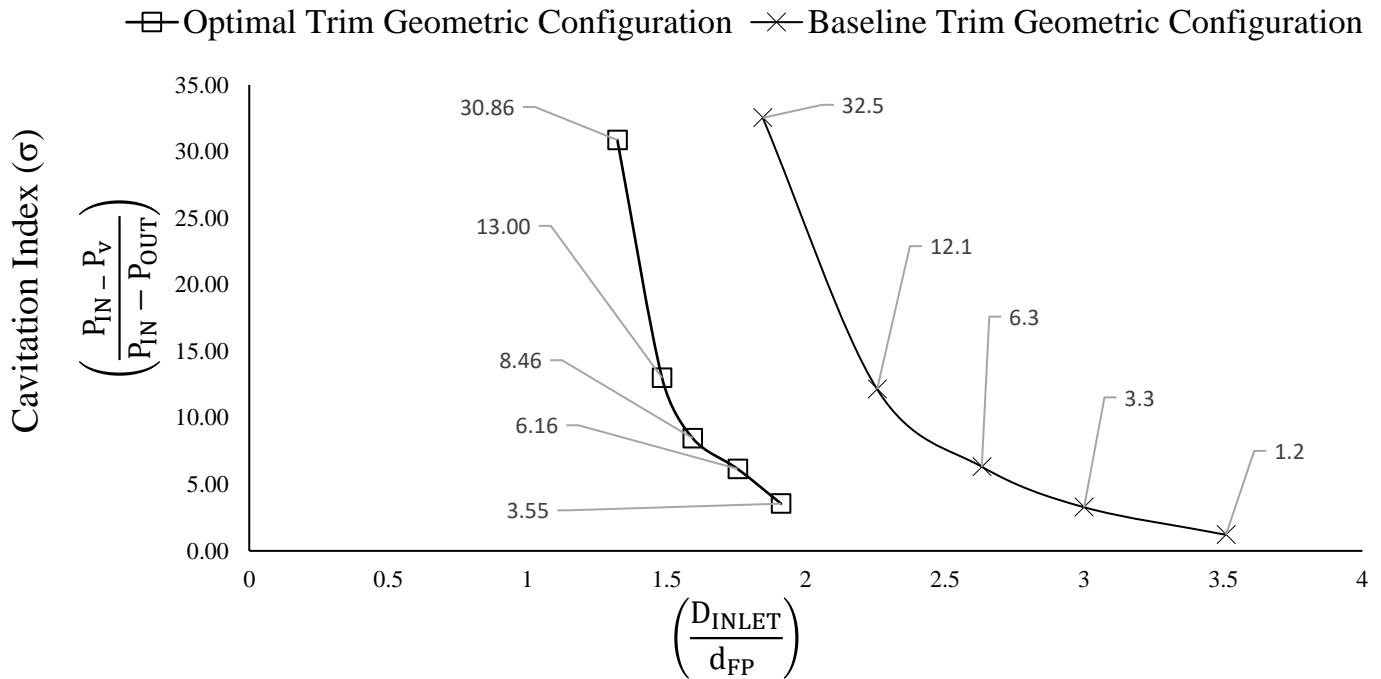


Figure 6-23: Variations of Cavitation Index for The Optimal and Baseline Trim Geometric Configurations

Further comparison of the hydrodynamic performance of optimal and baseline trim geometric configuration at the maximum allowable overall flow rate and pressure drop across the trim is depicted in figure 6-24 which reveals variations of the normalised pressure difference at each of the stages-flow passages along the trim flow path w.r.t the ratio of the control valve inlet diameter to the effective flow diameter of a respective stage flow passage along the trim flow path. The normalised pressure difference for the baseline trim geometric is significantly higher at all the stages-flow passages along the trim flow path as compared to the optimal geometric configuration. With emphasis on the trim exit pressure and flow structure, it can be observed that the normalised pressure difference at the stage-flow passage 5 of the baseline geometric configuration is 797.4 and 81.9 for the optimal geometric configuration at the same global flow rate. The normalised pressure difference is seen to increase exponentially as the ration of the control valve inlet diameter to effective flow diameter of a respective stage-flow passage increases, the high normalised pressure difference for the baseline trim geometric configuration of 797.4 at stage-flow passage 5 corresponds to the inlet to effective stage-flow passage diametric ratio of 3.51.

The normalised pressure difference at stage-flow passage 5 for the optimal geometric configuration of 81.9 corresponds to a diametric ratio of the control valve inlet to the effective stage-flow passage diameter of 1.91. This phenomenon indicates that the normalised pressure difference increase which defines an increase in the pressure drop across a stage-flow path increases relatively to a decrease in a stage-passage effective flow diameter. The pressure and flow structure at a stage-flow passage is dependent on the pressure and flow structure of the immediate upstream stage-flow passage, and the immediate downstream stage-flow passage of the designated stage-flow passage is also influential on the pressure and flow structure with respect to its effective stage-flow passage diameter magnitude. Hence, the pressure and flow structure along the trim flow path is governed by the stages-flow passages effective diameter magnitudes and most importantly and distinctly the combined effects of all the stages flow passages along the trim flow path as a function of the pattern and sequence of arrangement of the stages-flow passages w.r.t effective diameter magnitudes.

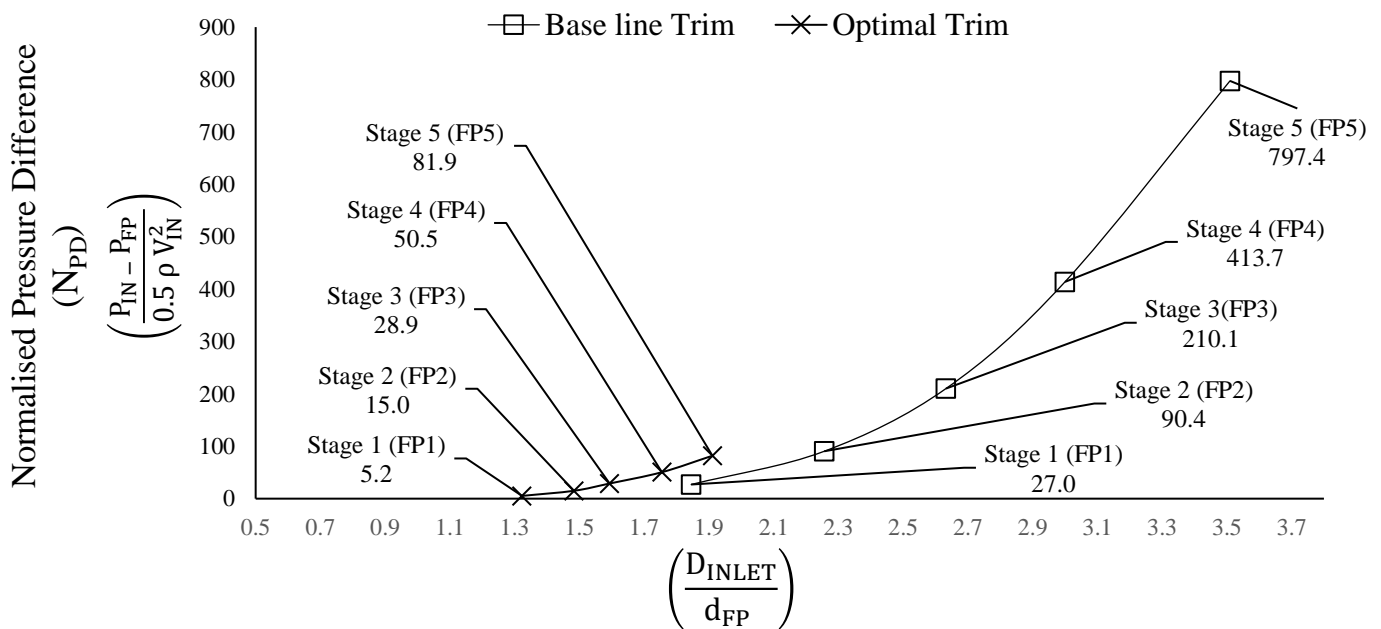


Figure 6-24: Variations of Normalised Pressure Difference for the Optimal and Baseline Trim w.r.t the Ratio of the Control Valve Inlet Diameter to the Effective Flow Diameter of a Respective Stage-Flow Passage Along the Trim Flow Path.

Figure 6-25 shows the variations of pressure drop across the stages-flow passages of the optimal and baseline trim geometric configurations, where the geometric configuration is characterized by the ratio of the inlet diameter to the effective flow diameter of a respective stage-flow passage along the trim flow path. It can be observed that excessively high pressure drop magnitudes are experienced across the stages-flow passages of the baseline geometric configuration, and in contrast with the optimal geometric configuration, at the last stage-flow path 5 of the baseline trim geometric configuration, the pressure drop is 191 psi and 15.6 psi for the optimal geometric configuration. Here again, the pressure drop across the stages-flow passages for both the baseline and optimal geometric trim geometric configuration increases with an increase of the ratio of the inlet diameter to the effective flow diameter of a stage-flow passage along the trim flow path. What is most importantly observed is that the baseline geometric configuration stages-flow passages present a substantially larger difference in the ratio of the control valve inlet diameter to the effective stage-flow passage diameters between the stages-flow passages along the trim flow path. Hence, in addition to the effects of the high ratio of the control valve inlet diameter to the effective stages-flow passages diameters, a larger difference between the stages-flow passages of the diametric ratio of the control valve inlet to the effective flow diameter of a stage-flow path is characteristic to high pressure drop across the stages-flow passages along the trim flow path.

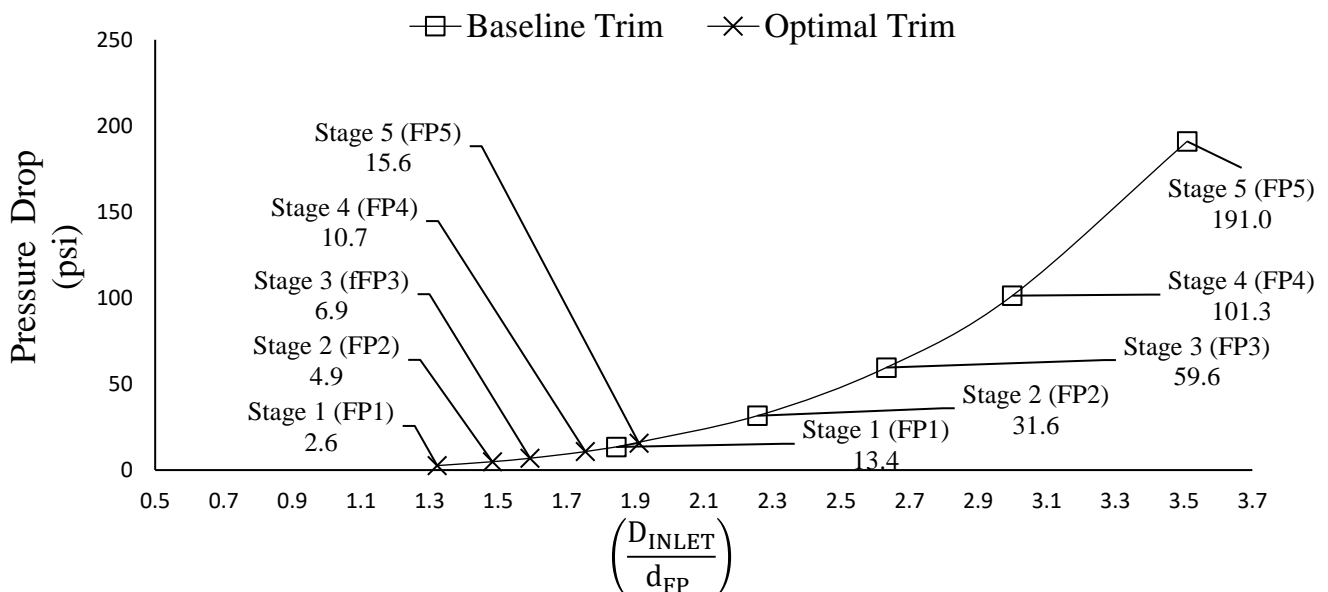


Figure 6-25: Variations of Pressure Drop Across the Trim Stages Flow Paths for the Optimal and Baseline Geometric Configurations.

Figure 6-26 depicts the variations of the local flow coefficient (CV) across the stages-flow passages of the optimal and baseline trim geometric configurations along the trim flow path as a function of the ratio of the inlet diameter to the effective flow diameter of a respective stage-flow passage. The overall magnitude of the flow coefficient of the trim is solely and directly dependent on the magnitudes and sequence of arrangement of the stages-flow passages effective flow diameters along the trim flow path. Hence, it can be observed that the optimal trim geometric configuration exhibits higher CV values across the stages-flow passages as compared to the baseline trim geometric configuration, and the values of the CV's between the stages-flow passages for the optimal trim geometric configuration are relatively less and proportional to the magnitudes of the stages-flow passages effective flow diameters. For the CV and geometric configuration characteristics. It can be observed that the CV increases as the ratio of the inlet diameter and effective flow diameter of a stage-flow passage decreases which relates to an increase in the flow passage effective flow diameter with corresponding less resistance to flow. In addition, the sequence and arrangement of the stages-flow passages w.r.t the effective flow diameter magnitudes is highly influential on the trim local flow and pressure structure through the combined interaction of the stages effective flow diameters along the trim flow path.

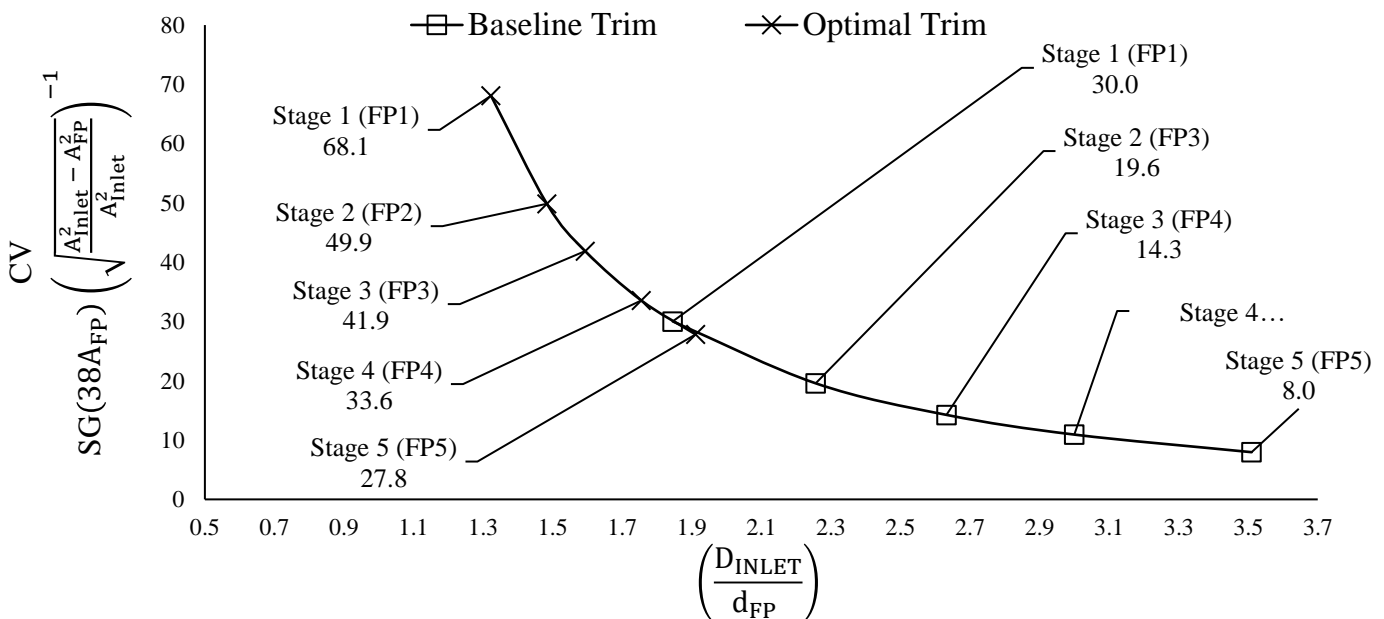


Figure 6-26: Variations of Flow Coefficients (CV) Across the Stages-Flow Passages of the Optimal and Baseline Trim Geometric Configurations.

Further comparison of the hydrodynamic performance characteristics of the optimal and baseline trim geometric configurations is presented in figure 6-27 which shows the variations of the local pumping energy requirements at each of the trim's stages-flow passages along the trim flow path for the optimal and baseline geometric configurations. It can be observed that there is an exceptional high pumping energy demand at the baseline trim stages-flow passages, and where the pumping energy requirement is seen to increase with an increase in the ratio of the inlet diameter to the effective diameter of a respective stage-flow path along the trim flow path. The pumping energy requirement at the trim last stage-flow passage 5 (Fp5) is 121.9 KW for the baseline geometric configuration, and 10 KW for the optimal geometric configuration at stage-flow passage 5 respectively where there is significantly less power requirement for the optimal trim geometric configuration. The pumping energy requirement is seen to increase with an increase in the ratio of the inlet diameter to the effective flow diameter of a stage-flow passage, and in addition, the sequence of arrangement of the stages-flow passages w.r.t the effective flow diameters has a direct effect on the pumping energy requirement at each stage-flow passage. The optimal sequence of arrangement of the stages-flow passages of the trim for the specific optimal hydrodynamic output objective functions has been determined iteratively.

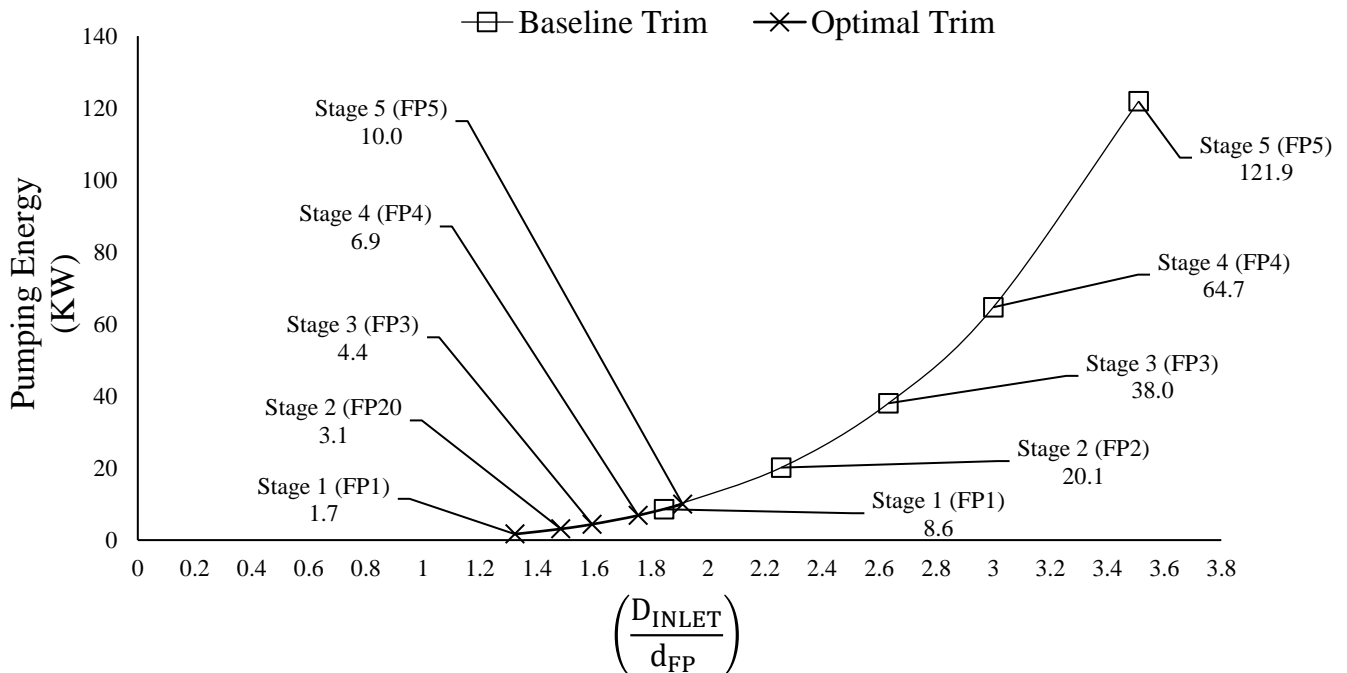


Figure 6-27: Variations of Pumping Energy Requirements Across the Trim Stages-Flow Passages Effective Flow Diameters Along the Trim Flow Path for the Optimal and Baseline Trim Geometric Configurations.

In order to highlight the interrelations between the local pumping energy requirements across the trim stages-flow passages and global pressure and flow parameters, the pumping energy and normalised pressure difference have been plotted as a function of the ratio of the control valve inlet diameter to the effective flow diameter of a stage-flow passage along the trim flow path for the optimal trim geometric configuration. Figure 6-28 shows the variations of the pumping energy requirements and normalised pressure difference at the trim stages-flow passages along the trim flow path for the optimal trim geometric configuration. It can be observed that the pumping energy requirements increase with an increase in the ratio of the control valve inlet diameter to the effective flow diameter of a respective stage-flow passage, and the normalised pressure difference relatively follows a similar trend. From this characterization the designer can relate the extent of the pumping energy requirement to the control valve global inlet pressure, density, and flow rate as a function of the local trim geometry for multi-stage-flow passage trims.

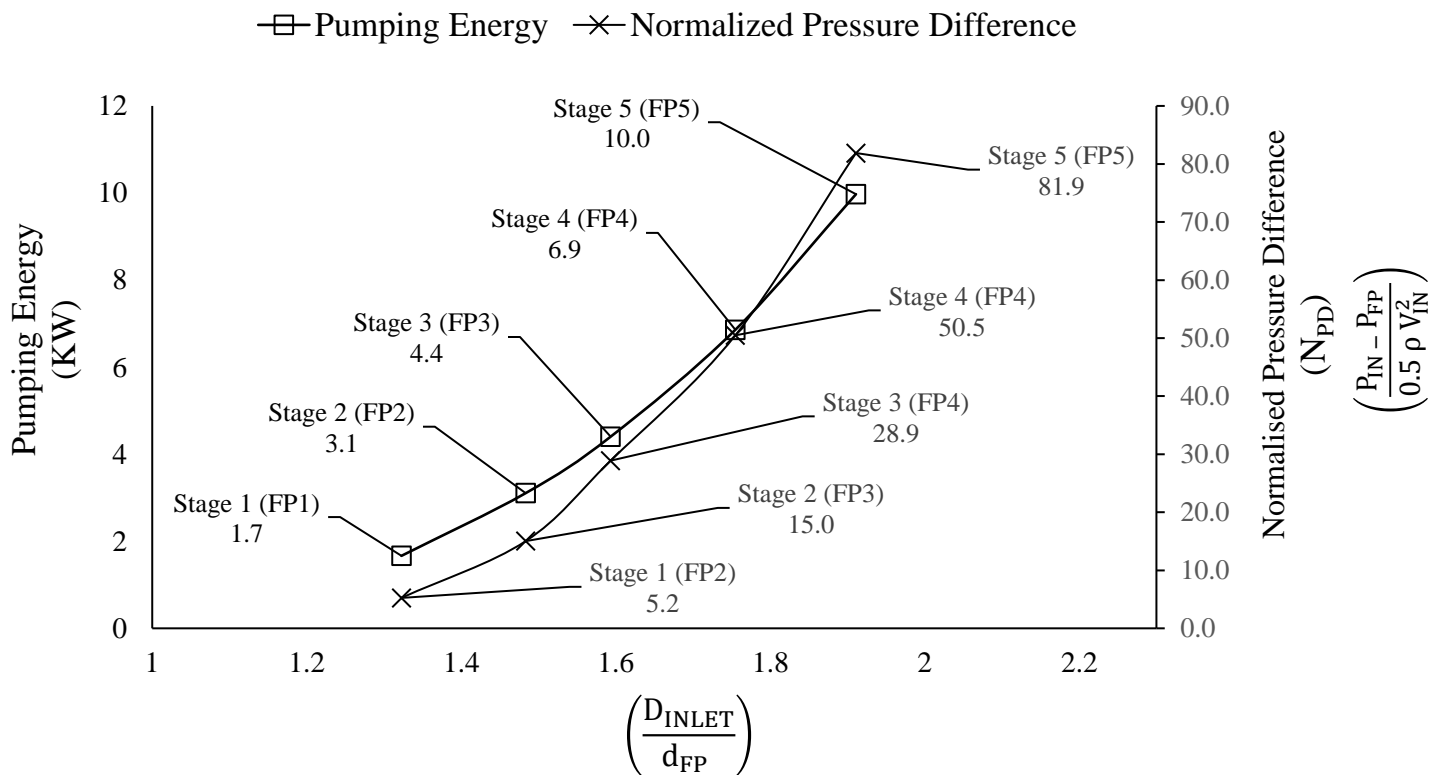


Figure 6-28: Variations of Pumping Energy Requirements and Normalised Pressure Difference at the Stages-Flow Passages of the Optimal Trim Geometric Configuration.

CHAPTER 7

CONCLUSIONS

The results obtained in the previous chapters regarding the hydrodynamic performance of a control valve and the development of the optimization model of a control valve hydrodynamic performance characteristic, extensive conclusions have been presented in this chapter. The details in this chapter include a summary of the achievements and contributions to the existing knowledge scope. In addition, the extent of the work carried out in this work is then evaluated and requirements for future work in the hydrodynamic performance of a control valve are defined.

7.1. Research Problem

The hydrodynamic performance of a control valve is particularly important as flow and pressure limitations need to be explicitly known to allow for efficient and safe operation. There have been numerous reports of detrimental failure of control valves due to cavitation damage that has compromised the valve body and component's stress integrity, and seat damage that has compromised the sealing capabilities. Control valve hydrodynamic performance is at present determined through the widely referenced standard ISA-75-01.01.01 (IEC 60534-2-1) where the hydrodynamic performance of a control valve is determined from empirical equations and coefficients that have been derived from extensive experimental tests from which only global parameters have been used to assume the extent of the local flow structure. Furthermore, the empiricism accounts for specific valve group types within the scope of the standards. The standards derived empirical equations and coefficients cannot be accurately referenced for control valves with geometry outside the scope of the standards, hence presenting a high risk of inaccurate hydrodynamic performance predictions of multi-stage trim control valves. The advent of highly advanced and complex software for flow field analysis, it is now feasible to accurately model the flow within complex multi-stage trim control valve computationally and analyse and map the complex local flow field under varying geometric and flow conditions. Over empiricism has led to numerous publications of coefficients and factors specific for different geometric configurations and flow parameters where accurate reference is not always possible, thus introducing significant ambiguity in the predictions of the critical hydrodynamic performance of a multi-stage trim control valve.

7.2. Research Aims and Major Achievements

From the extensive literature review on this subject, the defined main aims of this thesis are as follows:

Research Aim # 1: Standard Based Hydrodynamic Performance Diagnostics of a Control Valve

Achievement # 1: the study presents an extensive standards-based investigation on the application of the empirically derived methodology used to predict the hydrodynamic performance of a control valve. A study on the flow of water in a multi-flow passage control valve has been presented. The experimentally derived data available in the published literature within the scope of the Instrumentation Society of America (ISA) 75-01-01) standards, and other widely acceptable empirical flow equations on the geometric and flow characteristics within control valves have been implemented on a baseline multi-flow passage control valve to determine the hydrodynamic performance limits of (a) allowable flow rate (b) allowable differential pressure, and (c) choked flow characteristics.

The results of the hydrodynamic performance predictions of a control valve obtained from the standards methodology defined the performance limits within which the control valve can operate, and the corresponding flow coefficient (CV) available. the information provided from this aim facilitated the implementation of advanced CFD techniques as presented in the next aim to evaluate the appropriateness of the standards-based methodology in predicting the allowable differential pressure, allowable flow rate, and choked flow characteristics. Furthermore, widely accepted flow equation based on continuity hypothesis have been used in addition with the standards methodology to predict the flow field characteristics have also been evaluated in detail through computational fluid dynamics (CFD) in the next aim.

Research Aim # 2: CFD Based Hydrodynamic Performance of a Control Valve

Achievement # 2: Comprehensive CFD based diagnostics have been carried out in a multi flow passage control valve. The evaluation of the standard's hydrodynamic performance predictions through a numerical study has been presented. The numerical study has been carried out under similar conditions to those presented in the standard's empirically based hydrodynamic performance prediction models as detailed in aim 1.

Detailed numerical diagnostics of the complex local flow and pressure structure within a control valve have been carried out through a dedicated single and multi-phase mixture model. The local static pressure distribution within the control valve has been qualitatively and quantitatively analysed, the pressure structure has been qualitatively represented through contour plots depicting the local pressure distribution in detail. The maximum allowable differential pressure across the valve, at which respective flow rate does not increase any further regardless of further increase in the differential pressure have been quantitatively analysed w.r.t the vapour volume fraction. The results obtained in this aim have been compared with the results obtained from the standard's methodology where substantial discrepancies have been realised. The CFD model overpredicted the maximum flow rate by 14.4%, the maximum differential pressure by 18.1%, and the CV by 9.5%, however what is interesting was that the standard's published fluid pressure recovery factor for a control valve type that closely resembles the baseline valve seat and plug arrangement is in good agreement with the CFD predicted fluid pressure recovery factor.

The overprediction of the maximum allowable differential pressure and flow rate is quite significant, and it does indicate that the CFD model is more efficient as it extends the performance limits of a control valve substantially. This prevents oversizing of valves with higher cost implications, however based on performance predictions, this highlights inconsistencies in accurately predicting the flow field using present methodologies as they do not consider actual local geometric parameters. Due to these inconsistencies, it is thus justified to carry out further comprehensive investigations with direct considerations of local trim geometry, and this is presented in the next aim.

Research Aim # 3: CFD Based Parametric Investigations of a Control Valve

Achievement # 3: This study provides a comprehensive CFD based analysis on the geometric effects on the local and global flow characteristics in a control valve. A detailed numerical study on the flow of water within a control valve has been presented. Based on the information provide in aim 2, it has been concluded that the published empirical data may not be accurately referenced for valves outside the scope of valve types accounted for in the standards. In addition, there is substantially limited published data on hydrodynamic performance of multi-flow passage control valves. To gain an in depth understanding of the geometric and flow interactions, novel characterizations and correlations of geometric and flow parameters have been developed.

To determine the flow field sensitivities to the local trim geometry, each flow passage along the flow path has been defined through the effective flow area. The entrance and exit pressure at each flow passage and the corresponding differential pressure across each flow passage have been defined as the dependent flow field parameters. In order to facilitate a wide range of investigations to quantify the local and global geometric and flow interrelations gain an in depth understanding on the complex local and global geometric and flow relations, numerical simulations have been carried out for various (a) flow passages effective area sizes, (b) various effective flow area sequence of arrangement along the flow path w.r.t effective flow area sizes, (c) global differential pressure, (d) flow rates. These exhaustive investigations were crucial w.r.t to attaining valuable data to facilitate the development of semi-empirical prediction models.

The novel geometric and flow parameter characterization are a major achievement of this study. The results disclosed in this study provide clear insight into the complexity of the flow sensitivities to the geometry, and henceforth provides clarity into the flow behaviour within a control valve.

Research Aim # 4: Development of Analytical Model Tools for Optimum Hydrodynamic Performance Prediction and Optimization of a Control Valve

Achievement # 4: In this study an analytical model for hydrodynamic performance prediction and optimization has been developed. The optimization tool utilises an iterative method to obtain a solution for an objective function output for any given initial condition. The pressure and flow structure along the entire flow path can be explicitly optimized for any objective global function output within the geometric flow passage area maximum limit constraints. The optimization model presented in this study utilises the semi-empirical characterizations developed for the prediction of the local entrance and exit pressure and corresponding differential pressure across each flow passage along the entire flow path, the inherent global differential pressure, and corresponding flow coefficient (CV) for a wide range of flow conditions. One most important and novel aspect of the developed models is that they are scalable for both geometric and dynamic similarities. Through the developed optimization model, one can map the entire flow path of a multi-stage trim and have accurate data of the pressure structure within the vicinity of the flow passages and in addition, have accurate information for critical limits at which the valve can operate without cavitation, flashing, and choked flow. In addition, the optimization model provides corresponding information on the mean flow velocity, and flow rate of water along the entire flow path of the control valve. Hence the optimization model developed in this work can be accurately implemented in the design of multi and single flow passage control valves with ease of application and robustness.

7.3. Thesis Conclusions

Based on the extensive literature regarding flow within control valves, a detailed study has been carried out to evaluate the appropriateness of application of present state of the art hydrodynamic performance predictions on geometric configurations that are not published or are non-existent. Novel additions have been provided to enhance and improve the present understanding of the flow field sensitivities to the geometric configuration and overall hydrodynamic performance of a control valve. A summary of the major conclusions for each of the stipulated objectives of this Research study are as follows.

Research Objective # 1: To Determine the Hydrodynamic Performance of a Control Valve Using Existing State of The Art Standard Based Methodologies.

Conclusion # 1: Based on the investigations concerning the prediction of the hydrodynamic performance of a control valve using the current existing empirical methodologies, it is conclusive that published data of empirical equations and reference data of valve types and trim geometry outside the scope of the standards cannot be accurately referenced so as to closely predict the hydrodynamic performance. From a design perspective, published standard's data of a control valve type trim that closely resembles the baseline valve in this study has been used to predict the allowable global differential pressure, and allowable flow rate at the corresponding choked flow conditions. In addition, it has been established that the present standard methodologies only account for the global parameters to assume the local pressure and flow behaviour. This objective was important in that it provided information to facilitate the evaluation of the results through advanced computational fluid dynamics (CFD) techniques presented in the next objective.

Research Objective # 2: To Evaluate the Published Standard's and Empirical Data Predictions of the Hydrodynamic Performance Using Advanced CFD Based Analysis

Conclusion # 2: Based on the investigations concerning the CFD analysis-based evaluations of published standard's and empirical data predictions carried out in this study of the allowable differential pressure, allowable flow rate and choked flow conditions within the baseline control valve, it can be concluded that the CFD model substantially overpredicts the global differential pressure, allowable flow rate, and subsequent choked flow conditions. This is attributed to the fact CFD model explicitly accounts for the local geometric effects on the flow field, furthermore, significant inconsistencies have been highlighted because of possible invalid reference of

published empirical data which may not always be applicable for valve trims outside the scope of the published specific valve trim types, and non-scalability attributed to the deterministic approach outlined in the present methodologies. The results from this objective have provided the impetus to further investigate the local flow behaviour w.r.t the flow field sensitivities to the geometric configuration.

Research Objective # 3: To Establish the Effects of the Inlet Average Velocity on The Differential Pressure Ratio at The Valve Seat Flow Passage

Conclusion # 3: based on the investigations concerning the effects inlet average velocity on the differential pressure ratio at the valve seat flow passage, defined in this study as flow passage 3 (FP3). The investigations were carried out varying velocities of 1, 2,3 and 4 m/sec, and for 4 different combinations of flow passages effective flow areas along the flow path. The differential pressure ratio (DPR) at the valve seat/ flow passage 3 (FP3) has been characterized with the combined flow passages effective flow areas here defined as the multiple of all the effective flow areas along the entire flow path and denoted as (CFAR). It has been observed that the differential pressure ratio varies linearly and proportionally to variations in the combined flow area ratio.

From the results in this study, it can be concluded that the differential pressure ratio at the valve seat inherently varies as well proportionally with variations in the average global inlet velocity, where an increase in the velocity sees an increase in the differential pressure ratio, which is consistent with a lower static pressure downstream of the valve seat. Furthermore, it has been observed that, differential pressure ratio at the valve seat flow passage increases proportionally to a decrease in the combined flow passages effective flow area ratio. The results presented in this study provide important information that has been used to define global and local characteristics that have been used to develop prediction models for the local and global hydrodynamic performance models in this study.

Research Objective # 4: To Establish the Effects of Local Trim Geometry on the Local and Global Overall CV

Conclusion # 4: Based on the investigations concerning the effects of the trim flow geometry on the local and global overall CV. From the developed parameters that have been defined in this study to characterise the geometry and CV, it can be concluded that the combination of the effective flow areas defined as the multiple of all the effective flow areas along the entire flow path w.r.t their sequence of arrangement have a substantial effect on the overall global differential pressure and corresponding flow coefficient (CV).

It has been observed that a low multiple value of all the effective flow passage areas corresponds to a low global differential pressure and vice versa, and in terms of the corresponding CV, where the CV increases proportionally with an increase in the combined effective flow area ratio, which as stated earlier is the multiple of all the flow passages effective flow area ratios along the entire flow path. The results of the parameter characterization and relations in this study are particularly important in that the global differential pressure and CV can be easily computed from the developed geometric parameter defined as the (Combined flow area ratio (CFAR)). However, having established these novel geometric characteristics, the local flow behaviour needed to be further understood, and hence, this objective provided the basis from which more parameters were developed to further characterise the geometry, pressure, and flow structure.

Research Objective # 5: To Establish the Effects of Local Trim Geometry on the Pressure Structure Within a Multi-Stage Trim Control Valve

Conclusion # 5: Based on the investigations carried out in this study concerning the effects of the local trim geometry on the pressure structure within the valve carried out in this study. Further parameters have been developed in the form of the differential pressure ratio, which is the ratio of a flow passage exit pressure to the entrance pressure, where the exit pressure of a flow passage becomes the entrance pressure to next flow passage in series along the entire flow path. Here, the flow area ratio which is defined as the ratio of the available effective flow passage area upstream of the *i*th flow passage to the effective flow passage area downstream of the *i*th flow passage has been characterised with the differential pressure ratio as defined earlier. From the results obtained at a constant velocity of 3m/sec of water flowing through the valve, it can be concluded that the pattern and sequence of arrangement of the flow passages effective flow areas w.r.t size has a significant effect on the local pressure structure.

It has been observed that an effective flow area ratio of 1.2 at flow passage 3 (FP3) which is immediately upstream of valve plug flow passage, and with a corresponding differential pressure ratio of 0.4 results in a differential pressure ratio of 0.026 between the pressure at the vena contracta downstream of the valve plug to the valve plug entrance pressure. It has also been observed that a flow area ratio of 1.74 again at (FP3) with a corresponding differential pressure of 0.53 results in a differential pressure ratio of 0.6 between the pressure at the vena contracta downstream of the valve plug to the valve plug entrance pressure. On a scale of 0 to 1, a differential pressure ratio close to 0 indicates a significantly low pressure downstream of the valve plug flow passage, and a differential pressure ration close to 1 signifies a higher pressure downstream of the valve plug flow passage. The results presented in this study are critical as they have disclosed an in depth and unique insight into the sensitivities of the pressure flow field

to the geometric configuration w.r.t to defined characterizations developed in this study. Furthermore, the results in this study are especially important as the developed characterization parameters formed the basis on which the prediction models were developed for explicit flow field behaviour as a function of geometric interrelations.

Research Objective # 6: To Establish the Effects of Global Differential Pressure Ratio Variations on the Valve Seat/Plug Flow Passage Downstream Pressure

Conclusion # 6: based on the investigations carried out in this study concerning the effects of the global differential pressure on the valve seat/plug downstream pressure. Here the global differential pressure ratio was defined as the ratio of the outlet pressure to the inlet pressure. This study was carried out at constant inlet velocity and various outlet pressure magnitudes, and it can be concluded that the pressure downstream of the valve seat/plug increases proportionally with an increase in the outlet pressure at constant global flow conditions.

The results from this study are particularly important in highlighting that the outlet pressure is a parameter which should be carefully considered in determining critical flow conditions because the ISA standards and other relevant published empirically based equations consider the inlet pressure alone together with the fluid pressure recovery factor to determine the critical conditions. Furthermore, the differential pressure is accounted for as a single value which can be for any given values of inlet and outlet pressure combinations with the same differential magnitude. In addition, it can also be concluded that the outlet pressure magnitude has an explicit effect on the local flow and pressure structure within a multistage trim control valve. Hence, the outlet pressure must be accounted for to achieve accurate predictions of the hydrodynamic performance of a multi-stage trim control valve.

Research Objective # 7: To formulate the explicit effects of local flow passages effective flow areas and sequence of arrangement on the flow and pressure structure within the valve.

Conclusion # 7: Based on the investigations carried out in this study concerning the explicit effects of local flow passages effective flow areas and sequence of arrangement on the flow and pressure structure within the valve. Further deterministic characterization of independent geometric parameters and dependent flow and pressure parameters have been developed in this study. Here the cavitation index has been implemented to determine the extent of the flow and pressure structure upstream and downstream of every flow passage along the entire flow path.

From the results obtained in this study, it can be concluded that the multiple flow passages constitute a complex nonlinear combined effect on the flow and pressure structure within the valve, with the flow and pressure structure within the vicinity of a flow passage exhibiting an explicit interdependence on its immediate downstream and upstream flow passages as a function of their effective flow areas.

Hence, the results presented in this study of the characteristics and relations are of significance as they have been used to develop prediction models which have been explicitly implemented in the design optimization of a control valve.

Research Objective # 8: Development of Local and Global Semi-Empirical Relations for Geometry, Velocity, Pressure Drop, and Flow Coefficient (CV) in a control Valve.

Conclusion # 8: Based on the results presented in this study where exhaustive investigations and analysis of the effects of various independent geometric and flow parameters within the control valve, semi empirical relations of geometry, velocity, pressure drop, and flow coefficient (CV) have been developed. A novel pressure loss coefficient (K_L) dependent on geometric flow passage's effective flow area has been developed through derivations from mass and momentum conservation principles. It does not require prior knowledge of the pressure drop and velocity across a flow passage, and the fluid density as is required from the existing energy loss coefficient. Following on, the local CV is uniquely computed as a function of a flow passage effective flow area and K value, and having established the CV, the differential pressure across the flow passage is inversely calculated, and where the flow passage exit/downstream pressure is the difference between the downstream flow passage entrance pressure and the calculated upstream differential pressure. Hence, to design a control valve as a function of trim geometric effective flow area variables, the prediction models require that an initial desired or known global or local flow passage flow or pressure value to be specified, and then from which flow and pressure structure along the entire flow path can be computed, and modified as required.

Research Objective # 9: Development of a Scalable and Robust Optimization Tool for the Hydrodynamic Performance of a Control Valve

Conclusion # 9: based on the prediction models developed in chapter 5 regarding the hydrodynamic performance of a control valve, it has been comprehensively determined that flow and pressure structure within the valve is explicitly dependent on the sequence of arrangement of the sequence of arrangement of the flow passages effective flow areas along the flow path.

The relations of the trim geometry with the flow and pressure parameters is non-linear where the flow and pressure structure within the vicinity of a flow passage is interdependent on the magnitude of the effective flow areas of its upstream and downstream flow passages.

Hence from the novel developed equations, the flow and pressure structure of the entire flow path can be computed through iteratively varying the flow passages effective flow areas from an initial specification of a local or global desired or known flow or pressure dependent parameter.

7.4. Thesis Contributions

A summary of the major contributions in this research study are presented here.

Contribution # 1:

The first major contribution in this study is the comprehensive investigations on the appropriateness of application of the current published standards, empirical and theoretical equations, and coefficients as characterised to calculate the hydrodynamic performance of a control valve. The present literature does not disclose any information on the local flow and pressure structure with a control valve, furthermore, to the knowledge of the author, there is no available literature on the hydrodynamic performance of valves that have multi-flow passages. The advent of advanced computational fluid dynamics tools has facilitated in depth investigations by the author of the local flow and pressure distribution within the valve over a wide range of geometric and flow conditions. To characterise the geometry with the flow field, new parameters were developed such as flow area ratio (FAR), combined flow area ratio (CFAR), and differential pressure ratio (DPR). The effects of the flow passages effective flow areas, flow passages sequence of arrangement with regards to size along the flow path, global differential pressure, velocity, on the upstream and downstream pressure at the valve seat flow passage have been recapitulated. The developed parameter characterizations have facilitated and contributed to the development of prediction models in this study.

Contribution # 2:

The second major contribution of this study is the comprehensive parametric investigations on the local and global geometric and flow parameter characteristics within the control valve. The existing literature and state of the art does not provide information on local flow and pressure structure and does not explicitly account for the local geometry within a control valve. The advent of advanced computational fluid dynamics tools have facilitated these parametric investigations to be carried out by the author. Here the explicit effects of the flow passages

effective flow areas on the differential pressure, velocity, and pressure upstream and downstream of a flow passage have been investigated. Hence, from the results, formulations of Semi-empirical equations to characterise the geometry and flow and pressure parameters have been developed. A new and novel pressure loss coefficient (K_L) has been developed which is characterised by geometry alone. The existing characterization for the extent of pressure loss through a flow restriction, the pressure loss coefficient also termed as (K), requires a pre-known differential pressure, fluid density and velocity. The developed pressure loss coefficient is characterized only by the effective flow areas of the flow passages or singularities without prior knowledge of the pressure drop, flow and fluid density. Based on the investigations carried out, novel prediction models have been developed to predict the flow and pressure structure within the valve. The unique geometric and flow parameter characterization and the developed prediction models provides a significant contribution to the design of single and multi-flow passage valves for which the hydrodynamic performance of a control valve can be closely predicted. This characterizations methodology is new and novel, and as detailed in the work, it encompasses local multiple geometric interactions and combined effects not as yet currently explored and published. It is scalable and is universally applicable for any flow passage geometry or singularity that an effective area can be deduced.

Contribution # 3:

At present, control and regulating valves designs are increasingly incorporating complex trims thus presenting multiple flow passages along the flow path, at most there is no detailed calculations on the local effects of such trims as there is no existing design methodology available to do so. This is a major knowledge gap in this area, and this gap has been assuaged through the novel design methodology for single and multi-flow passage control valves. The developed design methodology is user friendly and provides optimal solutions for local and global flow and pressure structure, which include the local CV at each flow passage, the differential pressure across each flow passage, upstream and downstream pressure at each flow passage, local velocity, local pumping energy requirements, global flow rate, global differential pressure, global pumping energy requirement, and global flow rate. The developed semi-empirical optimization methodology that maps the entire flow path's flow and pressure structure explicitly as a function of flow passages effective flow areas is a significant contribution of this study.

7.5. Recommendations for Future Work

The deterministic and design methodologies for the hydrodynamic performance of a control valve have been presented in this current study for the purpose of alleviating knowledge gaps discerned in literature. With hindsight of conclusive outcomes presented in the previous sections, there still exists a wide scope for further research in control valve flow field geometric sensitivities. Further work has been identified in areas of hydrodynamic performance, design and optimization of a control valve, and these areas are presented below.

Recommendation # 1:

The information on the hydrodynamic performance of a control valve presented in this thesis has been obtained within the vicinity of the flow passages along the flow passages along the entire flow path, and rightfully so, the relative effects have been quantified and satisfy continuity. However, further studies need to be carried out to account for the sensitivities of the flow field to changes in direction of the flow path, flow separation, and inherent development of secondary flows. These studies will provide additional important information on the complex geometric and flow field interactions w.r.t flow and pressure structure which will provide a complete account of the entire flow field in all areas inside a control valve.

Recommendation # 2:

The current research study has been carried out under the pressure-based model with constant fluid density, temperature, and dynamic viscosity, a density/ energy-based model can be incorporated to account for changes in the flow and pressure structure as a function of temperature and density. Furthermore, numerical investigations can be carried out on the structural integrity of the valve components through fluid structure interaction, and in addition, with the consideration of noise level and propagation as a design parameter.

Recommendation # 3:

Numerical investigations can be carried out to derive explicit characteristics geometric and flow parameters on the onset and extent of cavitation within the control valve. The cavitation index has been used in this study to define the potential of cavitation occurring within the vicinity of the valve trim flow passages. However, even though the unique parameter characterization defined in the prediction models can explicitly predict the pressure structure downstream of a flow passage, and it is prudent to further define the extent of cavitation as a function of geometry. The inclusion of additional critical geometric and flow field characteristics allows an enhanced understanding of the complex flow phenomenon within a control valve and increase the level of accuracy of the prediction models presented in this study.

REFERENCES

- [1]. ISA BS EN 605534-2-5 (2003): Flow Capacity-Sizing Equations for Fluid Flow Through Multi-Stage Control Valves with Interstage Recovery.
- [2]. Taimoor Asim, Antonio Oliveira, Mathew Charlton, Rakesh Mishra (2019). Improved Design of a Multi-Stage Continuous Resistance Trim for Minimum Energy Loss in Control Valves. *Energy* 174 (2019) 954 -971.
- [3]. Seungbin Ko and Simon Song (2015): Effects of Design Parameters on Cavitation in Solenoid Valve for an Electric Vehicle Braking System and Design Optimization: *Journal of Mechanical Science and Technology* 29 (11) (2015) 4757-4765.
- [4]. A.S. Tabrizi, M.Asadi, G. Xie, G. Lorenzini, and C. Biserni (2014): Computational Fluid Dynamics Based Analysis of a Ball Valve Performance in the Presence of Cavitation. *Journal of Engineering Thermo-Physics*, Vol. 23 No 1.
- [5]. LI Beibei, LI Wenhua, Jiao Mingli, Wang Bingyang and Liu Xiumei (2017): Analysis of Cavitation Characteristics in Throttle Valve with Different Structure Parameters. *Journal of Mechanics in Medicine and Biology* Vol 17, No 3- 1750047.
- [6]. Hojin Ha, Jonas Lantz, Magnus Ziegler, Belen Casas, Matts Karlson, Petter Dyverfeldt, Tino Ebbers (2017): Estimating the Irreversible Pressure Drop Across a Stenosis by Quantifying Turbulence Production Using 4D Flow MRI. *Scientific Reports* 7:46618 DOI 10.1038/srep46618.
- [7]. Claudio Alimonti, Gioia Falcone, Oladele Bello (2010): Tow Phase Flow Characteristics in Multiple Orifice Valves. *Experimental Thermal and Fluid Science* 34- 1324-1333.
- [8]. Sanchez Calvo, Raul and Juana Sirgado, Luis, and Laguna Penuelas, Fransisco and Rodriguez Sinobas (2008): Estimation of Cavitation Limits from Local Head Loss Coefficient. *Journal of Fluid Engineering* v 130; p. 101302-1. ISSN 0342-7188.
- [9]. Hamidzera Yaghoubi, Seyed Amir Hossein Madani, Mansour Alizadeh (2018): Numerical Study on Cavitation in a Globe Control Valve with Different Numbers of Anti-Cavitation Trims. *Journal of Central South University* 25(11): 2677-2687.
- [10]. Behrouz Ebrahimi, Guoliang He, Yingjie Tang, Matthew Franchek, Dong Liu, Jay Pickett, Frank Springett, Dan Franklin (2016): Characterization of High- Pressure Cavitation Flow Through a Thick Orifice Plate in a Pipe of Constant Cross Section. *International Journal of Thermal Sciences* 114-229-240.

- [11]. V.K Singh, T. John Tharakan (2015): Numerical Simulations for Multi-Hole Orifice Flow Meter. *Journal of Flow Measurement and Instrumentation*.
- [12]. Ma Haoyuan, Zhang Tong, AN Qingsong, TAO Yuhao, XU Yue (2020): Visualization Experiment and Numerical Analysis of Cavitation from Characteristics in Diesel Fuel Injector Valve with Different Structure Design. *Journal of Thermal Science*.
- [13]. Yang Ye, Jian Chen, Qiao Sheng Pan, Zhi Hua Feng (2019): Suppressing the Generation of Cavitation by Increasing the Number of Inlet Check Valves in Piezoelectric Pumps. *Journal of Sensors and Actuators*.
- [14]. Abdulrazaq A. Araoye, Hasan M. Badr, Wael H. Ahmed (2017): Investigation of Flow Through Multi-Stage Restricting Orifices. *Journal of Annals of Nuclear Energy* 104 75-90.
- [15]. Chaitanya R. Mali, Ashwin W. Patwardhan, G.K. Pandey, Indranil Banerjeer, V. Vinod (2020): CFD Study on the Effect of Various Geometrical Parameters of Honeycomb Type Orifices on Pressure Drop and Cavitation Characteristics. *Journal of Nuclear Engineering and Design* 370- 110880.
- [16]. P. Testud, P. Moussou, A. Hirschberg, Y. Auregan (2007): Noise Generated by Cavitating SINGLE Hole and Multi-Hole Orifices in a Water Pipe. *Journal of Fluids and Structures* 23_163-189.
- [17]. Wang Haimin, Xie Shujuan, Sai Qingyi, Zhou Caimin, Lin Hao, Chen Eryunn (2013); Experiment Study on Pressure Drop of a Multi-Stage Let-down Orifice Tube: *Journal of Nuclear Engineering and Design* 265 633-638.
- [18]. H.P Rani, Y. Divya, R.R. Sahaya, V. Kain, D.K. Barua (2013): Numerical Investigation of Energy and Reynolds Number Distribution for Turbulent flow in an Orifice. *Journal of Engineering Failure Analysis* 34_451-463.
- [19]. Raul Sanchez, Luis Juana, Fransisco V. Laguna, Leonor Rodfguez-Sinobas (2008): Estimation of Cavitation Limits from Local Head Loss Coefficient: *Journal of Fluids Engineering* 130 (10): 101302.
- [20]. G.K. Pandey, D. Ramdasu, G. Padmakumar, V. Prakash, K.K. Rajan (2013): Development of Honeycomb Type Orifices for Flow Zoning in PFBR. *Journal of Nuclear Engineering and Design*.
- [21]. AI Wan Zheng (2014): Hydraulic Characteristics of Multi-Stage Orifice Plate. *Journal Shangai Jiatong Univ. Sci*, 19(3): 361-366- DOI: 10.1007/s12204-014-1510-x.
- [22]. ISA -75-01.01 -2007-(60534-2-1) Flow Equations for Sizing Control Valves
- [23]. Daily DJ. (2013): Fluid-Structure Interactions with Flexible and Rigid Bodies. PhD Thesis (Brigham Young University, Provo, UT)
- [24]. Fatjo GGA. (2016); New Dimensionless Number to Predict Cavitation in Accelerated Fluid. *International Journal of Computing Methods-Exp Measurements*.- 4:484–492.

- [25]. Moncalvo D, Friedel L, Joergensen B, (2009): Sizing of Safety Valves Using ANSYS CFX-Flow. *Chem Eng Technol*; 32: 247–251.
- [26]. Srikanth C and Bhasker C. (2009): Flow Analysis in Valve with Moving Grids Through CFD Techniques. *Advanced Engineering Software*; 40: 193–201.
- [27]. J. A. Davis and M. Stewart, (2002): Predicting Globe Control Valve Performance-Part I: CFD Modelling”, *Journal of Fluids Engineering, ASME Vol.124, No.9, 2002a*, pp.772–777.
- [28]. J. A. Davis and M. Stewart, (2002): Predicting Globe Control Valve Performance- Part II: Experimental Verification”, *Journal of Fluids Engineering, ASME Vol.124, No.9, 2002b*, pp.778-783. 121
- [29]. A. Dawy, A. Sharara And A. Hassan, (2013): A Numerical Investigation of The Incompressible Flow Through A Butterfly Valve Using CFD”, *International Journal of Emerging Technology and Advanced Engineering, Vol. 3, No.11, 2013*, Pp. 1-7.
- [30]. C. J. Deschamps, R.T.S. Ferreira and A. T. Prata, (1966): Turbulent Flow Through Valves of Reciprocating Compressors”, *International Compressor Engineering , Conference paper 1135, 1966*, pp. 377-382.
- [31]. T. Dobben, (1998): Predetermination of the Noise Emission of Valves in Fluid Service, *Proceedings of the 2nd International Conference on Developments in Valves and Actuators for Fluid Control Manchester, England: 28–30 March 1988*, pp. 227-239.
- [32]. DOE-HDBK-1018/2-93 (1993): Department of Energy –Valve Fundamentals Handbook, pp. 1-50.
- [33]. D. Elger, B. Williams, C. Crowe, and J. Roberson (2012): *Engineering Fluid Mechanics, 10th ed.*, John Wiley & Sons Inc.
- [34]. J. H. Ferziger and M. Peric, (2002): *Computational Methods for Fluid Dynamics*, Springer, 2002
- [35]. Deepwater horizon blowout preventer failure analysis report. 2014.
<http://www.csb.gov/assets/1/19/Appendix>
- [36]. Saha BK, Chattopadhyay H, Mandal PB (2014): Dynamic Simulation of a Pressure Regulating and Shut-Off Valve. *Computational Fluids* 101: 231–240.

- [37]. E. Lisowski, J. Rajda (2013): CFD Analysis of Pressure Loss During Flow by Hydraulic Directional Control Valve Constructed from Logic Valves, *Energy Conversion and Management*, 65, 285 – 291
- [38]. BS EN 60534-2-1 (2011): Industrial-Process Control Valves. Part 2-1: Flow Capacity – Sizing Equations for Fluid Flow Under Installed Conditions
- [39]. X. G. Li, D. X. Liu, S. M. Xu And H. Li (2009): CFD Simulation of Hydrodynamics of Valve Tray, *Chemical Engineering and Processing*, 48, 145 – 151
- [40]. Davis, J.A. And Stewart, M. (2002): Prediction of Globe Control Valve Performance—Part I: CFD Modelling. *Trans. ASME Journal of Fluids Engineering*, 124, 772777.
- [41]. Davis, J.A. And Stewart, M. 2002, “Predicting Globe Control Valve Performance—Part II: Experimental Verification,” *Trans. ASME J. Of Fluids Engineering*, 124, 778-783.
- [42]. T. Asim, M. Charlton, R. Mishra (2017): Capacity CFD Based Investigations for The Design of Severe Service Control Valves Used in Energy Systems. *Energy Conversion and Management*.
- [43]. Qian J, Wei L, Jin Z (2014): CFD Analysis on The Dynamic Flow Characteristics of a Pilot-Control Globe Valve. *Energy Convers Manage*; 87: 220–226.
- [44]. S. K. Kang, J. Y. Yoon, S. H. Kang And B. H. Lee (2006): Numerical and Experimental Investigations on Backward Fitting Effects on The Valve
- [45]. A. Beune, J. G. M. Kuerten And J. Schmiddlet (2011): Numerical Calculation and Experimental Validation of A Safety Valve Flows at Pressures up To 600bar, *Aiche: Fluid Mechanics And Transport Phenomena*, 57, 3285 – 3298 Flow Coefficient, *ImechE Part E: Journal Of Process Mechanical Engineering*, 220, 217 – 220
- [46]. F. Lin And G. A. Schohl (2004): CFD Prediction and Validation of Butterfly Valve Hydrodynamic Forces, *Proceedings of World Water and Environmental Resources Congress*, Salt Lake City, U.S.A.
- [47]. Q. Yang, Z. Zhang, M. Liu, And J. Hu (2011): Numerical Simulation of Fluid Flow Inside the Valve, *Procedia Engineering*, 23, 543 – 550
- [48]. Y. J. An, B. J. Kim And B. R. Shin (2008): Numerical Analysis Of 3-D Flow Through LNG Marine Control Valves for Their Advanced Design, *Journal of Mechanical Science and Technology*, 22, 1998 – 2005

- [49]. A. Grace And P. Frawley (2011): Experimental Parametric Equation for The Prediction of Valve Coefficient (CV) For Choke Valve Trims, *International Journal of Pressure Vessels and Piping*, 88, 109 – 1148
- [50]. D. Wu, S. Li And P. Wu (2015): CFD Simulation of Flow-Pressure Characteristics of a Pressure Control Valve for Automotive Fuel Supply System, *Energy Conversion and Management*, 101, 658 – 665
- [51]. J. Qian, L. Wei, Z. Jin, J. Wang, H. Zhang, And A. Lu (2014): CFD Analysis on The Dynamic Flow Characteristics of The Pilot-Control Globe Valve, *Energy Conversion and Management*, 87, 220 – 226
- [52]. [11] J. R. Valdes, M. J. Miana, J. L. Nunez And T. Putz (2008): Reduced Order Model for Estimation of Fluid Flow and Flow Forces in Hydraulic Proportional Valves, *Energy Conversion and Management*, 49, 1517 – 1529
- [53]. Agarwal, V. C. Mishra, R. (1998): Optimal Design of a Multi-Stage Capsule Handling Multi-Phase Pipeline, *International Journal of Pressure Vessels and Piping*, 75, 27 – 35.
- [54]. R. Amirante, P. G. Moscatelli And L. A. Catalano (2007): Evaluation of The Flow Forces on a Direct (Single Stage) Proportional Valve by Means of a Computational Fluid Dynamic Analysis, *Energy Conversion and Management*, 48, 942 – 953 [15]
- [55]. [E. Lisowski, W. Czyzycki, J. Rajda (2014): Multifunctional Four-Port Directional Control Valve Constructed from Logic Valves, *Energy Conversion and Management*, 87, 905 – 913
- [56]. E. Lisowski, G. Filo (2016): CFD Analysis of The Characteristics of a Proportional Flow Control Valve with an Innovative Opening Shape, *Energy Conversion and Management*, 123, 15 – 28
- [57]. R. Mishra, E. Palmer and J. Fieldhouse (2009): An Optimization Study of a Multiple Row Pin-Vented Brake Disc to Promote Brake Cooling Using Computational Fluid Dynamics, *Proceedings of the Institution of Mechanical Engineers, Part D: Journal of Automobile Engineering*, 223, 865–875
- [58]. Taimoor Asim, Rakesh Mishra, Matthew Charlton, and Antonio Oliveira (2015): Capacity Testing and Local Flow Analysis of Geometrically Complex Trims Installed within a Commercial Control Valve, *International Conference of Jets, Wakes and Separated Flows*, June 15-18, Stockholm, Sweden
- [59]. James Green, Rakesh Mishra, Matthew Charlton, and Owen (2012): Validation of CFD predictions using process data obtained from flow through an industrial control valve, *Journal of Physics: Conference Series*, 364, 012074

- [60]. James Green, and Rakesh Mishra, Matthew Charlton, and Owen (2012): Local Analysis of Flow Conditions within a Geometrically Complex Control Valve Trim using CFD, *Journal of Physics: Conference Series*, 364, 012075
- [61]. R. Mishra, S. N. Singh, and V. Seshedri (1998): Study of Wear Characteristics and Solid Distribution in Constant Area and Erosion-Resistant Long-Radius Pipe Bends for the flow of Multi-sized Particulate Slurries, *Wear*, 217, 297–306 [30]
- [62]. R. Mishra, S. N. Singh, and V. Seshadri (1998): Velocity measurement in solid-liquid flows using an impact probe, *Flow Measurement, and Instrumentation*, 8, 157–165
- [63]. R. Mishra, S. N. Singh, and V. Seshadri (1998): Improved model for the prediction of pressure drop and velocity field in multi-sized particulate slurry flow through horizontal pipes, *Powder Handling and Processing*, 10, 279–287.
- [64]. H. K. Versteeg and W. Malalasekera (1995): *An Introduction to Computational Fluid Dynamics*, Longman Scientific and Technical, U.K., ISBN
- [65]. Ahmed, W.H., Bello, M.M, El Nakla, M, Al Sarkhi, A (2012): Flow and Mass Transfer Downstream of an Orifice Under Flow Accelerated Corrosion Conditions. *Nucl. Eng. Des.* 252, 52–67.
- [66]. Arun, N. Malavarayan, S, Kaushik, M, (2010): CFD Analysis on Discharge Coefficient During Non-Newtonian Flows Through Orifice Meter. *Int. J. Eng. Sci. Technol.* 2 (7), 3151–3164.
- [67]. Bull, M.K., Agarwal, N.G (1983): Characteristics of Flow Separation Due to An Orifice Plate in Fully Developed Turbulent Flow-Pipe.
- [68]. Dabiri, S, Sirignano, W.A, Joseph, D.D (2007): Cavitation in Orifice Flow. *Physics.-Fluids* 19 (7), 72112.
- [69]. Dempster, W.M, Arebi, B (2001): Experimental Characteristics of Steam Bubble Growth at Orifices in Sub-Cooled Liquid. *Int. Commun. Heat Mass Transfer* 28 (4),467–477.
- [70]. Deotte Jr, R.E, Morrison, G.L. Panak, D.L. Nail, G.H (1991): 3-D Laser Doppler Anemometry Measurements Of The Axisymmetric Flow Field Near An Orifice. *Flow Meas. Instrum.* 2, 115–123.

- [71]. Eiamsa-Ard, S. Ridluan, A. Somravysin, P. Promvonge, P. Chok, (2008): Numerical Investigation of Turbulent Flow Through a Circular Orifice. *KMITL Sci. J.* 8 (1), 44–50.
- [72]. Gronych, T. Jerab, M. Peksa, L. Wild, J. Stane. K, F. Vicar, M., (2012): Experimental Study of Gas Flow Through a Multi-Opening Orifice. *Vacuum* 86 (11), 1759–1763.
- [73]. Jankowski. T.A. Schmierer, E.N. Prenger, F.C., Ashworth, S.P. (2008): A Series Pressure Drop Representation for Flow Through Orifice Tubes. *J. Fluids Eng.* 130 (5), 51204.
- [74]. Kumar, H.M. Kumar, K.J. Seshadri, V. (2015): CFD Analysis of Flow Through Dual Orifice Plate Assembly. *Int. J. Emerg. Technol. Adv. Eng.* 5 (10), 136–144.
- [75]. Morrison, G.L. Deotte, R.E., Moen, M. Hall, K.R. Hostle, J.C. (1990): Beta Ratio, Swirl And Reynolds Number Dependence of Wall Pressure in Orifice Flowmeters. *Flow Meas. Instrum.* 1, 269–277.
- [76]. Munoz-Díaz, E. Solorio-Ordaz, F.J. Ascanio, G. (2012): A Numerical Study of An Orifice Flowmeter. *Flow Meas. Instrum.* 26, 85–92.
- [77]. Nygard, F. Andersson, H.I. (2013): Numerical Simulation of Turbulent Pipe Flow Through an Abrupt Axisymmetric Constriction. *Flow Turbul. Combust.* 91 (1), 1–8.
- [78]. Ramamurthi, K. Nandakumar, K. (1999): Characteristics of Flow Through Small Sharp- Edged Cylindrical Orifices. *Flow Meas. Instrum.* 10 (3), 133–143.
- [79]. Rani, H.P. Divya, T. Sahaya, R.R. Kain, V. Barua, D.K. (2013): Numerical Investigation of Energy and Reynolds Stress Distribution for Turbulent Flow in An Orifice. *Eng. Fail. Anal.* 34, 451–463.
- [80]. Reis, L.C.B.S., Carvalho, J.A, Nascimento, M.A.R., Rodrigues, L.O. Dias, F.L.G. Sobrinho, P.M. (2014): Numerical Modeling of Flow Through an Industrial Burner Orifice. *Appl. Therm. Eng.* 67 (1–2), 201–213.
- [81]. Roul, M.K. Dash, S.K. (2012): Single-Phase and Two-Phase Flow Through Thin And Thick Orifices In Horizontal Pipes. *J. Fluids Eng.* 134 (9), 91301.
- [82]. Shaaban, S. (2014): Optimization of Orifice Meter's Energy Consumption. *Chem. Eng. Res. Des.* 92 (6), 1005–1015.

- [83]. Shah, M.S. Joshi, J.B. Kalsi, A.S, Prasad, C.S.R., Shukla, D.S. (2012): Analysis of Flow Through an Orifice Meter: CFD Simulation. *Chem. Eng. Sci.* 71, 300–309.
- [84]. Shan. F, Fujishiro. A. Tsuneyoshi, T. Tsuji. (2014): Effects of Flow Field on the Wall Mass Transfer Rate Behind a Circular Orifice in a Round Pipe. *Int. J. Heat Mass Transfer* 73, 542–550.
- [85]. Enzo Fabio, Luca Fassitelli, Ed Petrollieri. (n.d.). *Roman Engineering and Industry-Valvias* [Infographic] [Last Accessed 02/01/2020] www.valvias.com/history.php
- [86]. Paktechpoint Valve Training Article. (n.d.). *Cage Guided Globe Valve* [Infographic]. [Last Accessed 02/01/2020] <https://paktechpoint.com/all-fluid-control-valves-types-instrumentaton/>
- [87]. Tameson B.V. (n.d.). *Angle Seat Valve* [Infographic]. [Last Accessed 02/01/2020] <https://tameson.co.uk/angle-seat-valve.html>.
- [88]. Control Automation. (n.d.). *Sliding Stem Valves-Single and Double Ported Globe Valve* [Infographic]. [Last Accessed 02/01/2020] <https://control.com/textbook/control-valves/sliding-stem-valves/>
- [89]. Thinktank Optimal Fluid Solutions. (n.d.). *Pressure Balanced High Pressure Cage Type Globe Valve* [Infographic] [Last Accessed 02/01/2020] https://www.valve-cn.com/cage_guided_globe_control_valve/high_perssure_globe_control_valve.html
- [90]. Trillium Flow Technologies Cage Guided Brochure Blackborough BV992. (n.d.). *Cage Trim Valve with Multi-Flow Cage* [Infographic]. [Last Accessed 02/01/2020] https://www.trilliumflow.com/wp-content/uploads/2019/11/TFTUK_201909-Cage-Guided-Brochure-PW.pdf
- [91]. Pneucon Automation. (n.d.). *Globe 3 way control valve* [Infographic]. [Last Accessed 02/01/2020] <https://in.pinterest.com/pin/409757266080918549/>
- [92]. GlobalSpec.com. (n.d.). *Diaphragm Valve* [Infographic]. [Last Accessed 02/01/2020] https://www.globalspec.com/learnmore/flow_control_flow_transfer/valves/diaphragm_valves
- [93]. Projectmaterials. (n.d.). *Butterfly Valve* [Infographic]. [Last Accessed 02/01/2020] <https://blog.projectmaterials.com/valves/butterfly-valve-api-609/>
- [94]. Pekos Valves. (n.d.). *V-Port Ball Valve* [Infographic]. [Last Accessed 02/01/2020] <https://www.pekos.es/v-port-control-ball-valve-n-8-en>

- [95]. Trimteck Optimux. (n.d.). *Eccentric Plug Rotary Valve* [Infographic]. [Last Accessed 02/01/2020] <https://trimteck.com/product/control-valves/opexl-eccentric-plug-rotary-control-valve>
- [96]. Projectmaterials.. (n.d.). *Eccentric Disk Valve* [Infographic]. [Last Accessed 02/01/2020] <https://blog.projectmaterials.com/valves/butterfly-valve-api-609/>
- [97]. Lunchbox Sessions Valve Training. (n.d.). *Directional Control Valve* [Infographic]. [Last Accessed 02/01/2020] <https://www.lunchboxsessions.com/materials/flow-directional-control-valves/intro-to-directional-control-valves-lesson>
- [98]. Automation Forum. Co. (n.d.). *Directional Spool Valve* [Infographic]. [Last Accessed 02/01/2020] <https://automationforum.co/what-is-a-spool-valve-what-are-the-types-of-the-spool-valve/>
- [99]. Trimteck Optimux. (n.d.). *Multi-Stage Anti Cavitation Trim* [Infographic]. [Last Accessed 02/01/2020] <https://trimteck.com/product/severe-service/st-2-multi-stage-anti-cavitation-trim/>
- [100]. Valve and Automation-Total Valve and Control Solutions. (n.d.). *Multi-Stage Angle Style Control Valve* [Infographic]. [Last Accessed 02/01/2020] <https://valve.co.za/arca-multi-stage-trim-blowdown-control-valve/>
- [101]. Control Valve Characteristics. (n.d.). *Installed Characteristics* [Infographic]. [Last Accessed 02/01/2020] <https://automationforum.co/control-valve-characteristics/>
- [102]. Instrumentation Tools. (n.d.). *Control Valve Cavitation and Flashing* [Infographic]. [Last Accessed 02/01/2020] https://instrumentationtools.com/control-valve-cavitation-and-flashing/#google_vignette
- [103]. Flotech . (n.d.). *Understanding and Predicting Cavitation in Control Valves* [Infographic]. [Last Accessed 02/01/2020] <https://www.flotechinc.com/understanding-predicting-cavitation-control-valves>

APPENDICES

A-1: Computational Fluid Dynamics

Introduction

Computational fluid dynamics (CFD) is a subdivision of fluid mechanics that is used to analyze and develop solutions for fluid flows, heat transfer, chemical reactions, and fluid structure interaction. Computer based calculations are carried out to simulate the free stream flow of fluids and fluid structure interactions where structures and surfaces are characterized through boundary conditions. At present Computational fluid dynamics now forms an integral part in providing solutions for numerous complex fluid and thermodynamic phenomenon in many industrial applications such as aerodynamics, biological, environmental engineering, weather simulation, melting and solidification, magnetism, and combustion dynamics.

Operation of CFD Codes

The numerical solvers in CFD constitute of 3 main numerical methodologies, which are the spectral methods, finite volume, and finite difference. The finite volume method forms the governing equations behind most of the robust and well ascertained CFD codes. The finite volume method (FVM) is advantageous primarily in its computer memory usage cost and solution speed. The finite volume method characterizes and assesses partial differential equations in algebraic equation form with solutions obtained through iterative methods.

The methodology of solving a fluid dynamics problem follows a defined procedure which is:

➤ Preprocessing

Here the fluid or flow domain is extracted from geometry which has been pre-defined within the substantial bounds of the problem through a 3-dimensional representation of the geometry produced in a designated computer aided design software.

- The fluid extracted from the geometry which represents the flow domain volume is divided into discrete cells which form the mesh. The mesh of the flow domain can be defined as uniform, non-uniform, structured or unstructured.

There are different types of mesh types available which can be used for different problems depending on performance w.r.t accuracy, ease of solution convergence, and robustness for a given application physics. The common types of mesh types available in most commercial packages are tetrahedral, prismatic, pyramidal, polyhedral, and hexahedral elements.

➤ Numerical Representation of Fluid Flow

Numerical representation of the flow of fluids through fluid dynamics methodologies is based on the principle governing axioms of laws of conservation for which the main laws observed are the mass conservation, momentum conservation and energy conservation. The fluid is assumed to be a continuum where the microscopic interactions of the molecules are ignored, and the fluid is taken as continuous macroscopic matter.

➤ Conservation law of Mass

The conservation of mass implies that for any closed system to any form of matter and energy transfer, there will be no change in the mass of a system, and hence over time the mass is conserved. The conservation of mass can be expressed as

$$\text{Rate of change of fluid mass inside a control volume} = \text{Net rate of change of fluid flow into volume} \quad (\text{A1.1})$$

In physical terms the fulfillment of the mass conservation statement obliges to the constraint that mass can neither be created nor destroyed within a control volume and is defined in the integral format from the following expression

$$\frac{\partial \rho}{\partial t} \iiint_V \rho dV = - \oint_S \rho \mathbf{u} \cdot d\mathbf{S} \quad (\text{A-1.2})$$

Where ρ is the fluid density, \mathbf{u} is the flow velocity and t is time. The rate of increase of the mass within the control volume is represented by the left-hand side of the equation defined by a triple integral over the volume, and the right and side of the equation represents the integral over the surface of the control volume mass transfer into the control volume. The mass flow

into the control volume is considered as positive and the flow into the system is thus negative relative to the normal vector of the surface.

Through the divergence theorem the differential representation of the continuity- mass conservation equation is defined as follows

$$\frac{\partial \rho}{\partial t} + \nabla \cdot (\rho \mathbf{u}) = 0 \quad (\text{A-1.2})$$

The unsteady three-dimensional representation of continuity- mass conservation of the fluid for incompressible flow which is the longhand form of equation (A-1.2) above is expressed as

$$\frac{\partial \rho}{\partial t} + \rho \frac{\partial u}{\partial x} + \rho \frac{\partial v}{\partial y} + \rho \frac{\partial w}{\partial z} = 0 \quad (\text{A-1.3})$$

➤ Conservation Law of Momentum

Newton's second law of motion applied to a control volume stipulates that the change in momentum of the fluid within a control volume is the result of the momentum net flow into the control volume external forces imparted on the fluid within the control volume. The momentum equation for a control volume is defined in the integral format

$$\frac{\partial}{\partial t} \iiint_V \rho dV = - \oint_S (\rho \mathbf{u} \cdot d\mathbf{S}) \mathbf{u} - \oint_S (p d\mathbf{S}) + \iiint_V \rho f_{body} dV + F_{surf} \quad (\text{A-1.4})$$

The left hand side of the equation represents the net change of momentum within the control volume, the momentum net rate of transfer of momentum into the control volume is represented by the first term on the right of the equation, the force due to the pressure on the volume's surface is represented by the second term, the third term denoted by f_{body} represents the net acceleration of the mass within the control volume due to body forces and surface viscous forces are represented by F_{surf} .

In a 3-dimensional space cartesian coordinate system representation of the control volume, the x component of the momentum equation is determined by setting the rate of change of the fluid particle's x-momentum equal to the sum of the total force in the x direction on the element due to surface stresses and sources induced rate of increase of x-momentum and is expressed as

$$\rho g_x + \frac{\partial \sigma_{xx}}{\partial x} + \frac{\partial \tau_{yx}}{\partial y} + \frac{\partial \tau_{zx}}{\partial z} = \rho \left(\frac{\partial u}{\partial t} + u \frac{\partial u}{\partial x} + v \frac{\partial u}{\partial y} + w \frac{\partial u}{\partial z} \right) \quad (\text{A-1.5})$$

The expressions for the y and x components are defined as follows:

$$\rho g_y + \frac{\partial \tau_{xy}}{\partial x} + \frac{\partial \sigma_{yy}}{\partial y} + \frac{\partial \tau_{zy}}{\partial z} = \rho \left(\frac{\partial v}{\partial t} + u \frac{\partial v}{\partial x} + v \frac{\partial v}{\partial y} + w \frac{\partial v}{\partial z} \right) \quad (\text{A-1.6})$$

$$\rho g_x + \frac{\partial \tau_{xz}}{\partial x} + \frac{\partial \tau_{yz}}{\partial y} + \frac{\partial \sigma_{zz}}{\partial z} = \rho \left(\frac{\partial w}{\partial t} + u \frac{\partial w}{\partial x} + v \frac{\partial w}{\partial y} + w \frac{\partial w}{\partial z} \right) \quad (\text{A-1.7})$$

➤ Conservation of Energy

The conservation law of energy stipulates that for an isolated system the total energy remains constant and this is represented by the energy equation which is derived from the first law of thermodynamics. And for a closed thermodynamic system the first law of thermodynamics is expressed as

$$\delta Q = dU + \delta W \quad (\text{A-1.8})$$

Where δQ is the amount of energy added to the system through a heat source, dU is the rate of change of internal energy of the system, and δW is the amount of energy lost by the system due to the work done by the system on its surroundings. The rate of change of internal energy can also be expressed as

$$dU = \delta Q - \delta W \quad (\text{A-1.9})$$

Equation (A-1.9) above implies that:

$$\begin{aligned} & \textit{The rate of change of internal energy} = \\ & \textit{Amount of heat energy added to the system} - \textit{amount of energy lost by the system} \\ & \textit{due to the work done by the system on its surroundings} \end{aligned} \quad (\text{A-1.10})$$

The energy equation in terms of internal energy is expressed as

$$\begin{aligned} \frac{\partial(\rho e)}{\partial t} + \nabla \cdot (\rho e \vec{V}) &= \rho q + \frac{\partial}{\partial x} \left(K \frac{\partial T}{\partial x} \right) + \frac{\partial}{\partial y} \left(k \frac{\partial T}{\partial y} \right) \\ &+ \frac{\partial}{\partial z} \left(K \frac{\partial T}{\partial z} \right) - p \left(\frac{\partial u}{\partial x} + \frac{\partial u}{\partial y} \frac{\partial w}{\partial z} \right) \end{aligned}$$

$$\begin{aligned}
& + \lambda \left(\frac{\partial u}{\partial x} + \frac{\partial u}{\partial y} + \frac{\partial w}{\partial z} \right)^2 + \mu \left[2 \left(\frac{\partial u}{\partial x} \right)^2 \right. \\
& + 2 \left(\frac{\partial v}{\partial y} \right)^2 + 2 \left(\frac{\partial w}{\partial z} \right)^2 + \left(\frac{\partial u}{\partial y} + \frac{\partial v}{\partial x} \right)^2 \\
& \left. + \left(\frac{\partial u}{\partial z} + \frac{\partial w}{\partial x} \right)^2 + \left(\frac{\partial v}{\partial z} + \frac{\partial w}{\partial y} \right)^2 \right] \quad (A-1.11)
\end{aligned}$$

➤ Equation of State

The equation of state relates state variables such as pressure, density, volume, temperature, and internal energy for which the fluid properties are described. Relations between the state variables are determined through notions of thermodynamic equilibrium. For thermodynamic equilibrium, the state of a substance can be determined by consideration of 2 state variables which are density and temperature and the relations between these two state variables are characterized through the ideal gas law. The ideal gas law is expressed in empirical form as

$$PV = nRT \quad (A-1.12)$$

Where P is the pressure, V is the volume, R is the ideal gas state, T is the temperature, and n is the amount of substance.

For incompressible flow and fluids where density variations are infinitesimal, such that the state of the substance is independent of density the energy equation is not linked to the mass and momentum equations. The energy equation is implemented and solved only for high velocity compressible fluid flows and heat transfer applications.

➤ Navier Stokes Equations

The Navier stokes equations describe the motion of viscous fluids and they mathematically express the conservation of mass and momentum for Newtonian fluids. With derivation based on newton's second law of fluid motion with assumptions that the sum of the diffusing viscous term proportional to the velocity gradient and a pressure term is the resulting stress in the fluid, and thus this characterizes viscous flow. The Navier stokes equations are expressed as follows

$$\rho g_x - \frac{\partial p}{\partial x} + \mu \left(\frac{\partial^2 u}{\partial x^2} + \frac{\partial^2 u}{\partial y^2} + \frac{\partial^2 u}{\partial z^2} \right) = \rho \left(\frac{\partial u}{\partial t} + u \frac{\partial u}{\partial x} + v \frac{\partial u}{\partial y} + w \frac{\partial u}{\partial z} \right) \quad (\text{A-1.13})$$

$$\rho g_x - \frac{\partial p}{\partial y} + \mu \left(\frac{\partial^2 v}{\partial x^2} + \frac{\partial^2 v}{\partial y^2} + \frac{\partial^2 v}{\partial z^2} \right) = \rho \left(\frac{\partial v}{\partial t} + u \frac{\partial v}{\partial x} + v \frac{\partial v}{\partial y} + w \frac{\partial v}{\partial z} \right) \quad (\text{A-1.14})$$

$$\rho g_x - \frac{\partial p}{\partial z} + \mu \left(\frac{\partial^2 w}{\partial x^2} + \frac{\partial^2 w}{\partial y^2} + \frac{\partial^2 w}{\partial z^2} \right) = \rho \left(\frac{\partial w}{\partial t} + u \frac{\partial w}{\partial x} + v \frac{\partial w}{\partial y} + w \frac{\partial w}{\partial z} \right) \quad (\text{A-1.15})$$

A-1.2: Empirical Flow and Pressure Relations and Derivations

A-1.2.1. Incompressible Flow CV and Resistance Coefficient

In a control valve application terminology, the flow coefficient of an incompressible fluid flowing through a valve is described as the capacity of flow of water at 60 degrees Fahrenheit that can pass through a valve at 1 psi pressure drop. The ANSI/ISA 75.01.01 standard definition states the CV is the maximum flow rate in US gallons per minute that can flow through a valve at a pressure drop of 1 psi and is generally expressed as

$$CV = Q \sqrt{\frac{SG}{\Delta P}} \quad (\text{A-1.16})$$

Where Q is the volumetric flow rate in US gallons per minute, ΔP is the pressure drop, and SG is the specific gravity of the fluid which is expressed as:

$$SG = \frac{\rho}{\rho_0} \quad (\text{A-1.17})$$

Where ρ_0 is the reference density which is the density of water for liquids, and ρ is the density of the fluid flowing through the valve. The ISA standards utilize two sets of equations to calculate the flow coefficient which account for non-choked and choked flow condition. According to the standard ISA 75.01.01 non choked flow conditions are applicable if

$$\Delta P < F_L^2 (P_1 - F_F P_V) \quad (\text{A-1.17})$$

Where P_1 is the inlet pressure, F_F is the fluid critical pressure ratio factor, P_V is the fluid vapour pressure, and F_L is the liquid pressure recovery factor. The liquid critical pressure ratio factor F_F is defined through the following expression:

$$F_F = 0.96 - 0.28 \sqrt{\frac{P_V}{P_C}} \quad (\text{A-1.18})$$

Where P_V is the vapor pressure, and P_C is the fluid thermodynamic critical pressure. The fluid pressure recovery factor which is the ratio of the pressure drop across the control valve at choked flow conditions and the differential pressure between the inlet pressure and the fluid vapor pressure. The fluid pressure recovery factor is determined experimentally and is specific for every valve type, and it can also be estimated from the following expression.

$$F_L = \sqrt{\frac{P_1 - P_2}{P_1 - P_{VC}}} \quad (\text{A-1.18})$$

The flow coefficient (CV) for choked flow conditions is predicted from the following expression:

$$CV = \frac{Q}{N_1} \sqrt{\frac{SG}{F_L^2 (P_1 - F_F P_V)}} \quad (\text{A-1.18})$$

The flow coefficient can be termed as an expression for the extent of flow resistance that is added to a pipeline. The empirical head loss coefficient is expressed as

$$H = K \frac{V^2}{2g} \quad (\text{A-1.16})$$

And substituting the head loss for pressure drop the expression becomes:

$$\Delta P = K 0.5 \rho V^2 \quad (\text{A-1.17})$$

Substitution of equation (A-1.17) into equation (A-1.16) and transposition yields the following Imperial relationship (established by Crane)

$$CV = 29.9 \frac{d^2}{\sqrt{K}} \quad (\text{A-1.18})$$

$$CV = \left(\frac{d}{4.654 \cdot K} \right)^2 \quad (\text{A-1.19})$$

$$CV = 0.004634 \frac{d^2}{\sqrt{K}} \quad (\text{A-1.20})$$

Further flow coefficient (CV) and resistance coefficient interrelation is expressed as:

$$K = 0.002148 \frac{d^4}{CV^2} \quad (\text{A-1.21})$$

In the case of flow passages or stages in series, the total head loss coefficient is expressed as follows:

$$K_{\text{TOTAL}} = \sum_n^1 K_1 + K_2 + \dots \dots K_n \quad (\text{A-1.22})$$

For multiple flow restrictions-passages in parallel the total head loss coefficient is expressed as follows

$$\frac{1}{K_{\text{total}}} = \sum_n^1 \frac{1}{K_n} = \frac{1}{K_1} + \frac{1}{K_2} + \dots \dots \frac{1}{K_n} \quad (\text{A-1.23})$$

The total flow coefficient (CV) for flow restrictions-passages in series is expressed as:

$$\frac{1}{CV_{\text{total}}} = \sum_n^1 \frac{1}{CV_n} = \frac{1}{CV_1} + \frac{1}{CV_2} + \dots \dots \frac{1}{CV_n}$$

The total flow coefficient (CV) for flow restrictions-passages in parallel is expressed as:

$$CV_{\text{total}} = \sum_n^1 = CV_1 + CV_2 + \dots \dots CV_n$$

The control valve standard flow passages made up from the standard parts of the body, seat, cage, trim and plug can be considered individually with the overall flow coefficient being expressed as:

$$CV_{\text{total}} = \sum_n^1 = CV_{\text{Body}} + CV_{\text{Cage}} + CV_{\text{Seat}} + \dots \dots$$

A-1.2.2. Derivations of Empirical Flow Equations

The Bernoulli's energy equation forms the benchmark from which most equations for incompressible and Newtonian flow are derived, and it is generally expressed as:

$$P_1 + \rho_1 \frac{1}{2} V_1^2 = P_2 + \rho_2 \frac{1}{2} V_2^2 \quad (\text{A-1.24})$$

In terms of the differential pressure between two points along a streamline the expression becomes:

$$P_1 - P_2 = \rho_2 \frac{1}{2} V_2^2 - \rho_1 \frac{1}{2} V_1^2 \quad (\text{A-1.25})$$

From mass conservation, the volumetric flow rate and effective flow area relations are derived as follows:

$$\begin{aligned} Q &= A_1 V_1 = A_2 V_2 \\ V_1 &= \frac{Q}{A_1} \\ V_2 &= \frac{Q}{A_2} \\ P_1 - P_2 &= \frac{1}{2} \rho \left(\frac{Q}{A_2} \right)^2 - \frac{1}{2} \rho \left(\frac{Q}{A_1} \right)^2 \\ 2(P_1 - P_2) \rho^{-1} &= \left[\left(\frac{Q}{A_2} \right)^2 - \left(\frac{Q}{A_1} \right)^2 \right] \\ 2(P_1 - P_2) \rho^{-1} &= \left[\left(\frac{Q}{A_2} \right)^2 - \left(\frac{A_2}{A_1} \right) \left(\frac{Q}{A_1} \right)^2 \right] = \left(\frac{Q}{A_2} \right)^2 \left[1 - \left(\frac{A_2}{A_1} \right)^2 \right] \\ \left(\frac{Q}{A_2} \right)^2 &= \frac{2(P_1 - P_2) \rho^{-1}}{\left[1 - \left(\frac{A_2}{A_1} \right)^2 \right]} \\ Q &= A_2 \sqrt{\frac{2(P_1 - P_2) \rho^{-1}}{\left[1 - \left(\frac{A_2}{A_1} \right)^2 \right]}} \quad (\text{A-1.26}) \end{aligned}$$

The effective flow area ratio can be re-written as:

$$B = \frac{A_2}{A_1} = \frac{0.25 \cdot \pi d_2^2}{0.25 \cdot \pi d_1^2} = \frac{d_2^2}{d_1^2} \quad (\text{A-1.27})$$

The equation that finally characterizes the pressure, density, and volume flow of a fluid as a function of the effective flow area is expressed as follows:

$$Q = A_2 \frac{C_d}{\sqrt{1-\beta^4}} \sqrt{\frac{2(P_1 - P_2)}{\rho}} \quad (\text{A-1.28})$$

For compressible flow, the ANSI/ISA 75.01.01 [1] stipulates that choked flow conditions are in effect when the following conditions are satisfied

$$\frac{P_1 - P_2}{P_1} \geq F_\gamma X_t \quad (\text{A-1.29})$$

The flow coefficient is expressed as

$$CV = \frac{\dot{m}}{N_6 0.677 \sqrt{F_\gamma X_t P_1 \rho_1}} \quad (\text{A-1.30})$$

The flow through an effective flow diameter can be characterized with the discharge coefficient through the following expression:

$$C_d = \frac{\dot{m}}{Y N_6 \left(\frac{d}{4.654}\right)^2 \sqrt{F_\gamma X_t P_1 \rho_1}} \quad (\text{A-1.31})$$

$$\dot{m} = C_d Y N_6 \left(\frac{d}{4.654}\right)^2 \sqrt{F_\gamma X_t P_1 \rho_1} \quad (\text{A-1.32})$$

The control valve flow coefficient and the discharge coefficient relationship is thus expressed as:

$$CV Y N_6 \sqrt{F_\gamma X_t P_1 \rho_1} = C_d Y N_6 \left(\frac{d}{4.654}\right)^2 \sqrt{F_\gamma X_t P_1 \rho_1}$$

$$CV = C_d \left(\frac{d}{4.654}\right)^2 \quad (\text{A-1.33})$$

$$Y = \left(1 - \left(\left(\frac{P_1 - P_2}{P_1}\right) (3F_\gamma X_t)^{-1}\right)\right) \quad (\text{A-1.34})$$

Compressible non choked flow are considered when the following conditions are met

$$\frac{P_1 - P_2}{P_1} \leq F_\gamma X_t$$

$$CV = \frac{\dot{m}}{N_6 Y \sqrt{x P_1 \rho_1}}$$

$$C_d = \frac{\dot{m}}{Y N_6 \left(\frac{d}{4.654}\right)^2 \sqrt{(P_1 - P_2) \rho_1}} \quad (A-1.35)$$

$$\dot{m} = C_d Y N_6 \left(\frac{d}{4.654}\right)^2 \sqrt{(P_1 - P_2) \rho_1}$$

$$CV Y N_6 \sqrt{(P_1 - P_2) \rho_1} = C_d Y N_6 \left(\frac{d}{4.654}\right)^2 \sqrt{(P_1 - P_2) \rho_1}$$

$$CV = C_d \left(\frac{d}{4.654}\right)^2 \quad (A-1.36)$$

For incompressible choked flow effective flow diameter discharge coefficient and flow coefficient relations are derived as follows. For the ANSI/ISA 75.01.01.01 standard stipulation, choked flow parameters for calculating the CV are considered when the following conditions exist:

$$\Delta P \geq F_L^2 (P_1 - F_F P_V) \quad (A-1.37)$$

The corresponding CV under choked flow conditions is

$$CV = \frac{Q}{N_1} \sqrt{\frac{SG}{F_L^2 (P_1 - F_F P_V)}}$$

$$CV = \frac{Q}{N_1 F_L} \sqrt{\frac{SG}{(P_1 - F_F P_V)}}$$

$$Q = CV N_1 F_L \sqrt{\frac{P_1 - F_F P_V}{SG}} \quad (A-1.38)$$

Where N_1 is a unit conversion factor of 0.865, and SG is the specific gravity of the fluid.

$$C_d = \frac{Q}{Y N_1 \left(\frac{d}{4.654}\right)^2} \sqrt{\frac{SG}{(P_1 - F_F P_V)}}$$

$$\begin{aligned}
Q &= C_d Y N_1 \left(\frac{d}{4.654}\right)^2 \sqrt{\frac{P_1 - F_F P_V}{SG}} \\
CV N_1 F_L \sqrt{\frac{P_1 - F_F P_V}{SG}} &= C_d Y N_1 \left(\frac{d}{4.654}\right)^2 \sqrt{\frac{P_1 - F_F P_V}{SG}} \\
CV &= C_d \left(\frac{d}{4.654}\right)^2
\end{aligned} \tag{A-1.40}$$

For non-choked incompressible flow, the CV and discharge coefficient relations are as derived For the following conditions:

$$\begin{aligned}
\Delta P &\leq F_L^2 (P_1 - F_F P_V) \\
CV &= \frac{Q}{N_1} \sqrt{\frac{SG}{P_1 - P_2}} \\
Q &= CV N_1 \sqrt{\frac{P_1 - P_2}{SG}} \\
C_d &= \frac{Q}{N_1 \left(\frac{d}{4.654}\right)^2} \sqrt{\frac{P_1 - P_2}{SG}} \\
Q &= C_d N_1 \left(\frac{d}{4.654}\right)^2 \sqrt{\frac{P_1 - P_2}{SG}} \\
CV N_1 \sqrt{\frac{P_1 - P_2}{SG}} &= C_d N_1 \left(\frac{d}{4.654}\right)^2 \sqrt{\frac{P_1 - P_2}{SG}} \\
CV &= C_d \left(\frac{d}{4.654}\right)^2
\end{aligned} \tag{A-1.41}$$

From the relations revealed in the derivations, the flow coefficient is characteristic of the diameter and the discharge coefficient of the effective flow diameter, the flow coefficient is however a function of the fluid properties and rate of flow. With imperial units' considerations with conversion factors of 4.654 which converts the effective flow diameter from mm to inches, and 38 which converts imperial units of flow to metric, the following characteristics ensue:

$$\left(\frac{25.4}{4.654}\right)^2 \approx 29.8 \approx 38(0.25 \pi d^2) \approx 38 \frac{\pi d^2}{4} \quad (\text{A-1.42})$$

Other derivations ensue from considerations of equations presented in the standards ISA 75.01.01 [1] and API 520 [4] which ensues in the following expression:

$$A = \frac{Q}{C_d} \sqrt{\frac{SG}{P_1 - P_2}} \quad (\text{A-1.44})$$

Combination of equation (A-1.39) with the flow coefficient equation for non-choked flow yields the following expression for liquid flows:

$$38AC_d = CV = \frac{Q}{N} \sqrt{\frac{SG}{P_1 - P_2}} \quad (\text{A-1.45})$$

For gaseous flows, the expression becomes:

$$CV = 27.66 A C_d \quad (\text{A-1.46})$$

A-1.3. Empirical Derivations of Multi-Stage-Flow Passages Flow and Pressure Characteristics as a Function of Effective Flow Diameter and Area.

For flow passages in series along a flow path, the relations, and interactions between the stages-flow passages w.r.t the effective flow areas is expressed as follows.

$$\left(\frac{1}{C_{deq}A_{eq}}\right)^2 = \left(\frac{1}{C_{dA_1}}\right)^2 + \left(\frac{1}{C_{dA_1}}\right)^2 + \dots \left(\frac{1}{C_{dn}A_n}\right)^2 \quad (\text{A- 1.47})$$

$$\left(\frac{1}{C_{deq}A_{eq}}\right)^2 = \sum_1^n \left(\frac{1}{C_{dn}A_n}\right)^2 \quad (\text{A- 1.48})$$

Then it is stipulated that the relationship between the effective flow areas is

$$\begin{aligned}
 A_2 &= A_1\sqrt{s} \\
 A_2 &= A_1\sqrt{s} \\
 A_n &= A_{n-1}\sqrt{s}
 \end{aligned}
 \tag{A- 1.49}$$

Where s is the area ratio between the successive effective flow areas along a flow path in series.

This follows through that from the hypothesis, a reduction in the pressure drop across a stage-flow passage effective flow area by a factor of s , the effective flow area characteristic with the pressure drop should increase by a factor of the square root of s such that the conservation of mass is satisfied as follows:

$$\begin{aligned}
 Q_1 &= A_1 \cdot C \sqrt{\frac{2\Delta P_1}{\rho}} \\
 Q_2 &= A_2 \cdot C \sqrt{\frac{2\Delta P_2}{\rho}} \\
 A_2 &= A_1\sqrt{s} \\
 A_1 \cdot C \sqrt{\frac{2\Delta P_1}{\rho}} &= A_1 \cdot \sqrt{s} \cdot C \sqrt{\frac{2\Delta P_1 s^{-1}}{\rho}} \\
 \left(\frac{1}{C_{deq} A_{eq}}\right)^2 &= \left(\frac{1}{C_d A_1}\right)^2 + \left(\frac{1}{C_d \sqrt{s} A_1}\right)^2 \\
 &= \left[\frac{1}{C_d^2 A_1^2 s C_d^2 A_1^2}\right]^{0.5} \\
 &= \left[\frac{C_d^2 A_1^2 + C_d^2 A_1^2}{C_d^4 A_1^4 s}\right]^{0.5} \\
 C_d A_{eq} &= \left[\frac{1+s}{C_d^2 A_1^2 s}\right]^{-0.5} = C_d A_1 \sqrt{\frac{s}{s+1}}
 \end{aligned}
 \tag{A- 1.50}$$

A second successive stage in series along the flow path is expressed as follows.

$$\begin{aligned}
 \left(\frac{1}{C_{d\text{eq}}A_{\text{eq}}}\right)^2 &= \left(\frac{1}{C_d A_1 \sqrt{\frac{s^2}{s+1}}}\right)^2 + \left(\frac{1}{C_d A_1 s}\right)^2 \\
 &= \left[\frac{C_d^2 A_1^2 \frac{s}{s+1} + C_d^2 A_1^2 s^2}{C_d^4 A_1^4 \frac{s^3}{s+1}} \right]^{-0.5} \\
 &= \left[\frac{C_d^2 A_1^2 \left(\frac{s}{s+1} + s^2\right)}{C_d^4 A_1^4 \frac{s^3}{s+1}} \right]^{-0.5} \\
 C_d A_1 \sqrt{\frac{s^2}{s^2+s+1}} & \tag{A- 1.51}
 \end{aligned}$$

For example, the equivalent area of a four stages-flow passages or particularly orifices in series can be derived as follows:

$$\begin{aligned}
 \left(\frac{1}{C_{d\text{eq}}A_{\text{eq}}}\right)^2 &= \left(\frac{1}{C_d A_1 \sqrt{\frac{s^2}{s^2+s+1}}}\right)^2 + \left(\frac{1}{C_d A_1 s^{1.5}}\right)^2 \\
 &= \left[\frac{C_d^2 A_1^2 \frac{s^2}{s^2+s+1} + C_d^2 A_1^2 s^3}{C_d^4 A_1^4 \frac{s^5}{s^2+s+1}} \right]^{-0.5} \\
 C_d A_{\text{eq}} &= C_d A_1 \sqrt{\frac{s^3}{(s^2+1)(s+1)}} \\
 C_d A_{\text{eq}} &= C_d A_1 \sqrt{\frac{s^3}{s^3+s^2+s+1}} \tag{A- 1.52}
 \end{aligned}$$

A-1.4. Derivations of Flow Coefficient (CV) From Crane TP-410 Parameter Characterization.

The flow coefficient (CV) is defined as the rate of flow of water with units of imperial gallons/minute at a temperature of 60 Fahrenheit at a pressure drop of 1 psi for a valve with an effective flow area A and resistance coefficient K. the flow coefficient CV can be expressed as

$$C_v = Q \sqrt{\frac{\rho}{\Delta P(62.4)}} = \frac{29.9d^2}{\sqrt{f \frac{L}{D}}} = \frac{29.9d^2}{\sqrt{K}} \quad (\text{A-1.53})$$

Where the 62.4 is the density of water in lb/ft³ and the specific gravity is then $\rho/62.4$,

$29.9d^2$ as a function of effective flow area is expresses as follows:

$$38.08 \frac{\pi}{4} d^2 = 38.08 A \quad (\text{A-1.54})$$

Where A is the effective flow area of a flow passage or restriction, and then the flow rate is expressed as follows:

$$Q = \frac{38.08A}{\sqrt{K}} \sqrt{\frac{\Delta P(62.4)}{\rho}} \quad (\text{A-1.56})$$

Hence, according to the definition of the flow coefficient CV, and at unity of resistance coefficient is 1, the effective flow area is 1in², and the pressure drop is 1 psi the flow rate is 38.08gpm. Hence, based on the unit system, the flow rate can be expresses as:

$$Q = \frac{38.08 \left(\frac{\text{gpm}}{\text{in}^2 \sqrt{\text{psi}}} \right) A}{\sqrt{K}} \sqrt{\frac{\Delta P \left(62.4 \frac{\text{lb}}{\text{ft}^3} \right)}{\rho}} \quad (\text{A-1.57})$$

A-2: ISA-75.01.01- Standard Hydrodynamic Performance Characteristics:

Table A-2.1. Typical values of valve style modifier, liquid pressure recovery factor, and pressure differential ratio factor at full rated travel

Valve type	Trim type	Flow direction 2)	FL	xT	F_d
Globe, single port	3 V-port plug	Open or close	0.9	0.70	0.48
	4 V-port plug	Open or close	0.9	0.70	0.41
	6 V-port plug	Open or close	0.9	0.70	0.30
	Contoured plug (linear and equal percentage)	Open	0.9	0.72	0.46
		Close	0.8	0.55	1.00
	60 equal diameter hole drilled cage	Outward ³⁾ or inward ³⁾	0.9	0.68	0.13
	120 equal diameter hole drilled cage	Outward ³⁾ or inward ³⁾	0.9	0.68	0.09
Characterized cage, 4-port	Outward ³⁾	0.9	0.75	0.41	
	Inward ³⁾	0.85	0.70	0.41	
Globe, double port	Ported plug	Inlet between seats	0.9	0.75	0.28
	Contoured plug	Either direction	0.85	0.70	0.32
Globe, angle	Contoured plug (linear and equal percentage)	Open	0.9	0.72	0.46
		Close	0.8	0.65	1.00
	Characterized cage, 4-port	Outward ³⁾	0.9	0.65	0.41
		Inward ³⁾	0.85	0.60	0.41
Venturi	Close	0.5	0.20	1.00	
Globe, small flow trim	V-notch	Open	0.98	0.84	0.70
	Flat seat (short travel)	Close	0.85	0.70	0.30
	Tapered needle	Open	0.95	0.84	
Rotary	Eccentric spherical plug	Open	0.85	0.60	0.42
		Close	0.68	0.40	0.42
	Eccentric conical plug	Open	0.77	0.54	0.44
		Close	0.79	0.55	0.44
Butterfly (centered shaft)	Swing-through (70°)	Either	0.62	0.35	0.57
	Swing-through (60°)	Either	0.70	0.42	0.50
	Fluted vane (70°)	Either	0.67	0.38	0.30
High Performance Butterfly	Offset seat (70°)	Either	0.67	0.35	0.57
Ball	Full bore (70°)	Either	0.74	0.42	0.99
	Segmented ball	Either	0.60	0.30	0.98

COMPUTATIONAL FLUID DYNAMICS BASED DIAGNOSTICS AND PREDICTION TOOL FOR OPTIMAL DESIGN OF MULTI-STAGE TRIM CONTROL VALVES. BY GILBERT MARANGWANDA, SCHOOL OF COMPUTING AND ENGINEERING, UNIVERSITY OF HUDDERSFIELD

Table A-2.2: Minimum Inlet Absolute Test Pressure in kPa (Bar) as Related to F_L and Δp

Δp kPa (bar) → F_L ↓	Minimum inlet absolute test pressure - kPa (bar)								
	35 (0,35)	40 (0,40)	45 (0,45)	50 (0,50)	55 (0,55)	60 (0,60)	65 (0,65)	70 (0,70)	75 (0,75)
0,5	280 (2,8)	320 (3,2)	360 (3,6)	400 (4,0)	440 (4,4)	480 (4,8)	520 (5,2)	560 (5,6)	600 (6,0)
0,6	190 (1,9)	220 (2,2)	250 (2,5)	270 (2,7)	300 (3,0)	330 (3,3)	360 (3,6)	380 (3,8)	410 (4,1)
0,7	150 (1,5)	160 (1,6)	180 (1,8)	200 (2,0)	220 (2,2)	240 (2,4)	260 (2,6)	280 (2,8)	300 (3,0)
0,8	150 (1,5)	160 (1,6)	160 (1,6)	170 (1,7)	170 (1,7)	190 (1,9)	200 (2,0)	220 (2,2)	230 (2,3)
0,9	150 (1,5)	160 (1,6)	160 (1,6)	170 (1,7)	170 (1,7)	180 (1,8)	180 (1,8)	190 (1,9)	190 (1,9)

NOTE 1 For large valves where flow source limitations are reached, lower pressure differentials may be used optionally as long as turbulent flow is maintained and differential pressure measurement accuracy is within specification.

NOTE 2 For pressures not listed, use the following equation to calculate the upstream pressure: $p_{1_min} = 2\Delta p/F_L^2$

Table A-2.3: Properties of Water

Temperature °C	Density ρ kg/m ³	Dynamic viscosity cP	Kinematic viscosity	
			cSt	m ² /s
5	1,000 865	1,5181	1,518 2	1,5182E-06
10	1,000 600	1,305 9	1,306 3	1,3063E-06
15	1,000 000	1, 137 5	1, 138 6	1, 1386E-06
20	0,999 104	1,001 6	1,003 4	1,0034E-06
25	0,997 943	0,890 1	0,892 7	8,9272E-07
30	0,996 544	0,797 3	0,800 8	8,0083E-07
35	0,994 926	0,719 3	0,723 6	7,2363E-07
40	0,993 108	0,653 0	0,658 1	6,5810E-07

Table A-2.4: Tabulated Values for Piping Geometry Factor F_P if upstream and Downstream pipe are the same size.

$\frac{c}{d^2\sqrt{N_2}}$	d/D_1 or d/D_2				
	1	0,95	0,9	0,85	0,8
0,05	1	0,999 982	0,999 932	0,999 856	0,999 757
0, 1	1	0,999 929	0,999 729	0,999 423	0,999 029
0,2	1	0,999 715	0,998 919	0,997 698	0,996 135
0,3	1	0,999 359	0,997 572	0,994 842	0,991 365
0,4	1	0,998 861	0,995 696	0,990 885	0,984 802
0,5	1	0,998 222	0,993 299	0,985 867	0,976 551
0,6	1	0,997 443	0,990 393	0,979 835	0,966 744
0,7	1	0,996 525	0,986 992	0,972 848	0,955 525
0,8	1	0,995 468	0,983 11	0,964 968	0,943 054
0,9	1	0,994 275	0,978 765	0,956 265	0,929 493
1	1	0,992 946	0,973 977	0,946 811	0,915 008

Table A-2.5: Tabulated Values for Piping Geometry Factor F_P if Downstream pipe is Larger than Pipe.

$\frac{c}{d^2\sqrt{N_2}}$	d/D_2				
	1	0,95	0,9	0,85	0,8
0,05	1	1,000 22	1,000 385	1,000 502	1,000 576
0, 1	1	1,000 881	1,001 543	1,002 011	1,002 312
0,2	1	1,003 538	1,006 213	1,008 118	1,009 345
0,3	1	1,008015	1,014 146	1,018548	1,021 404
0,4	1	1,014 383	1,025 573	1,033 71	1,039 036
0,5	1	1,022 752	1,040 848	1,054 237	1,063 108
0,6	1	1,033 267	1,060 479	1,081 069	1,094 934
0,7	1	1,046 122	1,085177	1, 115 585	1, 136 505
0,8	1	1,061 569	1, 115 938	1, 159 84	1, 190 908
0,9	1	1,079 93	1, 154 176	1,216981	1,263 142
1	1	1, 101 623	1,201 944	1,292 058	1,361 837

Table A-2.6: Numerical Unit Conversion Constants

Constant	Flow Coefficient C		Formulae units					
	KV	CV	Q	$P, \Delta P, P_v$	ρ	T	d	v
N1	1.0×10^{-1} 1.00	8.65×10^{-2} 8.65×10^{-1}	m ³ /h m ³ /h	kPa a bar	kg/m ³ kg/m ³	-	-	-
N4	7.07×10^{-2}	7.60×10^{-2}	m ³ /h	-	-	-	-	m ² /s
N_g ($t_s = 0^\circ\text{C}$)	2.46×10^1 2.45×10^0	2.12×10^1 2.12×10^3	m ³ /h m ³ /h	kPa a bar	-	K K	-	-
N_g ($t_s = 15^\circ\text{C}$)	2.60×10^1 2.60×10^3	2.25×10^1 2.25×10^3	m ³ /h m ³ /h	kPa a bar	-	K K	-	-
N18	8.65×10^{-1}	1.00	-	-	-	-	mm	-
N21	1.3×10^{-3} 1.3×10^{-1}	1.4×10^{-3} 1.4×10^{-1}	-	kPa a bar	-	-	-	-
N_{22} ($t_s = 0^\circ\text{C}$)	1.73×10^1 1.73×10^3	1.50×10^1 1.50×10^3	m ³ /h m ³ /h	kPa a bar	-	K K	-	-
N_{22} ($t_s = 15^\circ\text{C}$)	1.84×10^1 1.84×10^3	1.59×10^1 1.59×10^3	m ³ /h m ³ /h	kPa a bar	-	K K	-	-
N25	4.02×10^{-2}	4.65×10^{-2}	-	-	-	-	mm	-
N26	1.28×10^7	9.00×10^6	m ³ /h	-	-	-	-	m ² /s
N31	2.1×10^4	1.9×10^4	m ³ /h	-	-	-	-	m ² /s
N32	1.40×10^2	1.27×10^2	-	-	-	-	mm	-
NOTE Use of the numerical constants provided in this table together with the practical metric units specified in the table will yield flow coefficients in the units in which they are defined.								

Table A-2.7: General Properties of Gases.

Gas or vapor	Symbol	M	γ	F_γ	$P_c^{(2)}$	$T_c^{(3)}$
Acetylene	C_2H_2	26.04	1.30	0.929	6,140	309
Air	–	28.97	1.40	1.000	3,771	133
Ammonia	NH_3	17.03	1.32	0.943	11,400	406
Argon	A	39.948	1.67	1.191	4,870	151
Benzene	C_6H_6	78.11	1.12	0.800	4,924	562
Isobutane	C_4H_{10}	58.12	1.10	0.784	3,638	408
n-Butane	C_4H_{10}	58.12	1.11	0.793	3,800	425
Isobutylene	C_4H_8	56.11	1.11	0.790	4,000	418
Carbon dioxide	CO_2	44.01	1.30	0.929	7,387	304
Carbon monoxide	CO	28.01	1.40	1.000	3,496	133
Chlorine	Cl_2	70.906	1.31	0.934	7,980	417
Ethane	C_2H_6	30.07	1.22	0.871	4,884	305
Ethylene	C_2H_4	28.05	1.22	0.871	5,040	283
Fluorine	F_2	18.998	1.36	0.970	5,215	144
Freon 11 (trichloromonofluoromethane)	CCl_3F	137.37	1.14	0.811	4,409	471
Freon 12 (dichlorodifluoromethane)	CCl_2F_2	120.91	1.13	0.807	4,114	385
Freon 13 (chlorotrifluoromethane)	$CClF_3$	104.46	1.14	0.814	3,869	302
Freon 22 (chlorodifluoromethane)	$CHClF_2$	80.47	1.18	0.846	4,977	369
Helium	He	4.003	1.66	1.186	229	5.25
n-Heptane	C_7H_{16}	100.20	1.05	0.750	2,736	540
Hydrogen	H_2	2.016	1.41	1.007	1,297	33.25
Hydrogen chloride	HCl	36.46	1.41	1.007	8,319	325
Hydrogen fluoride	HF	20.01	0.97	0.691	6,485	461
Methane	CH_4	16.04	1.32	0.943	4,600	191
Methyl chloride	CH_3Cl	50.49	1.24	0.889	6,677	417
Natural gas ⁴⁾	–	17.74	1.27	0.907	4,634	203
Neon	Ne	20.179	1.64	1.171	2,726	44.45
Nitric oxide	NO	63.01	1.40	1.000	6,485	180
Nitrogen	N_2	28.013	1.40	1.000	3,394	126
Octane	C_8H_{18}	114.23	1.66	1.186	2,513	569
Oxygen	O_2	32.000	1.40	1.000	5,040	155
Pentane	C_5H_{12}	72.15	1.06	0.757	3,374	470
Propane	C_3H_8	44.10	1.15	0.821	4,256	370
Propylene	C_3H_6	42.08	1.14	0.814	4,600	365
Saturated steam	–	18.016	1.25 – 1.32 ⁴⁾	0.893 – 0.943 ⁴⁾	22,119	647
Sulphur dioxide	SO_2	64.06	1.26	0.900	7,822	430
Superheated steam	–	18.016	1.315	0.939	22,119	647

Table A-2.8: Typical Values of Liquid Pressure Recovery Factor F_L and Pressure Differential Ratio Factor x_T at full Rated Travel.

Valve Type	Trim Type	Number of Stages	Flow Direction ^b	F_L ^{c d}	x_t ^e
Globe and angle	Multistage Multipath	2	Either	0,97	0,812
		3	Either	0,99	0,888
		4	Either	0,99	0,925
		5	Either	0,99	0,950
Globe and angle	Multistage Single path	3	Either	0,97	0,896
		4	Either	0,99	0,935
		5	Either	0,99	0,960
<p>a These values are typical only; actual values should be stated by the manufacturer.</p> <p>b Flow tends to open or close the valve, i.e. push the closure member away from or toward the seat.</p> <p>c The value of F_L is considered to be constant at all percentages of C.</p>					

Table A-2.9: Values of Stage Interaction Factors k , and the Reheat Factors r

Number of stages	k	r
1	0,404	0
2	0,673	0,215
3	0,825	0,316
4	0,885	0,335
5	0,915	0,310

Incompressible fluids

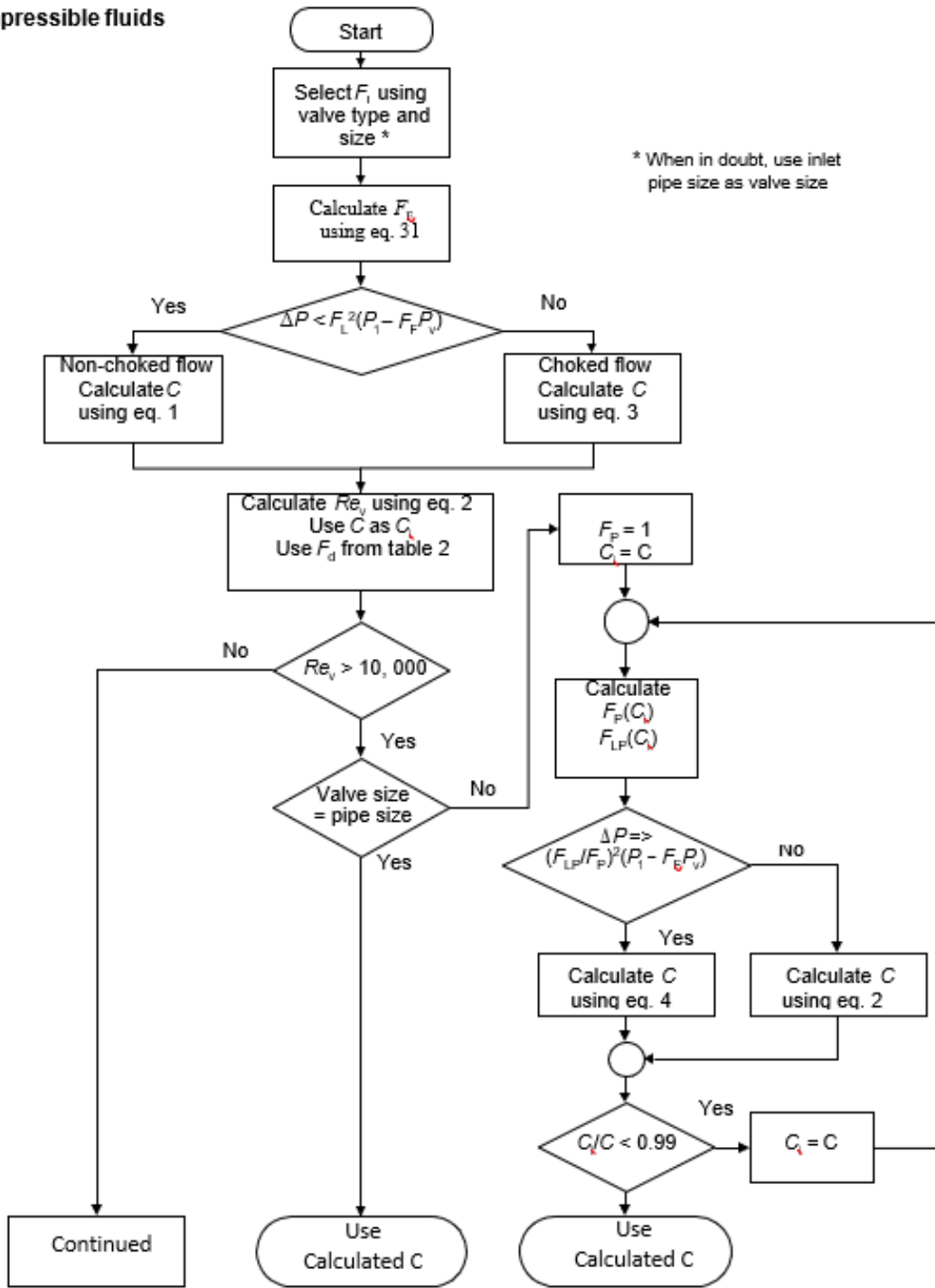
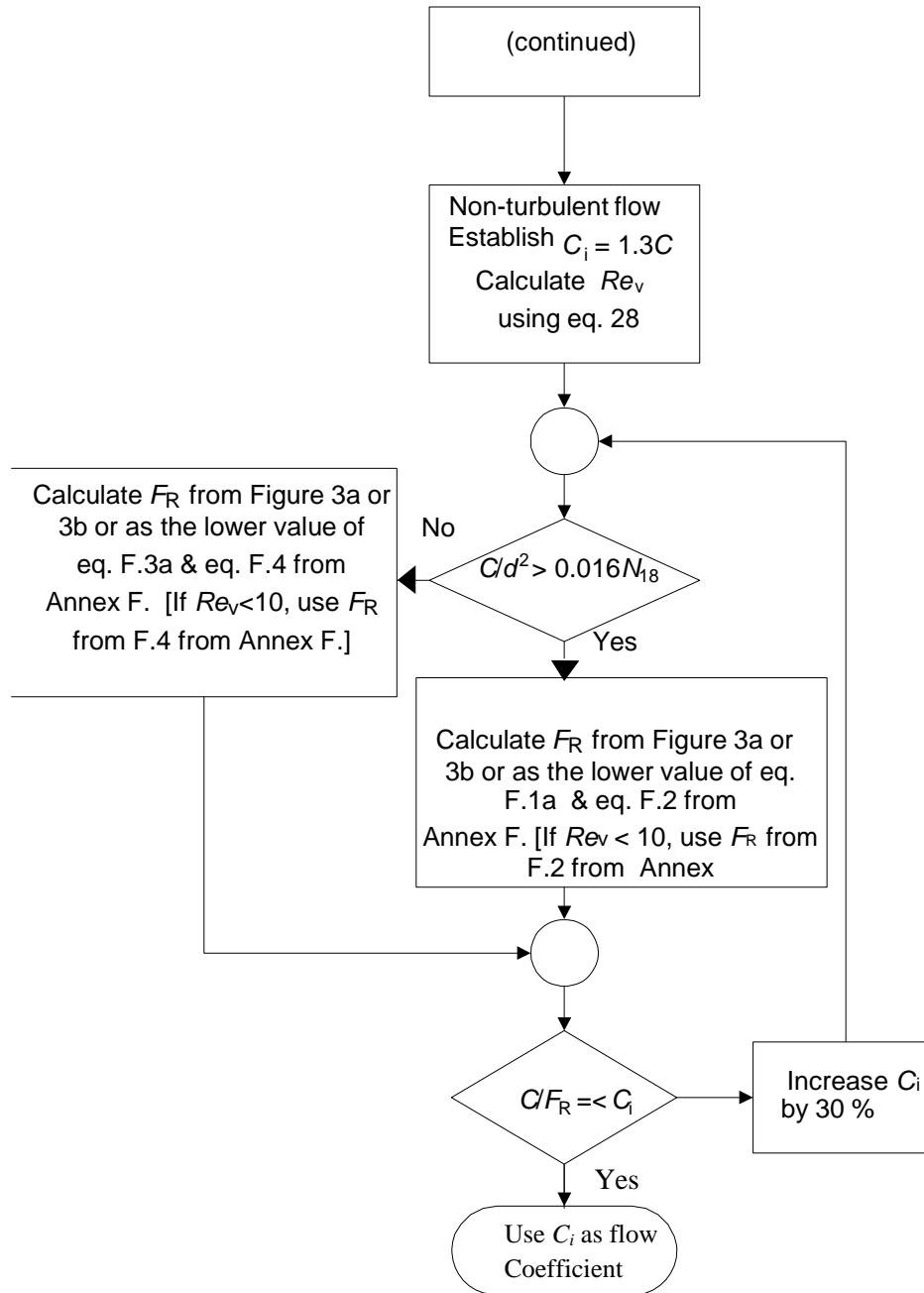


Figure A-2.1; ISA- 75.01.01 (IEC 60534-2-1) Standard Incompressible Flow Control Valve Flow Charts

COMPUTATIONAL FLUID DYNAMICS BASED DIAGNOSTICS AND PREDICTION TOOL FOR OPTIMAL DESIGN OF MULTI-STAGE TRIM CONTROL VALVES. BY GILBERT MARANGWANDA, SCHOOL OF COMPUTING AND ENGINEERING, UNIVERSITY OF HUDDERSFIELD

Incompressible fluids (continued)



A-3: Examples of Sizing Calculations

Example 1: Incompressible fluid – non-choked turbulent flow without attached fittings

Process data

Fluid:	water
Inlet temperature:	$T_1 = 356 \text{ K}$
Density:	$\rho_1 = 970 \text{ kg/m}^3$
Vapor pressure:	$p_v = 55,2 \text{ kPa}$
Thermodynamic critical pressure:	$p_c = 22 \text{ 120 kPa}$ Inlet
absolute pressure:	$p_1 = 680 \text{ kPa}$
Outlet absolute pressure:	$p_2 = 120 \text{ kPa}$
Flow rate:	$Q = 295 \text{ m}^3/\text{h}$
Pipe size:	$D_1 = D_2 = 150 \text{ mm}$

Valve data

Valve style:	globe
Trim:	3 stage, multipath
Flow direction:	flow-to-close
Valve size:	$d = 150 \text{ mm}$
Liquid pressure recovery factor:	$F_L = 0,99$ (from A-2.8)

Calculations:

$$F_F = 0.96 - 0.28 \sqrt{\frac{p_v}{p_c}} = 0.946$$

where

$$p_v = 55,2 \text{ kPa.}$$

$$p_c = 22 \text{ 120 kPa.}$$

Next, determine the type of flow

$$F_L^2(p_1 - F_F p_v) = 615 \text{ kPa}$$

which is more than the differential pressure 560 kPa; therefore, the flow is non-choked, and the flow coefficient C is calculated from the following expression:

$$C = \frac{Q}{N_1} \sqrt{\frac{\rho_1/\rho_0}{\Delta p}} = 123 \text{ m}^3/\text{h (K}_v\text{)}.$$

where

$$Q = 295 \text{ m}^3/\text{hr.}$$

$$N_1 = 1 \times 10^{-1}$$

$$\rho_1/\rho_0 = 0.97$$

$$\Delta p = 560 \text{ kPa.}$$

Example 2: Incompressible fluid – choked turbulent flow without attached fittings

Process data

Fluid:	water
Inlet temperature:	$T_1 = 366 \text{ K}$
Density:	$\rho_1 = 965 \text{ kg/m}^3$
Vapor pressure:	$p_v = 80 \text{ kPa}$
Thermodynamic critical pressure:	$p_c = 22\,120 \text{ kPa}$ Inlet
absolute pressure:	$p_1 = 680 \text{ kPa}$
Outlet absolute pressure:	$p_2 = 76 \text{ kPa}$
Flow rate:	$Q = 284 \text{ m}^3/\text{h}$
Pipe size:	$D_1 = D_2 = 150 \text{ mm}$

Valve data

Valve style:	globe
Trim:	3 stage, multipath
Flow direction:	flow-to-close
Valve size:	$d = 150 \text{ mm}$
Liquid pressure recovery factor:	$F_L = 0,99$ (from Table 2)

Calculations:

$$F_F = 0.96 - 0.28 \sqrt{\frac{p_v}{p_c}} = 0.943$$

where

$$p_v = 80,1 \text{ kPa.}$$

$$p_c = 22 \text{ 120 kPa.}$$

Next, determine the type of flow

$$F_L^2(p_1 - F_F p_v) = 593$$

kPa

which is less than the differential pressure 604 kPa; therefore, the flow is choked, and the flow coefficient C is calculated using equation (3):

$$C = \frac{Q}{N_1 F_L} \sqrt{\frac{\rho_1 / \rho_0}{p_1 - F_F p_v}} = 115 \text{ m}^3/\text{h (K}_v\text{).where}$$

$$Q = 284 \text{ m}^3/\text{h}$$

$$N_1 = 1 \times 10^{-1}$$

$$F_L = 0.99$$

$$\rho_1 / \rho_0 = 0.967$$

$$p_1 = 680 \text{ kPa}$$

$$F_F = 0.943$$

$$p_v = 80 \text{ kPa}$$

A-4: Specific Hydrodynamic Performance in a Multi-Stage Trim Control Valve

Table A-3.1. Specific Hydrodynamic Flow and Pressure Structure Within a Multi-Stage Trim Control Valve.

	Flow Passage Number	Normalised Effective Flow Diameter Ratio (D/d)	Flow Rate (Usgpm)	Inlet Pressure (PSI)	Outlet Pressure (PSI)	CV	Exit Pressure (PSI)	Normalised Pressure Difference	Pressure Drop (PSI)	Pressure Drop (N/M ²)	Pumping Energy Requirement (KW)	Cavitation Index (Σ)
Global			150	55.15	14.60	23.56			40.55	279564.18	35.28	
FP1	1	1.32				93.08	52.55	2.81	2.60	17905.07	2.26	21.16
FP2	2	1.48				68.16	47.71	8.04	4.84	33389.33	4.21	7.78

COMPUTATIONAL FLUID DYNAMICS BASED DIAGNOSTICS AND PREDICTION TOOL FOR OPTIMAL DESIGN OF MULTI-STAGE TRIM CONTROL VALVES. BY GILBERT MARANGWANDA, SCHOOL OF COMPUTING AND ENGINEERING, UNIVERSITY OF HUDDERSFIELD

FP3	3	1.59				57.25	40.84	15.46	6.87	47335.10	5.97	4.78
FP4	4	1.75				45.87	30.15	27.01	10.69	73726.79	9.30	3.80
FP5	5	1.91				38.04	40.00	43.81	15.55	107207.91	13.53	1.93

Table A-3.2. Specific Hydrodynamic Flow and Pressure Structure Within a Multi-Stage Trim Control Valve.

	Flow Passage Number	Normalised Effective Flow Diameter Ratio (D/d)	Flow Rate (Usgpm)	Inlet Pressure (PSI)	Outlet Pressure (PSI)	CV	Exit Pressure (PSI)	Normalised Pressure Difference	Pressure Drop (PSI)	Pressure Drop (N/M ²)	Pumping Energy Requirement (KW)	Cavitation Index (Σ)
Global	0		200	89.21	14.60	23.16			74.61	514380.58	86.55	
FP1	1	1.32				93.03	84.58	2.81	4.62	31866.24	5.36	19.26
FP2	2	1.48				68.26	76.00	8.03	8.58	59185.58	9.96	8.12
FP3	3	1.59				54.51	62.54	16.21	13.46	92814.74	15.62	4.54
FP4	4	1.75				45.87	43.53	27.76	19.01	131060.46	22.05	3.28
FP5	5	1.91				37.18	14.60	107.54	28.93	199453.55	33.56	1.49

	Flow Passage Number	Normalised Effective Flow Diameter Ratio (D/d)	Flow Rate (Usgpm)	Inlet Pressure (PSI)	Outlet Pressure (PSI)	CV	Exit Pressure (PSI)	Normalised Pressure Difference	Pressure Drop (PSI)	Pressure Drop (N/M ²)	Pumping Energy Requirement (KW)	Cavitation Index (Σ)
Global	0		200	63.90	14.60	28.49			49.30	339889.38	57.19	
FP1	1	1.26				107.08	60.41	2.12	3.49	24053.10	4.05	18.26
FP2	2	1.39				81.31	54.36	5.80	6.05	41710.26	7.02	7.52
FP3	3	1.48				68.26	45.77	11.01	8.58	59185.58	9.96	4.60

COMPUTATIONAL FLUID DYNAMICS BASED DIAGNOSTICS AND PREDICTION TOOL FOR OPTIMAL DESIGN OF MULTI-STAGE TRIM CONTROL VALVES. BY GILBERT MARANGWANDA, SCHOOL OF COMPUTING AND ENGINEERING, UNIVERSITY OF HUDDERSFIELD

FP4	4	1.59				57.34	33.61	18.41	12.17	83879.98	14.11	3.75
FP5	5	1.75				45.87	14.60	71.06	19.01	131060.46	22.05	1.75

	Flow Passage Number	Normalised Effective Flow Diameter Ratio (D/d)	Flow Rate (Usgpm)	Inlet Pressure	Outlet Pressure	CV	Exit Pressure (PSI)	Normalised Pressure Difference	Pressure Drop (PSI)	Pressure Drop (N/M^2)	Pumping Energy Requirement (KW)	Cavitation Index (Σ)
Global	0		200	59.40	14.60	29.88			44.80	308894.60	51.98	
FP1	1	1.26				107.08	55.91	2.12	3.49	24053.10	4.05	16.97
FP2	2	1.39				81.31	49.86	5.80	6.05	41710.26	7.02	6.78
FP3	3	1.48				68.26	41.28	11.01	8.58	59185.58	9.96	4.07
FP4	4	1.59				57.34	29.11	18.41	12.17	83879.98	14.11	3.38
FP5	5	1.65				52.50	14.60	64.58	14.51	100065.68	16.84	1.98

	Flow Passage Number	Normalised Effective Flow Diameter Ratio (D/d)	Flow Rate (Usgpm)	Inlet Pressure (PSI)	Outlet Pressure (PSI)	CV	Exit Pressure (PSI)	Normalised Pressure Difference	Pressure Drop (PSI)	Pressure Drop (N/M^2)	Pumping Energy Requirement (KW)	Cavitation Index (Σ)
Global	0		200	50.89	14.60	29.88			36.29	250204.63	37.89	
FP1	1	1.26				107.08	48.06	2.12	2.83	19483.01	2.95	17.94
FP2	2	1.39				81.31	43.16	5.80	4.90	33785.31	5.12	6.77

FP3	3	1.48				68.26	36.21	11.01	6.95	47940.32	7.26	4.07
FP4	4	1.59				57.34	26.36	18.41	9.85	67942.78	10.29	3.66
FP5	5	1.65				52.50	14.60	52.31	11.76	81053.20	12.27	2.21

	Flow Passage Number	Normalised Effective Flow Diameter Ratio (D/d)	Flow Rate (Usgpm)	Inlet Pressure (PSI)	Outlet Pressure (PSI)	CV	Exit Pressure (PSI)	Exit Pressure (N/M ²)	Normalised Pressure Difference	Pressure Drop (PSI)	Pumping Energy Requirement (KW)	Cavitation Index (Σ)
Global	0		200	56.29	20.00	29.88				36.29	37.89	
FP1	1	1.26				107.08	53.46	368615.62	2.12	2.83	2.95	19.85
FP2	2	1.39				81.31	48.56	334830.30	5.80	4.90	5.12	7.87
FP3	3	1.48				68.26	41.61	286889.99	11.01	6.95	7.26	4.84
FP4	4	1.59				57.34	31.76	218947.20	18.41	9.85	10.29	4.20
FP5	5	1.65				52.50	20.00	137894.00	52.31	11.76	12.27	2.66

	Flow Passage Number	Normalised Effective Flow Diameter Ratio (D/d)	Flow Rate (Usgpm)	Inlet Pressure (PSI)	Outlet Pressure (PSI)	CV	Exit Pressure (PSI)	Exit Pressure (N/M ²)	Normalised Pressure Difference	Pressure Drop (PSI)	Pumping Energy Requirement (KW)	Cavitation Index (Σ)
Global	0		150	45.20	20.00	29.88				25.20	21.93	
FP1	1	1.26				107.08	43.24	298117.34	2.12	1.96	1.71	22.94
FP2	2	1.39				81.31	39.84	274655.32	5.80	3.40	2.96	8.33
FP3	3	1.48				68.26	35.01	241363.43	11.01	4.83	4.20	5.17
FP4	4	1.59				57.34	28.16	194180.95	18.41	6.84	5.95	5.09
FP5	5	1.65				52.50	20.00	137894.00	36.33	8.16	7.10	3.39

	Flow Passage Number	Normalised Effective Flow Diameter Ratio (D/d)	Flow Rate (Usgpm)	Inlet Pressure (PSI)	Outlet Pressure (PSI)	CV	Exit Pressure (PSI)	Exit Pressure (N/M ²)	Normalised Pressure Difference	Pressure Drop (PSI)	Pumping Energy Requirement (KW)	Cavitation Index (Σ)
Global	0		100	31.20	20.00	29.88				11.20	6.50	
FP1	1	1.26				107.08	30.33	209104.38	2.12	0.87	0.51	35.55
FP2	2	1.39				81.31	28.82	198676.81	5.80	1.51	0.88	10.21
FP3	3	1.48				68.26	26.67	183880.42	11.01	2.15	1.24	6.49
FP4	4	1.59				57.34	23.63	162910.42	18.41	3.04	1.76	8.71
FP5	5	1.65				52.50	20.00	137894.00	16.15	3.63	2.10	6.29

	Flow Passage Number	Normalised Effective Flow Diameter Ratio (D/d)	Flow Rate (Usgpm)	Inlet Pressure (PSI)	Outlet Pressure (PSI)	CV	Exit Pressure (PSI)	Normalised Pressure Difference	Pressure Drop (PSI)	Pressure Drop (N/M ²)	Pumping Energy Requirement (KW)	Cavitation Index (Σ)
Global		120	119.5	76.43	14.60	15.20			61.83	426282.39	42.86	
FP1	1	1.32				35.11	64.84	19.72	11.58	79861.44	8.03	6.58
FP2	2	1.48				49.86	59.10	29.50	5.74	39607.40	3.98	8.70
FP3	3	1.59				41.87	50.96	43.36	8.14	56150.28	5.65	5.43
FP4	4	2.05				24.01	26.18	85.54	24.77	170801.83	17.17	2.05
FP5	5	1.72				35.11	40.00	105.26	11.58	79861.44	8.03	2.24

A-5: Expressions for Flow and Pressure Structure in Multi-Stage Control Valves and Trims

Flow Passage Pressure Drop	$\Delta P_{FP} = \left[\left(15852 Q_{FP} \left((SG) 38 A_{FP} \sqrt{\left(\frac{(A_{INLET}^2 - A_{FP}^2)}{A_{INLET}^2} \right)^{-1}} \right) \right)^2 \right]^2$
Flow Passage Flow Coefficient (CV)	$CV_{FP} = \left(\frac{1}{\sqrt{\left((SG) 38 A_{FP} \left(\sqrt{\left(\frac{(A_{INLET}^2 - A_{FP}^2)}{A_{INLET}^2} \right)^{-1}} \right) \right)^2}} \right)$

<p>Flow Passage Flow Rate</p>	$Q_{FP} = 0.0000631 \left[\sqrt{\Delta P_{FP}} \left((SG) 38 A_{FP} \sqrt{\left(\frac{A_{Inlet}^2 - A_{FP}^2}{A_{Inlet}^2} \right)} \right)^{-1} \right]$
<p>Local Flow Passages Pressure drop and Exit Pressure Along Flow Path, and Global Inlet Pressure Prediction Model</p>	$P_{IN} = \left(\frac{(15852 (Q_{FP1}))}{(SG) 38 A_{FP1} \left(\sqrt{\frac{A_{INLET}^2 - A_{FP1}^2}{A_{INLET}^2}} \right)} \right)^2 + \left(\frac{(15852 (Q_{FP2}))}{(SG) 38 A_{FP2} \left(\sqrt{\frac{A_{INLET}^2 - A_{FP2}^2}{A_{INLET}^2}} \right)} \right)^2 + \left(\frac{(15852 (Q_{FP3}))}{(SG) 38 A_{FP3} \left(\sqrt{\frac{A_{INLET}^2 - A_{FP3}^2}{A_{INLET}^2}} \right)} \right)^2 + \dots + P_{Out}$

<p>Local Flow Passages Flow Coefficient CV Along Flow Path, and Global Flow Coefficient (CV) Prediction Model.</p>	$\left(\frac{1}{\sqrt{(CV^2)^{-1}}} \right) = \frac{1}{\left(\frac{(SG) 38 A_{FP1}}{\sqrt{\left(\frac{A_{Inlet}^2 - A_{FP1}^2}{A_{Inlet}^2} \right)}} \right)^2} + \frac{1}{\left(\frac{(SG) 38 A_{FP2}}{\sqrt{\left(\frac{A_{Inlet}^2 - A_{FP2}^2}{A_{Inlet}^2} \right)}} \right)^2} + \frac{1}{\left(\frac{(SG) 38 A_{FP3}}{\sqrt{\left(\frac{A_{Inlet}^2 - A_{FP}^2}{A_{Inlet}^2} \right)}} \right)^2} + \dots + P_{out}$
--	---

